DOE/NASA/0167-10
NASA CR-179485
GARRETT NO. 31-3725(10)

ADVANCED GAS TURBINE (AGT) TECHNOLOGY DEVELOPMENT PROJECT

1985 ANNUAL REPORT
(JULY 1984 — JUNE 1985)

Engineering Staff of
Garrett Turbine Engine Company
A Division of The Garrett Corporation

July 1986

Prepared for
NATIONAL AERONAUTICS AND SPACE ADMINISTRATION
Lewis Research Center
Cleveland, Ohio 44135
Under Contract DEN3-167

(NASA-CR-179485) ADVANCED GAS TURBINE (AGT) TECHNOLOGY DEVELOPMENT PROJECT ANNUAL REPORT Interim Progress Report, Jul. 1984 - Jun. 1985 (Garrett Turbine Engine Co.) 175 p CSCL 20A G3/85

N86-33211

Unclas
44634

U.S. DEPARTMENT OF ENERGY
Office of Vehicle and Engine Research and Development
Technology Development and Analysis Division
Washington D.C. 20585

DOE/NASA/0167-10
NASA CR-179485
GARRETT NO. 31-3725(10)

ADVANCED GAS TURBINE (AGT) TECHNOLOGY DEVELOPMENT PROJECT

1985 ANNUAL REPORT (JULY 1984 — JUNE 1985)

Engineering Staff of
Garrett Turbine Engine Company
A Division Of The Garrett Corporation

JULY 1986

Prepared for
National Aeronautics and Space Administration
Lewis Research Center
Cleveland, Ohio 44135
Under Contract DEN3-167

for
U.S. DEPARTMENT OF ENERGY
Office of Vehicle and Engine Research and Development
Technology Development and Analysis Division
Washington D.C. 20585

TABLE OF CONTENTS

		Page
1.0	SUMMARY	1
1.1	Power Section Development	1
1.2	Combustor Development	1
1.3	Regenerator Development	1
1.4	Ceramic Development	2
2.0	INTRODUCTION	3
3.0	POWER SECTION DEVELOPMENT	5
3.1	Engine S/N 001	5
3.1.1	Ceramic Rotor Engine Testing	5
3.1.2	Ceramic Turbine Rotor Support Testing	6
3.1.3	Dog Bone Quill Shaft	7
3.1.4	Miscellaneous Motoring Tests	7
3.2	Engine S/N 002C	9
3.2.1	Build 6	9
3.2.2	Build 7	9
3.2.3	Build 8	10
3.2.4	Build 9	10
3.2.5	Build 10	12
3.2.6	Build 11	13
3.2.7	Build 12	13
3.2.8	Build 13	16
3.2.8.1	Build 13A	17
3.2.8.2	Build 13B	18
3.2.8.3	Build 13C	19
3.2.8.4	Build 13D	19
3.2.8.5	Build 13E	21
3.2.8.6	Build 13F	21
3.2.8.7	Build 13G	21
3.2.8.8	Build 13H	21
3.3	Engine S/N 003	26
3.3.1	Build 46	26
3.3.1.1	Build 46H	26
3.3.1.2	Build 46J	27
3.3.2	Build 47	27
3.3.4	Build 48	29
3.4	Engine S/N 004C	35

TABLE OF CONTENTS (Contd)

		Page
4.0	COMPONENT/SUBSYSTEM DEVELOPMENT	37
4.1	Compressor Development	37
4.2	Turbine Development	37
4.3	Combustion	37
4.3.1	Torch Ignitor	37
4.3.2	Combustion System Design Improvements	37
4.3.3	Fuel Nozzle Testing	40
4.4	Regenerator System - Ford	40
4.4.1	Regenerator Seal	40
4.4.2	Seal Coatings	45
4.4.3	Regenerator Core and Drive System	51
4.4.4	Regenerator Development Rig	57
4.4.5	Non-Diaphragm Seals	58
4.5	Ceramic Materials	60
4.5.1	Rotor Materials Evaluations	60
4.5.2	Static Components	60
4.5.3	Ceramic Turbine Rotor Deliveries	73
4.5.4	Screening Rigs	74
4.5.4.1	Ceramic Components Thermal Screen Tests	82
4.5.5	Ceramic Turbine Rotors	99
4.5.6	Ceramic Components Received	103
4.6	High Temperature Foil Bearing Development	106

APPENDICES

APPENDIX A	FORD MOTOR COMPANY ADVANCED GAS TURBINE (AGT) TECHNOLOGY DEVELOPMENT PROJECT 1985 ANNUAL TECHNICAL PROGRESS REPORT
APPENDIX B	AIRESEARCH CASTING COMPANY ADVANCED GAS TURBINE (AGT) TECHNOLOGY DEVELOPMENT PROJECT 1985 ANNUAL TECHNICAL PROGRESS REPORT
APPENDIX C	CARBORUNDUM UNIQUE WORK ADVANCED GAS TURBINE (AGT) TECHNOLOGY DEVELOPMENT PROJECT 1985 ANNUAL TECHNICAL PROGRESS REPORT

TABLE OF CONTENTS (Contd)

APPENDIX D LIST OF SYMBOLS, ABBREVIATIONS, AND ACRONYMS

APPENDIX E REFERENCES

NASA C-168 FORM

LIST OF FIGURES

Figure	Title	Page
1	AGT101 Program Schedule	4
2	Engine S/N 001 Build 26 Ceramic Rotor Failure	5
3	Lissajous Trace of the Thrust Rotor Clearance Probes During Failure Initiation	6
4	Rotor Interference Diagram	7
5	Rotor Blade Damage	8
6	Ceramic Rotor Strain Test - Exducer and Fracture	8
7	Ceramic Rotor Strain Test - Inducer Instrumentation and Fracture	8
8	Dog Bone Quill Shaft Configuration	8
9	Turbine Shaft Excursions, Wayne-Kerr Probes	9
10	Dual Alloy Turbine Wheel Backface Crack	10
11	Flow Separator Housing Damage Locations	10
12	Turbine Shroud Fracture	11
13	No Performance Deterioration During Test	12
14	Hot (Inner) Regenerator Seal Distress	12
15	Performance Parameters Tracked During 100-Hour Endurance Test	13
16	Ceramic Parts After 100 Hours at 2050 ±50F and Cruise Speed	15
17	Programmed Temperature Control for Development Starts	16
18	First 2100F Development Start, S/N 002C, Build 11	16
19	Fractured Flow Separator Housing, S/N 002C, Build 11.	17
20	S/N 002C, Flow Separator Housing to Turbine Shroud Fit	17
21	Required and Actual Thermal Transient Results, S/N 002C, Build 12	18
22	Exhaust Housing With Insulation and Displacement Probe	23
23	S/N 002C, Build 13H Regenerator Core Removed	24
24	S/N 002C, Build 13H Teardown Showing Rotor	24
25	S/N 002C Flow Separator Housing Failure Mode	25
26	Heat Shield to Combustor Cap Clearance-Versus-ΔT	26
27	Case 1 - Exhaust Housing Temperatures	27
28	Regenerator Drive Pressure Relationship to Combustor Inlet Temperature (T3.5)	27
29	Seal Leakage Areas Individually Tested	29
30	Metal Engine Flow Distribution	30
31	Piston Ring Seal Showing Added Inserts at Splitline	31
32	Engine Performance as a Function of Speed (1600F)	31
33	Engine Performance as a Function of IGV Position (1600F)	32
34	Performance Model Results	33
35	Total Parasitic Power Loss (Aero to Dynamometer)	35
36	Powertrain Parasitic Loss (Engine Gear to Dynamometer)	35
37	Performance Rating Stations	38
38	Torch Ignitor - Multi-Fuel	39
39	Torch Test Data Using JP-4	40
40	T/3 Torch Configuration	41
41	T/4 Torch Upgraded Configuration with Cooling Air Provisions	41
42	Combustion System Conceptual Design	42
43	Modularized Fuel Nozzle/Ignitor Development Configuration	43
44	Garrett (View A) and Delavan (View B) Fuel Nozzle Installations	44

LIST OF FIGURES (Contd)

Figure	Title	Page
45	Garrett Fuel Nozzle	45
46	Combustor Mixer Modification	45
47	Phase V Static Seal Leakage	46
48	Phase VI Static Seal Leakage	47
49	Phase VI Diaphragm Cooling Design	47
50	Phase VI Initial Design Concept	48
51	Phase VI Second Design Concept	49
52	Phase VI Third Design Concept	50
53	Seal Coating Evaluation (18-Hours at 1000F)	52
54	Location of Linear Transducer on Exhaust Cover	55
55	Test Results to Measure Effect of Increased Cooling Air	56
56	Ford Regenerator Development Rig Modifications	57
57	Non-Diaphragm Seal Configurations	58
58	Flexure Strength of AGT101 Rotors	65
59	Representative: Fracture Origins For NGK SN-54	69
60	Fracture Origins For NGK SN-54	70
61	Turbine Shroud S/N 545 Density Summary	73
62	Fracture Origins for Test Bars Cut From ACC RBM 104 Baffle S/N-593	73
63	Flow Separator Housing Cut-Up Test Bar Location	74
64	Internal (a) and Surface (b) Fracture Origin and As-Machined Surface (c) For LAS Flexure Tested at Room Temperature (70F)	75
65	Fracture Origin (A) and Surface (b) of LAS Flexure at 1800F	76
66	Fracture Origin (a and b) and surface (c) of LAS Flexure Tested at 2000F	77
67	Fracture Origin at 200X(a) and 400X(b) of LAS Flexure Tested at 2050F. Note Glazed Surface of Interior of Origin	78
68	Ceramic Component Qualification Sequence	81
69	Cutback of Stator Vane Trailing Edge	82
70	AGT101 Static Components Proof Test Cycles	85
71	Erosion of Lockheed HTP-12	89
72	Static Structures Rig	89
73	Diagram of Rig With Associated Instrumentation	94
74	Origin of Turbine Shroud Fracture	96
75	Turbine Shroud Mechanical Screening Test Setup	100
76	RBSN Turbine Shroud Showing Failure in Mechanical Screening Test	100
77	Slotted Versus Slotless Turbine Shroud Configuration	100
78	Mechanical Screening Rig Test Setup	101
79	Dial Indicator Locations for Turbine Shroud Load Test	102
80	Increasing Consistency Evident in Cold Spin Test	104
81	Ceramic Rotor S/N 344 Installed in Cold Spin Pit	105
82	New Design Spin Pit Arbor	105
83	Ceramic Rotor S/N 344 Installed in Spin Pit with New Arbor Arrangement	105
84	Laser Marking of Ceramic Rotor S/N 552	106
85	Wear on Foils Supporting the Shaft Loads After 263 Starts	106
86	Foil Bearing Surface Coating Development	108
87	Dynamic Properties Test Rig Schematic	108

LIST OF FIGURES (Contd)

Figure	Title	Page
88	Typical Results of Dynamic Friction Test	110
89	AGT101 Single Bearing Test Rig Schematic	110
90	Wear Typical of 1000 Starts at 1-g Load, Aμ Coated Foil Versus SiN_4 Journal	111
91	Si_3N_4 Turbine Rotor with Integral Bearing Journal and Aμ Coated Foil Bearing	111
92	RM 20 Powder Reduction Flow Chart	114
93	Dispex A-40 and Cooloids of California 226/35 SRII Powder	115
94	Dispex Concentraction Versus Viscosity for 3 Powder Distributions	116
95	Dispex A-40 SRIII Powder	116
96	Colloids of California 226/35 SRIII Powder	116
97	Particle Size Distribution of Several Denka Si_3N_4 Powders - Manufacturer's Data	135
98	Particle Size Distribution Curve of Toyo Soda Si_3N_4 Powders - Manufacturer's Data	136
99	Particle Size Distribution of As-Received UBE Si_3N_4 EO-2 and EO-5 Powders and EO-5 After Milling for 1 Hour	137
100	Particle Size Distribution of As-Received UBE EO-2 Si_3N_4 Powder and the Effective Change in Distribution After 5 and 25 Hours Milling	138
101	Particle Size Distribution of As-Received Starck H-2 Si_3N_4 Powders and Effects of 10, 12, and 16 Hours Milling Time	139
102	Stress Rupture, Room and Elevated Temperature Flexure Test (Specimens Cut from Plate Cast with Rotor S/N 552)	143
103	Room Temperature Flexure Testing	144
104	Ceramic Slip Cast AGT101 Turbine Rotor	145
105	$Si_{3}N_4$ Rotor with Shaft Attachment Ready for Spin Testing	145
106	Si_3N_4 Rotor Completely Assembled for Engine Test	145
107	EDX at 2,700 KEV of Powder Samples	145
108	EDX at 5.2 KEV of Powder Samples	146
109	An Expanded EDX Microprobe Spectrum of Blade Sample	146
110	An EDX Microprobe Spectrum Obtained on the Cleaned Area of the Sample Using a 39kV Beam Voltage	146
111	Modification of "A" Generation Rotor	149
112	Changes in Mold Design	150
113	AGT101 Turbine Shroud Evolution	150
114	AGT101 Transition Duct Evolution	151
115	Iterations in Plaster Mold - Flow Separator Housing	153
116	Trial Casting from First Iteration Mold Design - Flow Separator Housing	154
117	AGT101 Ceramic Ring Components	154
118	On Right Side of Photograph is a Leeds and Northrup Microtrak Particle Size Distribution Analyzer. On Left is a Haake Rotor Viscometer	155
119	Haake Rheometer for Characterizing Flow Behavior of Injection Molding Mixes	156
120	Micromerities Flow Sorb II - 2300, Surface Area Analytical Equipment	157
121	Injection Molded Transition Duct with Port Holes	162

LIST OF TABLES

Table	Title	Page
1	Test/Computer Performance Comparison	14
2	S/N 002C, Regenerator Systems Configurations	19
3	Comparison of S/N 002C Engine Test With Performance Match Model	20
4	AGT101, S/N 002C Performance Model	22
5	Exhaust Housing Data Reduction Cases	26
6	S/N 003 Motoring Test Summary - July 1984	28
7	Component Leakage	31
8	Test Points	32
9	S/N 003 Motoring Test Summary - July 1984	34
10	NGK Regenerator Core Performance	53
11	Corning Regenerator Core Performance	54
12	Thermal Distortion of Flow Separator Housing and Core	59
13	AGT101 Component and Material Summary	61
14	AGT Ceramic Material Characterization at Garrett	62
15	AGT101 Static Component Predicted Stress and Temperatures	63
16	AGT101 SI_3N_4 Rotor Predicted Stresses and Temperatures	64
17	ACC Code 1 Sintered Silicon Nitride Stress Rupture Test Results	66
18	ACC Code 2 SSN Stress Rupture Test Results	67
19	Stress Rupture Results For NGK SN-50 Sintered Si_3N_4	68
20	Flexure Strength Test Results for NGK SN-54	69
21	Component Cut-Up Room Temperature Flexure Strength Summary	71
22	Component Cut-Up Room Temperature Flexure Strength Summary	72
23	Flexure Strength Results for Cut-Up LAS Flow Separator Housing S/N 17	74
24	Stress Rupture Results for LAS Test Bars Cut From Flow Separator Housing S/N-17	78
25	Flexure Strength and Fracture Origins of Laser Marked Test Bars	79
26	ACC Rotors Received July 1, 1984 - June 30, 1985	80
27	AGT101 Static Components Proof Test Cycles	81
28	Turbine Shroud and Stator Screening Tests	83
29	Inner and Outer Diffuser Housing Screening Results	86
30	Transition Ducts/Combustor Baffles Screened	88
31	Fractography Results	90
32	Ceramic Components Tested in Structures Rig, Build 12, September 12-14, 1984	91
33	Parts Built Into Static Structures Rig, Build 13	93
34	Hot Stator Rig, Build 1	95
35	*Components Used in 2500F Turbine Shroud Screening Rig*	97
36	April 18, 1985 Testing at 2500F (Vertically Configured Rig)	98
37	May 13, 1985 Testing at 2500F (Vertically Configured Rig)	99
38	Axial and Radial Deflections of RBSN Turbine Shroud During Mechanical Screen Test	103
39	Cold Spin Test Results	104
40	Summary of Foil and Journal Coatings Evaluated	107
41	Wear Test Sequence	109
42	Comparison of Test Results for High Temperature Foil and Journal Coatings at Ambient Conditions	111

LIST OF TABLES

Table	Title	Page
43	Silicon Nitride Survey	122
44	GTE Sylvania Si_3N_4 - Manufacturer's Analysis	123
45	Denka Si_3N_4 Powder - Manufacturer's Analysis	124
46	ELKEM Si_3N_4 Powder - Manufacturer's Analysis	125
47	Kemanord Si_3N_4 Powder - Manufacturer's Analysis	126
48	H.C. Starck H-1 Si_3N_4 Powder - Manufacturer's Analysis	128
49	H.C. Starck H-2 Si_3N_4 Powder - Manufacturer's Analysis	129
50	Toshiba Si_3N_4 Powder - Manufacturer's Analysis	130
51	Toyo Soda Si_3N_4 Powder - Manufacturer's Analysis	131
52	UBE SN-E02 Si_3N_4 Powder - Manufacturer's Analysis	132
53	UBE SN-E05 Si_3N_4 Powder - Manufacturer's Analysis	133
54	UBE SNE-10 Si_3N_4 Powder - Manufacturer's Analysis	134
55	Comparison of PSD and Surface Area of Si_3N_4 From Various Suppliers	140
56	Rotors Shipped July 1984 - June 1985	141
57	Rotors in Stress Rupture, Room and Elevated Temperature Testing	142
58	Comparison of GTE Powders Received October 1983 - June 1985	147
59	Chemical Analyses of GTE Powders	148
60	Component Delivery	159
61	Turbine Shroud Densities	160

1.0 SUMMARY

This report describes progress and work performed by the Garrett Turbine Engine Company/Ford Motor Company Team during July 1984 through June 1985 to develop technology for an Advanced Gas Turbine (AGT) engine for automotive applications. This work was performed for the Department of Energy under NASA Contract DEN3-167. This is the tenth in a series of semiannual reports, however, per agreement between contracting parties, the period covered encompassed a full calendar year of contract activity. Work performed during the first nine periods (References 1 through 9) initiated design and analysis, ceramic development, component testing, and test bed evaluation.

Project effort conducted under this contract is part of the DOE Gas Turbine Highway Vehicle System Program. This program is oriented at providing the United States automotive industry the high-risk long-range technology necessary to produce gas turbine engines for automobiles with reduced fuel consumption and reduced environmental impact. Technology resulting from this program is intended to reach the marketplace by the early 1990's.

The advanced automobile gas turbine, when installed in a Ford vehicle (3000 pounds inertia weight), will provide:

- o A combined federal driving cycle (CFDC) fuel economy of 42.8 miles per gallon based on Environmental Protection Agency (EPA) test procedures using diesel No. 2 (DF-2) fuel. The AGT-powered vehicle will substantially give the same overall vehicle driveability and performance as a comparable production vehicle powered by a conventional spark-ignition powertrain system
- o Emissions less than federal standards
- o Ability to use a variety of fuels

1.1 Power Section Development

Eight builds of the ceramic structures engine were tested accumulating over 125 hours of test time including a 100-hour durability test at cruise conditions (2100F, 68,000 rpm). Baseline performance was established at 2100F and 100,000 rpm, demonstrating 43.4 hp-shaft output.

Metal engine performance characterization testing was completed with excellent correlation between analytical model and engine test data. This completed Milestone 2 of the program.

1.2 Combustor Development

Effort in combustor development concentrated on fuel nozzle testing. A revised nozzle configuration was designed, fabricated, and tested. The nozzle incorporates the centerline ignition source. Successful ignition and fouling tests were conducted.

1.3 Regenerator Development

Diaphragm tooling for Phase V-A seals was received and several sets of seals fabricated. Static seal testing indicated the Phase V-A configurations are a significant improvement over Phase V seals. The next generation Phase VI seals (increased cooling) are currently being designed.

Regenerator drive torque variations were determined through testing to be a function of exhaust housing distortion. Analytical modeling is currently underway to define modifications to the housing.

1.4 Ceramic Development

Testing conducted in the ceramic component rigs to qualify hardware for engine testing. Design modifications were incorporated in the stator trailing edge, turbine backshroud, and turbine shroud to reduce stress and alleviate problems experienced during test.

Testing continued at 2500F with over 1 hour of test time accumulated without problems.

Rotor fabrication continued at ACC, Ford, and NGK-Locke. All vendors are showing progress. Kyocera was contacted regarding rotor fabrication.

2.0 INTRODUCTION

This report is the tenth in a series of Technical Summary Reports for the Advanced Gas Turbine (AGT) Technology Development Project, authorized under NASA Contract DEN3-167 and sponsored by the DOE. This report has been prepared by the Garrett Turbine Engine Company (hereinafter referred to as Garrett), a Division of the Garrett Corporation, and includes information provided by the Ford Motor Company (hereinafter referred to as Ford), Sohio Engineered Materials Company/Carborundum, and AiResearch Casting Company (ACC). The project was administered by Mr. Thomas Strom, Project Manager, NASA-Lewis Research Center, Cleveland, Ohio. This report presents plans and progress from July 1984 through June 1985.

Project effort conducted under this contract is part of the DOE Gas Turbine Highway Vehicle System Program. This program is oriented at providing the United States automotive industry the high-risk, long-range technology necessary to produce gas turbine engines for automobiles that will have reduced fuel consumption and reduced environmental impact. The intent is that technology resulting from this program be capable of reaching the marketplace by the early 1990s.

The advanced gas turbine, when installed in a Ford vehicle (3000 pounds inertia weight) would provide:

- A CFDC fuel economy of 42.8 miles per gallon based on EPA test procedures and DF-2. The AGT-powered vehicle shall give substantially the same overall vehicle driveability and performance as a comparable production vehicle powered by a conventional spark-ignition powertrain system
- Emissions less than federal standards
- Ability to use a variety of fuels

The Garrett/Ford advanced gas turbine has been designated the AGT101.

The program is oriented toward developing advanced gas turbine long-range, high-risk technology such that the automotive industry can carry forward to production in the 1990s. Emphasis on ceramics, gas bearings, low emission combustion, and improved component performance shall continue. The AGT101 is being used as a test bed in which to develop these technologies.

The program schedule is depicted in Figure 1. The program continues technology work through FY86, culminating in demonstration of the original goals of engine specific fuel consumption, power output, and emissions. In addition, the viability of ceramics will have been demonstrated in the AGT101 test beds, and the potential of economically producing the ceramic parts in automotive production quantities will have been assessed. When these goals are achieved, Ford will be in a position to proceed, without Government support, through the typical preproduction tasks that then could lead to production in the 1990s.

The primary technology challenge in the program continues to be ceramic components development and related high performance gas turbine aerothermodynamic components development for the AGT101. The AGT101 nominally is a 100 shp engine, capable of speeds to 100,000 rpm and operating at turbine inlet temperatures (TIT) to 2500F with a specific fuel consumption level of 0.3 pounds/horsepower/hour over much of the operating range.

This report reviews the power section (metal and ceramic) effort conducted to date, followed by a review of the components/ceramic technology development. Appendices include reports of progress from Ford, ACC, and Carborundum.

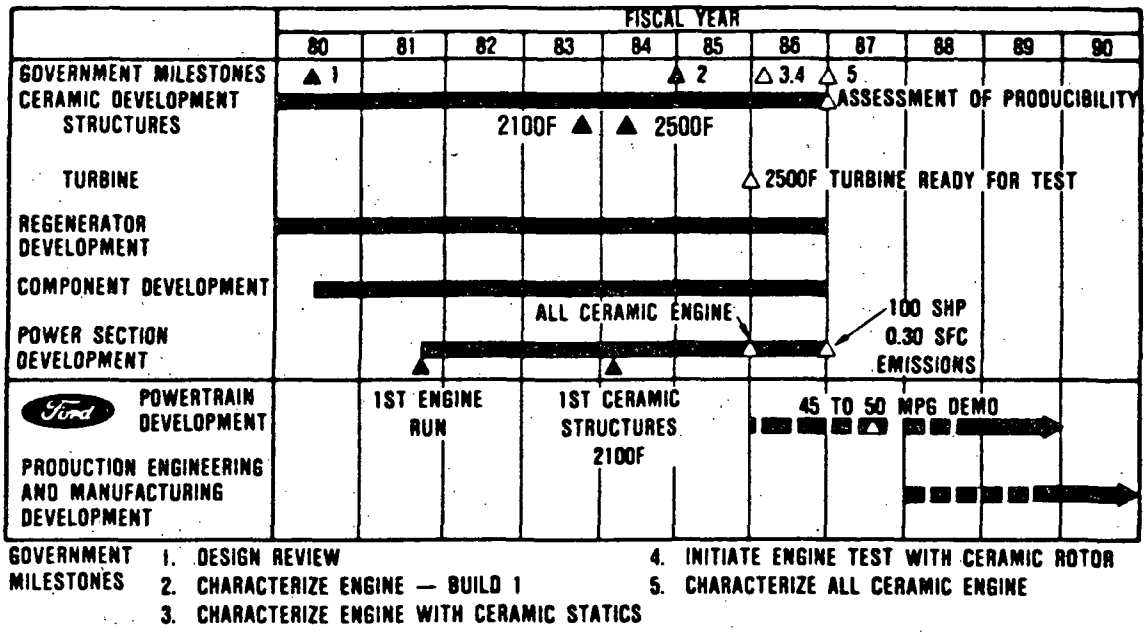

Figure 1. AGT101 Program Schedule.

3.0 POWER SECTION DEVELOPMENT

3.1 Engine S/N 001

Over the past year, engine S/N 001 has been used as a ceramic rotor and rotor dynamics test bed. The ceramic rotor work was performed on engine Builds 25 and 26. Builds 27 and 28 evaluated a "dog bone" quill shaft and its effect on rotor stability at high speeds. Most recently, Builds 29 through 33, tested various rotor/gearbox couplings and bearing mount configurations.

3.1.1 Ceramic Rotor Engine Testing

Build 25 was assembled and tested using metal 1600F structures and a ceramic turbine rotor. The objective of the test was to demonstrate ceramic rotor operation to full engine speed under 1600F engine operating conditions. During that test the rotor failed at 97,300 rpm. Figure 2 shows the condition of the engine rotor during disassembly.

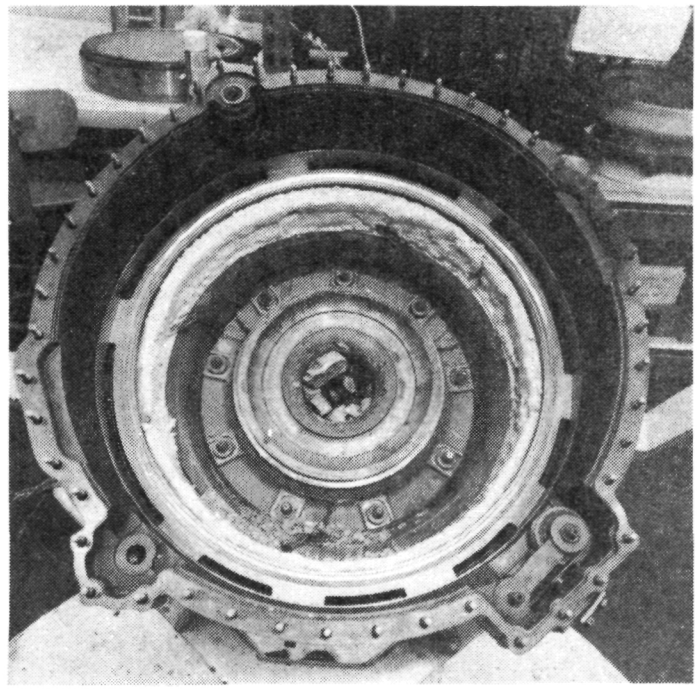

Figure 2. Engine S/N 001 Build 26 Ceramic Rotor Failure.

Results of the failure analysis indicated that the rotor failed due to excessive ceramic turbine rotor blade vibration. This conclusion was supported by the following observations:

- Several large rotor hub fragments were recovered, atypical of hub burst. Fractographic examination did not reveal any fracture origins

- A review of the rotor shaft motion during failure revealed instantaneous departure from a stable orbit. This is an indication that an instantaneous imbalance (blade loss) was imposed on the rotating group at the onset of failure. Figure 3 shows the rotor shaft motion during the failure

- Rotor dynamic analysis of the rotor motion did not indicate backward whirl at the time of failure--a classic response induced by rubbing

- Three blade resonances are potentially excitable during operation, with one close to the failure speed

- Acoustic blade ring tests of similar rotors indicated the presence of these blade resonance modes within the operating range

Build 26 was a retest of the metal engine structure/ceramic rotor configuration. However, prior to test the rotor was "tuned" to eliminate blade resonance from the upper region of the engine operating speed range. Blade resonant frequencies were checked and material removed to "tune out" the exducer second mode and inducer first modes in the 20 to 35 kHz range (70,000 to 102,000 rpm).

Due attention was given to the fact that blade modifications increasing the exducer

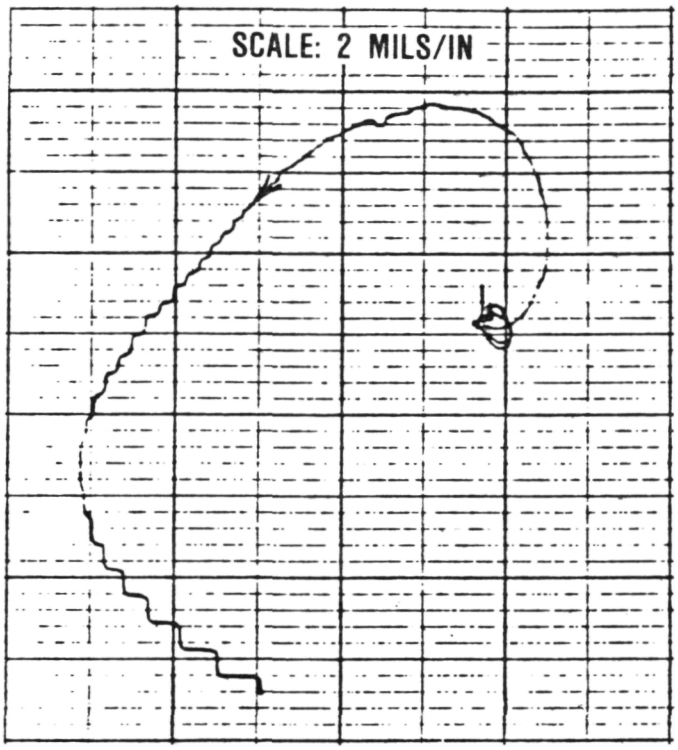

Figure 3. Lissajous Trace of the Thrust Rotor Clearance Probes During Failure Initiation.

second mode beyond the engine operating range also increase the exducer fundamental resonance into the lower end of the operating range, as shown in the Campbell diagram on Figure 4. Full recognition was made that this resulted in a potential low-speed (55,000 to 65,000 rpm) blade excitation. This risk element was accepted since the rotor must pass through these low speed resonances enroute to the engine design speeds and had done so in Build 25.

Two starts were made on Build 26. During the first start, an engine speed control problem allowed the engine to accelerate quickly to 77,000 rpm before an emergency shutdown was executed. A second start was attempted and at an engine speed of 62,000 rpm the rotor failed. It should be noted that the engine experienced a "hung start" at this speed and dwelled there for approximately 2.5 minutes. The engine speed at the time of failure was 62,000 rpm.

Engine damage was less extensive during this second failure. As shown in Figure 5, the rotor hub was completely intact with only broken blades. Given the rotor condition and the pretested blade resonant data, the conclusion was drawn that blade vibration again was the cause of the engine failure.

3.1.2 Ceramic Turbine Rotor Support Testing

In support of future engine tests, static vibration test of the ceramic rotor blades on the Bullen machine was conducted and an engine strain-gage test planned.

The objective of the shake table (Bullen machine) test was to determine the strain amplitude required to fracture ceramic turbine rotor blades. Testing was performed on rotor S/N 638. The blades were acoustically rung, strain mapped, and strain-gaged to provide information on the peak strains in the inducer and exducer regions of selected blades. The rotor was mounted on a Bullen machine and oriented to apply maximum vibration energy to the instrumented blades.

The results of this test are shown on Figures 6 and 7. The instrumented inducer blade fractured at a strain peak-to-peak amplitude of more than 2000 micro in/in while dwelling at the blade natural frequency of 13,900 Hz. The exducer blade with strain-gage instrumentation showed a maximum strain amplitude of 1600 micro in/in at 16,300 Hz, but did not fracture despite repeated passes through the blade natural frequency at maximum energy input level. An exducer blade did break during the test, however, since the blade was not instrumented, the strain level was not known.

The Bullen test provides insight into required strain level for fracture, but, energy input levels are not quantified. Therefore, an engine strain gage test is planned to map the excitation energy levels present during operation.

Testing will be conducted on a cold engine since strain gage attachment at elevated temperatures for ceramic application has not been

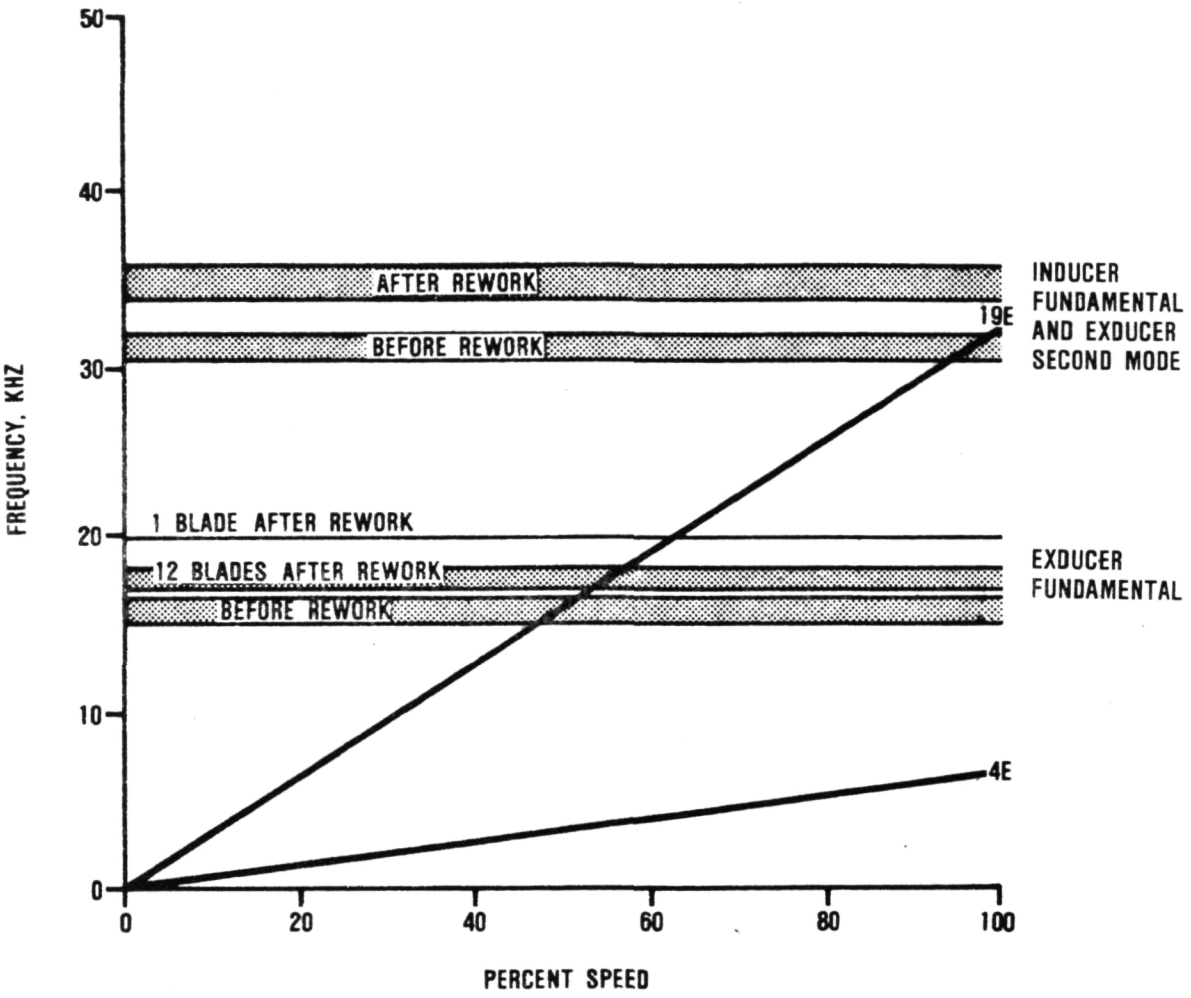

Figure 4. Rotor Interference Diagram.

successfully accomplished. Upon receipt of suitable quality rotors (full blading, no discernable flaws) testing will be initiated.

3.1.3 Dog Bone Quill Shaft

The "dog bone" quill shaft was configured as a possible alternative to the copper plated splined spacer (Reference 9). By minimizing the quill shaft mass, the destabilizing effects of excessive quill shaft spline clearance can be minimized. The configuration, shown in Figure 8 incorporates an oil film bearing and hydraulically mounted ball bearing.

Builds 27 and 28 evaluated the configuration. During test, engine operation was limited to 81,000 rpm by excessive subsynchronous rotor whirl at 104 Hz. Higher speeds were possible by reducing turbine bore cooling, however, this entailed risk to the foil bearing due to thermal failure. Testing did not show improved rotor dynamics.

3.1.4 Miscellaneous Motoring Tests

Builds 29 through 33 tested a variety of different rotor dynamic configurations. Included among these were:

- Locked up quill shaft
- Full land-width hydraulic mount

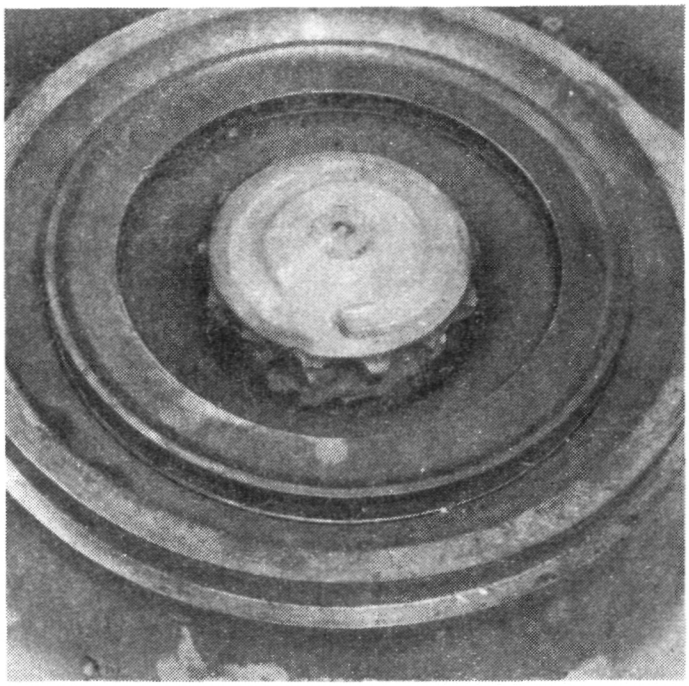

Figure 5. Rotor Blade Damage.

Figure 6. Ceramic Rotor Strain Test - Exducer and Fracture.

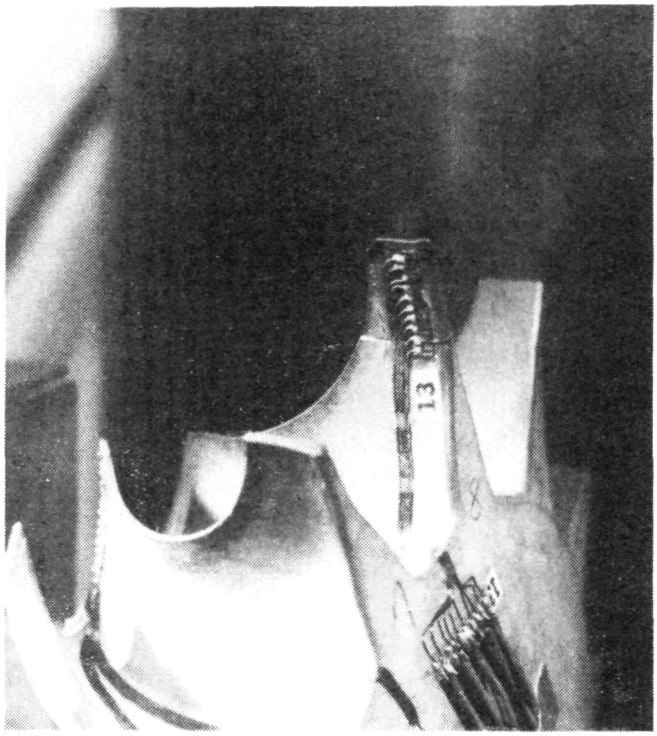

Figure 7. Ceramic Rotor Strain Test - Inducer Instrumentation and Fracture.

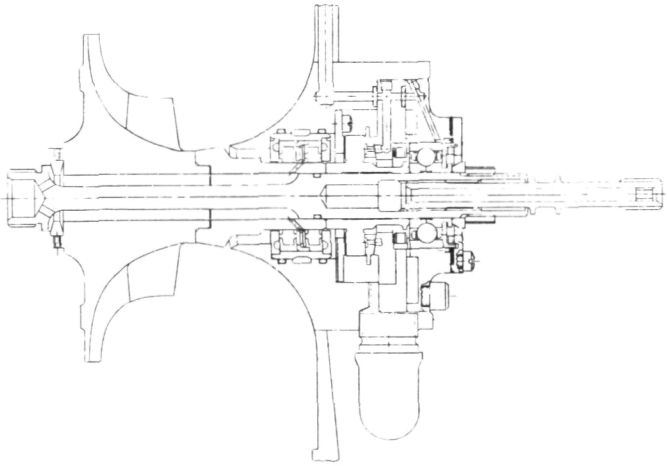

Figure 8. Dog Bone Quill Shaft Configuration.

- o AGT101 baseline configuration without gearbox or quill shaft

- o Without a hydrodynamic thrust bearing

Data from these tests currently are being evaluated and will be reported during the next period.

3.2 Engine S/N 002C

Eight builds of S/N 002C were tested accumulating 125 hours of test time and accomplishing several key milestones, including:

- o 100 hours "continuous" operation at 2100F cruise power conditions

- o Baseline performance at 100,000 rpm and 2100F, demonstrating 43.4 hp

- o Investigative housing distortion testing which influences regenerator drive torque and leakage

- o Accumulation of approximately 150 hours of total test time

The following paragraphs discuss these results.

3.2.1 Build 6

The Build 6 configuration differed from Build 5 by including a thermally isolated foil bearing housing, oil film thrust bearing, and a second set of ceramic structures. Additionally, new insulation was installed.

The engine was preheated to 160F by motoring, followed by a light-off and acceleration to 55,000 rpm. One thermal cycle was successfully completed to 2100F and a second cycle was holding for 3 minutes at 2100F when an increasing 1/revolution synchronous motion was detected on the proximity probes at the turbine end (see Figure 9). The engine was shut down when the maximum allowable 1-mil excursion was reached.

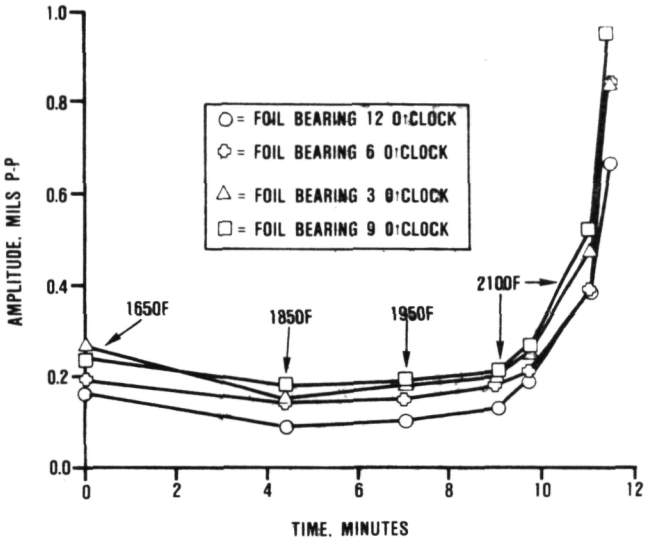

Figure 9. Turbine Shaft Excursions, Wayne-Kerr Probes.

The engine was returned to the assembly area for teardown. Inspection revealed that the dual-alloy turbine wheel was cracked on the backface contour near the material junction as shown in Figure 10.

Additional teardown findings revealed two broken flange segments and a chipped area on the flow separator housing. All flow separator housing crack origins were noted to be at the support point locations of the retaining ring (Figure 11). Probable cause of the distress was the tight fit of the insulation ring surrounding the flow separator housing, forcing the housing against the locating pins.

3.2.2 Build 7

Build 7 was assembled with a second set of ceramic structures from Build 10 of the structures rig (Reference 9). The engine was installed into the test cell, but shortly thereafter was removed to reduce regenerator drive torque following reshimming, the engine was returned to the test facility where it successfully completed 11 cycles to 2100F.

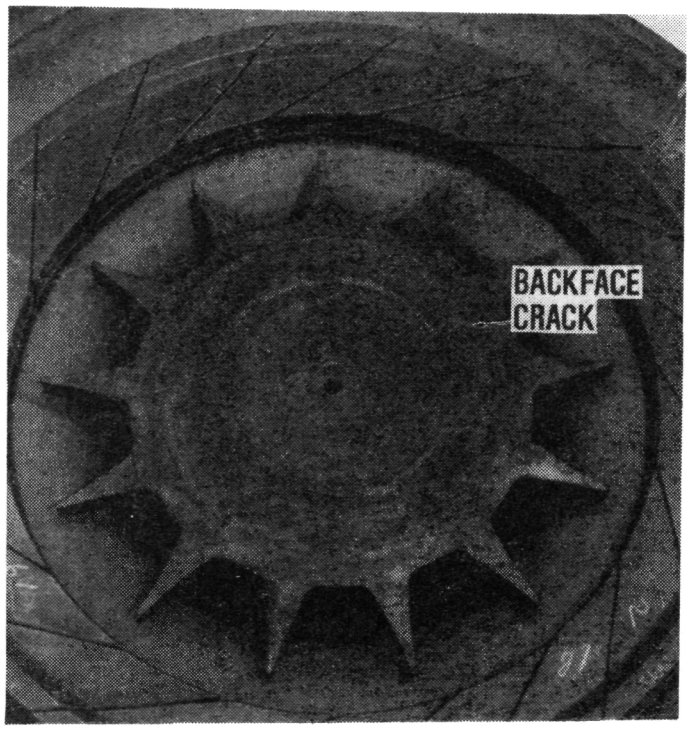

Figure 10. Dual Alloy Turbine Wheel Backface Crack.

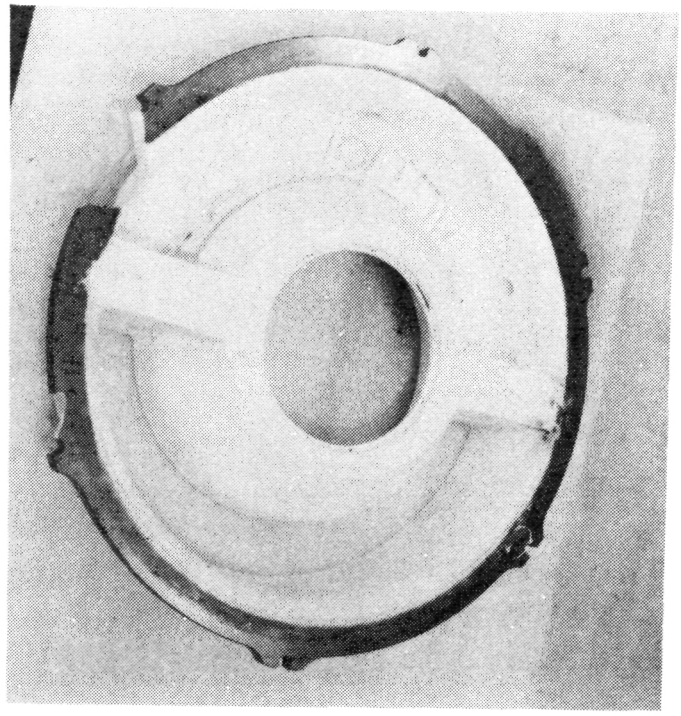

Figure 11. Flow Separator Housing Damage Locations.

Teardown inspection revealed 3 minor chips on the flow separator housing seal ring and a major fracture of the turbine shroud originating at one of the load spacers in a contact stress location and propagating into the stator platform area (Figure 12). As discussed in Section 4.5 herein, the shroud support has been redesigned to alleviate this local stress condition.

3.2.3 Build 8

Build 8 was returned after motoring tests due to high synchronous (1/revolution) at the turbine end. The engine was disassembled and the rotating group was resubmitted for component and group balancing.

3.2.4 Build 9

Along with a rotating group imbalance a flattened wave spring was found in the thrust mount area on Build 8. The wave spring was replaced, components rebalanced and along with a new set of regenerator seals Build 9 was completed.

The rotor dynamics signature was greatly improved, and after corrections were made to the fuel system the engine sustained speed and temperature. Operating at 60,000 rpm with a turbine inlet temperature ($T_{4.1}$) of 2050 ±50F, the engine completed approximately 7 hours of continuous operation. The speed then was increased to 68,000 rpm. Testing proceeded round-the-clock for the next three days without incident until the end of the 79th hour. Shutdown was prompted by a massive oil leak that developed in a high pressure oil supply line to the engine from the remote lube cart (Laboratory supplied).

During the test, engine parameters were recorded on an hourly basis to monitor any

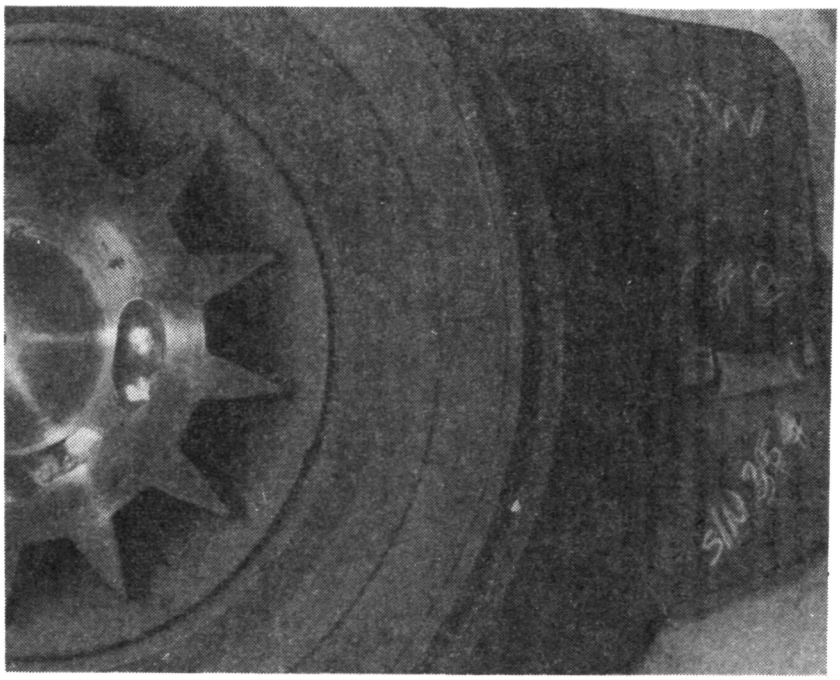

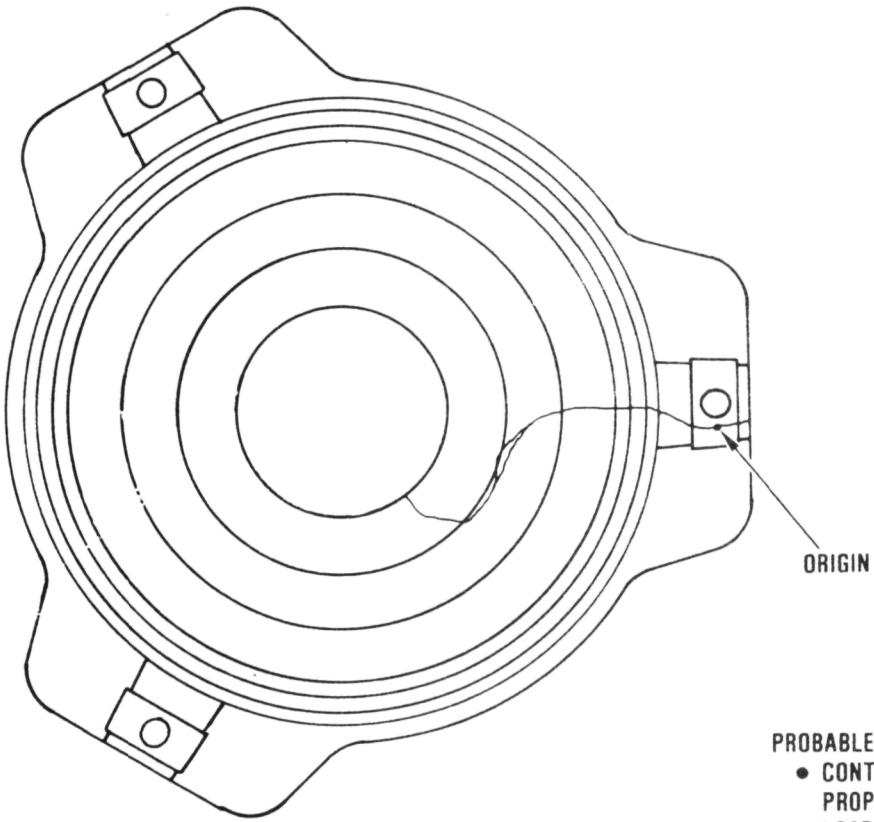

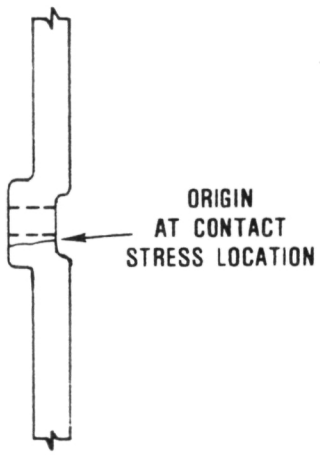

PROBABLE CAUSE

- CONTACT STRESS INITIATED. THERMAL STRESS PROPAGATED. CONTACT STRESS AT SHROUD-LOAD SPACER INTERFACE
- ECCENTRIC NOT IN NULL POSITION MAY HAVE CONTRIBUTED TO LOCAL STRESS

Figure 12. Turbine Shroud Fracture.

deterioration in performance. No measurable performance deterioration was noted throughout the test. A slight increase in performance was indicated and was attributed to a 1- to 2-percent reduction in overall engine leakage. Figure 13 shows a series of plots compiled from raw engine data.

The engine was disassembled prior to completing the remaining 21 hours. Teardown inspection revealed all major ceramic structural components survived without incurring any major distress, Minor chipping was found on the flow separator housing support surface that was judged not to be detrimental to engine performance.

Extensive cracking and delamination of the regenerator seal ceramic coating was noted during disassembly. Figure 14 shows the degree of distress on the hot (inner) seal. A less severe condition was visible on the cold (outer) seal inner periphery.

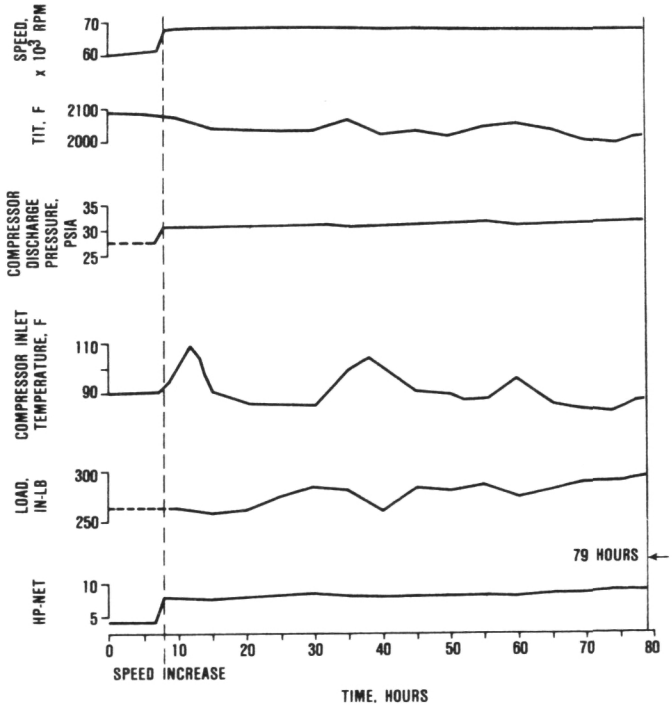

Figure 13. No Performance Deterioration During Test.

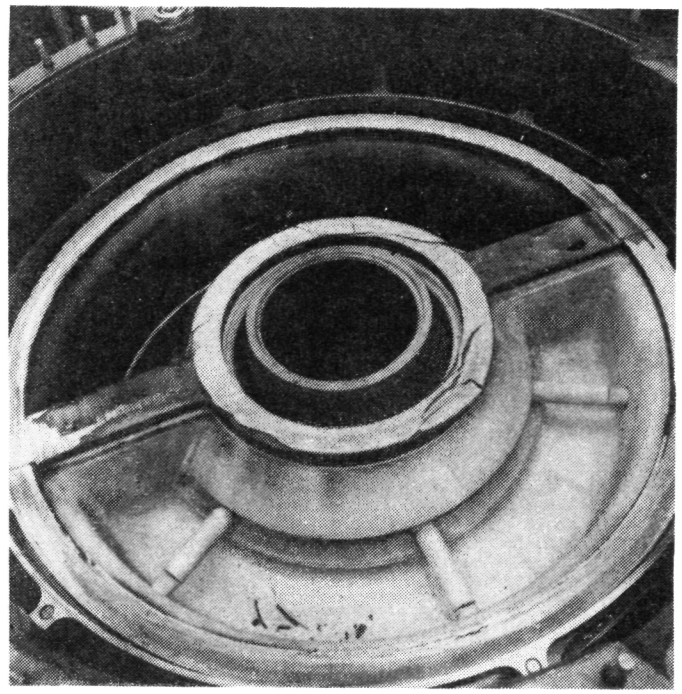

Figure 14. Hot (Inner) Regenerator Seal Distress.

3.2.5 Build 10

The engine was reassembled and run for an additional 21 hours completing an 100-hour endurance test.

Engine parameters again were monitored and logged once per hour. Engine speed, T4.1, compressor discharge pressure, load, and power are plotted during the 100-hour endurance test, and depicted in Figure 15. The performance model was checked at 21.5, 78.5, 80, and 100 hours. The test results are compared in Table 1 and indicate no performance degradation during the 100 hours.

The engine was subsequently torn down and all parts visually (30X) inspected. No cracks were found on any of the ceramic parts. Some minor chipping was noted on three stators and the piston ring seal. Figure 16 documents the excellent condition of the ceramic parts.

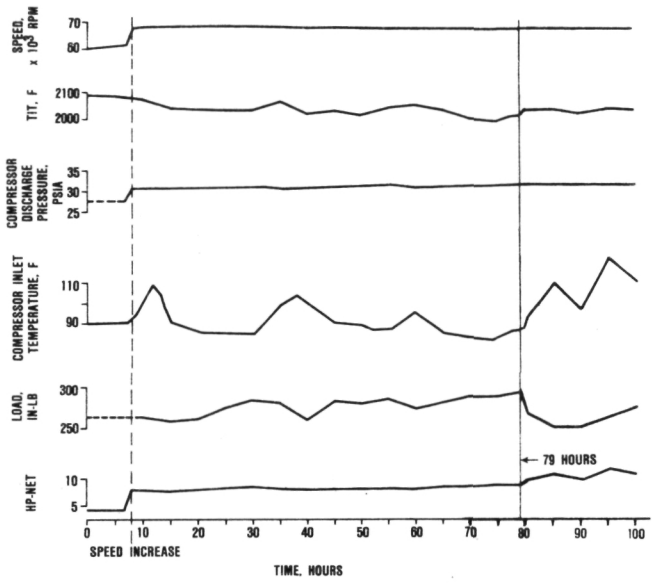

Figure 15. Performance Parameters Tracked During 100-Hour Endurance Test.

Successful completion of the 100-hour endurance test was a major milestone in the AGT program.

3.2.6 Build 11

Build 11 was completed with the ceramic structures set, S/N SR12, which had been tested to 5 transient thermal cycles of 1800F, in 15 seconds (Section 4.5 herein). A similar thermal cycle was defined for the test of this build as shown in Figure 17. The ECU had been modified to accomplish this thermal transient. As programmed, the engine would be ready-to-load after 6 minutes at 1800F, $T_{4.1}$.

Figure 18 shows the analog data chart of this first development start. The required transient programmed into the ECU microprocessors also is superimposed on this chart. A significant difference between the required and actual temperature profile is evident. During the run, the starter remained engaged which may have caused some of the control problem. However, poor performance was indicated by not being able to drop the starter to become self sustaining. Area C of Figure 18 shows the speed droop when the starter power was reduced, indicating that it was still supplying power assist to the engine. The engine was shut down after 4 minutes and 20 seconds at this condition.

The start torque had increased to such a high level that the engine could not be started. The engine was returned to assembly. Teardown revealed oil in the foil bearing, which explained the high start torque. A more significant finding, however, was a fractured flow separator housing. This explains the poor performance noted during the brief test run.

The fracture areas were confined to the flow separator housing crossarms. One crossarm, depicted in Figure 19, shows three major cracks in this view from the turbine side. The cracks are highlighted by the labeled end points, i.e.; cracks extend from points A to B, C to D, and E to F. The probable cause of these fractures is contact between the housing and the recently replaced turbine shroud in the piston ring area. Figure 20 shows a close-up of this area indicating the possible contact point. During the 260 seconds of hot operation the original contact turned to interference, because of expansion differences in the two parts, and overstressed the flow separator housing. A fractography analysis agrees with these observations.

3.2.7 Build 12

Build 12 included a new flow separator housing and rework in the area of previously noted contact (Figure 20) to achieve a minimum 0.050 inch clearance between the flow separator housing and turbine shroud. The test plan emphasized full speed performance at 2100F, $T_{4.1}$.

The engine was motored 8 to 10 times without becoming self-sustaining. Each time the speed was limited below 43,000 rpm, which is estimated as the minimum motoring speed for a successful start.

Table 1. Test/Computer Performance Comparison.

		Test Results				Computer Model			
Hours		21.5	78.5	80	100	21.5	78.5	80	100
T_{CELL}	F	84.14	84.4	76.2	77	84.15	84.41	76.2	77
P_{BAR}	psia	14.08	14.08	13.995	14.0896	14.08	14.08	13.99	14.08
$P_{3.0}$	psia	30.81	31.68	31.142	31.291	29.80	30.60	29.62	29.8
$T_{3.0}$	F	301	306	37	314	309	313	300	301
$T_{3.5}$	F	1530	1640*	1505	1538	1529	1503	1534	1534
$T_{4.1}$	F	2033	2006	2035	2035	2033	2006	2035	2035
$T_{5.1}$	F	1603	1622	1569	1609	1604	1575	16505	1605
$T_{6.0}$	F	456	464	502	512	471	471	461	462
HP_{NET}	HP	7.72	8.60	9.23	10.57**	7.92	8.87	8.58	8.66
N_E	rpm	68455	69718	68720	68810	68455	69718	68720	68810
N_{REG}	rpm	14.4	14.5	18.3	19.0	14.4	14.5	18.3	19.0
IGV	degrees	0.0	0.0	8.0	8.0	0.0	0.0	8.0	8.0
Leakage	Percent W_1	--	--	--	--	25.5	24.5	24.8	
							Same leakage model		

*At approximately 52 hours, $T_{3.5}$ began to increase while no other temperatures showed significant change. Therefore, $T_{3.5}$ reading at 78.5 hours may be incorrect.

**The integrity of this data point questionable (after 94 hours).

On two occasions, the engine was fired and the ECU subjected the static ceramic structures to the thermal cycles shown in Figure 21. Even during these two cycles, the engine did not achieve a higher speed. While making a hot restart a foil bearing failure caused an abrupt shutdown. At the same time, the regenerator core appeared to be stopped due to excessive drive torque. The engine was returned to assembly.

During engine teardown the following findings were made:

- An oily substance was found in the vee-seal and curvic area
- The regenerator core and seals were mechanically sound except for a 6-inch area where some ring gear polymer delamination occurred
- A turbine rub was experienced on the shroud and backshroud resulting in metallic buildup on both ceramic parts as well as some pitting or pullout of ceramic material out of the backshroud surface
- The impeller also may have touched the mating shroud but if so, only very slightly
- The turbine shroud shifted radially and was located 6.5 mils off center

Figure 16. Ceramic Parts After 100 Hours at 2050 ±50F and Cruise Speed.

- One rocker assembly bolt, S/N 019, was broken and part of the head, or one-half the load carrying area, was broken off
- The foil bearing foils and backing springs were damaged severely and required replacement

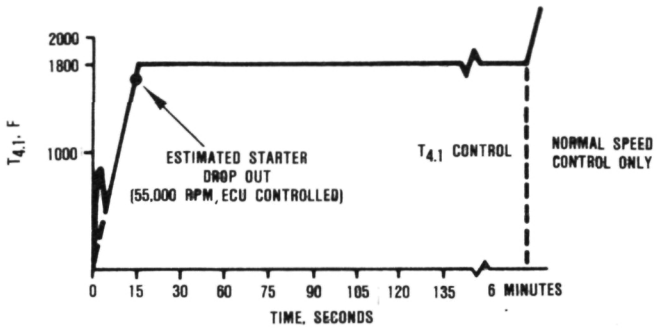

Figure 17. Programmed Temperature Control for Development Starts.

3.2.8 Build 13

Table 2 summarizes the regenerator build configurations for engine Builds 13 through 13H. The configuration for Build 13 remained the same as Build 12, except the regenerator pocket was increased from 0.044 to 0.050 inch. The purpose of these builds was to measure the effect of regenerator seal clearances on performance and to test various seal shoe material to note effects on regenerator drive torque.

Highlights of the Build 13 series tests include:

- Operated at steady-state, full speed, and full load (10 minutes) for the first time
- Established the 2100F baseline performance (43.4 shp)
- Completed seven development start cycles (this brings the total thermal cycles to 14 for most of the ceramic structural parts)

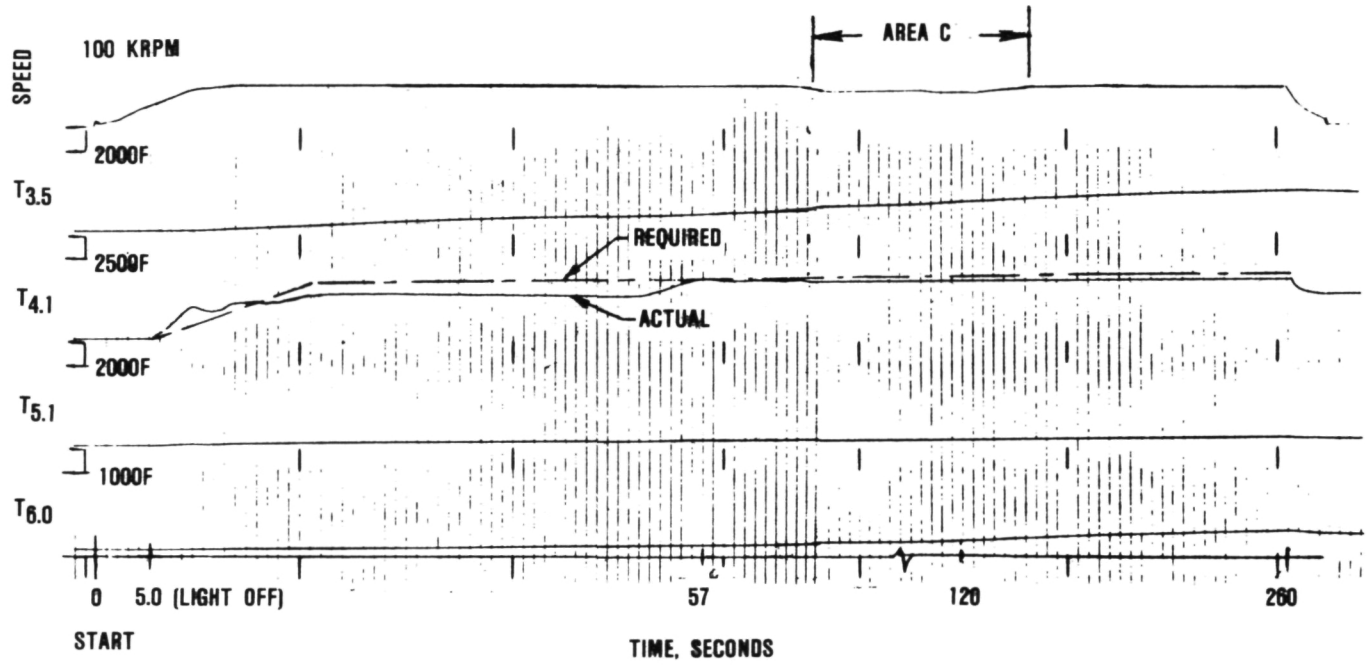

Figure 18. First 2100F Development Start, S/N 002C, Build 11.

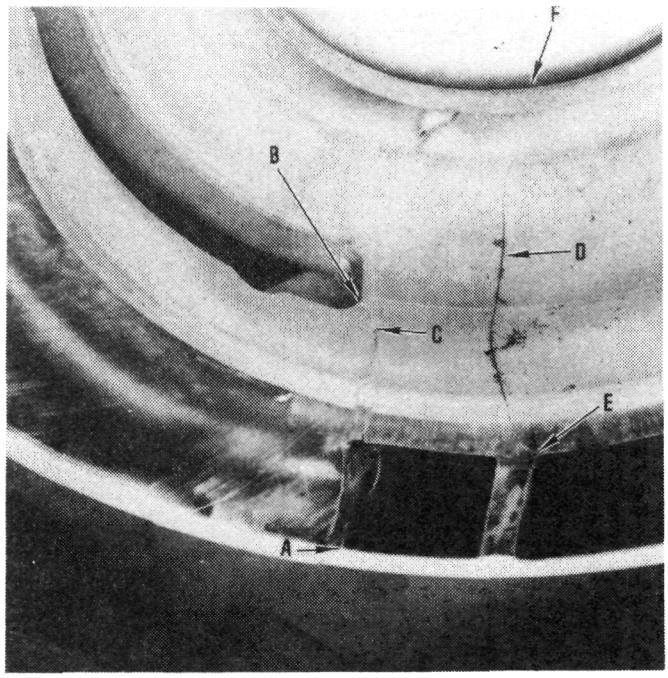

Figure 19. Fractured Flow Separator Housing, S/N 002C, Build 11.

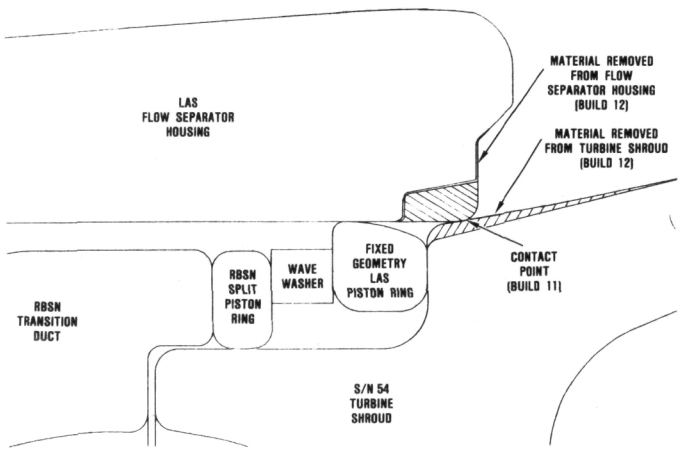

Figure 20. S/N 002C, Flow Separator Housing to Turbine Shroud Fit.

- Ran for 4 hours and 40 minutes, with most of the time spent at 90,000 rpm or higher speeds and over one-half the time at full load (2100F)
- Accumulated 25 starts
- Showed a primary cause-effect relationship between the exhaust housing thermal distortion and the regenerator drive power requirement

The engine was run to full speed and full load. This is the first time a ceramic engine has been tested to these severe temperature and speed conditions.

After the first successful start was made, the self-sustaining $T_{4.1}$ was recorded at 1530F at 59,000 rpm. The engine was accelerated to 86,210 rpm and loaded to 2000F, $T_{4.1}$. The measured torque at the dynamometer was 577 inch-pounds, which equates to 21.3 hp at the dynamometer or 25.2 hp at the engine output gear (bare engine power). During a subsequent run, the regenerator torque slowly increased above the operating limit and the engine was shut down and returned to assembly.

The fixed roller support for the regenerator core seized, which caused the roller to slide along the regenerator ring gear; this explains the excessive drive torque. The roller was replaced and the regenerator pocket increased by another 0.010 inch (to 0.060 inch) to decrease the drive torque.

3.2.8.1 Build 13A

Build 13A was installed in the test cell and operated at 100,000 rpm during the next run. While trying to bring the engine to full load with the newly installed water brake, the $T_{4.1}$ temperature limit of 2100F was exceeded and the engine was shut down by the ECU. While trying to set the full-speed, full-load operating condition a torque equivalent to 28.7 hp bare engine power was noted. During a second run, steady state conditions at 95,000 rpm and 2008F were achieved. The test results and computer model match is presented in Table 3. High engine leakages were of primary concern.

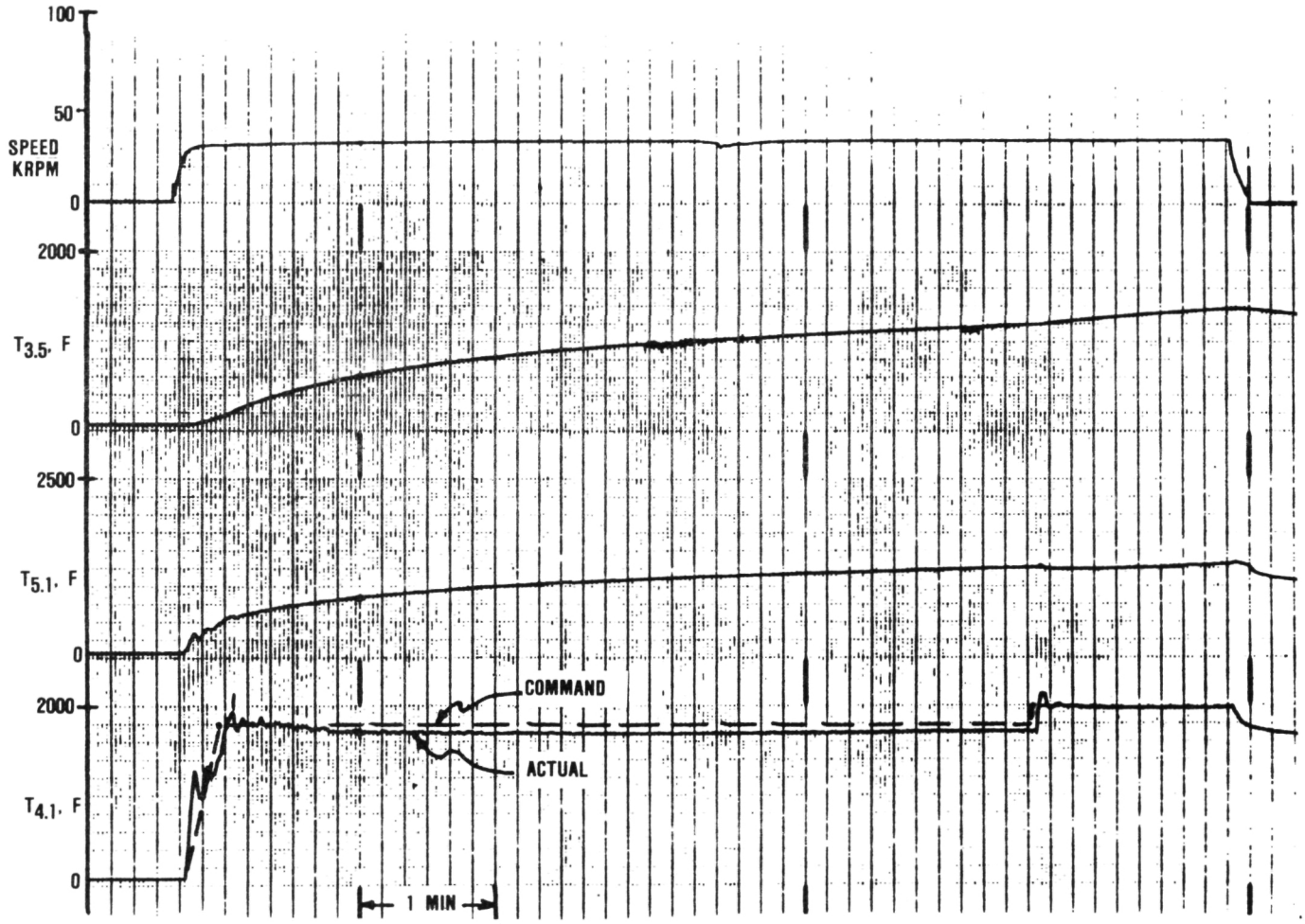

Figure 21. Required and Actual Thermal Transient Results, S/N 002C, Build 12.

3.2.8.2 Build 13B

Build 13B was running at self-sustained conditions and while slowly accelerating to 70,000 rpm the regenerator stopped turning. This was due to increased friction and consequently high drive torque. This drive torque is measured by the hydraulic pressure applied to the drive motor that rotates the regenerator. When this pressure exceeds the relief valve pressure, approximately 1750 psig, the regenerator stops and the exhaust temperature climbs rapidly to its operating limit of 1000F. A cell automatic shutdown system is set to shut off the fuel solenoid at this limit point. After letting the engine cool down for several hours, the drive torque again was measured (without running the engine) and registered as twice that when first installed. The engine was returned to assembly and the regenerator system disassembled. The fixed roller again showed end contact so the assembly was reworked to create a 5 mil axial clearance to the clevis in which it rotates. This rework decreased the drive torque from 190 lb-in (as received from cell) to 140 lb-in. The regenerator seal clearance was increased 5 mils to 0.063 inch (2 mil gasket set during test) and the torque decreased to 85 lb-in.

Table 2. S/N 002C, Regenerator Systems Configurations.

Build	Core S/N and Material*	Hot Seal C-SHOE, X-ARM Coating	Cold Seal C-SHOE, X-ARM Coating	Seal Clearance, inch	Cold-Static Drive Torque Before/After Test, in-lbs
13	FM44-006/AS	HX-037 I-112, I-112	CX035 I-85, I-112	0.050	80/190
13A	Same	Same	Same	0.060	80/180
13B	Same	Same	Same	0.058	80/190
13C	Same	Same	Same	0.063	85/155
13D	Same	HX028* I-85, I-112	CX027 I-85, I-85	0.059	100/175
13E	A-26/MAS	Same	Same	0.059	85/105
13F	A-29/MAS	Same	Same	0.059	90/150
13G(1)	Same	HX034T I-85, I-112	CX037 I-85, I-85	0.061	75/140
13H	FM44-006/AS	Same	Same	0.064	65/-

*AS stands for aluminum-silicate
MAS stands for magnesium-aluminum-silicate

(1)Hot seal was machined with a 0.015 taper (thinner shoe inner versus outer periphery)
Cold seal used an improved parameter I-85 coating

3.2.8.3 Build 13 C

Build 13C was run to full speed and full load. The performance, however, was not as good as the base case, which may have been due to the increased seal clearance. The engine was rebuilt to try to lower the friction by replacing I-112 with I-85 seal shoe coatings. The hot seal outer periphery shoes (C-shoes) coated with I-112 were replaced with I-85 coated shoes. The cold seal inner periphery and crossarm area (x-arm) coated with I-112 was replaced with I-85 coating. These seal changes allowed reduction of the seal clearance by 4 mils to 0.059 inch, based on the breakaway torque in assembly.

3.2.8.4 Build 13D

Build 13D experienced a regenerator stoppage about 17 minutes into the run while at 75,000 rpm engine speed and 1940F, $T_{4.1}$.

Table 3. Comparison of S/N 002C Engine Test With Performance Match Model.

Parameter	Engine Test	Computer Model
Engine Speed, rpm	95,163	95,163
Regenerator Speed, rpm	21.6	21.6
IGV Angle, degrees	0	0
P_{BAR}, psia	14.153	14.153
$T_{1.0}$, F	80	80
$T_{3.0}$, F	407	413
$T_{3.1}$, F	463	449
$T_{3.5}$, F	1387	1342
$T_{4.1}$, F	2000	2000
$T_{5.0}$, F	—	—
$T_{5.1}$, F	1408	1445
$T_{6.0}$, F	602	587
Gross Power, hp	--	32.78
Parasitic Losses, hp	--	11.60
Net Power at Dynamometer, hp	21.13	21.18
Powertrain Losses, hp	--	4.69
Bare Engine Power, hp	--	25.77
Bare Engine Power at SL, 59F, hp	--	31.76
Total Leakage (Percent of compressor inlet flow)	--	22.3

Teardown revealed debris in the seal area downstream of the regenerator. A hairline crack also was found through the piston ring seal, and the transition duct had major cracks. The damage to the latter part is probably due to a misaligned combustor installed against the transition duct. This chipped a small piece from the edge of the duct that served as the origin for crack propogation. The piston ring seal and transition duct were replaced for the next build. In addition, the regenerator was replaced to note the effect of the core material change from aluminum-silicate (AS) to magnesium-aluminum-silicate (MAS).

3.2.8.5 Build 13E

Build 13E made three separate runs totaling 44 minutes. During the first run at high speed (90,000 rpm) while trying to load the engine, the control system could not hold speed. This was apparently due to fuel flow limits. The MAS regenerator core has lower cell density and consequently lower effectiveness, which translates to higher fuel flow requirements. After 5 minutes into the third run a significant number of acoustic signals were recorded from the flow separator housing. The number and energy level of these acoustic emissions (AE) were of concern and the engine was shut down. To isolate the problem the regenerator alone was rotated and the same level of AE signal was recorded. During teardown the only damage found was to the regenerator core; none to the flow separator housing. The core had two cracks extending from the support ring/elastomer to the bore. The debris from the failed core was cleaned out of the engine seal areas and the core replaced with an equivalent design part.

3.2.8.6 Build 13F

Build 13F was tested to full speed and load with intermediate performance points taken at 67; 75; 90; and 95,000 rpm. Five starts were made on this build and the engine run for 2 hours and 25 minutes with all but 15 minutes spent at 2100F and 30 minutes at speeds exceeding 90,000 rpm. The computer performance comparison at cruise and full speed is shown in Table 4. Although the regenerator drive torque was at reasonable levels during the test, afterwards during disassembly, the torque was determined to be unacceptably high. Partial teardown revealed damaged regenerator seals. The I-112 coating on the hot seal inner periphery spalled off after removal from the engine.

3.2.8.7 Build 13G

Both regenerator seals were replaced for Build 13G. The hot seal was machined to have the inner periphery shoe 0.015-inch thinner than the outer periphery shoes. The crossarm areas of the shoes also were cut at a constant taper from the outer to the inner periphery. This seal was configured with the taper to unload the inner periphery. Also, the cold seal was replaced with a seal coated with improved parameter I-85. Improved parameter refers to the plasma spray application method for coating the substrate. Earlier seals were coated with coating parameters that were not optimized for this application of the I-85 coating system.

Build 13G was started two times, both times the regenerator drive torque exceeded operating limits and the engine had to be shut down. The first time the limit was reached 17 minutes into the run with the engine at 94,000 rpm. The second run lasted 12 minutes, with the engine at 75,000 rpm. Teardown revealed some I-85 coating wear on the cold seal inner periphery. One area showed pull-out of the coating and deposition of the material elsewhere. This buildup area scored the regenerator core (one local groove approximately 0.05-inch deep). The cold seal was lapped flat in this area and the regenerator core replaced.

3.2.8.8 Build 13H

For Build 13H, the regenerator core was replaced with an aluminum-silicate (AS) material. In addition, the exhaust cover also was insulated during the test as shown in Figure 22.

Table 4. AGT101, S/N 002C Performance Model.

Parameter	Engine Test	Computer Model	Engine Test	Computer Model
N_e, rpm	100,000	100,000	74,670	74,670
N_{Reg}, rpm	--	23.3	--	17.4
IGV Slew Rate, deg/sec	0.0	0.0	0.0	0.0
T_{Cell}, F	85	85	82	82
P_{Bar}, psia	14.096	14.096	14.104	14.104
$P_{3.0}$, psia	--	56.71	--	34.21
$T_{3.0}$, F	445	466	292	292
$T_{3.1}$, F	502	501	358	365
$T_{3.5}$, F	1383	1404	1528	1543
$T_{4.0}$, F	2139	2139	2108	2108
$T_{5.0}$, F	--	1597	--	1766
$T_{6.0}$, F	620→750	658	470→580	517
Power, HP				
Dynamometer	30.07	30.08	13.21	14.63
Gross		42.88		21.43
Bare Engine	35.07	35.08	16.56	17.98
Bare Engine (Sea Level, Std Day)		43.40		22.09
Leakage, percent				
Overboard	--	1.0	--	1.0
Foil Bearing	--	2.0	--	2.0
Turbine Piston-Ring	--	7.86	--	7.82
Regenerator Seals	--	9.88	--	10.28
Total	--	20.74	--	21.1

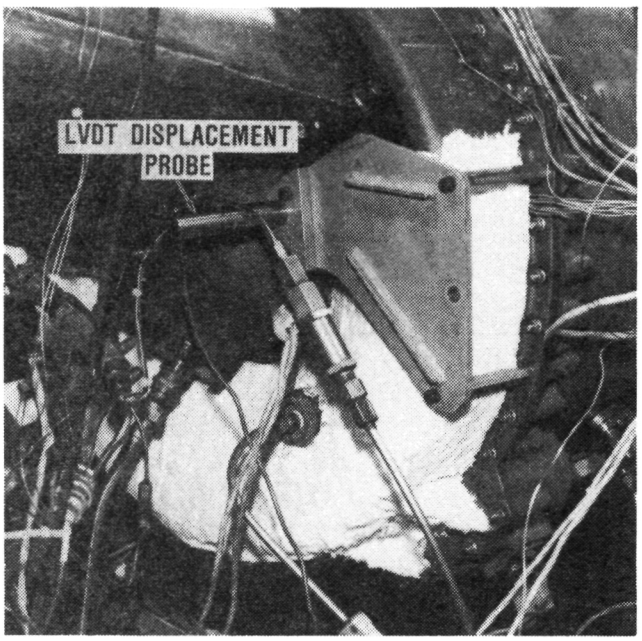

Figure 22. Exhaust Housing With Insulation and Displacement Probe.

Build 13H accumulated 105 minutes running time and 18 starts. The large number of starts was due to ECU executed automatic shutdowns. Soon after lighting off, the fuel was shut off by the ECU with an ECU indication of an over-temperature fault. The ECU was modified to eliminate the 200F band between the commanded temperature ramp (1800F in 15 seconds) and the overtemperature limit. The limit was raised to 2000F, which is the same as the limit for the 6-minute hold at 1800F.

The purpose of Build 13H testing was to see what effect exhaust housing distortion has on regenerator drive torque.

During the first run, the regenerator locked up when the drive pressure exceeded the limit at 90,000 rpm, while trying to load the engine to 2100F, $T_{4.1}$. During the second run, facility air (room temperature) was used to cool the combustor cap and exhaust housing flange area. The circumferential location of this cooling jet was midspan of the low pressure side of the exhaust housing. The exhaust duct curvature then distributed the jet circumferentially around the combustor cap, which aided in more evenly cooling the exhaust housing on the low pressure side. An additional piece of instrumentation was added to measure exhaust housing deflection (see Figure 22). This consisted of one linear variable displacement transformer (LVDT) mounted to a bracket with the spring loaded rod resting against the exhaust housing in the high-to-low pressure crossover area radially near the combustor cap flange.

With the cooling system in place the regenerator did not lock up while running the engine at 70,000 rpm and partial load. However, the drive pressure would change when the cooling jet was moved to different circumferential locations. With the jet in one area, the regenerator drive pressure was close to the operating limit. When the jet was returned to the center position, the drive pressure reverted to the original values. This also was evident from the LVDT, which indicated a maximum displacement of 0.008 inch in a direction to close the seal gap at the inner periphery of the regenerator cold seal.

After this run, insulation was added on all exposed surfaces of the high pressure side of the exhaust housing to increase the metal temperature on this side in an attempt to decrease the temperature differential between the high and low pressure sides of the exhaust housing.

With the insulation in place and the cooling air on steady-state conditions, the engine was run at 90,000 rpm and 2100F, $T_{4.1}$. The engine then was operated at 95,000 rpm and again, steady-state conditions were reached. The cooling jet effect again was demonstrated by circumferentially moving the jet. With the jet near the low-to-high pressure crossover point, the deflection was at a minimum and acceleration to full speed was attempted. During the acceleration (at about 98,000 rpm), a loud sound was heard and the engine coasted to a stop. The ECU displayed an underspeed fault indication. Dynamics of the rolldown

appeared normal, however, the regenerator could not be rotated. The engine was returned to the assembly area where teardown revealed a major fracture in the flow separator housing with secondary damage to the transition duct, baffle, regenerator core and hot seal, turbine shroud bolt, and stators. In addition, slight rubs were found in the foil bearing, and compressor and turbine shrouds. Figures 23 and 24 show the damage found during disassembly. Failure analysis was initiated.

Failure Analysis - Analyses of the test results of the flow separator housing failure were completed. Extensive examination of the flow separator housing fracture surfaces could not isolate the primary origin. Many crack origins were found, including the area where the regenerator shield contacts the flow separator housing. This points to the probable failure mode depicted in Figure 25. The cooling flow impinging on the combustor cap may have cooled an area of the cap used as a pilot. If the pilot diameter (Surface 1) was smaller (than in the normally uncooled condition) due to lower temperature, the heat shield that slides inside this pilot seizes. Once the heat shield locks up in the combustor cap a rigid load path is created through the structures between the heat shield, regenerator shield, and flow separator housing. If these parts continue to expand (even a few mils due to increased speed and/or temperature), the flow separator housing support land would be overstressed. Figure 26 shows the thermal difference between the cap and shield that could cause the thermal lockup as a function of the clearance between the parts (from blueprint minimum to maximum clearances). With nominal clearance, a thermal differential of 510F would cause lockup. Based on cap temperatures, there is a high probability that this temperature differential (ΔT) was achievable during engine operation with the unusual applied cooling flow.

To ascertain the effect of exhaust housing distortion on regenerator lockup, seven operating conditions were examined. Table 5

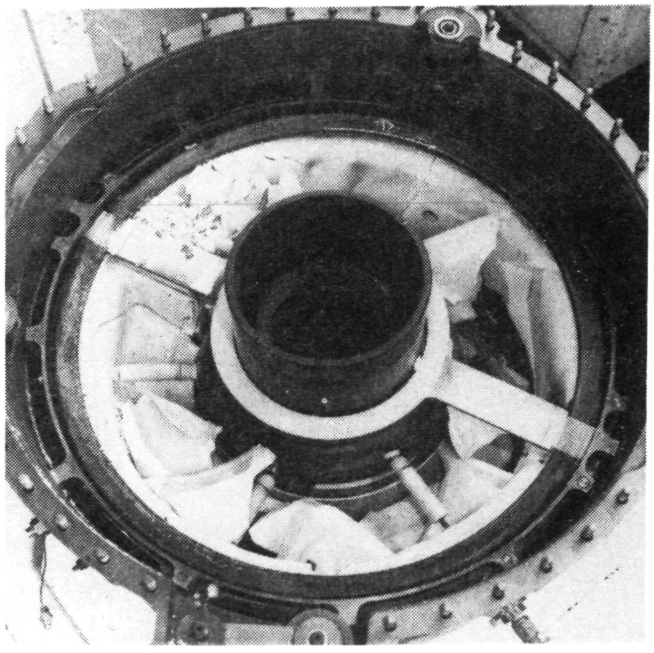

Figure 23. S/N 002C, Build 13H Regenerator Core Removed.

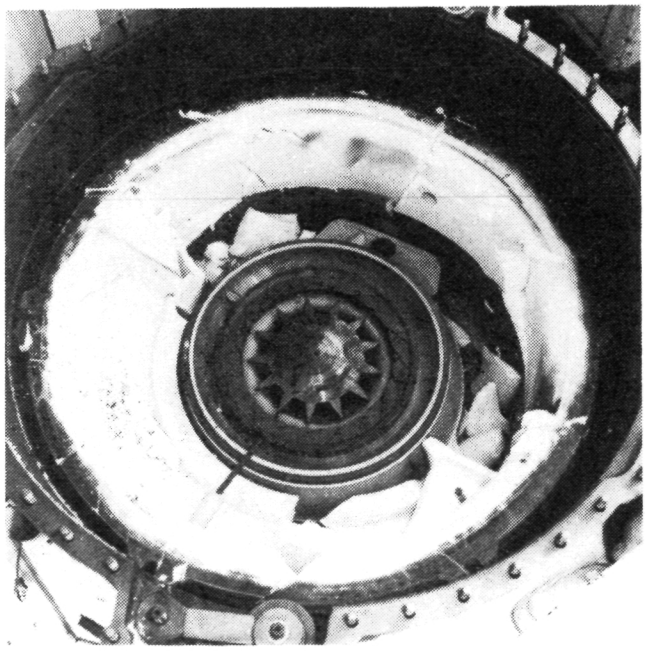

Figure 24. S/N 002C, Build 13H Teardown Showing Rotor.

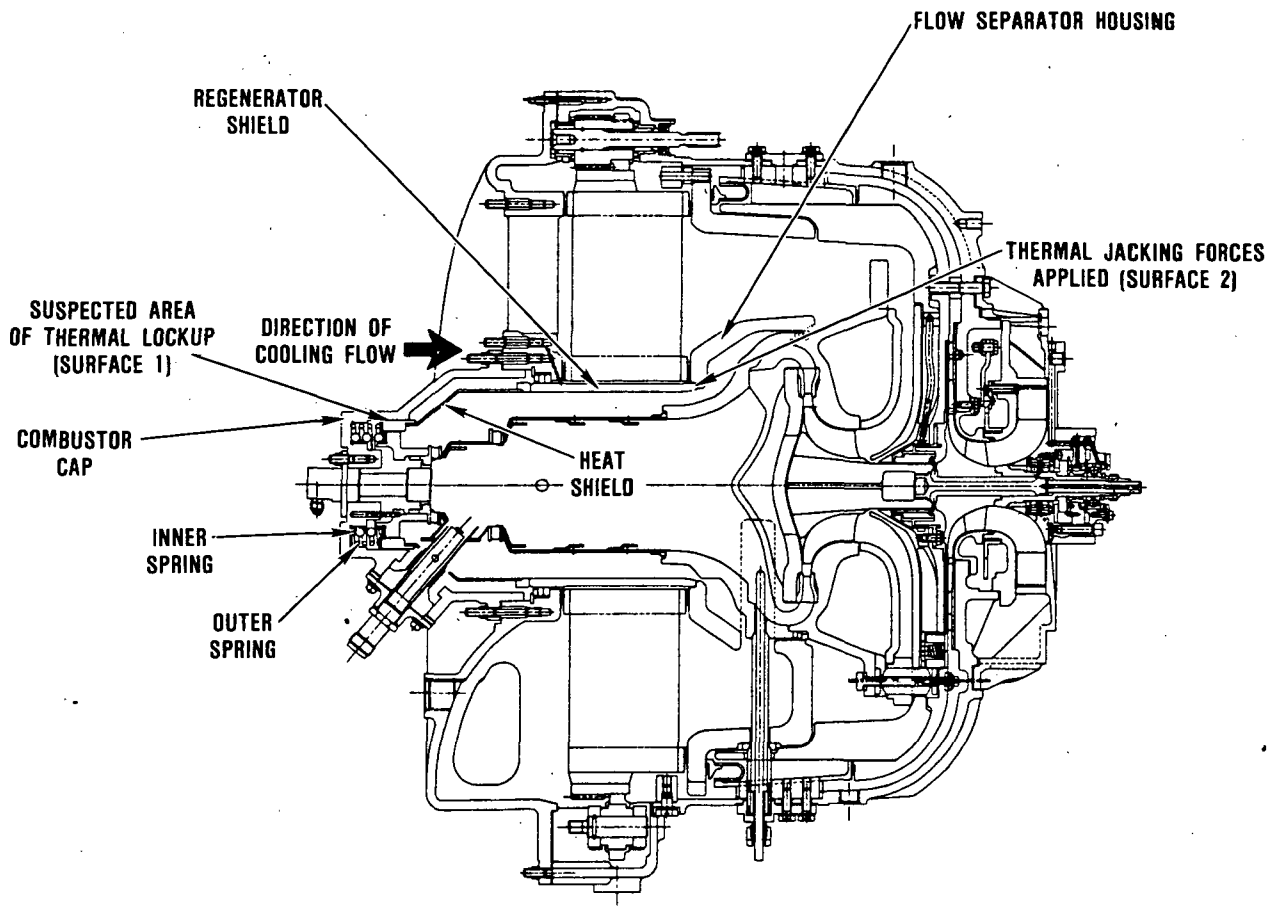

Figure 25. S/N 002C Flow Separator Housing Failure Mode.

summarizes these cases. The temperature distribution and deflection data of the exhaust housing were investigated for each case. However, because deflection was measured at only one point, correlation of thermal distortion to regenerator drive pressure is nearly impossible. When the deflection is low at one measured point, it may be high at another point not being measured, where core lockup could be occurring. The exhaust housing temperature distribution just before core lock up (Case 1) is shown in Figure 27. Figure 28 shows the relationship between regenerator drive pressure and combustor inlet temperature (T3.5), which is the temperature reading closest to the regenerator support structure. This data clearly shows the problem to be thermally induced.

However, this was not considered to be conclusive. Therefore, in future tests the number and circumferential distribution of thermocouples and deflection indicators will be increased. Based on observations while operating the engine, thermal distortion is a primary cause of regenerator lockup. Garrett concluded that because of no cooling air or insulation, the engine could not be loaded at 90,000 rpm without locking up the regenerator. Conversely, with cooling air and insulation there was no problem running steady state with full load at 95,000 rpm.

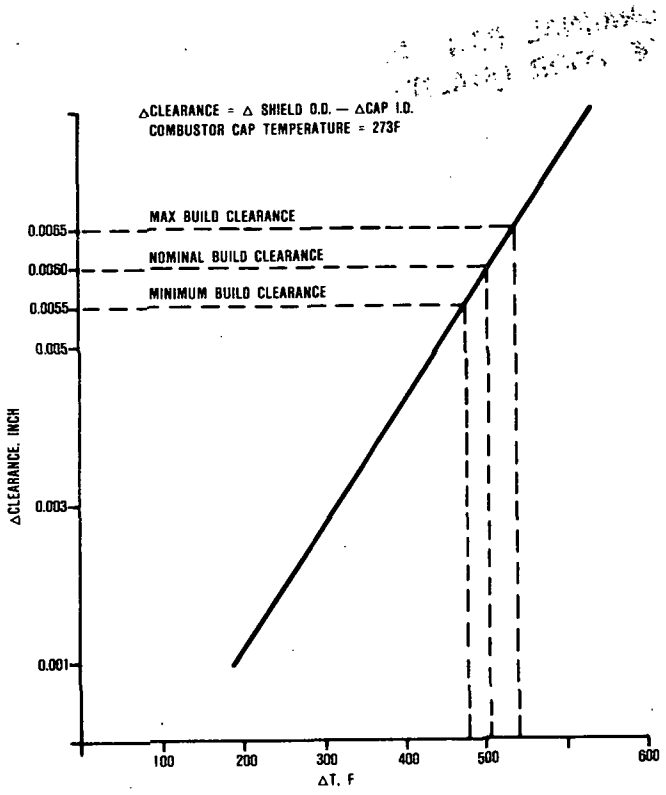

Figure 26. Heat Shield to Combustor Cap Clearance-Versus-ΔT.

3.3 Engine S/N 003

The rotor dynamic tests reported in the previous report were completed during this reporting period. In addition, the contract milestone, Metal Engine Characterization was also successfully completed.

3.3.1 Build 46

Build 46 of this engine was tested four times to evaluate the effects of a longer axial foil bearing on engine rotor dynamics. These test results are summarized below and on Table 6.

3.3.1.1 Build 46H

This engine was assembled in the same configuration as Build 46G with the exception that a new quill shaft/spline spacer set and a new ball bearing was used replacing those parts damaged from the previous build. This engine was tested to determine hot engine

Table 5. Exhaust Housing Data Reduction Cases.

Case	Build	Test Date	Engine Speed, rpm	With Cooling Air	With HP Insulation	Comment
1	G	04/17/85	67,000	No	No	Reading before regenerator lockup
2	H	04/29/85	60,000	No	No	No regenerator lockup
3	H	04/29/85	89,000	No	No	Reading before regenerator lockup
4	H	04/30/85	90,000	Yes	No	Reading before regenerator lockup
5	H	05/01/85	90.000	Yes	Yes	No regenerator lockup
6	H	05/01/85	94,000	Yes	Yes	Reading before flow separator housing failure
7	H	04/30/85	72,000	Yes	No	No regenerator lockup

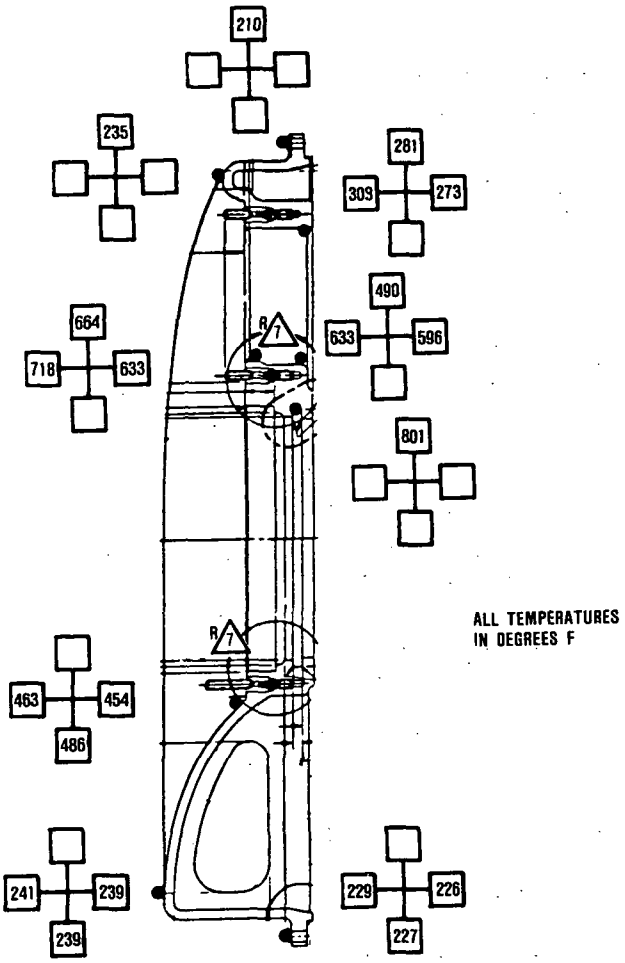

Figure 27. Case 1 - Exhaust Housing Temperatures.

rotor dynamics in test cell C-102. The maximum speed attained was 89,400 rpm and was limited by excessive subsynchronous turbine motion of 1.1 mils at 150 Hz. This same engine build was motored for a cold test comparison. Again, the maximum speed (75,000 rpm) was limited by excessive subsynchronous motion.

3.3.1.2 Build 46J

The quill shaft/splined spacer set was changed to one with copper-plated splined spacer. This spacer was plated producing a

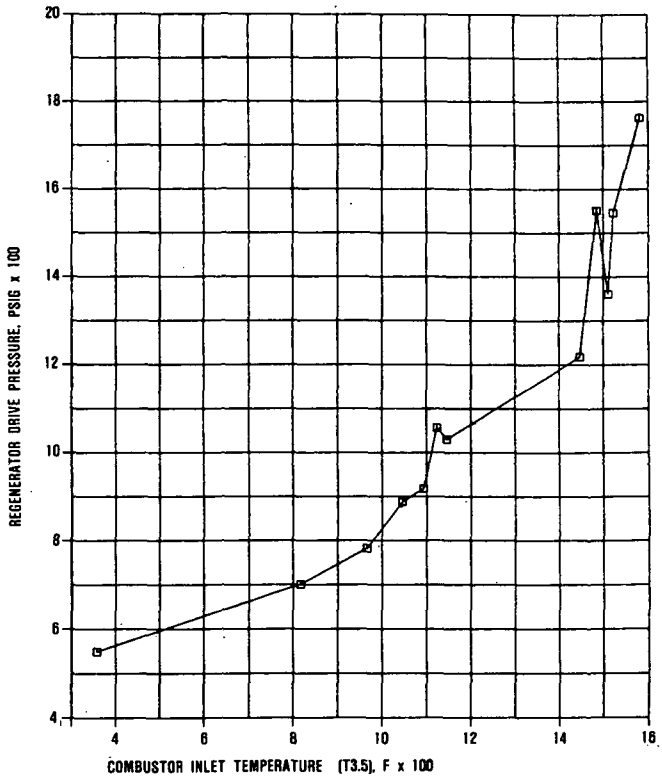

Figure 28. Regenerator Drive Pressure Relationship to Combustor Inlet Temperature (T3.5).

0.0018-inch interference fit with the quill shaft. This engine then was cold motored to 98,000 rpm with a 0.6 mil synchronous and 0.5 mil subsynchronous motion. A hot test then was conducted in test cell C-102. The maximum speed during this test was 90,000 rpm limited by 1.12 mils subsynchronous motion at 140 Hz. Teardown revealed that the copper plating had worn to the point where the spline spacer/quill shaft fit was loose. These two series of tests indicate that the longer axial foil does not provide sufficient damping to solve the subsynchronous motion.

3.3.2 Build 47

After completing the motoring test, this engine was assigned to run the characterization test. This test was to map the performance of the metal engine at 1600F between

Table 6. S/N 003 Motoring Test Summary - July 1984

Test Date	Build	Compressor	Turbine	Foil Bearing	Speed, krpm	Turbine Motion		Quill Motion		Comments
						Frequency, Hz	Amplitude, Mils	Frequency, Hz	Amplitude Mils	
7/2	46H	Ti	Astroloy	Long Axial 6:1-No Hole	89.4	1490 150	0.9 1.1			New quill set; New ball bearing; Hot operation Hot operation C-102
7/3	46H	Ti	Astroloy	Same	75	1255	0.9 1.6	1255	0.9	New ball bearing; new quill shaft
7/12	46J	Ti	Astroloy	Same	98	1635	0.6	1635 150	0.5 0.5	Plated spline spacer
7/13	46J	Ti	Astroloy	Same	90	1505 140	0.63 1.12	1505	1.02	Plated spacer; hot test C-102

idle and full speed, and various inlet guide vane (IGV) positions.

The Phase III regenerator seals were replaced with Phase V seals.

After performance testing, sources of high leakage were investigated. Figure 29 shows the seal areas tested. The foil bearing was flow checked in a separate fixture. The resulting leakage flow amounted to over 6 percent. This high flow is thought to be due to the new support structure and bearing design which were previously introduced for thermal isolation and rotor dynamics. The piston ring leakage also was found to be high at 4.5 percent.

The regenerator seals were tested in the hot regenerator rig and exhibited a leakage flow of about 7 percent. The "C" seal, on the other hand, showed "zero" leakage. The various flows are plotted versus upstream pressure and speed in Figure 30. The total engine flow also has been plotted. Efforts to reduce the leakage in two areas were successful. By adding a baffle upstream of the foil bearing, the leakage was decreased by over 3 percent (see dashed line in Figure 30). The baffle is a thin sheet-metal shim with a tight clearance to the shaft (0.005-inch radial).

The piston rings also were modified with a sheet-metal insert. The split line of each of the three rings creates leakage areas as shown (shaded) in Figure 31. A Hastelloy X insert was installed into the ring to cover the split line gap. With this insert installed, the leakage decreased to 1.5 percent.

3.3.4 Build 48

Build 48 of this engine was reassembled with the modifications discussed in the previous paragraph. Testing proceeded with the same test plan as the previous build.

Successful testing of engine S/N 003, Build 48B, during this reporting period, completed the Metal Engine Characterization Test. Mapping the engine performance at 1600F,

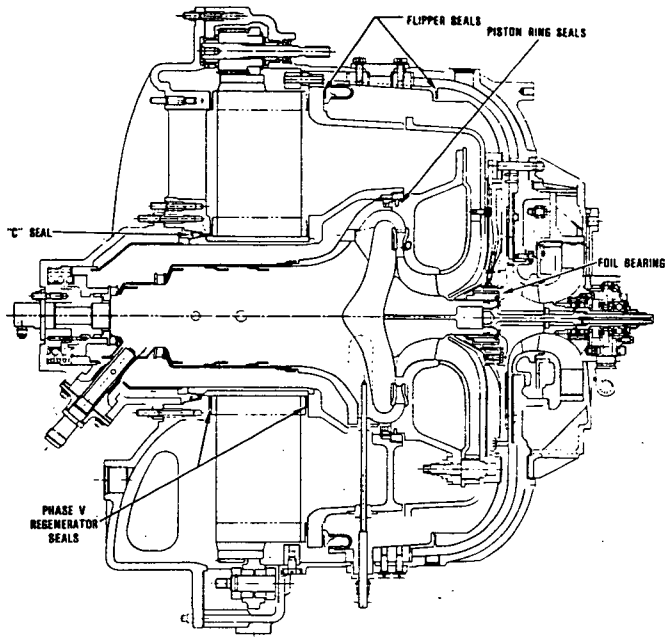

Figure 29. Seal Leakage Areas Individually Tested.

$T_{4.1}$, fulfills this contract milestone. During the test, the engine accumulated 5.6 hours and 4 starts (total of all builds: 100.2 hours and 272 starts).

Build 48B was configured with the latest regenerator seals available (Phase V-A). The leakage flows of the Phase V-A regenerator seals showed improvement over Phase V seals. At pressure equivalent to 80,000 rpm, the component leakages are tabulated as a percentage of total engine flow in Table 7. The total leakage was estimated at 12 percent based on this data.

Performance data was measured at 70,000, 80,000, 90,000 and 95,000 rpm and at 0, 20, 40 and 60 degree IGV positions at 80,000 rpm.

The drag torque applied by the hydraulic load motor was measured at each operating condition. The resulting net power output is plotted as a function of engine speed in Figure 32 and as a function of IGV position in Figure 33.

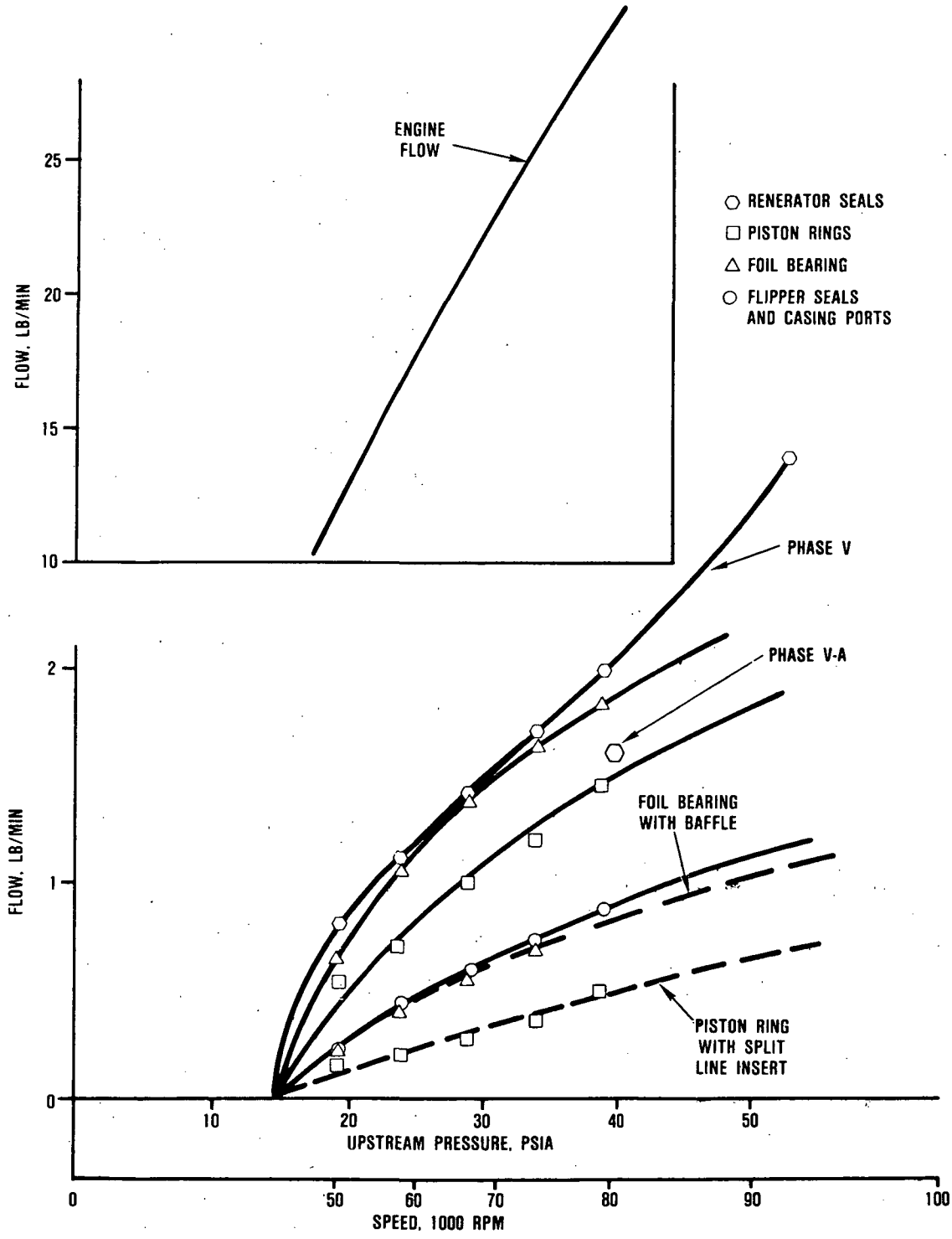

Figure 30. Metal Engine Flow Distribution.

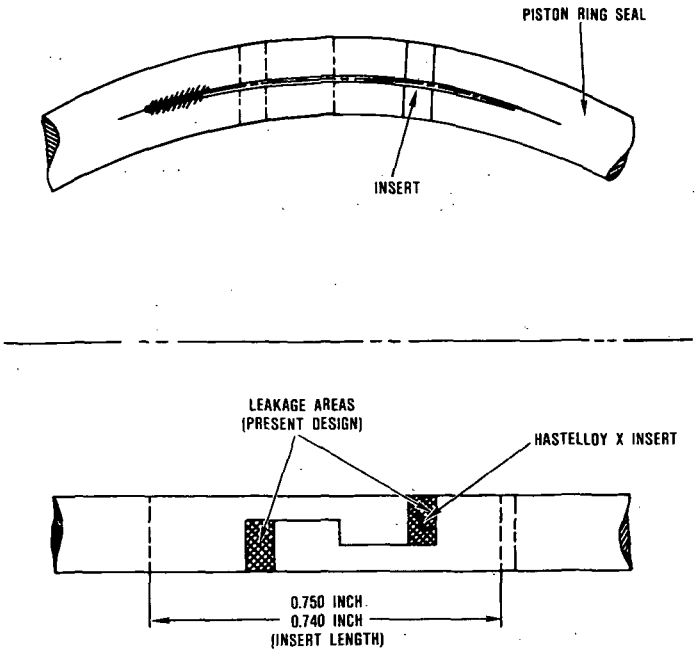

Figure 31. Piston Ring Seal Showing Added Inserts at Splitline.

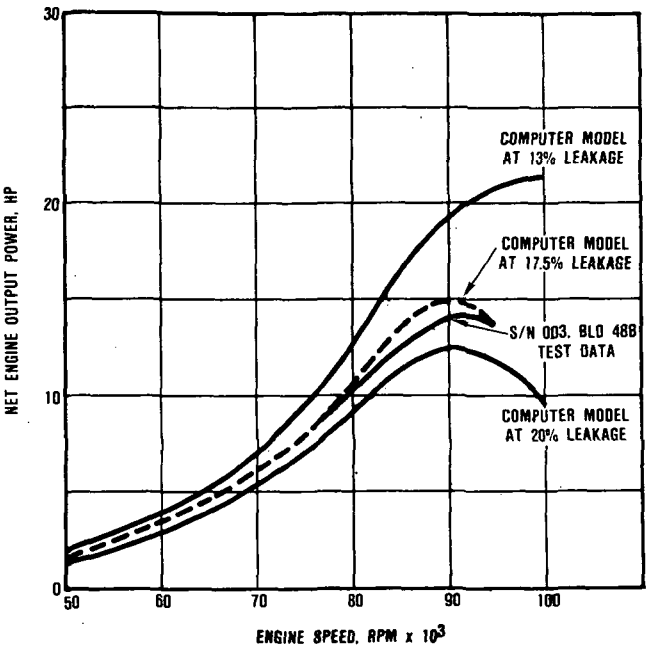

Figure 32. Engine Performance as a Function of Speed (1600F).

Table 7. Component Leakage

(All data for 80,000 rpm pressures)		
Component	*Cold Static* Test Data, Percent*	*Computer Model* Percent Total Flow
Piston Rings	1.8	4.5
Foil Bearing	2.8	1.65
Flipper Seals and Overboard	3.1	0.53
Regenerator System	4.3	11.5
Total	12	18.18 = 17.5*

*Percent of total engine flow

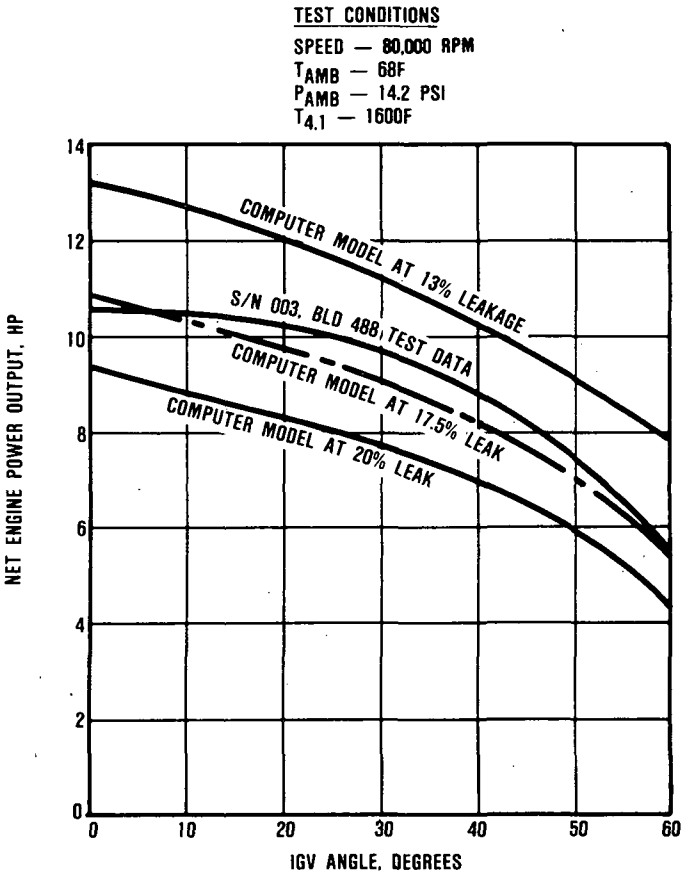

Figure 33. Engine Performance as a Function of IGV Position (1600F).

The engine was tested and accumulated 2.6 hours and 13 starts. Performance was measured at 90,000 and 93,500 rpm, and the engine was accelerated to full speed.

Performance testing was initiated and the engine was tested to steady state conditions at 90,000 rpm with the IGVs (inlet guide vanes) set at 0 degrees. This is Point 17 of the data points that were to be run (see Table 8). The IGVs then were closed down to 20 and 40 degrees (points 18 and 19, respectively) and the engine allowed to come to steady state conditions at each position. Next, the speed was increased to 95,000 rpm. However, two events required a decrease in speed; the high forced vibration, and more importantly, the

Table 8. Test Points

Point	Speed* (rpm)	IGV Position (Degrees)
1	50,000	0
2	50,000	20
3	50,000	40
4	50,000	70
5	60,000	0
6	60,000	20
7	60,000	40
8	60,000	70
9	70,000	0
10	70,000	20
11	70,000	40
12	70,000	70
13	80,000	0
14	80,000	20
15	80,000	40
16	80,000	70
17	90,000	0
18	90,000	20
19	90,000	40
20	95,000	0
21	95,000	20
22	100,000	0
23	100,000	20

* ±200 rpm

** ±2 degrees

$T_{4.1}$ was significantly increasing with increasing speed. This indicates that peak power had been reached between 93,000 and 94,000 rpm. Therefore, the last point run was 93,500 rpm, 0-degree IGVs, and 1600F $T_{4.1}$ (designated Point 20 on Table 8).

Figure 34 shows the computer model flow chart with the component efficiencies and cycle conditions, as well as heat losses and leakages. Table 9 compares these results with the values measured during the test for data point 17.

The following observations were made from this data:

- o Excellent correlation can be achieved between the computer model and engine test data
- o The apparent leakage is higher than predicted. Sources of high leakage should be investigated and repaired
- o Additional pressure data would be required to get better leakage correlation

The latest parasitic loss curve is shown in Figure 35. which represents the total power loss from the aerodynamic power output of the engine to the dynamometer. This value is added to the dynamometer to match the computer performance model calculated output power. Figure 36 represents the power loss between the engine output shaft gear (to which the quill shaft gearbox is attached) and the dynamometer.

A significant point becomes apparent when comparing the hot operating leakage at 80,000

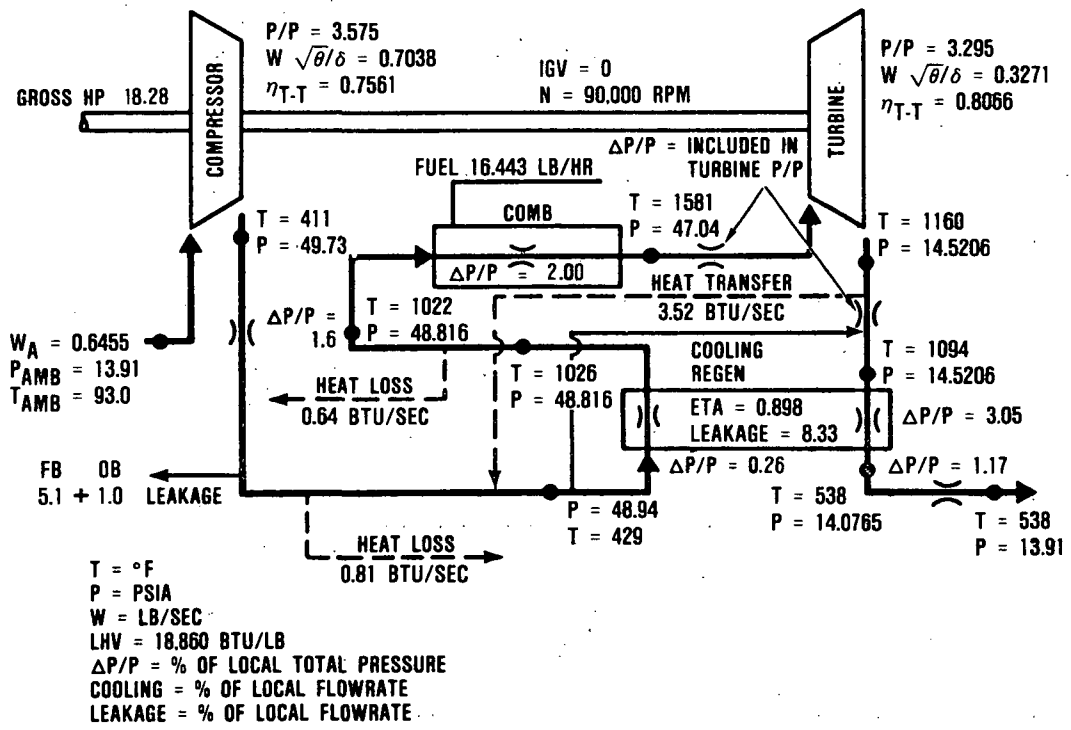

Figure 34. Performance Model Results.

Table 9. S/N 003 Motoring Test Summary - July 1984

Test Date	Build	Compressor	Turbine	Foil Bearing	Speed, krpm	Turbine Motion		Quill Motion		Comments
						Frequency, Hz	Amplitude, Mils	Frequency, Hz	Amplitude Mils	
7/2	46H	Ti	Astroloy	Long Axial 6.1-No Hole	89.4	1490 150	0.9 1.1			New quill set; New ball bearing; Hot operation Hot operation C-102
7/3	46H	Ti	Astroloy	Same	75	1255	0.9 1.6	1255	0.9	New ball bearing; new quill shaft
7/12	46J	Ti	Astroloy	Same	98	1635	0.6	1635 150	0.5 0.5	Plated spline spacer
7/13	46J	Ti	Astroloy	Same	90	1505 140	0.63 1.12	1505	1.02	Plated spacer; hot test C-102

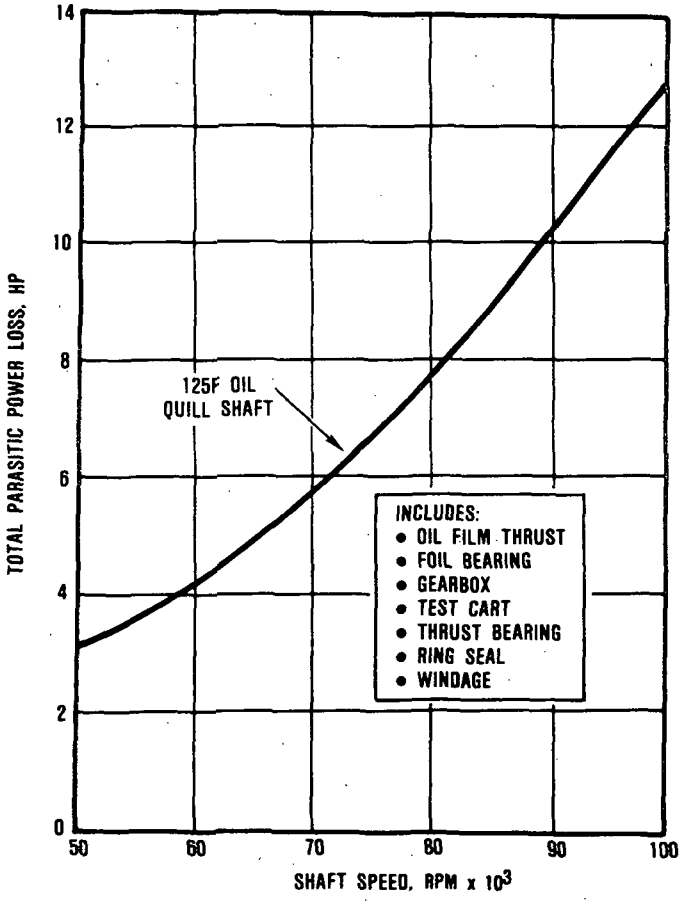

Figure 35. Total Parasitic Power Loss (Aero to Dynamometer).

rpm to the pre-test cold static leakage. The computer model data also is listed in Table 7 for comparison. The hot leakage is significantly higher than the cold static leakage. From this, GTEC concluded that the thermal and/or pressure distortion of the housings with sealing surfaces causes increased leakage. The AGT101 design consists of ceramic housings which analytically show much less distortion; therefore, this is presumed not to be a problem unique to the ceramic engine. For this reason, the characterization test of the 1600F metal engine is considered a complete success.

A meeting was held with NASA/DOE/ Sandia principals on the January 24, 1985 to review this test as it relates to the Solar Advanced Gas Turbine (SAGT-1A) program (Contract DEN3-181). The decision to transfer any further testing of S/N 003 engine to the SAGT-1A program/contract was approved.

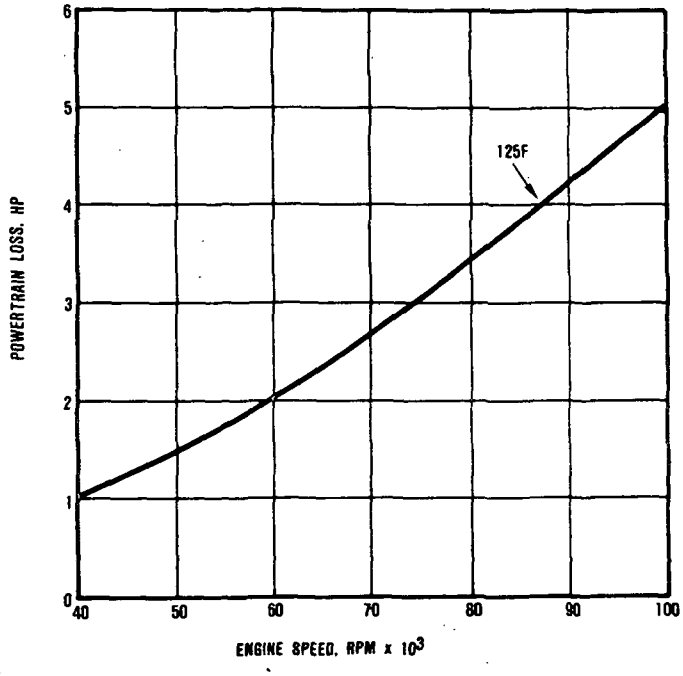

Figure 36. Powertrain Parasitic Loss (Engine Gear to Dynamometer).

3.4 Engine S/N 004C

This engine was assembled in the 2100F configuration, it incorporated ceramic structures Set 3 which were qualified to normal start conditions, a zirconia-coated combustor, and a dual-alloy turbine rotor. Basically, this engine was similar to engine S/N 002C with a few exceptions. The regenerator support structure was the same as that used on engine S/N 001 engine which was designed to be more thermally stable than the original AGT101 structure, and sealing around the engine station thermocouple ports was improved.

Objectives of the first test on this engine are listed below:

- o Characterize the engine performance over the engine speed range with turbine inlet

temperatures at 2100F and zero degree VIGV angle.

- Perform several development starts.

- Inject Fullers Earth into the engine during the final engine shutdown of the test to determine leakage paths.

During the first start of this engine, the rotor went unstable and the foil bearing failed. The damage was limited to the foil bearing and one stator segment. The cause of the problem was traced to contamination of the hydraulic mount by an unidentified foreign substance which somehow entered the oil supply lines during engine installation on the test cart.

The engine was rebuilt with a new foil bearing and stator segment. To preclude a recurrence of the contamination problem, all test cart lines were carefully flushed before engine installation and additional oil filters were installed at each oil inlet fitting to the engine. The retest is scheduled for July 1985.

4.0 COMPONENT/SUBSYSTEM DEVELOPMENT

Component/subsystem development activities during this reporting period were concentrated on supporting AGT101 2100F engine testing, ceramic component development at 2100 and 2500F, combustion nozzle tests, and hot regenerator testing. Figure 37 shows the performance rating stations for the AGT101 engine and components.

The following sections discuss major efforts and accomplishments during the reporting period for each component subsystem.

4.1 Compressor Development

No activity during this reporting period.

4.2 Turbine Development

No activity during this reporting period.

4.3 Combustion

Activities encompassed additional fuel nozzle evaluation of the Delavan Simplex systems and an in-house designed fuel nozzle. Effort on this torch ignitor continued with demonstration ignition testing of the main combustor using the torch. Initial testing of the in-house nozzle show very promising results and indicate no need for the torch system.

4.3.1 Torch Ignitor

Feasibility testing of the torch ignition system (Figure 38) was demonstrated (Reference 9) and showed satisfactory results. Continued evaluation of this torch system was conducted with two different swirler geometries, 30 and 45 degrees. Figure 39 shows the lean stability characteristic of the T/3 torch configuration as a function of air assist pressure. Torch combustion performance generally was better for the 45-degree swirler geometry as represented by a wider stability envelope. However, lean stability was not as good as the 30-degree swirler.

Minor modifications were incorporated in the T/3 configuration to introduce air assist directly to the fuel supply line (in addition to that applied to the air assist plenum) as shown in Figure 40 and replacing the flush electrode with a protruding type. With this configuration, a minimum ignition fuel flow of 1.6 lb/hr was obtained at 15-percent speed. Numerous lightoffs were obtained with delay times of 1-3 seconds.

During atmospheric testing, a new configuration was investigated in which the torch ignitor was replaced by an ignitor located within the simplex envelope at the centerline (Figure 41). This configuration demonstrated lightoffs that were generally cleaner than the T/3 configuration. At 15-percent speed and air assist of 5 psid, lightoffs were obtained with flows of 2 and 4.2 lb/hr at times of 6 and 3 seconds, respectively.

Based on this data, both T/3 and T/4 torch configurations are considered satisfactory for continued evaluation with the simplex nozzle.

4.3.2 Combustion System Design Improvements

Conceptual schematics to upgrade the present ceramic combustion system configuration have been prepared. An objective is to relocate the ceramic pre-load springs to a region that is more effectively isolated from the high temperature burner inlet environment, and also to improve the combustor head and ceramic components. Figure 42 shows a layout under review in which the existing ceramic pre-load springs and some of the pre-load components are utilized. Also, incorporated into this design is a modular main fuel nozzle design arrangement that incorporates an axial ignitor, which exhibited acceptable ignitor performance in development tests.

Figure 43 is a conceptual view of development hardware for the modularized fuel nozzle/ignitor assembly. The air assisted fuel jet injection system of the standard fuel nozzle is retained, but in this case, injection is in a radially outward direction. The fuel and air assist tubing is routed to the fuel nozzle head

1.0 AMBIENT
2.0 COMPRESSOR INLET (IGV)
2.05 IMPELLER INLET
2.5 DIFFUSER INLET
3.0 DIFFUSER DISCHARGE
3.05 DUCT COMMON INSTRUMENTATION PLANE (RIGS)
3.1 REGENERATOR HP INLET
3.5 REGENERATOR HP EXIT
3.6 COMBUSTOR INLET
4.0 COMBUSTOR EXIT, TURBINE INLET
4.1 STATOR INLET
4.5 STATOR DISCHARGE
5.0 TURBINE ROTOR EXIT
5.05 DIFFUSER EXIT (RIGS)
5.07 DIFFUSER EXIT BEND (RIGS)
5.1 REGENERATOR LP INLET
5.5 REGENERATOR LP EXIT
7.0 POWER SECTION EXHAUST

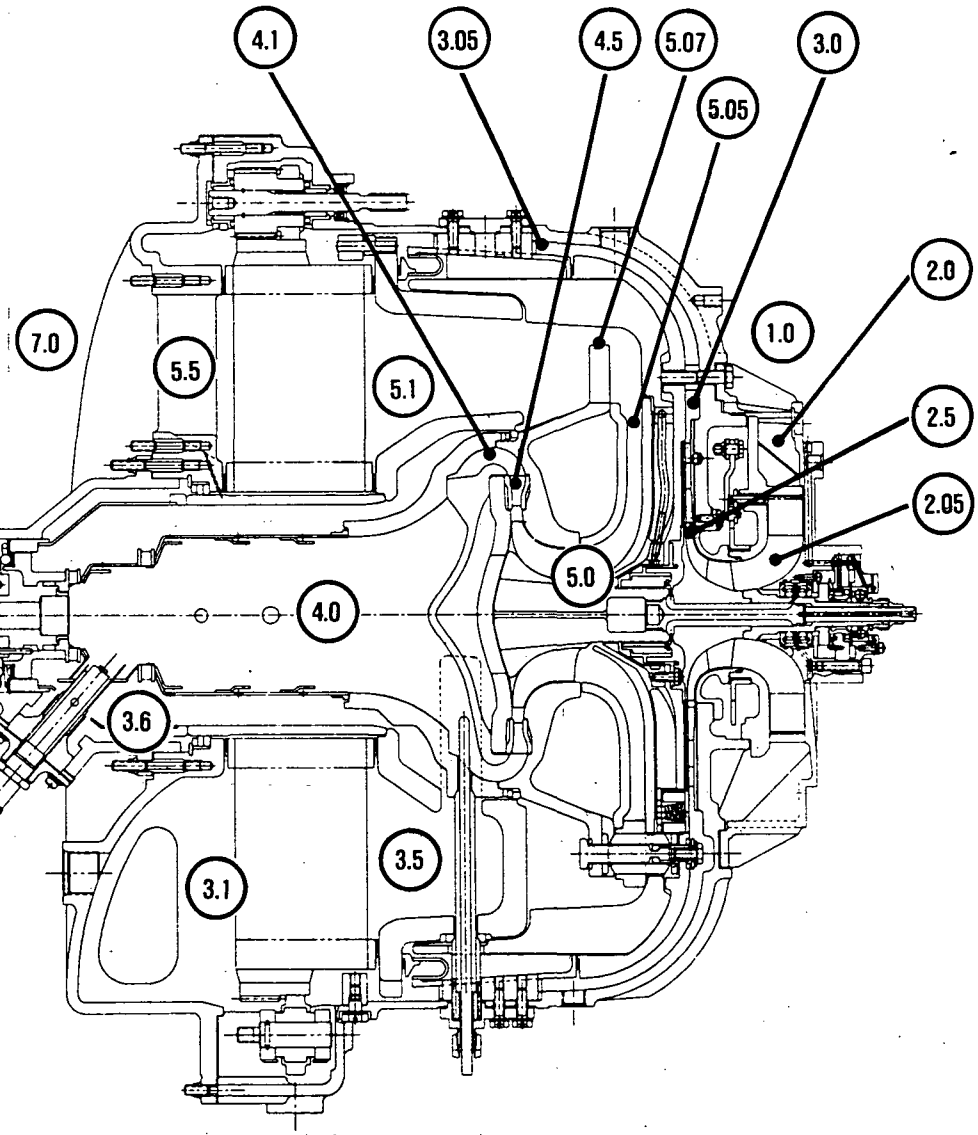

Figure 37. Performance Rating Stations.

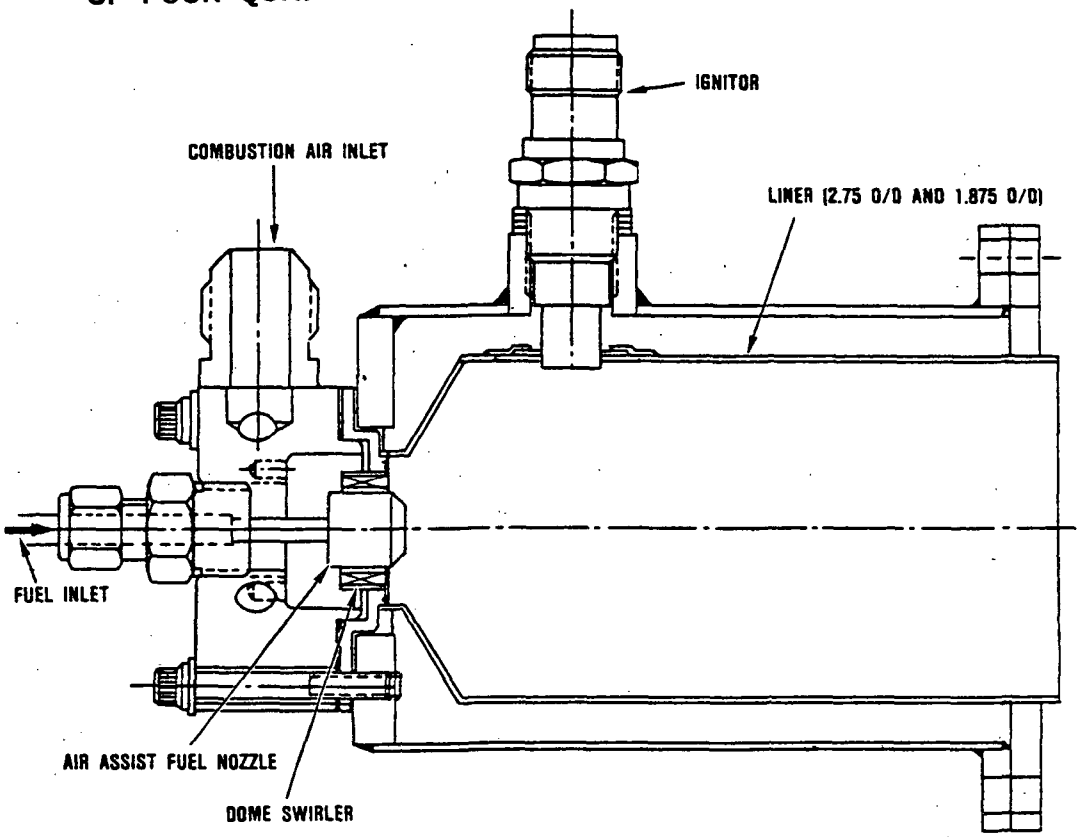

Figure 38. Torch Ignitor - Multi-Fuel.

through the fuel nozzle body, which is supplied with low temperature cooling air. Additional cooling air is supplied to the fuel nozzle head to provide convective cooling in the tip air cooling plenum and also in the circumferential cooling air plenum. These cooling air plenums are incorporated to reduce heat soak to the fuel distribution ring and maintain fuel wetted surface temperature low enough to prevent thermal degradation and plugging. This cooling air is discharged to the fuel nozzle cavity.

An alternative technique of ignition is being explored in which the spark ignitor is replaced by a glow plug. Kyocera manufacturers ceramic-hot-end glow plugs that are used in Isuzu diesel engines. Applicable glow plugs are being obtained for test evaluation and burner compatibility.

At this time the use of glow plugs, if they are functionally satisfactory, appear to have merit in that:

- Cooling with regenerator bypass air (and consequent SFC penalty) may not be required
- The predominant use of ceramics in parts exposed to the aggressive burner thermal environment is more consistent with ceramics utilization in the combustion system design.

A more refined layout of the combustion system is shown in Figure 44. The layout provides for a dual approach in that the Garrett nozzle and Delavan Simplex nozzles are accommodated within the same envelope.

Figure 45 shows an updated fuel nozzle design. The design is shrouded with cooling air, which also serves as air assist flow. Fuel injection is concentrated at the nozzle ID, with the ignitor located on the nozzle centerline. Fuel spray is directed toward the nozzle centerline creating a locally rich zone for ignition. Once stability has been achieved, acceleration can be accomplished.

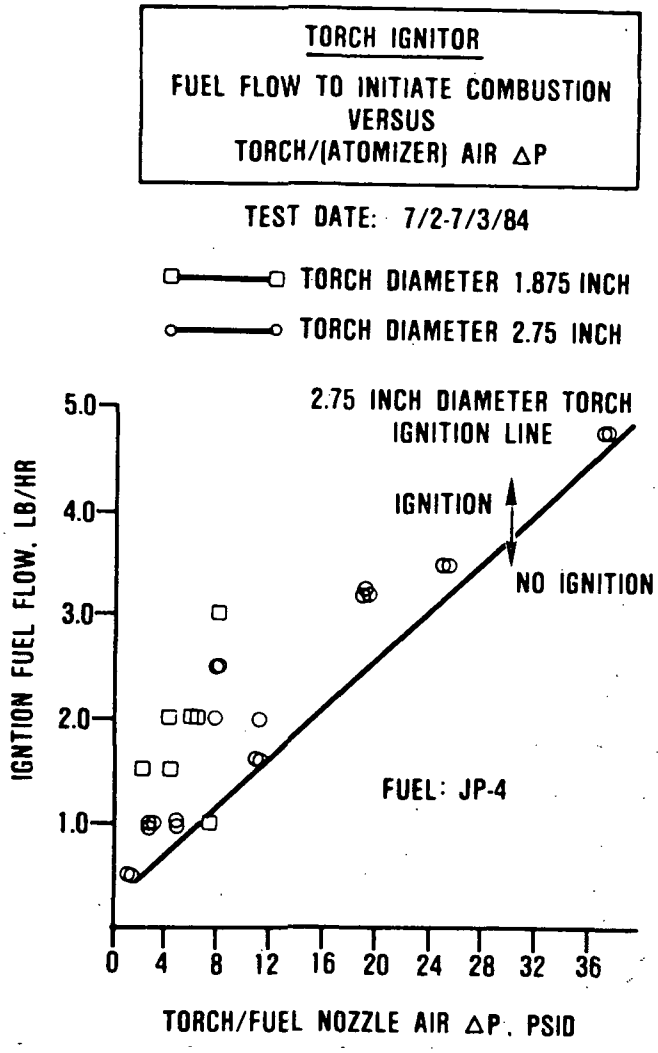

Figure 39. Torch Test Data Using JP-4.

4.3.3 Fuel Nozzle Testing

Testing of prototype Conax nozzles has been initiated. Successful ignition has been achieved at 15, 25, and 35 percent engine operating conditions with ignition delay times of 2-10 seconds at air assist pressures of 10-15 psid. Continued testing is scheduled.

Initial testing of the Garrett nozzle showed acceptable ignition with lightoff occurring within 3-6 seconds over a range of 15 to 45 percent speed. However, difficulties were experienced in stabilizing at idle fuel flow conditions. Modifications were incorporated, as shown in Figure 46, and significant improvements realized. Ignition was obtained at idle in 1-2 seconds with an air-assist pressure of 8 psid and fuel flows of 8-10 lb/hr.

Short duration (30 minute) fuel plugging tests were conducted on the Garrett nozzle using JP-4 and diesel grade DF-2 at burner inlet temperatures of 1650F and fuel flows of less than 1 lb/hr. No plugging was evidenced based on fuel pressure monitored and post spray testing.

Additional testing is planned using the metal and ceramic hardware.

4.4 Regenerator System - Ford

4.4.1 Regenerator Seals

The initial Phase V regenerator seals contained diaphragms that were fabricated by hand and heat treated in an oxidizing atmosphere. Although static seal leakage rig testing demonstrated a significant reduction in leakage level and sensitivity to seal working height (Figure 47) when compared to previously designs, additional improvements were expected after receiving new diaphragm dies. In addition, heat treatment of the diaphragms in an inert atmosphere will improve the assembly procedure.

All final diaphragm tooling dies were received during this report period and several seal assemblies, designated as Phase V-A, were fabricated for evaluation in the static seal rig, dynamic hot rig and engines at Garrett. Based on static seal rig leakage data (Figure 47), the Phase V-A seals demonstrated the expected improvements of the initial Phase V design. A set of Phase V-A seals is currently being installed in the hot structure rig at Garrett to establish the dynamic leakage characteristics utilizing the helium leakage detection system.

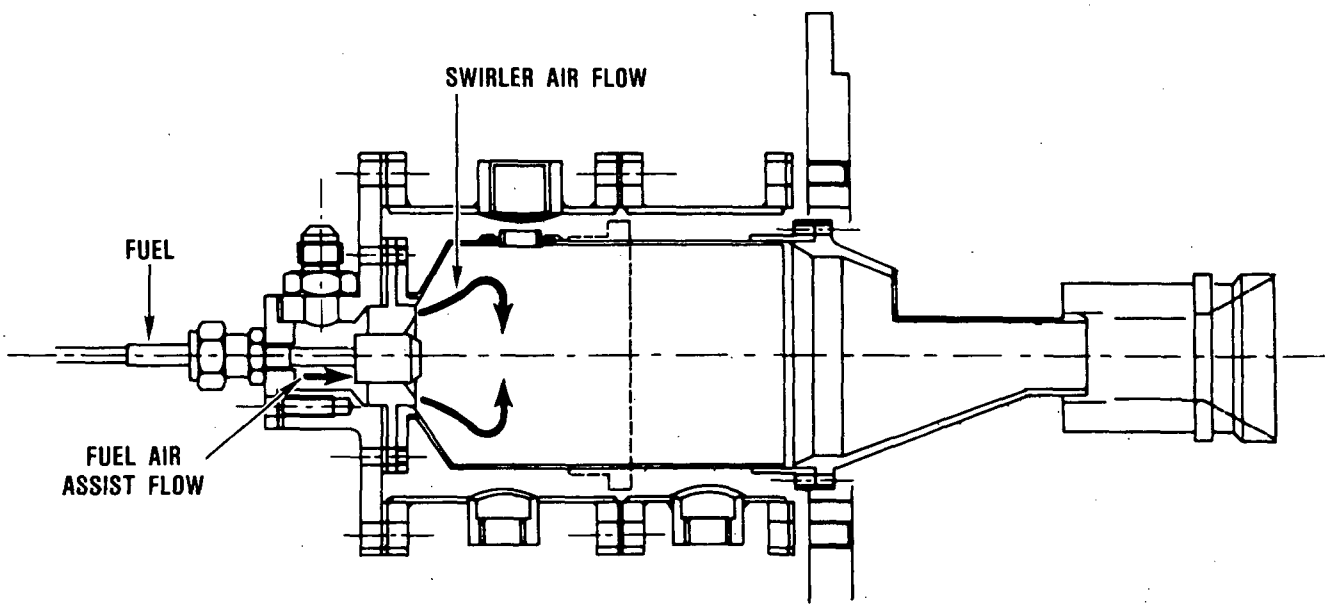

Figure 40. T/3 Torch Configuration.

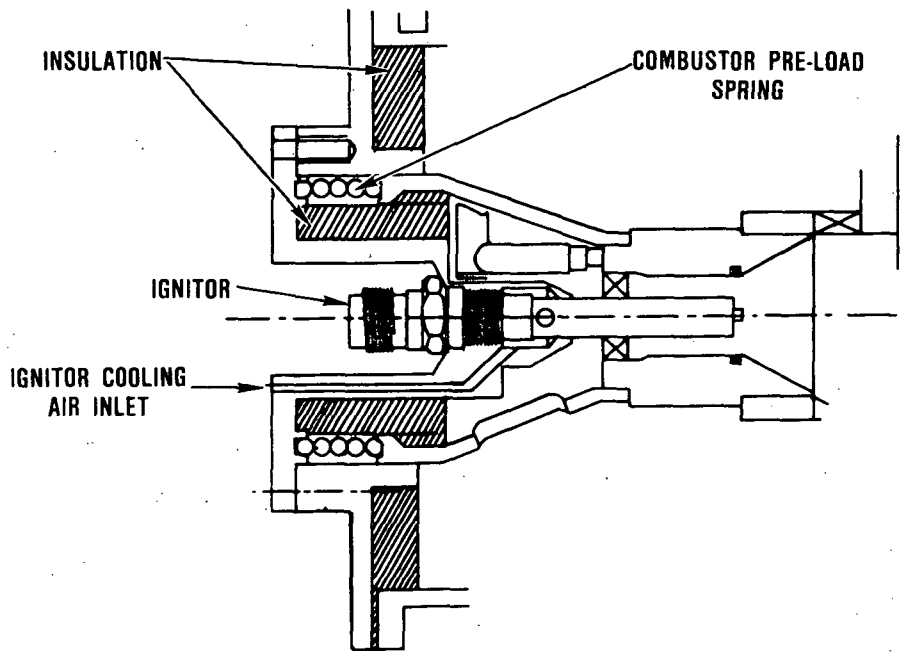

Figure 41. T/4 Torch Upgraded Configuration with Cooling Air Provision.

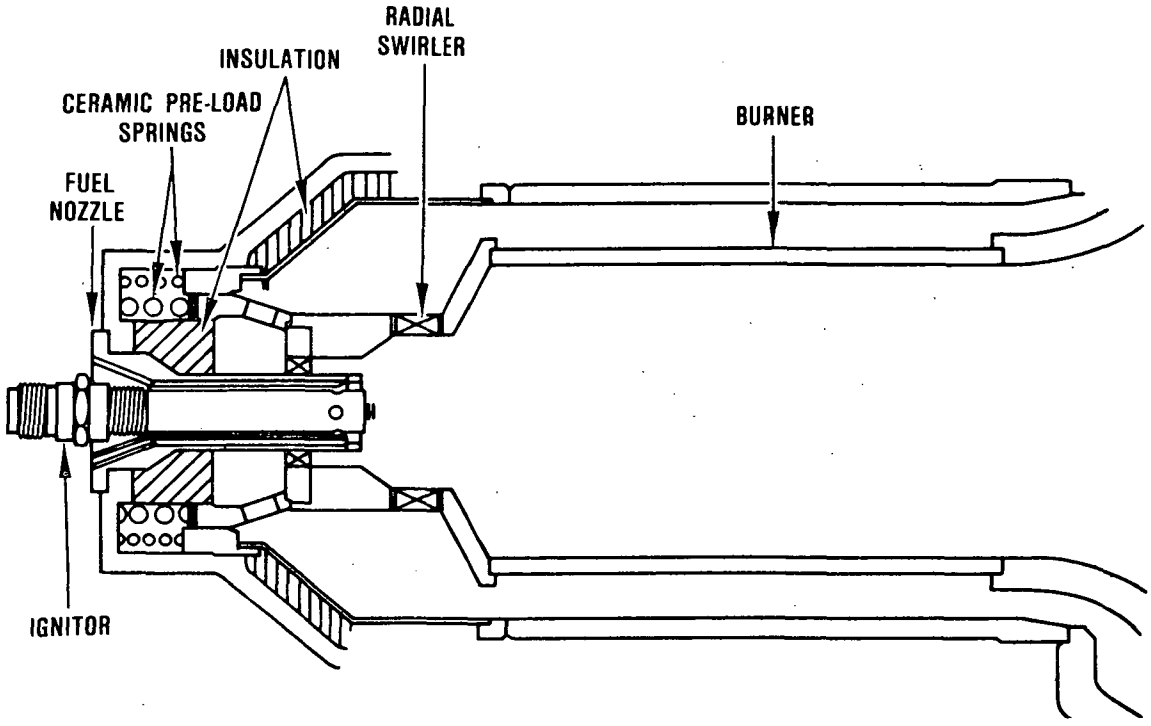

Figure 42. Combustion System Conceptual Design.

Additional testing in the static seal rig with symmetrical upper and lower outer peripheral diaphragms and equal length retainer legs showed a 20-percent reduction in static leakage. This concept was adopted as the basis for the next generation seal design, which is designated as Phase VI, as illustrated on Figure 48. In addition, the Phase VI design can accommodate more cooling air for the inboard (hot) crossarm seal compared to Phase V. The initial tooling for the Phase VI outer peripheral diaphragm was received at the end of the report period. Design changes for the crossarm diaphragms are being evaluated.

To accommodate the higher operating temperatures associated with the 2500F engine, the regenerator inboard (hot) seal crossarm will require diaphragm cooling. The design objective is to keep the middle (support) diaphragm (Figure 49) below 1650F, which should provide adequate strength using Rene 41 or Waspaloy materials for the expected diaphragm stress levels.

A finite element model utilizing solid instead of shell elements was incorporated into a 3-D heat transfer analysis program. The model, which consists of 231 nodes and 98 elements, is used as a design tool to support the prototype seal configurations. The amount of cooling air flow is dependent on the pressure differential that exists in the channel. For discharge holes in the middle diaphragm at the center of the periphery, the pressure differential (less than 0.25 psi) establishes the minimum rate of cooling air flow. For maximum cooling, holes in the retainer (Figure 49) allow the air to discharge into the center hole cavity, which is vented to the exhaust duct.

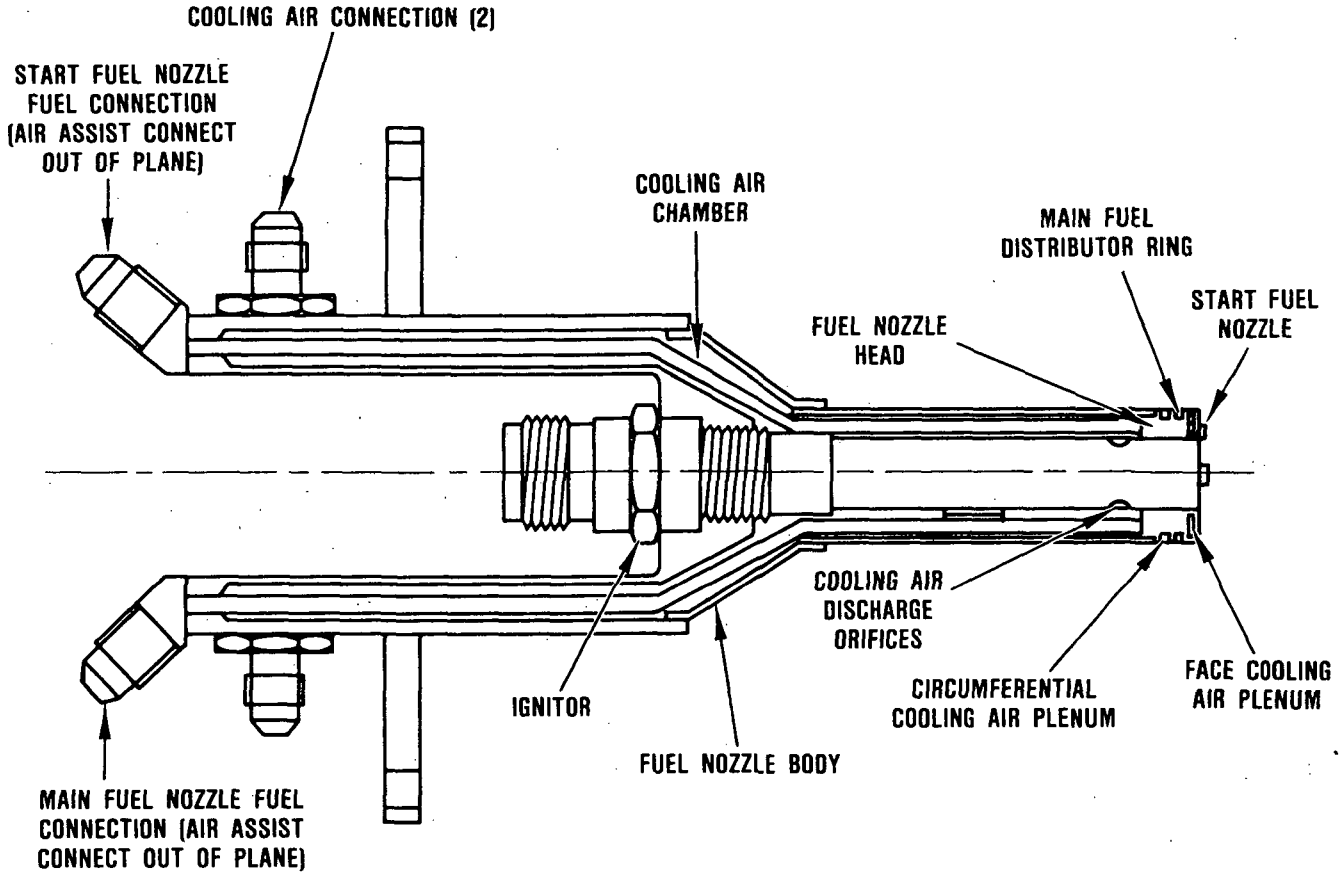

Figure 43. Modularized Fuel Nozzle/Ignitor Development Configuration.

The initial design concept (Figure 50) evaluated allowed cooling air to flow between the middle (support) and lower diaphragms. In addition, a barrier coating was applied to the back side of the coated shoe. The barrier coating is required because the trailing edge portion of the middle diaphragm represents a direct conduction path between the flow separator housing (FSH) and rubbing shoe.

For the 2500F engine flow conditions at cruise (60-percent engine speed) approximately 0.5 to 0.9 percent of compressor discharge air combined with 0.030 inch barrier coating thickness (Figure 50) was required to allow the middle diaphragm to operate at a safe temperature. Since cooling flow requirements were excessive, a second design concept was evaluated.

The second design concept (Figure 51) allowed cooling air to flow between the middle and upper diaphragm. For the 2500F engine flow conditions, approximately 0.25 to 0.50-percent of the compressor discharge air (Figure 51) in addition to 0.050 inch barrier coating on the back side of the metal substrate would be required to allow the middle diaphragm to operate at a safe temperature. This represents a reduction of 50-percent of the cooling air required for the initial design concept, which allowed cooling air between the lower and middle diaphragms.

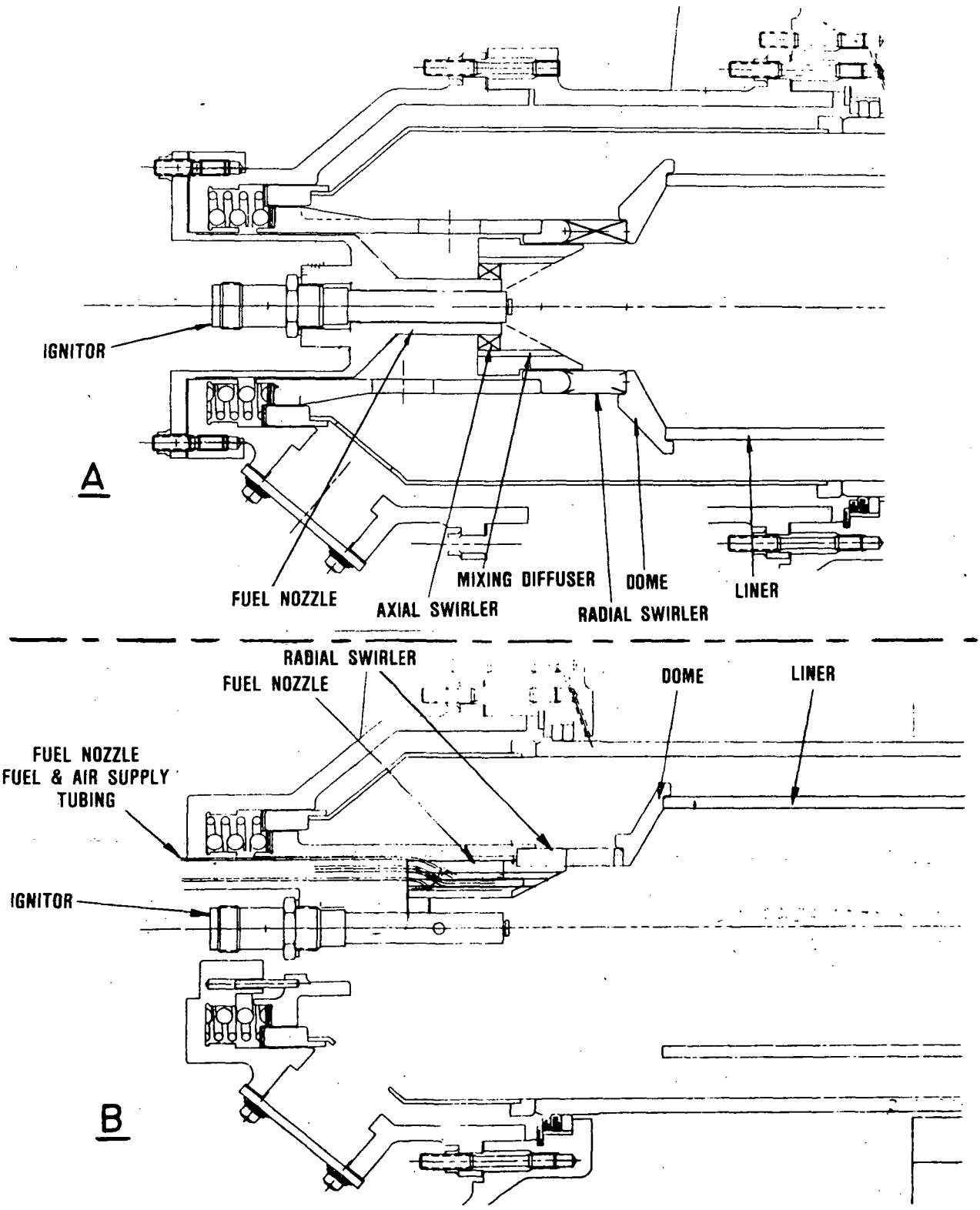

Figure 44. Garrett (View A) and Delavan (View B) Fuel Nozzle Installations.

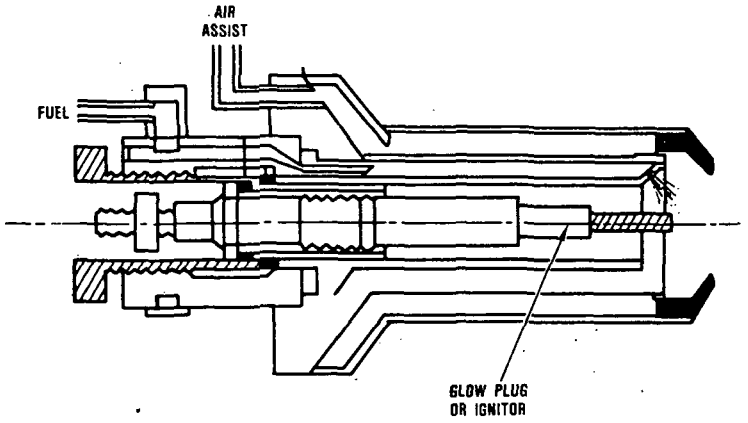

Figure 45. Garrett Fuel Nozzle.

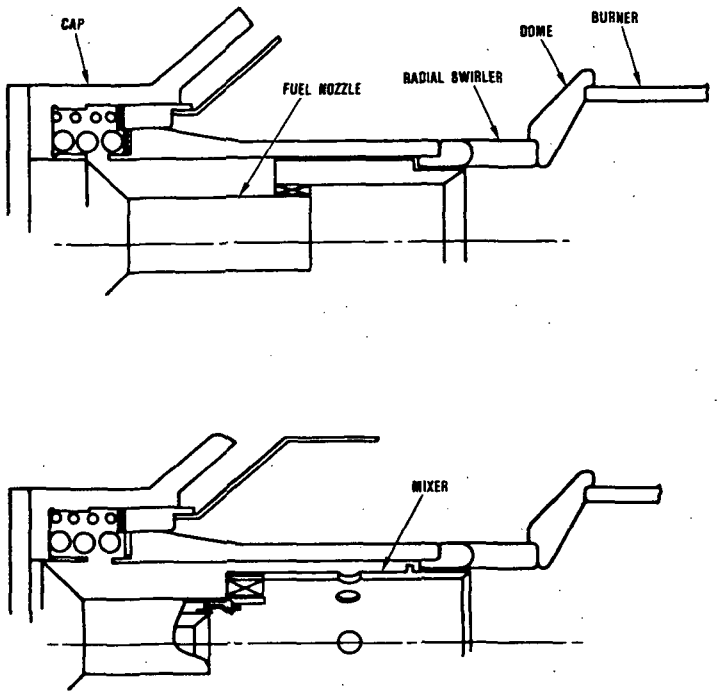

Figure 46. Combustor Mixer Modification.

To further reduce the cooling air requirement, a third design concept was evaluated featuring cooling air on both sides of the middle diaphragm (Figure 52). An additional feature for this design concept is the flexibility to interrupt the flow to prevent boundary layer build-up and promote localized turbulence by modifying the geometry of the middle diaphragm in the flow direction. Consequently, the convection coefficient can be increased by as much as 25-percent.

Another important consideration is to maintain the cooling flow discharge holes in the middle diaphragm at the center of the inner peripheral seal, which establishes the minimum rate of cooling airflow. Cooling air requirements above the minimum would necessitate throttling the air, which would be difficult to control, prior to discharge into the center hole cavity through holes in the retainer (Figure 49).

Minimum cooling air for the three design concepts was evaluated for 2500F engine flow conditions at 60-percent engine speed with the FSH varying from 1400 to 1700F (Figure 52). The results indicate the middle diaphragm will operate at an acceptable temperature level with cooling flow on both sides and 0.06 inch barrier coating on the back side of the metal substrate.

Recent finite element analysis of the FSH at Garrett indicates the temperature level at the inner circular portion will be 1900 to 1950F. Consequently, a barrier coating will also be required on the FSH in this region (Figure 52). The analysis will be repeated during the next report period to update the barrier coating thickness and cooling airflow requirements.

4.4.2 Seal Coatings

The impetus for replacing I-85 with I-151 was based on visual observations of hot flow path components tested in the hot structures rig and ceramic engine. At 2000 to 2100F turbine inlet temperatures, the I-85 coating for the hot seal outer peripheral shoes and cold seal crossarm may have been marginal. Although the I-85 did not delaminate, soften or experience significant wear, trace amounts of copper caused some sticking to occur between ceramic components.

Based on wear rig tests at Ford in the early 1970's, the I-151 had 200 degrees (F) higher

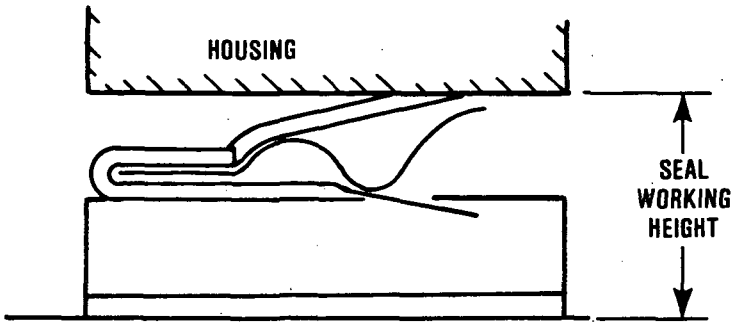

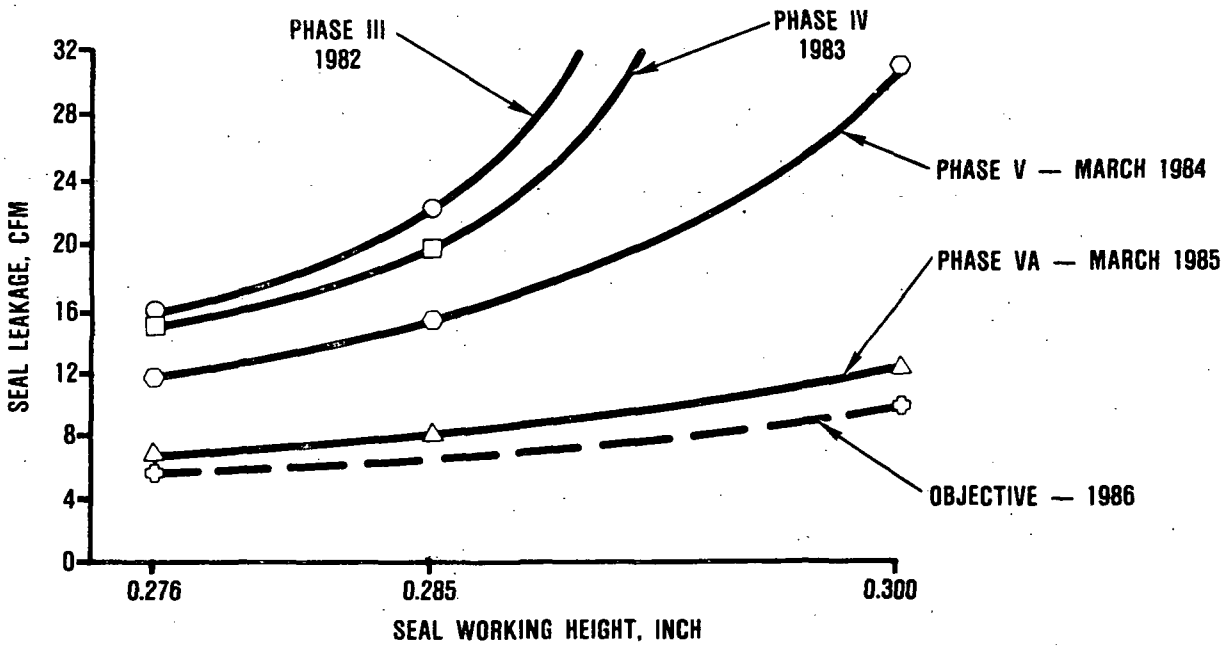

Figure 47. Phase V Static Seal Leakage.

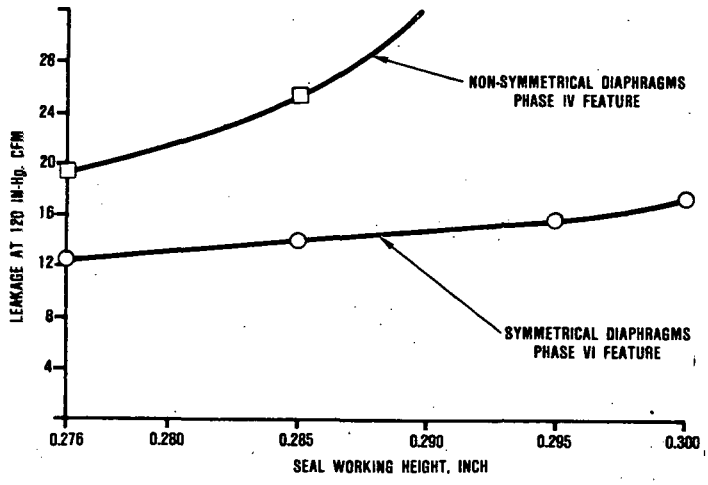

Figure 48. Phase VI Static Seal Leakage.

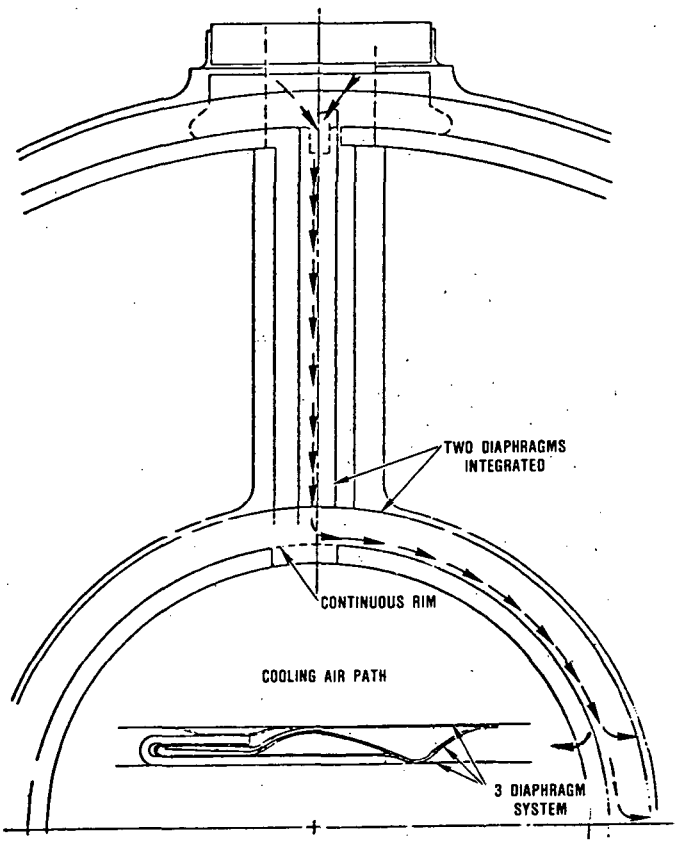

Figure 49. Phase VI Diaphragm Cooling Design.

temperature capability compared to I-85. A purchase order was submitted to Ferro Corporation to produce I-151 powder on a best effort basis. After considerable difficulty in producing powder that satisfies the Ford specification for particle size distribution, a small yield (60 lb) was delivered to Ford.

The initial seals with I-151 installed in the ceramic engine at Garrett experienced delamination in the I-151, I-39 interface bond region. Since the delaminations occurred in the higher temperature regions of the seal (800-900F), the initial suspicion centered on the moisture content in the I-39 powder prior to spraying. In addition, the I-39 powder appeared to be too soft, with indications that corrosion may have occurred.

Since the seal components that experienced delaminations were from a recent group sprayed at APS, the remaining components were put in a furnace at 1000F overnight. Every component with I-151 experienced delamination to some extent. Components with I-112, I-00 interface coatings did not delaminate.

To resolve which of the coatings, I-39 or I-151, were causing delaminations to occur, modifications to the plasma spray procedure were incorporated at APS. An external overspray deflecting air jet was attached to the plasma gun at a right angle to the stream, to prohibit fines from impinging on the substrate. In addition, the I-39 may require a higher spraying temperature compared to the other intermediate coating (I-00). The higher temperature, which is controlled by increasing the amperage, would also help nullify the effect of any moisture content in the powder.

To evaluate the effect of these modifications, a set of six samples were sprayed as follows:

a) I-39 (high amperage)+ I-151
b) I-39 (low amperage) + I-151
c) I-39 (high amperage)+ I-85
d) I-39 (low amperage) + I-85
e) I-00 + I-151
f) I-00 + I-85

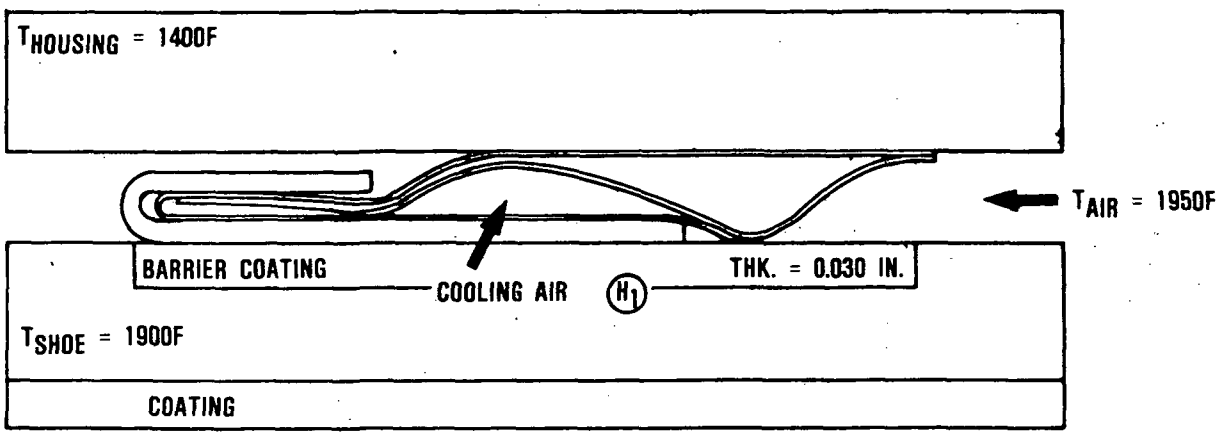

DESIGN NO. 1

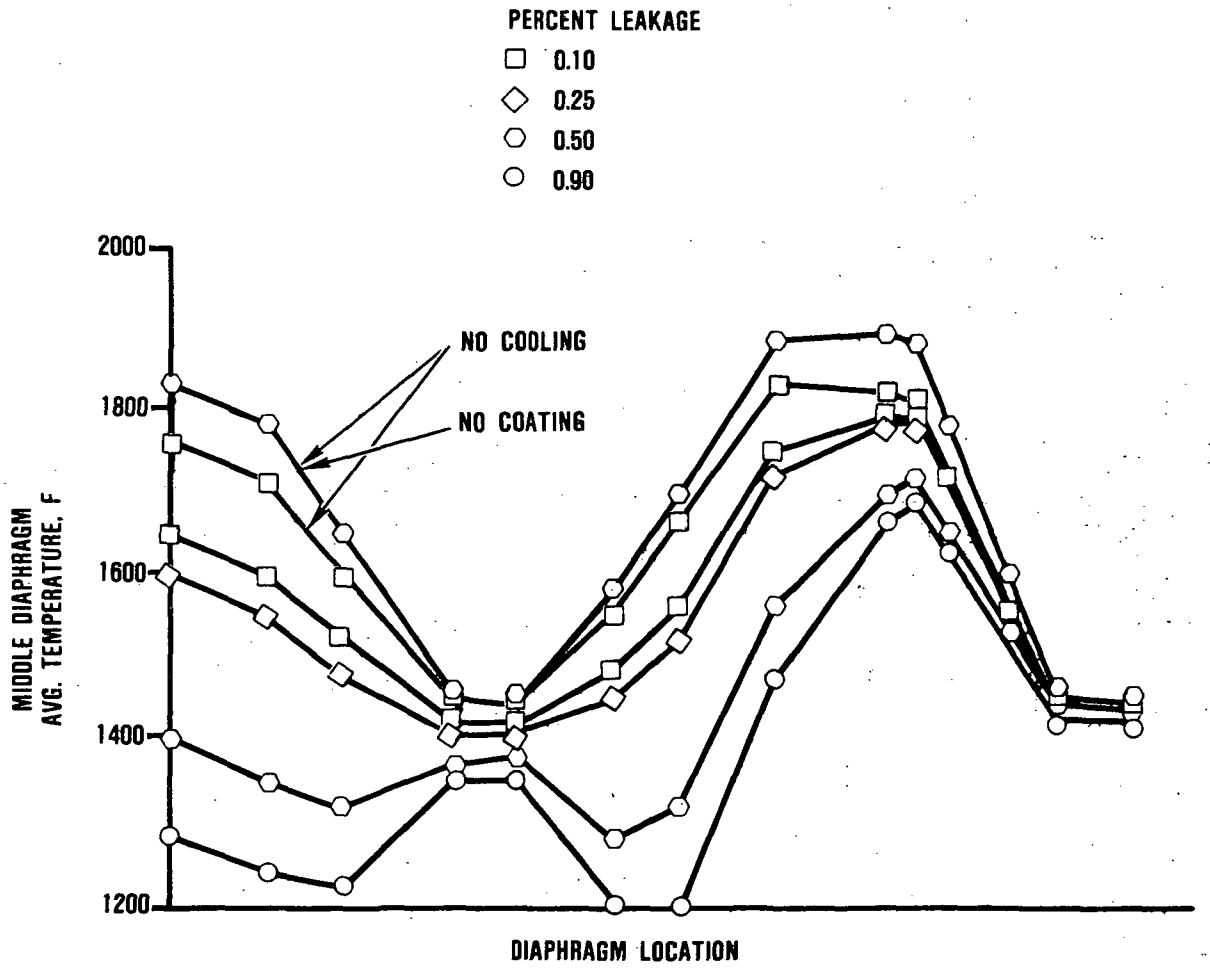

Figure 50. Phase VI Initial Design Concept.

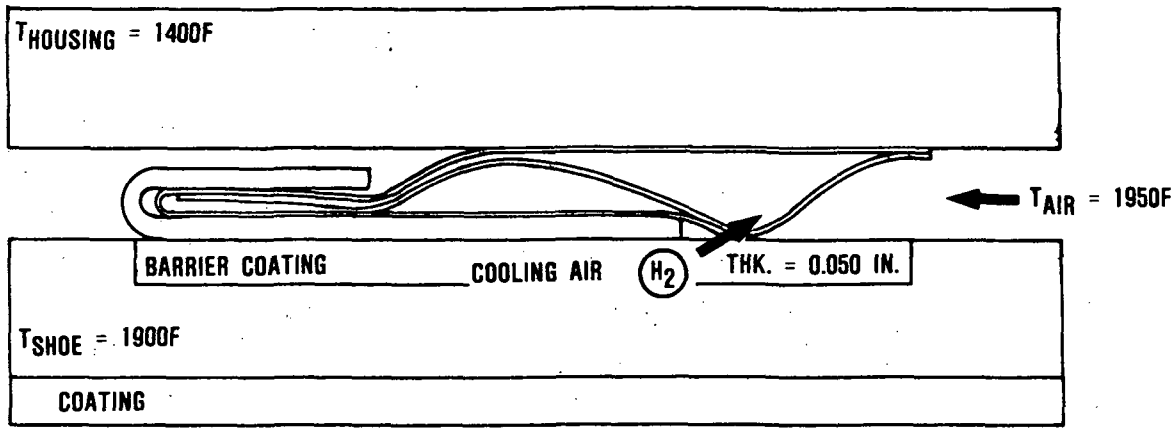

DESIGN NO. 2

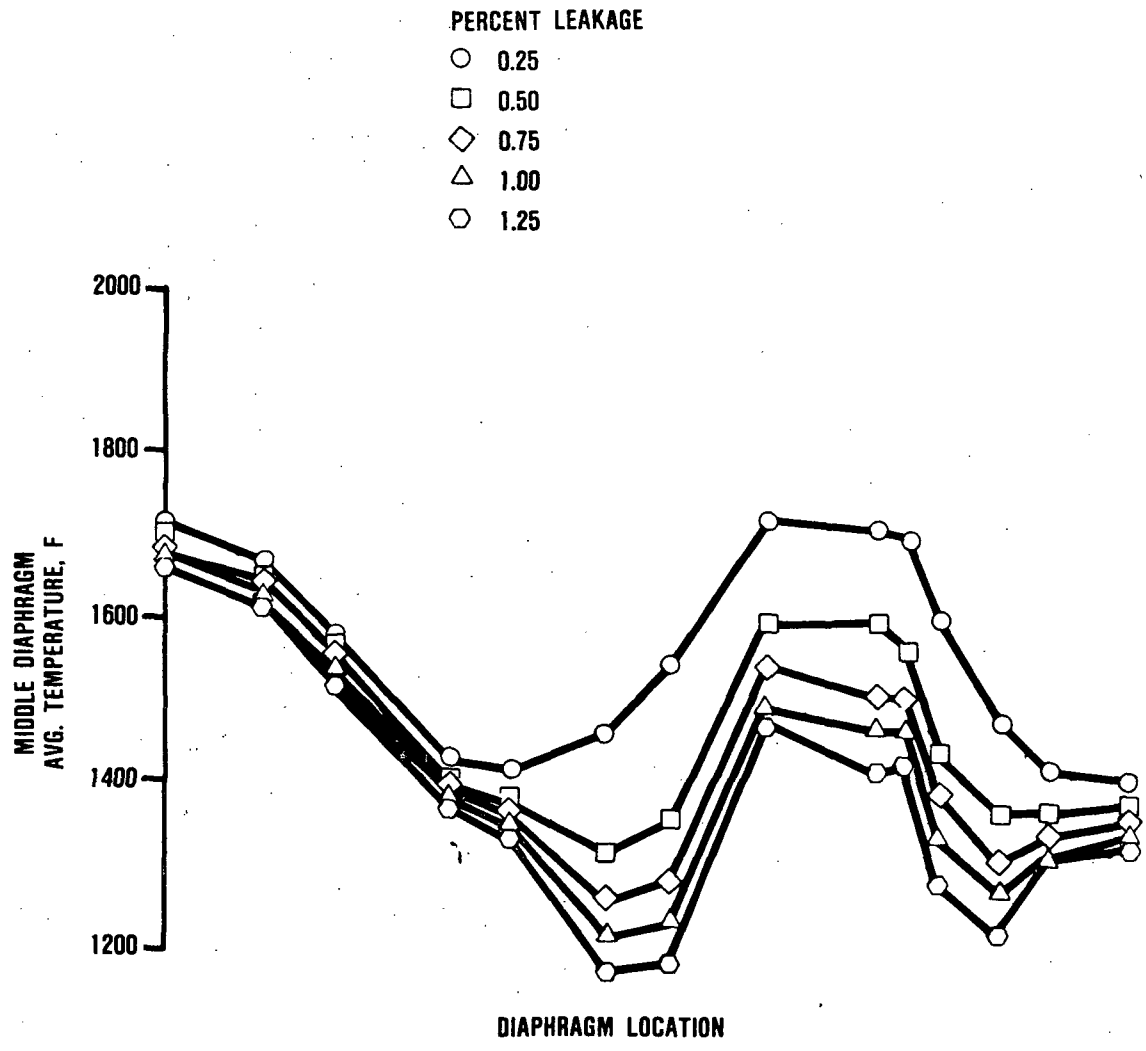

Figure 51. Phase VI Second Design Concept.

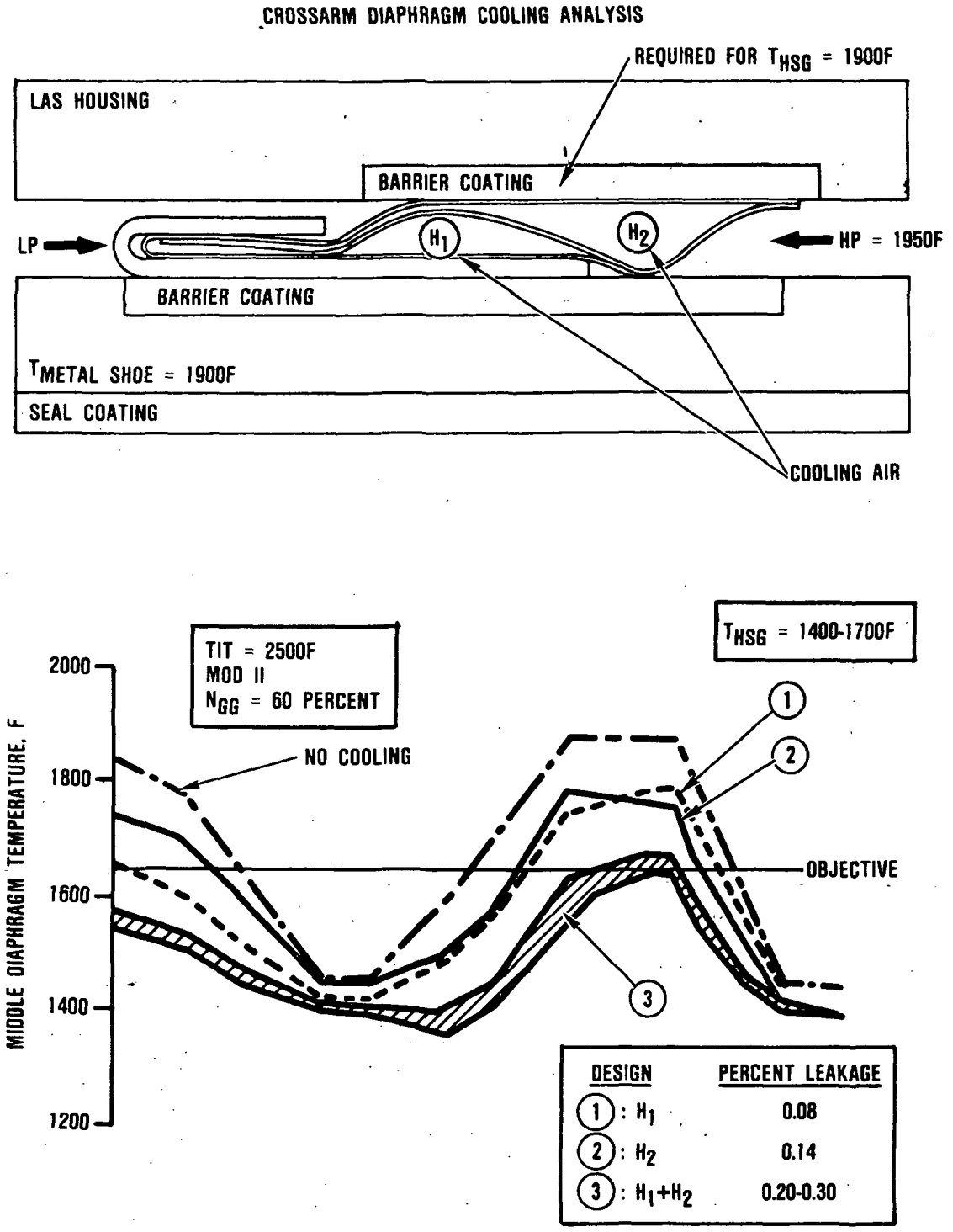

Figure 52. Phase VI Third Design Concept.

Each of the 430 stainless substrates had the same bond coating. All of the powders were dried prior to spraying with an overspray deflecting air stream mounted to the plasma gun. The samples were installed in a furnace at 1000F for 18 hours. Each of the samples with I-151, regardless of the modifications to the intermediate coating (I-39 or I-00), spalled severely (Figure 53). Conversely, samples with I-85 did not delaminate.

At the same time, a wear sample had been accumulating time in the seal wear rig. Unlike the seals in the Garrett engine, the I-151 coating became powdery prior to delamination at 1000F. However, seal friction remained very low throughout the test.

Samples of the as-received powders and scrapings off the wear sample were submitted for plasma emission spectrometry evaluation. In addition, samples of I-49 and I-85 were also submitted. All of the coatings evaluated, except for the I-151 powder, appeared to be within specification. Since I-151 is a mixture of I-49 (within specification) and I-40 (not available for measurement), the problem is attributed to the I-40 being out-of-specification or the blending process was improper. Regardless, the remaining amount of I-151 will not be utilized.

As a replacement for I-151, modified versions of I-85 with improved plasma spray parameters as well as I-112 components were assembled for engine evaluation at Garrett. Limited testing in the ceramic engine S/N 002 of seal assemblies with I-112 in place of I-85 have, however, indicated higher regenerator drive torque requirements.

Additional engine and hot structures rig testing during the next report period will determine if the problem is resolved. In the event that I-85 or I-112 are not acceptable, a purchase order will be submitted for a second attempt at formulating acceptable I-151 powder.

4.4.3 Regenerator Core and Drive System

NGK has demonstrated the ability to extrude MAS material in three different matrix fin geometries (CO.3, CO.7, CO.9) in the form of full size cores. In addition, tooling has been developed for a fourth fin shape (CO.8). The CO.3 and CO.7 matrix geometries are isosceles triangular fins with 0.0055 and 0.0035 inch wall thicknesses, respectively. The CO.8 and CO.9 structures are rectangular with a nominal 0.0045 inch wall thickness. The predicted performance for the four NGK fin geometries are listed on Table 10.

For NGK to satisfy the three performance objectives, a new dense material is required for the thin-wall isosceles triangular structure (CO.7). The current effort at NGK is aimed at developing a new dense material with a compatible cement, which can accommodate shrinkage during firing without adversely affecting thermal properties.

A dimensionless parameter that relates mechanical properties to thermal properties of the matrix is defined as the thermal stress factor (θ), which is the ratio of strain tolerance to the maximum expansion difference (ΔPPM) between the temperature extremes of the regenerator. Strain tolerance (ST) is defined as the ratio of modulus of rupture (MOR) to modulus of elasticity (MOE) for the matrix. This parameter can be considered a relative measure of the intrinsic resistance of a matrix to thermal stress. Since the probability of thermal failure increases with decreasing thermal stress factor, it is a convenient criterion to compare matrix materials on an equivalent basis. A large thermal stress factor indicates good resistance to thermal stress failure. A low thermal stress factor does not necessarily imply that the matrix material is not suitable for a regenerator application. It does indicate that stress relief techniques are required at the regenerator rim to provide sufficient thermal stress capacity.

Once, the regenerator has been designed for sufficient thermal stress capacity, the

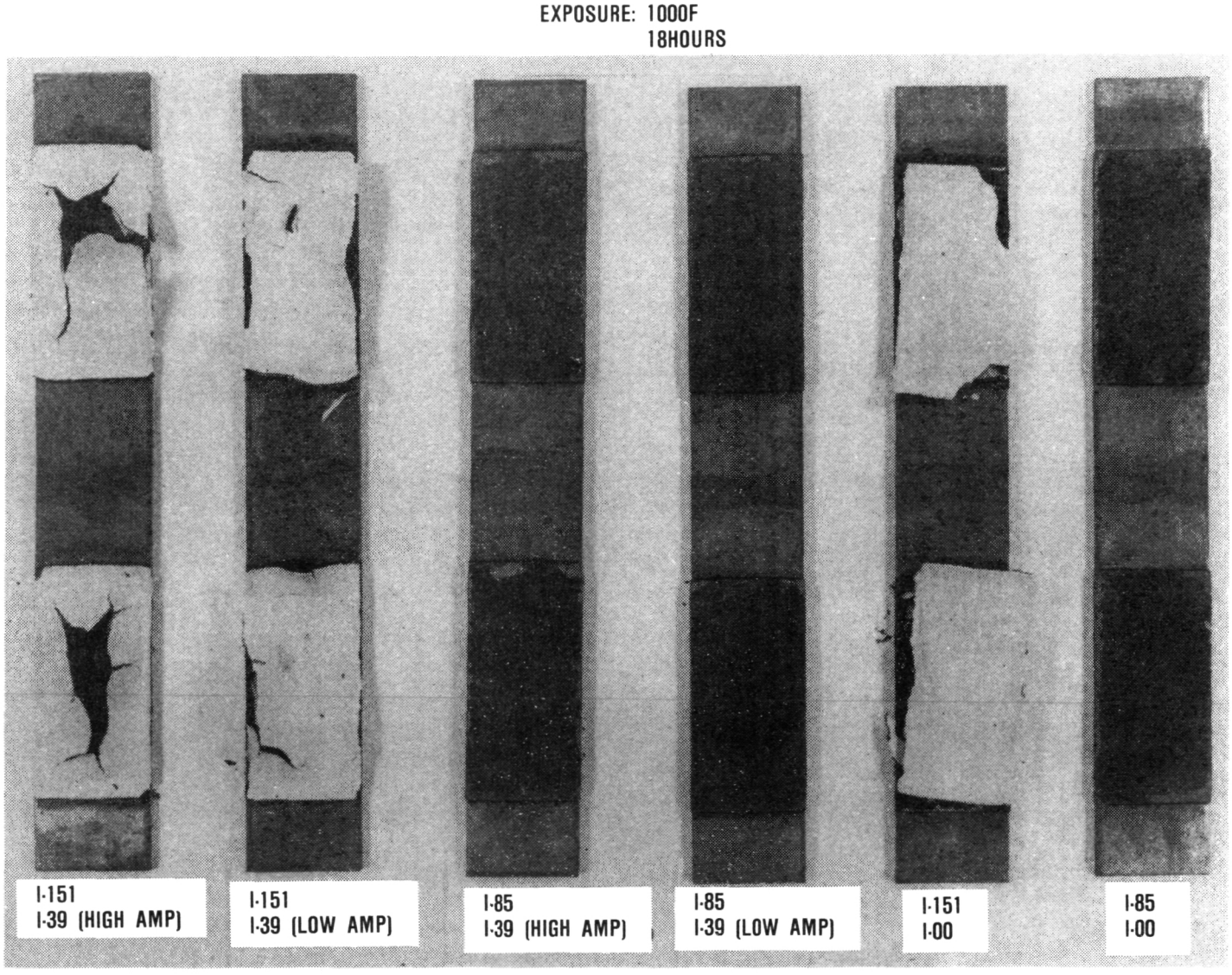

Figure 53. Seal Coating Evaluation (18-Hours at 1000F).

Table 10. NGK Regenerator Core Performance

Objectives: 100 Percent Engine Speed Effectiveness = 92.9% Minimum Pressure Drop = 7.5% Maximum Porosity Leakage = 0.5% Maximum						
NGK (MAS) Extrusion	Fin Configuration	Wall Thickness, inch	Cell Density, Openings / in^2	ε, %	ΔP/P, %	Leakage, %
Isosceles	CO.3	0.0055	920	90.1	6.0	0.30
Isosceles	CO.7	0.0030	1510	93.6	7.3	1.7
Rectangle	CO.9	0.0047	1115	91.4	7.2	0.80
Rectangle	CO.9	0.0043	1390	93.3	9.2	1.0 (Est.)

NOTE: NGK Leakage based on GE-Cordierite, coating and impregnation

thermal stability of the material must be taken into account. If the material has reasonable stability with time at temperature then stress can be maintained at an acceptable level. By comparing the thermal stress factors, before and after time at temperature exposure, an insight into allowable instability can be made. If thermal stress factor increases, then the instability that has occurred should not impair thermal stress levels. If thermal stress factor decreases, then the lower limit for each matrix material must be established based on the original safety factors. Based on thermal stress analysis of the AGT regenerator and thermal stability characteristics of the present material, the stress factor (θ) requirements for the new material for the as-received and 1100C exposure condition are 1.0 and 0.4, respectively, as per the following equation:

$$\theta = \frac{(MOR/MOE)}{\Delta PPM}$$

A recent version of NGKs new material, designated as MX, has virtually eliminated thermal instability at 1000C with a significant reduction at 1100C. In addition, a modified version of their current cement has demonstrated a significant increase in strength. Development effort will be concentrated on reducing instability of MX material at 1100C and reduction of wall porosity of the present Cordierite (CO.3) material.

The current aluminum-silicate (AS material 9461) from Corning has acceptable thermal stability up to 1100C. The predicted performance for the current wrapped sinusoidal matrix geometry (T.14.20) from Corning indicates acceptable pressure drop and leakage as listed on Table 11. Since this geometry is 1 percent below the effectiveness objective, an analytical study has been completed to optimize extruded matrix geometries that will satisfy the performance objectives. The matrix performance characteristics for an

extruded isosceles triangular and rectangular fins with two different aspect ratios were estimated based on existing shuttle rig test data. Based on analytical results, the three extruded fin geometries listed on Table 11 will satisfy the AGT regenerator performance objectives. Selection will be based on the extruded configuration that would be best from a die tooling development standpoint.

Sudden increases in regenerator core drive torque were experienced in the ceramic engine S/N 002. Six of the last nine engine builds (Builds 12 and 13A through 13H) experienced core seizure despite modifications in build clearance, drive system components, core and seal hardware. Prior to Build 12, this engine had successfully completed a 100-hour durability test with drive torque varying between 100 to 250 ft-lb and without any regenerator drive system problems. A test sequence was established for Build 13H to evaluate potential causes of this problem. The engine was run from 60,000 to 90,000 rpm with TIT below 1700F. As TIT was increased to 2100F, drive torque increased accordingly until rotation stopped. An attempt was made to rotate the core approximately 30 minutes after shutdown without success. It was then decided to install a linear transducer on the exhaust cover (Figure 54) to monitor axial movement as a function of gas generator speed and burner inlet temperature. In addition, cooling air was impinged on the exhaust cover in a circular direction as illustrated in Figure 54.

The results of the second day of testing are shown on Figure 55. The axial movement of the cover toward the engine centerline was proportional to the burner inlet temperature for a constant engine speed. Regenerator drive torque increased with cover inboard movement, which tends to reduce seal operating clearance. While at 90 percent engine

Table 11. Corning Regenerator Core Performance

Objectives: 100 Percent Engine Speed

Effectiveness = 92.9% Minimum
Pressure Drop = 7.5% Maximum
Porosity Leakage = 0.5% Maximum

Fin Shape	X Fins/in	Y Rows/in	N Holes/in^2	Aspect Ratio PH/H	Wall Thickness inch	σ	DH inch	ε %	ΔP/P %	Porosity Leakage %
Wrapped Sinusoidal	38.0	34.5	1310	2.0	0.0024	0.79	0.0228	91.9	7.3	0.20
Extruded Isosceles	52.0	29.0	1510	1.2	0.003	0.73	0.0194	93.6	7.3	
Extruded Rectangle No. 1	22.9	51.0	1165	2.7	0.0035	0.76	0.0230	92.9	7.4	
Extruded Rectangle No. 2	15.7	54.1	850	4.2	0.0035	0.77	0.0240	92.9	7.5	

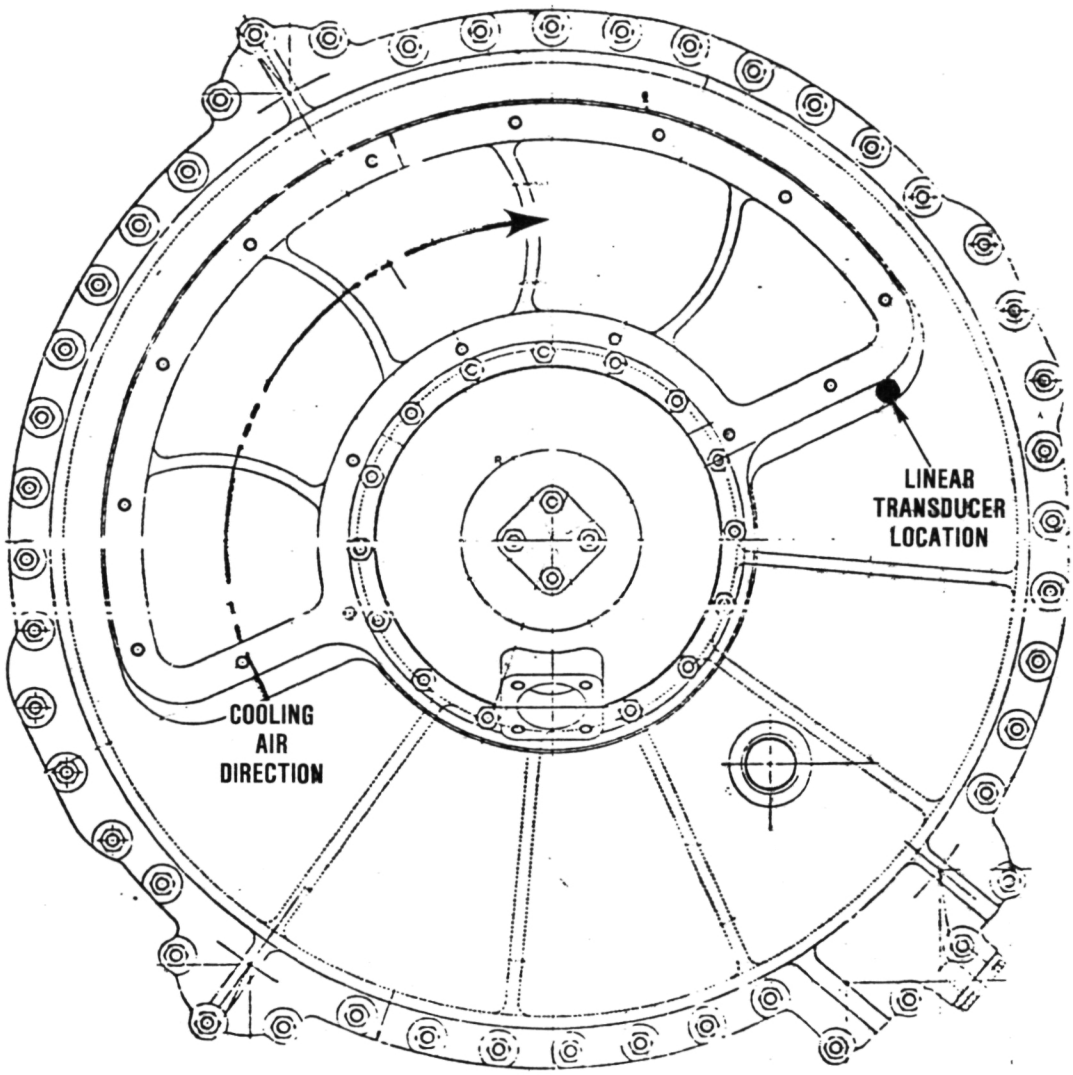

Figure 54. Location of Linear Transducer on Exhaust Cover.

speed and attempting to increase TIT, drive torque increased suddenly to the upper limit causing the core to stop rotating. Cooling air impinging the cover allowed the cover to move outboard and unlike the previous day, the core was free to rotate 5 minutes after shutdown.

The test was repeated and the engine was held at 70 percent speed with constant TIT and resulting burner inlet temperature (Figure 55). After increasing the cooling air the inboard axial movement of the cover was reduced from 0.0067 to 0.0032 inch. The cooling air was then redirected by direct impingement on the high pressure (HP) side of the cover, which caused the cover movement to increase from 0.0032 to 0.0078 inch. Drive torque increased accordingly from 260 to 325 ft-lb. This occurrence indicated the cover movement is an oblique axial plane.

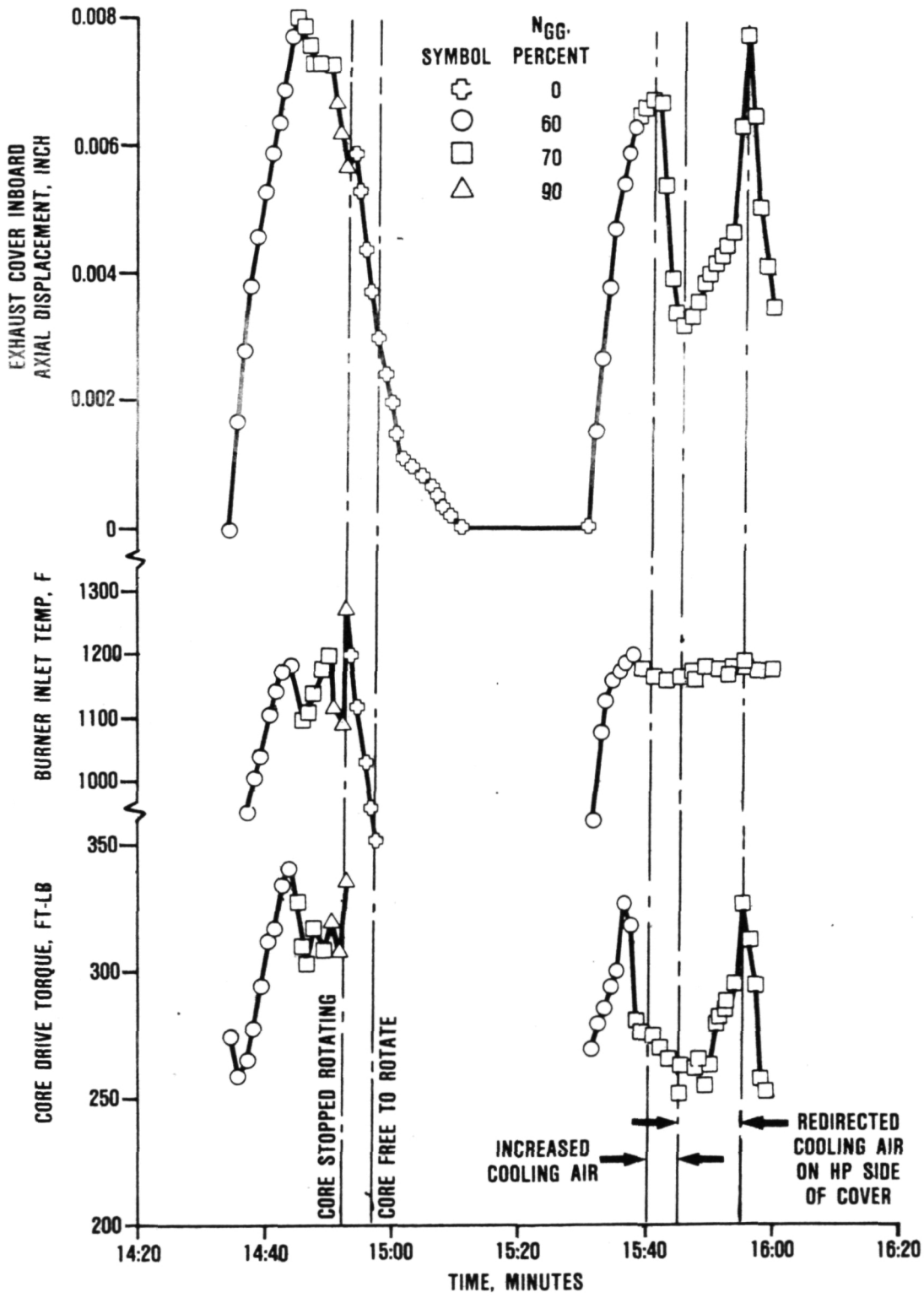

Figure 55. Test Results to Measure Effect of Increased Cooling Air.

For the third day of testing, the HP half of the exhaust cover was covered with a layer of wet blanket insulation in addition to the cooling air applied in the original direction. For this combination the axial inboard movement of the cover was reduced approximately 0.002 inch for comparable test conditions of the previous day at 60 to 70 percent speed. Correspondingly, the drive torque level was also reduced in spite of increased oscillation. Engine speed was increased to 90 percent. Correspondingly, the drive torque level was also reduced in spite of increased oscillation. Engine speed increased to 95 percent with burner inlet temperature held between 1000 to 1050F, the cover movement was reduced from 0.0056 to 0.0032 inch and drive torque oscillated between 240 and 290 ft-lb. After stabilization at 95 percent engine speed with the cover movement at 0.006 inch and drive torque below 300 ft-lb. an attempt was made to achieve 100 percent engine speed. At approximately 98 percent speed a loud noise was heard and the cover movement increased and then suddenly decreased while drive torque increased sharply to the upper limit, and core rotation stopped. Disassembly of the engine revealed a FSH failure.

As a result of this testing, the primary cause of excessive regeneration drive torque is due to exhaust cover distortions, which is proportional to combustion inlet temperature level regardless of engine speed. During the next report period, additional linear transducers will be installed to determine the exhaust cover distortion plane. Insulation will be added to the exhaust cover and additional modifications will be predicated on these results.

4.4.4 Regenerator Development Rig

The Ford regenerator development rig was modified during this report period to provide provisions for measuring dynamic regenerator seal leakage. A crossover duct was incorporated (Figure 56) to provide an exit orifice on the HP side in addition to the existing inlet orifice. A tapered disc with an internal variable throttle drive replaced the stationary

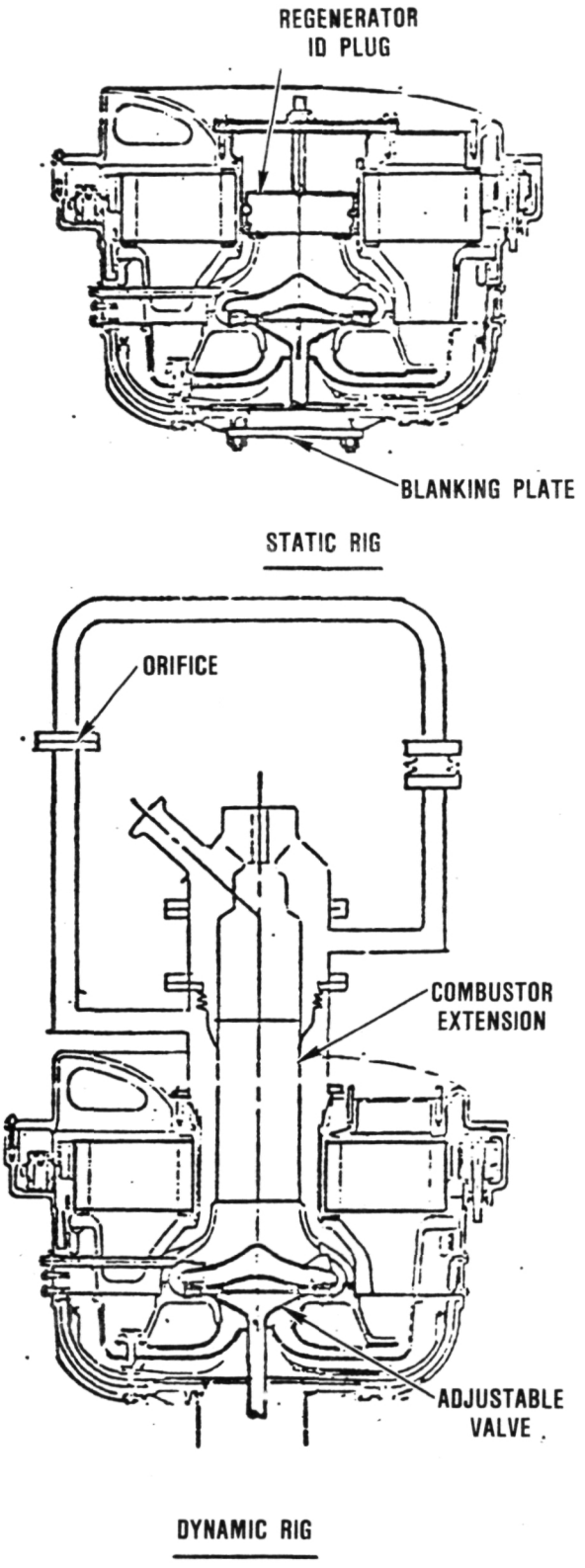

Figure 56. Ford Regenerator Development Rig Modifications.

rotor to simulate the turbine pressure drop. In addition, a "flipper" seal was fabricated to replace the piston rings that were used to seal internal leakage between the regenerator shield and exhaust housing. A fixture similar to the one used by Garrett was also fabricated so that rig static leakage can be measured (Figure 56).

The rig with the leakage measurement modifications and valve that simulates turbine pressure drop was run during this period. The initial 7.5 hours of hot (1200F) testing and 8.3 hours of cold (70F) testing were directed at establishing repeatability of leakage measurement. Cold test data was repeatable up to 30 psig, the current testing limit, provided no hot tests were run in between. Leakage is about 20 percent, but is not repeatable within ±3 percent after a hot test. Lack of repeatability is currently being investigated and is believed to be due to repositioning of some components due to thermal loads. Components will be changed one at a time to determine their contribution to total leakage. In addition, linear transducers will be mounted to the regenerator cover to record its displacement during hot tests. The rig is scheduled to be updated with all ceramic components supplied by Garrett during the next report period. Since the regenerator cover deflection and four of the six non-regenerator seal leak paths are the same in the ceramic flow path as in the metal version, these investigations will apply to the ceramic engine.

4.4.5 Non-Diaphragm Seals

As an alternate approach to cooling the inboard (hot) seal crossarm diaphragm, a feasibility study was initiated to eliminate diaphragms from this seal (Figure 57). The work plan for this study consists of the following:

a) Thermal analysis

   1) Three dimensional finite element analysis of FSH distortion

   2) Two dimensional finite element analysis of the regenerator matrix distortion

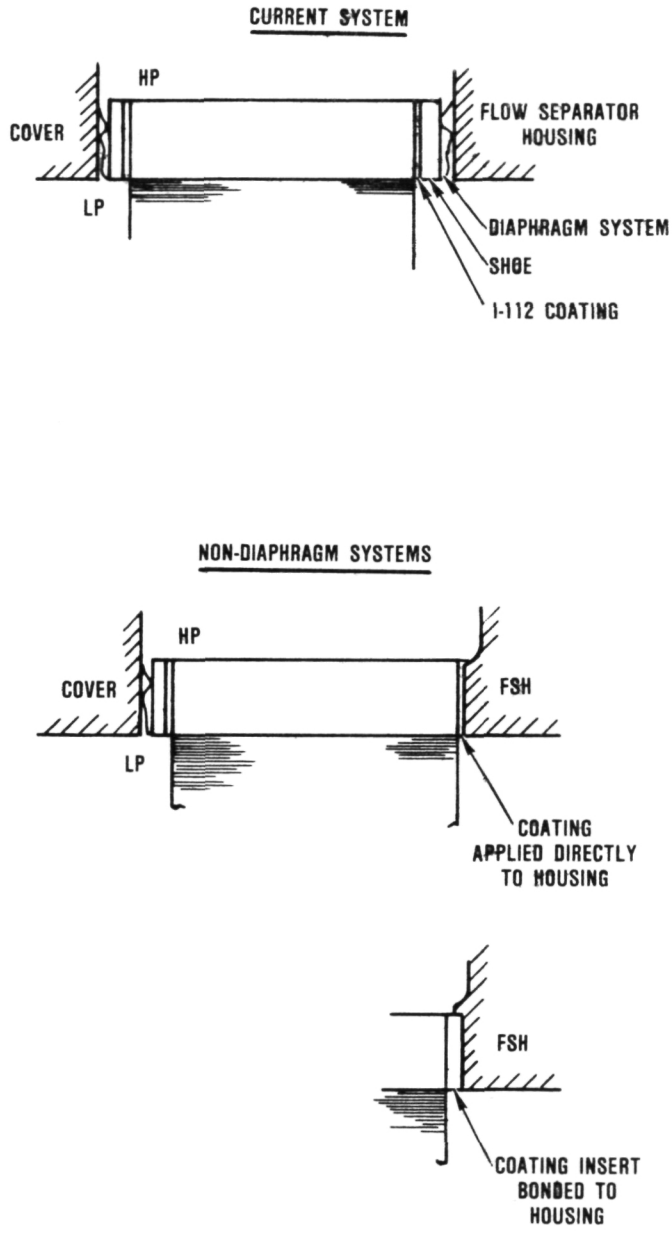

Figure 57. Non-Diaphragm Seal Configurations.

3) Labyrinth seal leakage analysis for regenerator core - FSH gap

b) Attachment of ceramic coatings to the FSH

c) Evaluate wear and friction characteristics in the seal wear rig

The hot face thermal distortion for the current Corning (AS) and NGK (CO.3) materials were evaluated for cruise and full power conditions, which correspond to engine speeds of 60 and 100 percent, respectively. The results (Table 12) indicate the Corning material has acceptable distortion variance, whereas the present NGK material is unacceptable for a non-diaphgragm seal system.

A low-distortion FSH is desirable to minimize leakage in a non-diaphragm seal. Six low-distortion RBSN flow separator housing design concepts proposed by Garrett were reviewed and one configuration was selected for further analysis. The initial finite element analysis of the FSH at cruise power conditions was completed at Garrett and indicated that the gap between the housing and core was less than 0.0015 inch (Table 12).

The development of an analytical model based on labyrinth seal theory was initiated to estimate undershoe seal leakage. This model, together with the distortions calculated for the FSH and regenerator core, is required to determine total system leakage of a non-diaphragm seal system.

Candidate coatings attached to LAS samples are being evaluated on a continuous basis as they become available. During this report period the following coatings have been investigated:

a) SCA-1000

b) I-112

c) S-77

Three LAS samples coated with SCA-1000 from Kaman Sciences Corp. with different application treatments accumulated a total of 130 hours in the seal wear rig at 500F. Although friction was very low, the coating was too soft causing the core passages to plug. Two additional samples have been ordered with the SCA-1000 coating to be densified with DES-1000 to reduce wall porosity and evaluate friction and wear characteristics against an LAS sample.

The initial I-112 coating, which was plasma sprayed on an LAS bar, was tested for 80 hours in the seal wear rig at 500 to 800F at 50 rpm and 3 psi. Wear was negligible and friction was very low but one section delaminated. The intermediate coating consisted of a mixture of I-112 and LAS powder.

The next set of samples consisted of a Ford ATLAS frit (ground LAS), which should improve bonding, as a constituent for plasma spraying I-112 on LAS sample bars for the seal wear rig.

Table 12. Thermal Distortion of Flow Separator Housing and Core

Component	Engine Speed	
	60%/Distortion, Inch	100%/Distortion, Inch
FSH (RBSN)	0.0015	
FSH (LAS)	0.0033	
Core (Corning)	0.0012	0.0006
Core (NGK)	0.0090	0.0060

Samples with ATLAS bonded directly to LAS were subjected to 2300F without coating failure. However, samples coated with ATLAS and an overcoat of I-112 after a 1500F furnace exposure showed a reaction between the ATLAS frit and the I-112. Processing techniques were developed to plasma spray I-112 coating on a pre-heat treated bond coating of ATLAS, which was subjected to 2000F exposure without failure of the LAS sample.

A LAS sample was plasma sprayed with a Ford S-77 coating over a non-heat treated ATLAS bond coating. Unlike a similar sample with I-112, there was no adverse reaction between the two coatings at 1500F exposure, indicating that the S-77 is more stable than I-112.

LAS samples with I-112 and S-77 seal coatings are currently being evaluated in the seal wear rig for friction and wear characteristics.

4.5 Ceramic Materials

A summary of the AGT101 material property results is presented in Table 13. To assist in the use of this table, a material characterization reference chart is presented in Table 14, and a summary of the predicted stress and temperature conditions for lightoff, maximum power, and idle conditions for each of the major ceramic static components and rotor are presented in Tables 15 and 16.

4.5.1 Rotor Material Evaluations

Room temperature, 1800F, and 2200F flexure testing was conducted on test specimens cut from six, high density, good quality, ACC Code 1 and 2 rotors densified at ACC, Ford and ASEA. Each AGT rotor yielded approximately 26 test specimens. Ten specimens from each rotor were tested at room temperature and 5 each at 1800F and 2200F. The flexure results are summarized in Figure 58. The lower additive Code 2 material should have increased high temperature strength over the Code 1 material. Although this is not the case at this time, with increased development the Code 2 material should have improved properties over the Code 1. The ACC Code 1 and 2 sintered silicon nitride materials have significantly higher room and elevated temperature flexure strength than both Ford and ASEA densified Code 1 materials.

The 2200F flexure strength value reflected in Figure 58 for ACC Code 2 appears to be unusually low. Testing will be repeated when another high density ACC densified Code 2 rotor becomes available. The suspect data points will be checked.

Stress rupture tests were conducted on ACC Codes 1 and 2 sintered silicon nitride specimens. The test specimens were cut from plates which had been processed with AGT rotors. The Code 1 material was sintered at Ford and has a density of 3.27 g/cm^3. The Code 2 material was sinter HIPped at ACC to a density of 3.24 g/cm^3. Temperature and stress levels were chosen to simulate AGT rotor operating conditions. Test conditions and results are listed in Tables 17 and 18. All sixteen test samples survived 100 hours at temperatures ranging from 1650 to 2150F, and loads of either 6 or 30 ksi. The samples then were fractured at room temperature. The resulting strength data for both the Codes 1 and 2 material shows considerable scatter but no severe strength loss occurred due to being under stress. The Code 2 baseline flexure strength of this lot of material is 63.2 ksi, which is abnormally low for Code 2.

4.5.2 Static Components

Stress Rupture Testing of NGK SN-50 Sintered Silicon Nitride (SSN)

NGK SN-50 (SSN) has been tested in flexural stress rupture to obtain a preliminary assessment of material performance under anticipated peak-temperatures at steady-state conditions. Temperatures of interest were those anticipated for the turbine shroud and inner/outer diffuser housings, as summarized below:

Table 13. AGT101 Component And Material Summary.

Supplier	Material	Process	Condition	Qualification Bar							Ceramic Component						
				Room Temperature			Elevated Temperature				Room Temperature			Elevated Temperature			
				σ_θ[2]	M[3]	Population	σ_θ[2]	M[3]	F	Population	σ_θ[2]	M[3]	Population	σ_θ[2]	M[3]	F	Population
ACC																	
Inner Diffuser Outer Diffuser Turbine Shroud Baffle	RBSN (RBN104)	Slip Cast	As-Fired Longitudinally Ground Heat Treated	49.7 53.2 54.8	4.5 5.5 8.5	30 10 29	52.1	10.1	2200	10	44.3[4] 46.3	8.0 5.3	21 27				
Stator	RBSN (RBN124)	Injection Molded	As-Fired[1]	40.1	4.8	19	44.5	8.4	2200	23							
Rotor	Sintered Si_3N_4[7] Code 1	Slip Cast	Longitudinally Ground								123.9	16.4	10	98.6 71.0	5.7 36.8	1800 2200	5 5
	Sintered Si_3N_4[7] Code 2	Slip Cast	Longitudinally Ground	89.8	7.2	9	50.3	13.0	2200	10	119.0	21.4	10	99.0 63.7	10.3 9.3	1800 2200	5 5
Carborundum																	
Turbine Shroud, Stator	Sintered -SiC	Injection Molded	As-Fired	48.6	9.5	30	45.0	5.0	2500	10	55.4[5]	7.1	9				
Combustor Baffle	Sintered -SiC	Slip Cast	Longitudinally Ground	49.4	5.8	30	41.4	6.7	2500	10	53.0 51.6	7.3 8.9	9 4				
Transition Duct, Regenerator Shield, Backshroud	Sintered -SiC	Isopressed	Longitudinally Ground	57.7	7.7	30	56.2	11.9	2500	10							
Ford																	
Rotor	SRBSN (RM-2)	Slip Cast	Longitudinally Ground	109.3	19.8	6	73.1	16.4	2200	6							
Rotor	SRBSN (RM-3)[8]	Slip Cast	Longitudinally Ground	98.6[6]	19.0	10	77.6[6] 71.6[6] 70.8[6]	10.9 12.9 11.3	1832 2192 2552	5 5 5							
Rotor	SRBSN (RM-20)[8]	Slip Cast	Longitudinally Ground	130.4	13.3	10											
Stator	RBSN	Injection Molded	As-Fired	43.1	9.2	39	45.8	7.7	2200	10							
NGK																	
Backshroud, Transition Duct, Diffusers	Sintered Si_3N_4 (SN-50)	Isopressed	Longitudinally Ground	87.6	10.5	10	47.1	13.6	2000	7							
Turbine Shroud	Sintered Si_3N_4 (SN-54)	Isopressed	Longitudinally Ground	109.5	10.3	5	67.9 53.0 40.7 23.2	3.6 6.1 25.0 7.0	1800 2000 2200 2500	2 5 5 2							
Kyocera Turbine Shroud	Sintered SiC SC201	Isopressed	Longitudinally Ground	65.4	5.2	5											
			Ground and Heat Treated	78.5	10.4	5					66.5 70.5	19.7 12.0	5 5				
Corning																	
Flow Separator Housing	LAS	Slip	Longitudinally	14.0	18.8	11	13.5	9.7	2000	12	12.9	5.3	10	13.4 15.4 16.0	3.4 8.1 7.7	1800 2000 2050	5 10 9

All test bars 0.250 x 0.125 inch cross section unless noted. Bars tested in 4-point flexure, 1.50 inch outer span and 0.75 inch inner span. Cross head speed, 0.02 inch/minute

[1]Test bar cross section 0.31 x 0.15 inch

[2]Characteristic strength, ksi

[3]M = Weibull Modulus

[4]Test bar cross section 0.236 x 0.1 inch

[5]As machined, longitudinally ground

[6]Average flexure strength, ksi

[7]Code 1 = 8%-Y_2O_3, 4%-Al_2O_3
Code 2 = 6%-Y_2O_3, 2%-Al_2O_3

[8]Data supplied by vendor

Table 14. AGT101 Ceramic Material Characterization at Garrett.

	AiResearch Casting Co.					Carborundum Co.							Corning	Ford Motor Co.			NGK Locke	Pure Carbon	Kyocera
	Reaction-Bonded Si_3N_4			Sintered Si_3N_4		Sintered SiC			Reaction-Sintered SiC				LAS	SRBSN	RBSN	LAS			
	SC	IM		SC	IM	SC	IM	IP	CP	CM	IP	Hot Pressed SiC		SC	IM		IP	IP	IP
	RBN-104	RBN-124	RBN-126	SSN-502	SSN-522					KX-01	KX-02			RM-2			SN-50, SN-54	SC201	Refel
Flexure Strength																			
Room Temperature	S1-245	S1-251	S1-249	S3-46	S1-256	S2-61 S6-97	S1-266 S6-99	S1-265	S1-264 S2-59				S6	S4-28	S2-68	S6	S3-45, S10	S9-40	
Elevated Temp. T_1 (1800-2000F)		S1-251			S1-256				S1-264	S3-51	S4-25		S6			S6	S3-45, S10		
T_2 (2200F)	S1-245		S1-249		S1-257				S2-59 S1-264					S4-28	S2-68				
T_3 (2500F)	S1-245	S1-251	S1-249		S1-258	S2-61	S1-266	S1-265	S2-59 S1-264						S2-68		S10, S10		
Transverse Machined	S1-248				S1-255				S2-58 S1-277										
Longitudinal Machined	S1-248				S1-255		S1-266		S1-277	S3-51	S4-25			S4-28			S3-45		S3-48
Cut from Components	S6 CCM81 S10			S-9 S3-46 S4-		S10		S2-87 S10				S3-49	S10					S10	S3-38
Post-Machining Oxidation	S1-248 S7					S2-61			S2-59 S1-277		S4-25								S3-48
Oxidation																			
Gradient Furnace					S4-30									S4-30					
Dynamic Durability Rig	*								*					S4-28					
Stress Rupture																			
Static, Air					S4-31 S1-262 S2-63									S4-31			S10		
Dynamic, Gas Fired	S2-65								S2-65										
Interface Considerations																			
Compatibility Test	S5-38 CCM82					S5-38 CCM82	S5-38 CCM82		S5-38 CCM82	S5-38 CCM82			S5-38 CCM82				S5-38 CCM82	S9-46	
Sliding Tests	S2-74 S1-281						S9-46		S2-75										
Coating Development	S2-78 S1-280								S2-78 M15-13										
Shrink Fit/ Ratchet Tests				S6-52															
Thermal Shock (Stators)		S4-35					S4-35												
Spin Test (Rotor)																			
Bladeless Rotor				S3-46			S2-85	S2-85						CCM81					S3-48
Bladed Rotor				S5-35										CCM82					

*Tested under NASA 3500-Hour Durability Program, Contract DEN3-27.

SC = Slip Cast
IM = Injection Molded
IP = Isopressed
CP = Cold Pressed (Uniaxial)
SRBSN = Sintered Reaction Bonded Si_3N_4

Examples of References:

S1-245 = Page 245, First Semi-Annual Report

CCM82 = Paper presented at 1982 CCM

Table 15. AGT101 Static Component Predicted Stress and Temperatures.

	Normal Engine Lightoff	Steady-State Maximum Power N = 100 Krpm T_4 = 2500F		Steady-State Idle N = 50 Krpm T_4 = 2146F	
Component (Type) Material	Peak Stress, ksi/ Temperature, F	Peak Stress, ksi/ Temperature, F	Peak Temperature, F/ Stress, Ksi	Peak Stress, ksi/ Temperature, F	Peak Temperature, F/Stress, ksi
Outer Diffuser (A3A)					
RBSN	14.9/861	<2.0/1850	1950/<1.0	<1.0/2025	2050/<1.0
Turbine Shroud (B3)					
RBSN	16.7/1219	<5.0/2400	2450/<3.0	<5.0/2050	2100/<3.0
SSN	34.1/1155	<5.0/2400	2450/<3.0	<5.0/2050	2100/<3.0
Stators (Single-Vane)					
RBSN	26.2/1550	<3.5/2475	2475/<3.5	<3.0/2125	2125/<3.0
SASC	32.5/1100	<5.0/2475	2475/<5.0	<4.0/2125	2100/<4.0
Flow Separator Housing (Without Stators)					
LAS	13.1/1980	<7.9/1730	1995/<1.8	<2.0/1990	1740/<0.2
RBSN	19.4/1280	<14.2/1300	1990/<1.7	<19.7/1260	1735/<0.2
Transition Duct					
RBSN	5.3/1383	<2.0/2175	2300/<1.0	<1.0/2050	2075/<1.0
Combustor Baffle					
SASC	18.1/1355	<3.0/2550	2600/<1.0	<3.0/2175	2225<1.0
Backshroud (Hollow Core)					
SSN	5.3/563	<1.0/2500	2500/<1.0	<3.0/2145	2145<1.0

Table 16. AGT 101 SI_3N_4 Rotor Predicted Stresses And Temperature.

Condition	Peak Stress, ksi/ Temperature, F	Peak Temperature, F/ Stress, ksi
1 N = 50,000 rpm TIT = 2241F	18.0/1750	2100/ 5.0
2 N = 77,000 rpm TIT = 2500F	22.0/1750	2200/ 8.0
3 N = 100,000 rpm TIT = 2500F	33.0/1950	2150/ 14.0

Component	Peak Temperatures, F	Engine Condition
Turbine shroud	2500	Maximum power
Diffuser housings	1750	Maximum power
Diffuser housings	2000	Idle

Testing at 1750 and 2000F was performed using a stepped stress rupture approach with an initial load of 15 ksi. Loads were held for 24 hours and were increased in 5 ksi increments to 30 ksi.

At the completion of the 96-hour test, the test bars were measured for deflection, and then loaded to failure at the respective stress rupture temperature.

To assess the material behavior at 2500F, two test bars were tested for 5 and 30 minutes, at 5 and 2.3 ksi respectively (these short durations were selected in anticipation of creep at this temperature). At the completion of the 2500F exposure the test bars were measured for deflection, and then flexure tested at room temperature.

Results of this testing are summarized in Table 19. As the tabulated data indicates, no test bars failed during stress rupture loading, but all showed some degree of creep deflection. Post stress rupture flexure testing indicated no strength loss as a result of the exposure when compared with the baseline flexure results presented in Reference 3 and also summarized in Table 19 herein. However, the occurrence of significant creep at the 2500F load conditions indicates that the use of SN-50 must be limited to temperatures well below 2500F. Additionally at 2000F, stress levels must be maintained below 30 ksi to avoid the occurrence of creep.

Flexure Testing of NGK SN-54 (SSN)

Isopressed SN-54 sintered Si_3N_4 received from NGK as certification material for turbine shrouds was flexure tested at room and elevated temperatures. Bars were tested in the machined condition as received from NGK. Test temperatures were 70, 1800, 2000, 2200 and 2500F. Results are summarized in Table 20. Scanning electron microscopy (SEM) photomicrographs of typical fracture surfaces are presented in Figures 59 and 60. As summarized, slow crack growth was observed on test bars tested at 2000F and higher temperatures. The SEM photographs illustrate a coarser and more glassy appearance of the

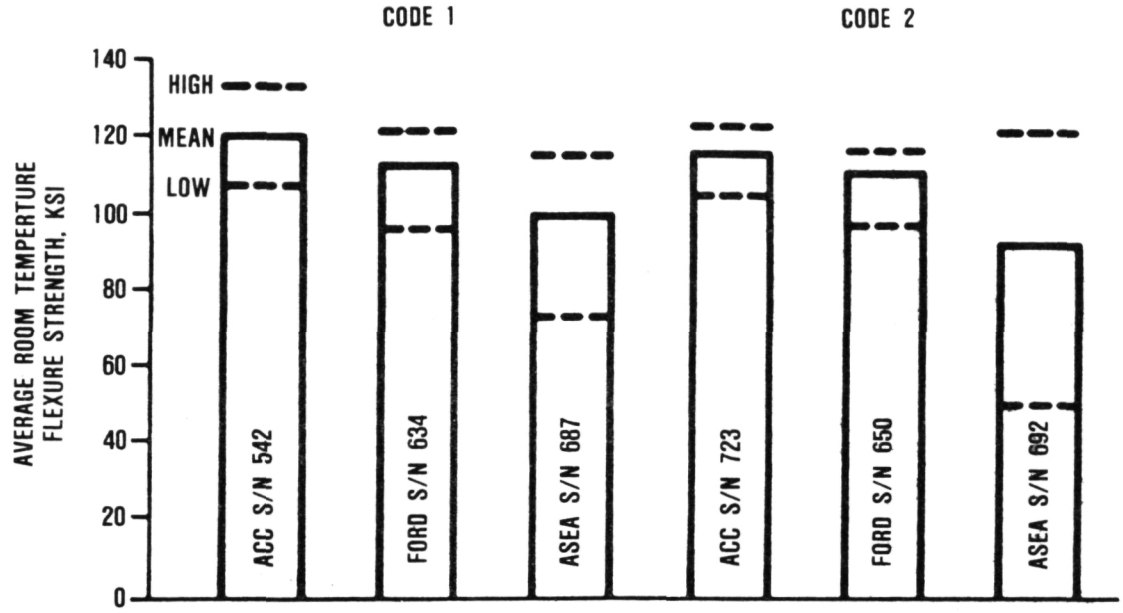

	ACC S/N 542 3.26 g/cm^3	FORD S/N 634 3.29 g/cm^3	ASEA S/N 687 3.25 g/cm^3	ACC S/N 723 3.25 g/cm^3	FORD S/N 650 3.27 g/cm^3	ASEA S/N 692 3.25 g/cm^3
ROOM TEMPERATURE 10 DATA POINTS	120.3	111.9	99.3	116.3	111.1	91.8
1800F 5 DATA POINTS	91.5	78.2	80.5	94.7	81.5	80.5
2200F 5 DATA POINTS	70.0	50.5	52.6	60.7	65.9	68.3

All bars tested were 0.125 x 0.250 inch in cross section. Loads were applied in 4-point flexure using 0.75 and 1.5 inch inner and outer spans, respectively. Fracture strengths were obtained at 0.02 in/min crosshead speed.

Figure 58. Flexure Strength of AGT101 Rotors.

fracture and surface as the test temperature is increased.

Component Cut-Up Flexure Testing

Several ceramic components which fractured in thermal screening and engine tests have been machined to provide test bars for strength evaluation. Component cut-up, certification, and/or baseline flexure strengths are summarized in Tables 21 and 22.

Density Study of Reaction Bonded Silicon Nitride (RBSN) Turbine Shroud

ACC RBSN Turbine Shroud S/N 545 was fractured during thermal screening as discussed later. Fracture segments from this component were measured for density using the ASTM C20-74 immersion technique. A summary of the density measurements, presented in Figure 61, indicates that the RBSN part is uniformly dense at an acceptable density of 2.7 g/cm^3.

Table 17. ACC Code 1 Sintered Silicon Nitride Stress Rupture Test Results.

Temperature	Stress Level, ksi	Time Under Stress, hrs	Room Temperature Strength After Stress Rupture, ksi	Location of Fracture Origin
1650	30	100	67.0	Tensile face
1650	30	100	79.9	At machining flaw
1750	6	100	107.5	Tensile face
1750	6	100	104.3	Chamfer
2050	30	100	89.9	Internal
2050	30	100	109.6	Internal metallic inclusion
2150*	6	100	80.8	Tensile surface
2150*	6	100	73.5	Tensile surface

*Maximum deformation measured is 0.001 inch.

All bars tested were 0.125 x 0.250 inch in cross section. Loads were applied in 4-point flexure using 0.75 and 1.5 inch inner and outer spans, respectively. Fracture strengths were obtained at 0.02 in/min crosshead speed.

RBSN Baffle S/N 593 Cut-Up Analysis

A summary of the results for RBSN Baffle S/N 593, were reported in Table 22. However, the cut-up flexural results were well below acceptable strength values.

SEM photographs of several fracture origins of these test bars are presented in Figure 62.

Lithium Aluminum Silicate (LAS) Flow Separator

S/N 17 Cut-up Analysis

Flow separator housing S/N 17, fabricated from Corning Code 9458 LAS, which fractured during engine 002C Build 11 testing, was cut up for material evaluation. Test bars were machined from the area indicated in Figure 63. Flexure testing was performed at room temperature (70F), 1800, 2000, and 2050F, and was followed by SEM examination of fracture origins in selected bars. Results are summarized in Table 23 and Figures 64 through 67. In addition to the modulus of rupture (MOR) testing, two test bars were tested in flexural stress rupture at 5 ksi and 2000F for 100 and 165 hours, respectively. Neither test bar fractured during stress rupture exposure, so both were measured for deflection, and then flexure tested to fracture at room temperature. A summary of these results is presented in Table 24.

Table 18. ACC Code 2 SSN Stress Rupture Test Results.

Temperature, F	Stress Level, ksi	Time Under Stress, hrs	Room Temperature Strength After Stress Rupture, ksi	Comments
1650	30	100	68.6	Chamfer
1650	30	100	84.6	Metallic inclusion
1750	6	100	66.2	Chamfer
1750	6	100	71.4	Chamfer
2050	30	100	44.9	Tensile surface
2050	30	100	42.2	Chamfer
2150	6	100	54.5	Tensile surface
2150	6	100	57.6	Tensile surface

Bars cut from plate with a density of 3.24 g/cm^3.

Maximum deformation measured 0.001 inch.

Room temperature baseline strength of this Code 2 material is 63.2 ksi.

*All bars tested were 0.125 x 0.250 inch in cross section. Loads were applied in 4-point flexure using 0.75 and 1.5 inch inner and outer spans, respectively. Fracture strengths were obtained at 0.02 in/min crosshead speed.

As tabulated, these results show no strength degradation over the ambient (70F) to 2050F temperature range in fast fracture, however, creep does occur at 2000F. Examination of the test bars flexure tested at 2050F also reveal a glazing or blunting of the surface features within the pore origin.

Laser Marking of Ceramic Materials

The effect of laser marking on the strength of five ceramic materials was investigated to determine whether this technique would be suitable for permanently marking AGT101 parts. Positive identification of engine hardware for the AGT program is necessary to keep component traceability. Samples of the five ceramic materials (RBSN, SASC, LAS, NC132 and SSN-501) were used to determine the laser parameters that would clearly mark the ceramic surface without visible damage. Only laser marking of the LAS materials was unacceptable, due to visible damage of acceptably marked materials. Subsequently, test bar samples were marked with a series of XHs along the length of the test bars to simulate worst case marking orientations.

Table 19. Stress Rupture Results For NGK SN-50 Sintered Si_3N_4.

S/N	Temperature, F	Load, ksi*	Time, hrs	Deflection, inch	Creep, percent	Fracture Strength, ksi at F	Comment
10019	1750	15	24				
		20	24				
		25	24				No SR** failure
		30	24	0.002	0.18	63.4 at 1750	Tensile face fracture
10030	2000	15	24				
		20	24				
		25	24				No SR failure
		30	24	0.020	1.77	43.3 2000	Slow crack growth
10024	2500	5	0.08	0.011	0.98	94.2 at 70	No SR failure Tensile face fracture
10029	2500	2.3	0.5	0.008	0.67	91.9 at 70	Both bars showed oxide penetration

*All bars tested were 0.125 x 0.250 inch in cross section. Loads were applied in 4-point flexure using 0.75 and 1.5 inch inner and outer spans, respectively. Fracture strengths were obtained at 0.02 in/min crosshead speed.

**SR = Stress Rupture

One-half of the test bars from each material were given the established heat treatment for healing surface flaws. All test bars were flexure tested at room temperature with the laser marked surface in tension. Table 25 summarizes the flexure strength data of laser marked specimens. Carborundum SASC and ACC RBN-104 laser-marked and heat-treated materials showed no reduction in strength due to the laser marking and did not fracture in the laser marked area, as long as the materials were heat treated. The flexure strength after laser marking of these materials without heat treating showed a reduction in strength and all fractures originated at the laser marking.

ACC SSN-501 and Norton NC132 test specimens failed at the laser marking, both with and without heat treatment. But the flexure strength of the specimens was adequate in all cases.

In summary, laser marking parameters have been established for marking four ceramic materials frequently used on the AGT101 program. Properly processed laser

Table 20. Flexure Strength Test Results for NGK SN-54.

Temperature F	Characteristic Strength, ksi (average, ksi)	Weibull Modulus (Standard Deviation)	Number of Bars	Remarks
70	109.5 (104.8)	10.3 (10.1)	5	
1800	67.9 (61.2)		2	
2000	53.0 (49.4)	6.1 (7.0)	5	Slow crack growth
2200	40.7 (39.9)	25.1 (1.6)	5	Slow crack growth
2500	23.2 (21.9)		2	Oxidized surface

All bars tested were 0.125 x 0.250 inch in cross section. Loads were applied in 4-point flexure using 0.75 and 1.5 inch inner and outer spans, respectively. Fracture strengths were obtained at 0.02 in/min crosshead speed.

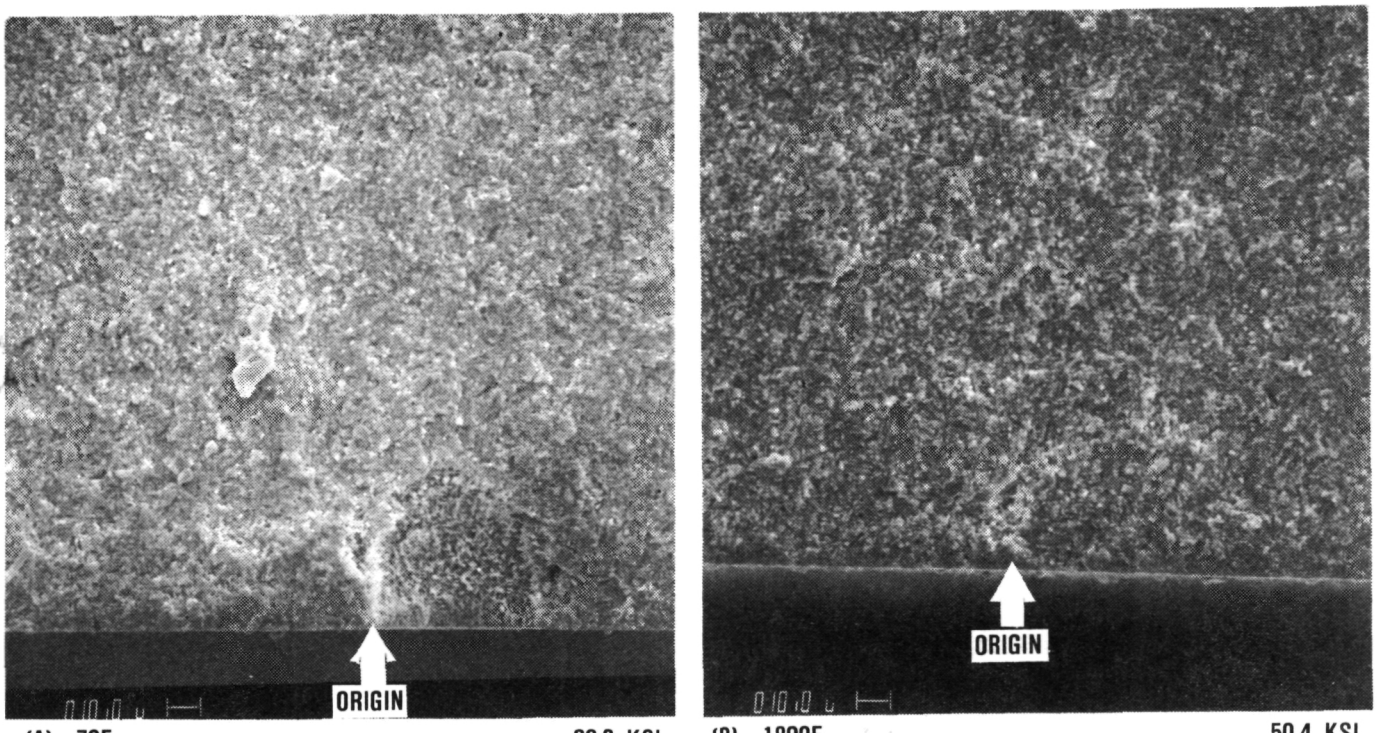

(A) 70F 89.3 KSI (B) 1800F 50.4 KSI

Figure 59. Representative: Fracture Origins for NGK SN-54.

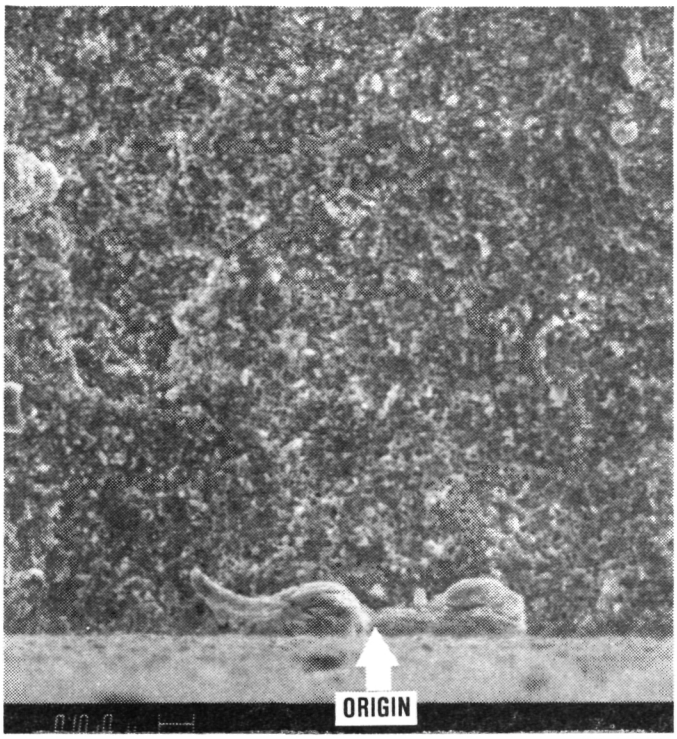

(A) 2000F 37.4 KSI

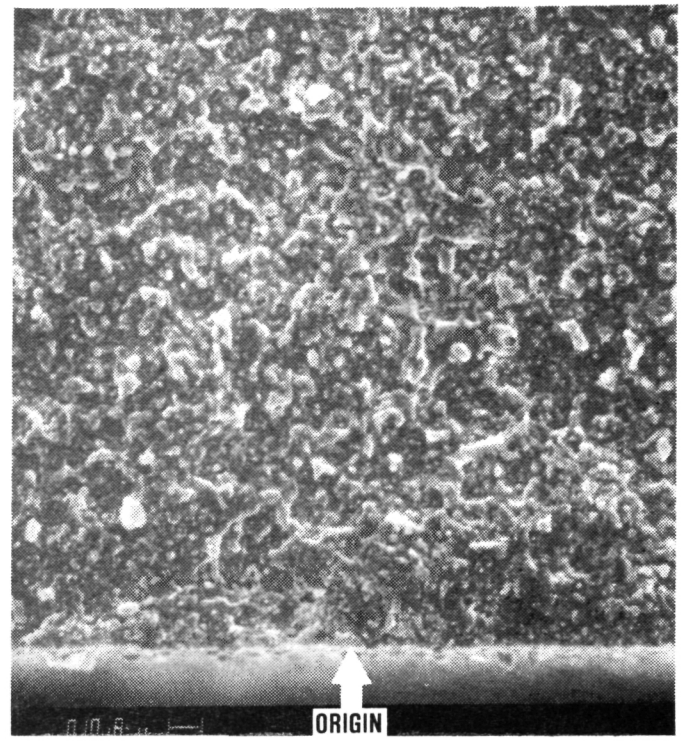

(B) 2200F 42.3 KSI

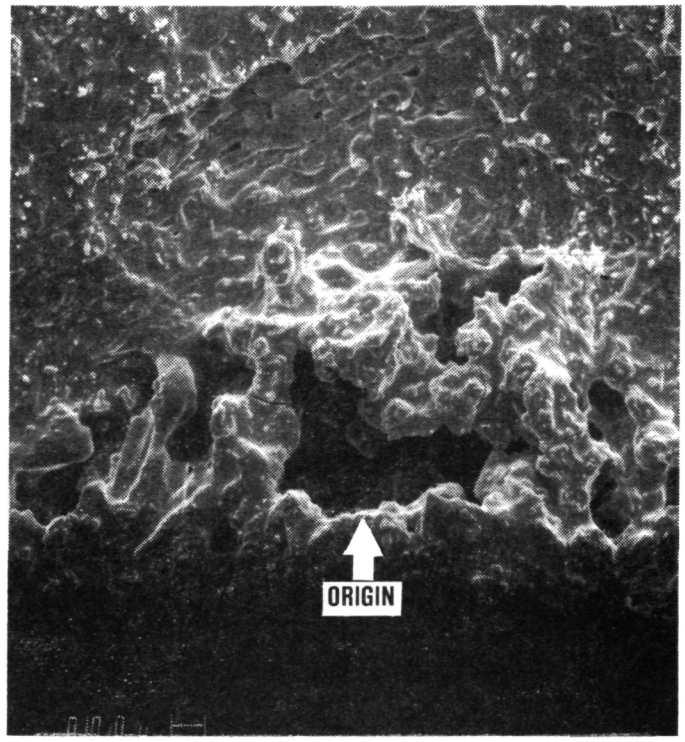

(C) 2500F 23.9 KSI

Figure 60. Fracture Origins For NGK SN-54.

Table 21. Component Cut-Up Room Temperature Flexure Strength Summary.

Component/ Source Material	Test Bar Orientation	Component Cut-Up			Certification Bars			Baseline Test Bars		
		No. of Bars	Strength, ksi Characteristic (average)	Modulus (Standard Deviation) Weibull	No. of Bars	Strength, ksi Characteristics (average)	Modulus (Standard Deviation) Weibull	No. of Bars	Strength, ksi Characteristic (average)	Modulus (Standard Deviation) Weibull
Turbine Shroud S/N 468/ ACC/RBN104		17 cone 6 tab	59.0 (57.1) 57.2 (54.6)	15.4 (5.0) 10.00 (5.6)		Not Tested		29	54.8 (51.8)	8.5 (6.9)
Transition Duct S/N 113/ CBO/SASC		23	34.3 (32.6)	9.1 (4.0)	5	36.9 (34.6)	6.8 (4.6)	30	57.7* (54.3)*	7.7 (8.0)
Turbine Backshroud S/N 101A/ CBO/SASC		12	41.8 (40.4)	14.2 (3.1)		Not Tested		30	57.7* (54.3)*	7.7 (8.0)
Turbine Shroud S/N 106/ Kyocera/ SC 201		5	70.5 (67.8)	12.0 (5.4)	5	78.5 (75.2)	10.4 (7.4)		Not Tested	
Baffle S/N 122/ CBO/SASC		5	51.6 (49.1)	8.9 (5.3)	4	67.5 (65.7)	16.6 (3.8)	30	49.4	5.8

ACC - AiResearch Casting Company
CBO - Carborundum

*Not heat treated

All test bars have a 0.250 x 0.125 inch cross section and have been ground in longitudinal direction and heat treated 2 hours at 2200F. Flexure testing was performed at 0.02 inch per minute cross head speed with 1.5 inch outer span, 0.75 inch inner span.

Table 22. Component Cut-Up Room Temperature Flexure Strength Summary.

Component/ Source Material	Test Bar Orientation	Component Cut-Up			Certification Bars			Baseline Test Bars		
		No. of Bars	Strength, ksi Characteristic (average)	Modulus (Standard Deviation Weibull	No. of Bars	Strength, ksi Characteristics (average)	Modulus (Standard Deviation) Weibull	No. of Bars	Strength, ksi Characteristic (average)	Modulus (Standard Deviation) Weibull
Turbine Shroud S/N 101/ Kyocera/ SC 101		5	66.5 (64.5)	14.7 (4.2)	5	78.5 (75.2)	10.4 (7.4)		Not Tested	
Flow 4. Separator Housing S/N 17/ Corning/ LAS		10 5 10 9	12.9 (11.9)* 13.4 (12.0)[1] 15.4 (14.6)[2] 16.0 (15.0)[3]	5.3 (2.2) 3.4 (3.2) 8.1 (1.9) 7.7 (2.1)		Not Tested		11 12	14.0* 13.5[2]	18.8 9.7
Turbine Backshroud S/N 104A CBO/SASC		5	54.4 (49.0)	6.2 (7.7)		Not Tested		30	57.7* (54.3)	7.7 (8.0)
Baffle 4. S/N 593/ ACC/ RBN104		5	31.1 (28.9)	5.7 (4.8)	4	Not Tested		29	54.8 (51.8)	8.5 (6.9)

ACC - AiResearch Casting Company
CBO - Carborundum

*Not heat treated 1. Tested at 1800F 2. Tested at 2000F 3. Tested at 2050F 4. Additional studies discussed elsewhere in report

All test bars have a 0.250 x 0.125 inch cross section and have been ground in longitudinal direction and heat treated 2 hours at 2200F. Flexure testing was performed at 0.02 inch per minute cross head speed with 1.5 inch outer span, 0.75 inch inner span.

marked materials show little or no material strength loss as a result of laser marking.

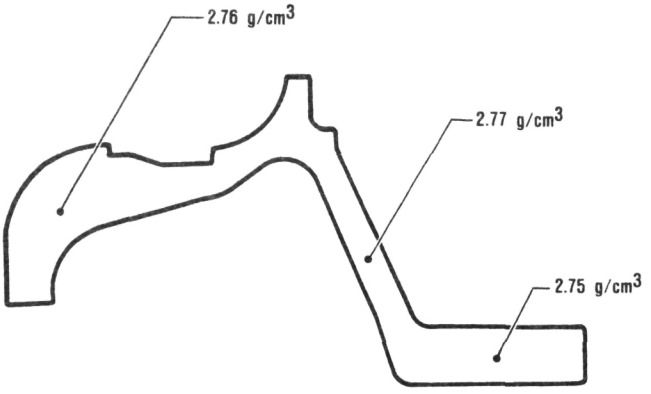

Figure 61. Turbine Shroud S/N 545 Density Summary.

4.5.3 Ceramic Turbine Rotor Deliveries

ACC has fabricated rotors of both the Code 1 (8-percent Y_2O_3, 4-percent Al_2O_3) and the Code 2 (6-percent Y_2O_3, 2-percent Al_2O_3) composition during the past year. Final densification is accomplished at ACC, ASEA or Ford. Table 26 summarizes the Codes 1 and 2 rotors received between July 1, 1984 and June 30, 1985. ACC is currently concentrating their rotor efforts on the lower additive Code 2 material. Work is continuing on development of a sintered reaction bonded Si_3N_4 composition.

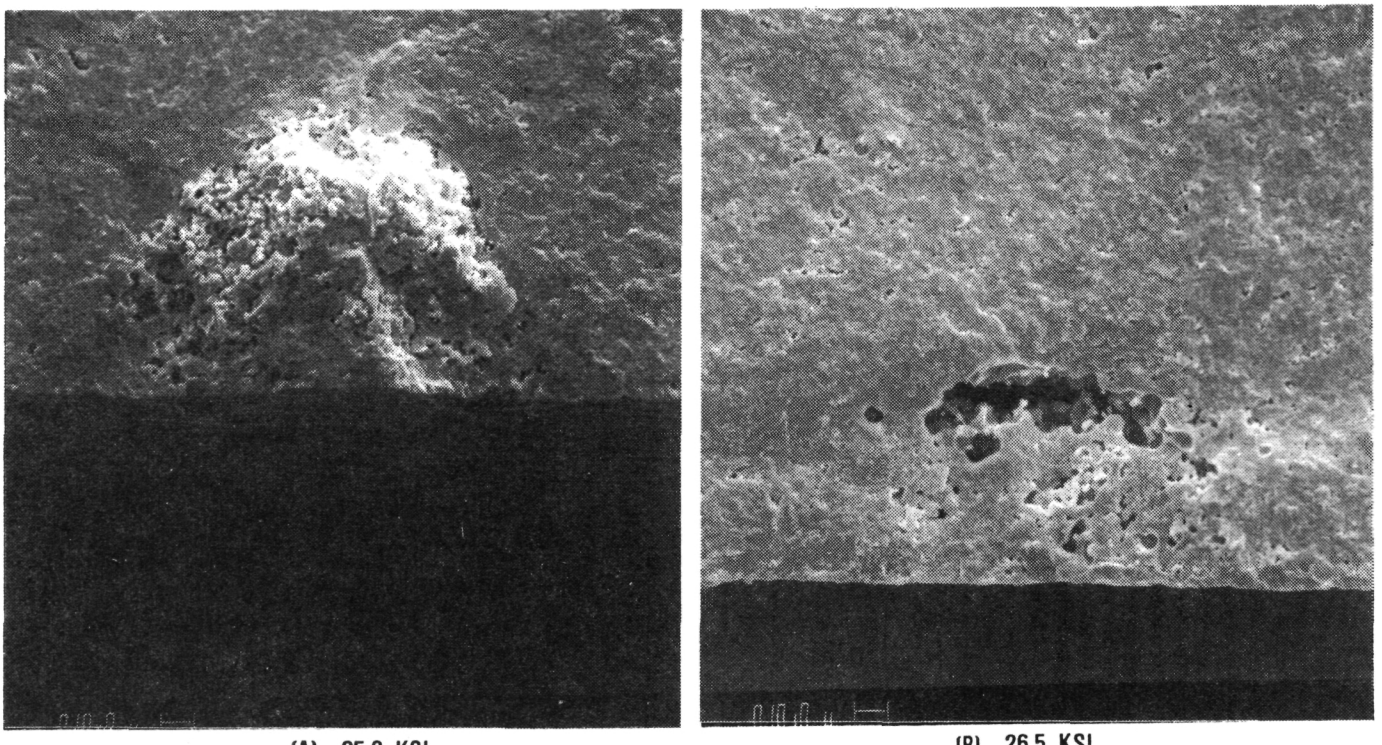

(A) 25.9 KSI (B) 26.5 KSI

Figure 62. Fracture Origins for Test Bars Cut From ACC RBSN 104 Baffle S/N-593.

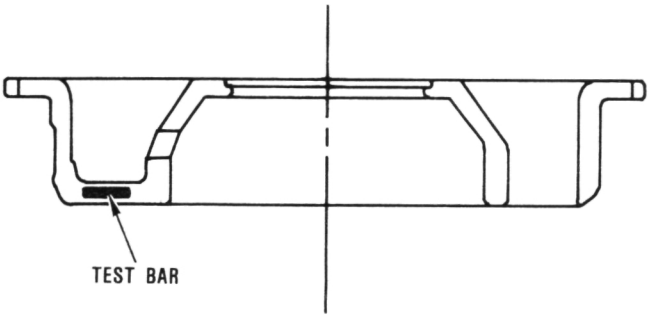

Figure 63. Flow Separator Housing Cut-Up Test Bar Location.

4.5.4 Screening Rigs

The ceramic structural parts received from AGT101 program suppliers continue to be qualified for engine testing according to the flow chart shown in Figure 68. Logic for the iterative design/inspection/test/redesign approach in developing engine quality hardware was to eliminate discrepant parts before reaching the engine test phase. Each component is, therefore, subjected to 40X visual and dimensional inspection, non-destructive evaluation (NDE), and mechanical and thermal proof/screening rigs for final qualification prior to engine installation.

Table 23. Flexure Strength Results for Cut-Up LAS Flow Separator Housing S/N 17.

	Temperature, F			
	70	1800	2000	2050
MOR, ksi*	13.0 14.4 10.1 13.4 13.7 7.5 10.9 10.1 12.1 13.8	13.8 8.6 13.2 15.6 8.6	15.0 18.1 13.8 12.1 16.1 16.1 15.3 13.8 11.8 13.7	19.3 14.8 15.4 16.8 15.8 13.5 13.8 12.8 13.2
Characteristic Strength, ksi	12.9	13.4	15.4	16.0
Weibull Modulus	5.3	3.4	8.1	7.7
Average Strength, ksi	11.9	12.0	14.6	15.0
Standard Deviation, ksi	2.2	3.2	1.9	2.1

*All bars tested were 0.125 x 0.250 inch in cross section. Loads were applied in 4-point flexure using, 0.75 and 1.5 inch inner and outer spans, respectively. Fracture strengths were obtained at 0.02 in/min crosshead speed.

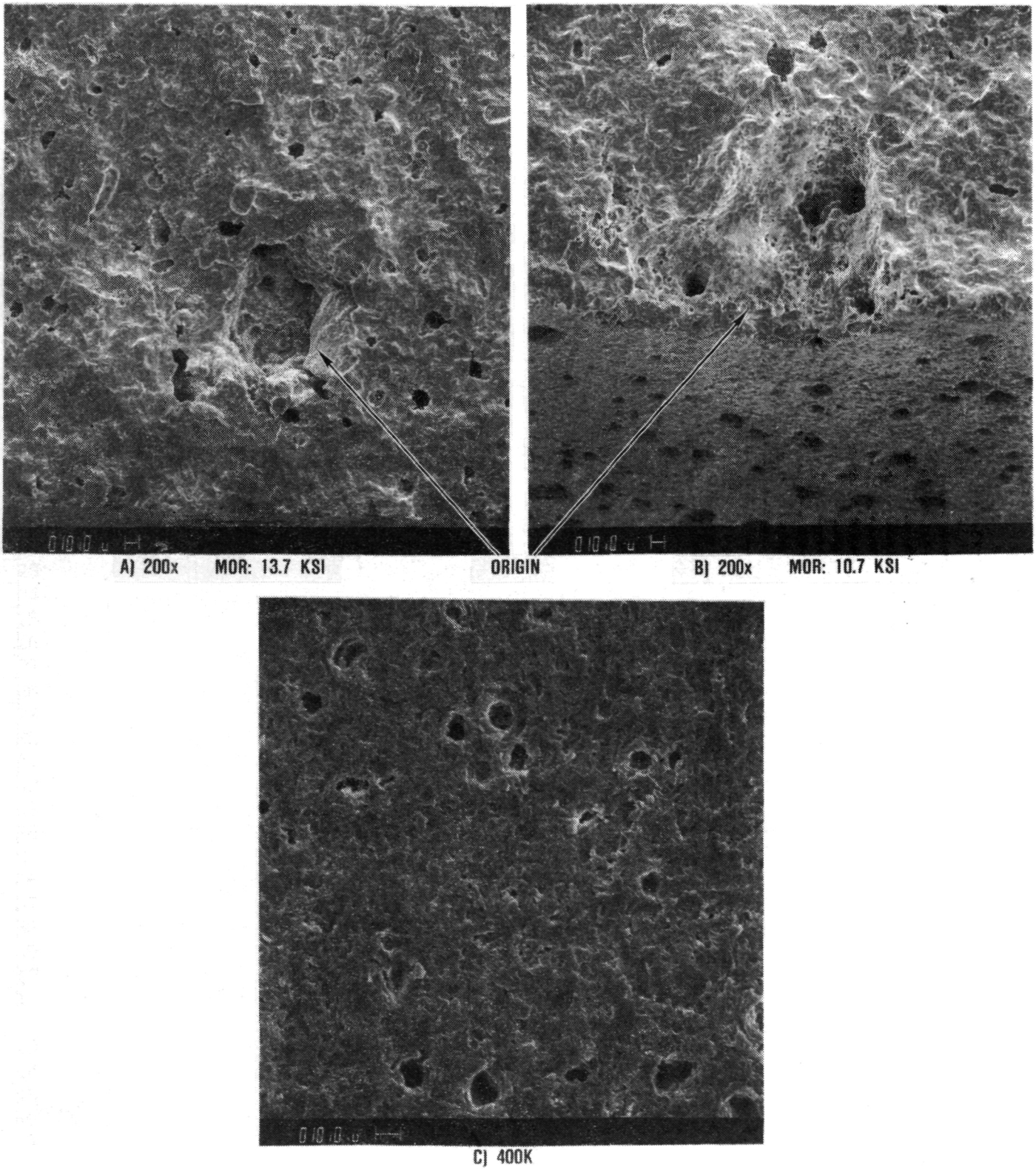

Figure 64. Internal (a) and Surface (b) Fracture Origin and As-Machined Surface (c) For LAS Flexure Tested at Room Temperature (70F).

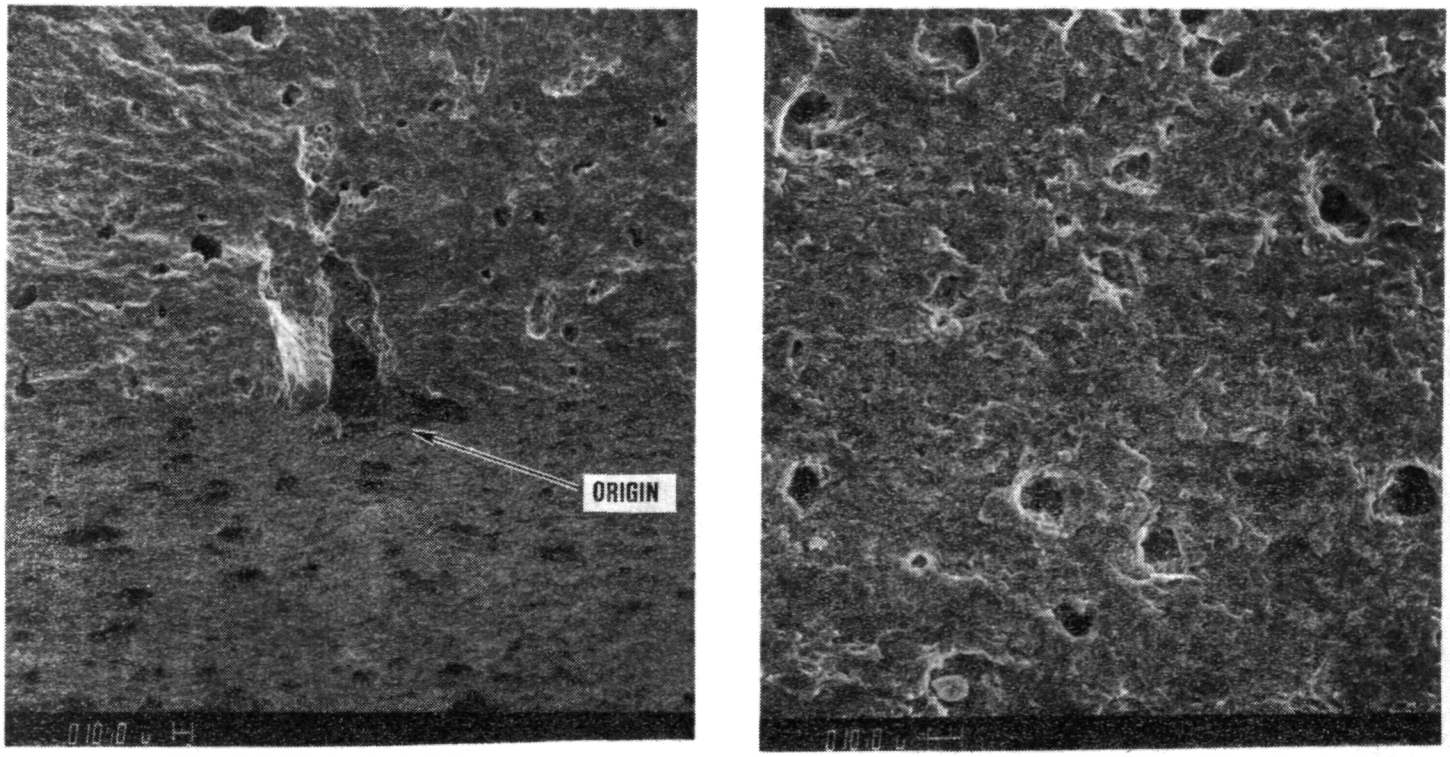

Figure 65. Fracture Origin (a) and Surface (b) of LAS Flexure at 1800F.

Major structural components are first tested in mechanical rigs to simulate the pressure and contact loading encountered in engine operation. These tests then are followed by a proof test in thermal screening rigs to simulate the maximum principal stresses encountered in engine operation. During this reporting period the thermal cycles for the screening rigs were defined so as to simulate stresses which exceed predicted engine stresses under normal start conditions by 25 percent. These proof cycles are given in tabular form in Table 27.

Testing at 2500F temperatures was initiated during this reporting period to investigate the high temperature effects on ceramics, such as static fatigue, contact loading, and endurance. This rig configuration was changed from the initial conception, due to concerns over rig inlet housing distortions when using pre-heated inlet air. The new rig is oriented vertically. Also, the rig eliminates the flow separator housing, an expensive and long lead time item, which would have been unnecessarily placed at risk in the previous rig design.

The final proof/qualification rig test (static structures rig) utilizes all of the ceramic components in an assembly of the engine structure, without the rotor, and checks the mechanical functioning of the assembly. Further, the static structures rig evaluates the sealing capability, component capability, axial and radial pilots, contact loading, and stresses at elevated temperature. Components fractured during any phase of this evaluation undergo intensive fractography and analytical reevaluation to determine the cause and recommended solutions.

The following events mark some of the significant steps made in the development of ceramic hardware during this reporting period:

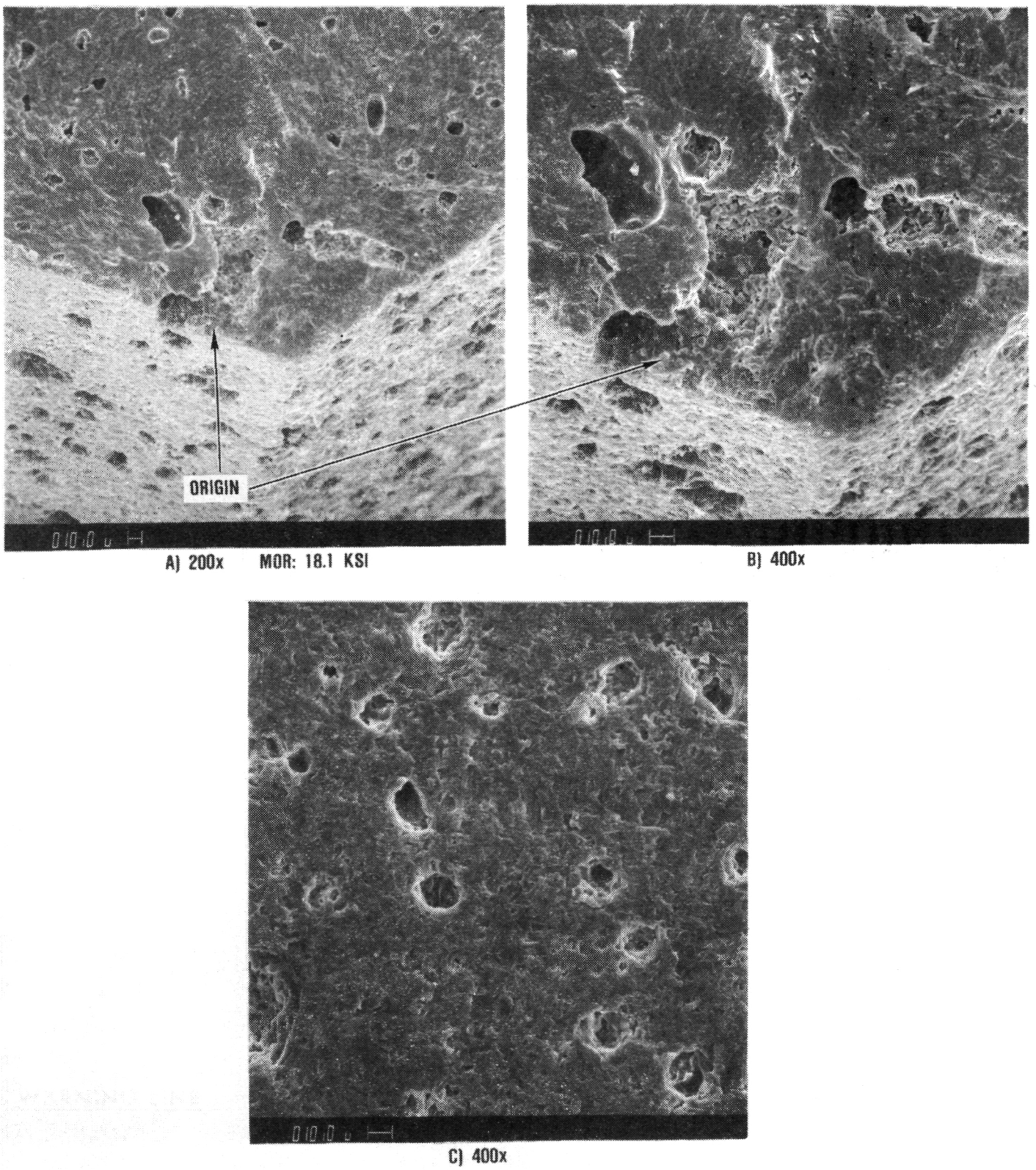

Figure 66. Fracture Origin (a and b) and surface (c) of LAS Flexure Tested at 2000F.

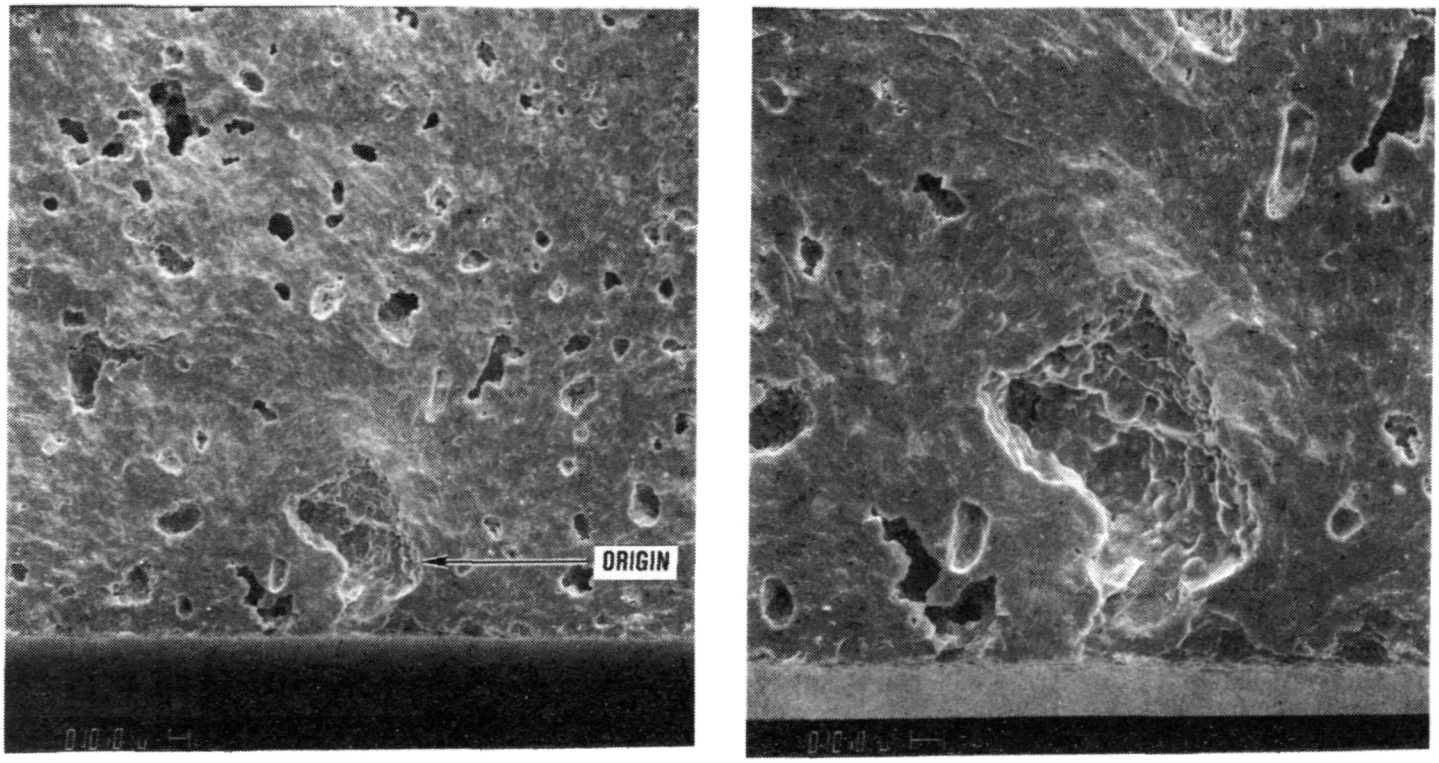

Figure 67. Fracture Origin at 200X(a) and 400X(b) of LAS Flexure Tested at 2050F. Note Glazed Surface of Interior of Origin.

Table 24. Stress Rupture Results for LAS Test Bars Cut From Flow Separator Housing S/N-17.

Temperature, F	Load, ksi	Time, hrs	Deflection, inch	Creep, percent	Fracture Strength, ksi at Room Temperature
2000	5	100	0.006	0.54	8.9
2000	5	165	0.016	1.44	12.1

*All bars tested were 0.125 x 0.250 inch in cross section. Loads were applied in 4-point flexure using 0.75 and 1.5 inch inner and outer spans, respectively. Fracture strengths were obtained at 0.02 in/min crosshead speed.

Table 25. Flexure Strength and Fracture Origins of Laser Marked Test Bars.

	Laser Marked		Laser Marked and Heat Treated	
	Mean Strength	Fracture Origin	Mean Strength	Fracture Origin
Carborundum SASC	32.7 ksi (5 samples)	At laser marking	51.1 ksi (5 samples)	Not at laser marking
ACC RBN-104 RBSN	33.2 ksi (5 samples)	At laser marking	38.2 ksi (5 samples)	Not at laser marking
ACC SN-501 SSN	98.1 ksi (7 samples)	At laser marking	84.6 ksi (7 samples)	At laser marking
Norton NC132 HPSN	89.2 ksi (8 samples)	At laser marking	105.0 ksi (8 samples)	At laser marking

1) A change was made from a liquid fuel burner to a natural gas burner, for the operation of thermal screening rigs. The advantages are better light-off characteristics and more stable operation under severe transient conditions, leading to more repeatable screening tests.

2) The acquisition and use of new acoustic emissions monitoring equipment from Physical Acoustics Corporation allows for diskette recording of acoustic emission (AE) data and hard copy graphics display of the AE data generated by the test. This equipment also is used to monitor AE during engine tests.

3) Fracture of a ceramic turbine backshroud during a structures rig qualification test in August 1984 led to a design change which incorporates a hole in the center of the turbine backshroud. In this way the highly stressed area of the part was, in fact, physically eliminated from the design. A piece of insulation is installed between the backshroud and the baffle to avoid thermally stressing the combustor baffle. This is particularly significant in the 2100F configuration engine, where bore cooling is used to cool the dual-alloy rotor.

4) Laser marking of ceramic components was initiated, with the locations for marking being selected to coincide with areas of low stress. Guidelines for marking also dictate that the lowest power setting consistent with legibility be used. To date, no ceramic fractures have been caused by the laser markings.

5) The fracture of stator segments during thermal screening, with fracture origin at the trailing edge, led to a design change for the stator segments. This change consists of a radial cutback to the trailing edge, as shown in Figure 69.

6) The repeated failure of RBSN turbine shrouds to withstand a mechanical screening test simulating engine maximum power pressure loading led to a design change in this part as well. The locating slots at the turbine shroud mounting flange were eliminated. The turbine shroud mounting system, which includes the rocker and bolt assemblies, was shown to adequately retain

Table 26. ACC Rotors Received July 1, 1984-June 30, 1985.

Rotor Serial Number	Composition	Status	Density, g/cm^3	Comments
573	Code 1	Sintered at Ford	3.27	Burst at 78 krpm
632	Code 1	Sintered at Ford	3.28	
633	Code 1	Sintered at Ford	3.29	
634	Code 1	Sintered at Ford	3.29	Cut-up for flexure strength
637	Code 1	Sintered at Ford	3.27	
638	Code 1	Sintered at Ford	3.27	
641	Code 1	Sintered at Ford	3.29	
642	Code 1	Sintered at Ford	3.28	
643	Code 1	Sintered at Ford	3.29	
648	Code 1	Sintered at Ford	3.27	
650	Code 2	Sintered at Ford	3.27	Cut-up for flexure strength
651	Code 1	Sintered at Ford	3.30	
652	Code 1	Sintered at Ford	3.30	Burst at 121 krpm
658	Code 1	Sintered at Ford	3.29	
686	Code 1	Sintered at ASEA	3.26	
687	Code 1	Sintered at ASEA	3.25	Cut-up for flexure strength
688	Code 1	Sintered at ASEA	3.27	Failed NDE - burst at 101 krpm
689	Code 2	Sintered at ASEA	3.24	
690	Code 2	Sintered at ASEA	3.24	
691	Code 2	Sintered at ASEA	3.24	
692	Code 2	Sintered at ASEA	3.25	Cut-up for flexure strength
723	Code 2	Sintered at ACC	3.25	Cut-up for flexure strength
724	Code 2	Sintered at ACC	3.24	

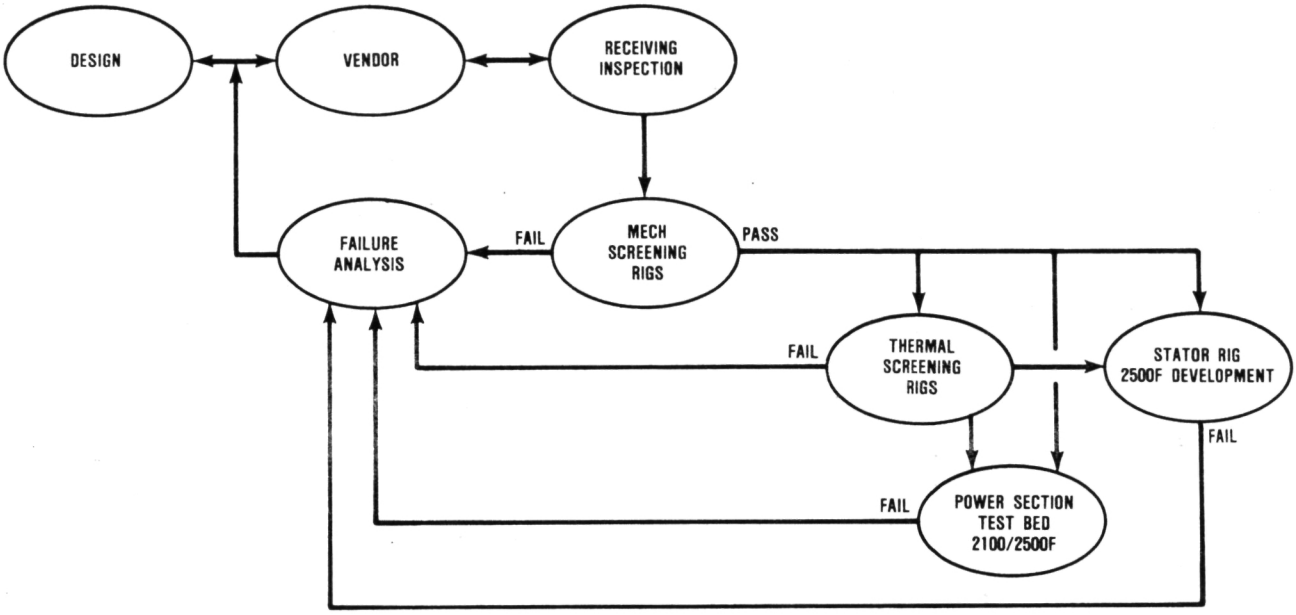

Figure 68. Ceramic Component Qualification Sequence.

Table 27. AGT101 Static Components Proof Test Cycles.

Component(s)	Material	$\dot{m}$, lbm/min	To, F	T_{rig}, F	$\Delta t_{L/O}$, sec	$t_{S/D}$, sec	Number of Cycles
Transition Duct, Baffle	All Materials	22.6	70	1800	10	600	1.5
Inner + Outer Diffusers	RBSN SSN	17.1	70	2000 2000	10	600	1.5
Turbine Shroud	RBSN SSN SASC	10.0	200	1575 1630 1720	15	600	1.5
Stators	All Materials	17.1	70	2225	10	35	1.5

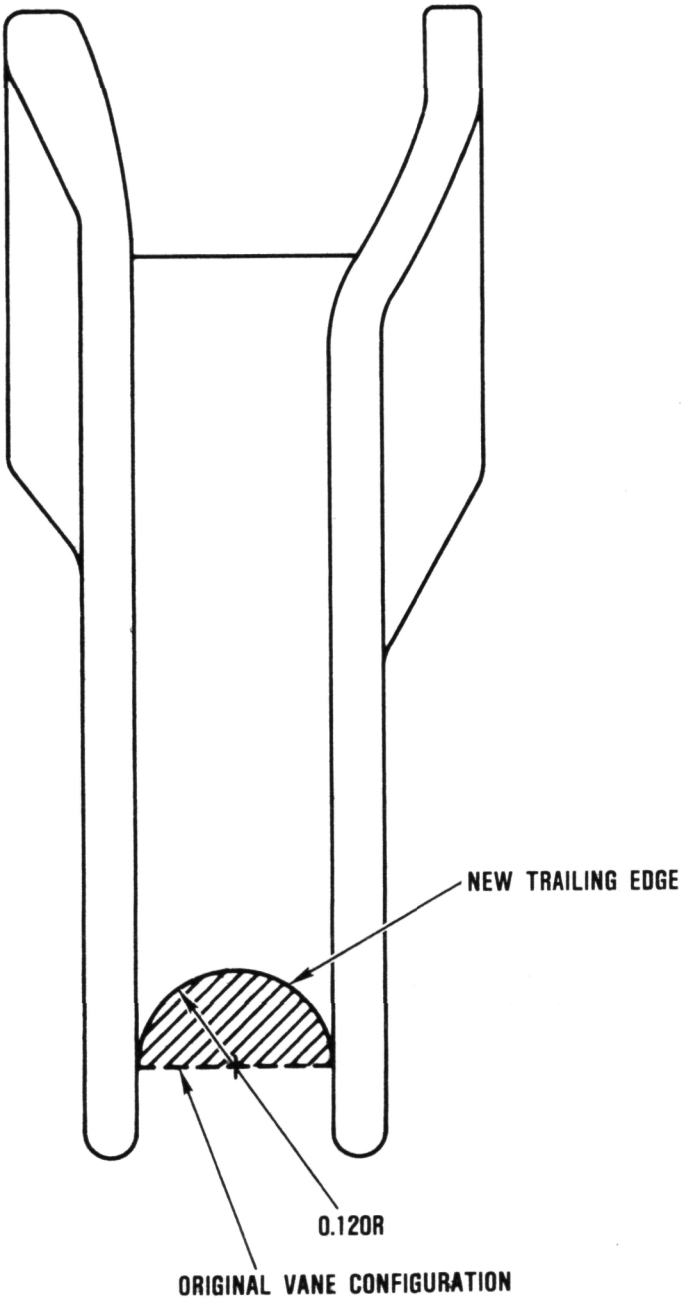

Figure 69. Cutback of Stator Vane Trailing Edge.

the turbine shroud in position in a shake-table test. The slotless configuration, which relies upon frictional loads alone to maintain turbine shroud position, withstood a 12-g load.

7) Sufficient confidence was gained in the ceramic static structures rig testing so that ceramic structural components are now considered qualified for engine use without passing through this phase of screening. The emphasis upon structures rig testing will thereby be shifted to leakage investigations.

4.5.4.1 Ceramic Components Thermal Screen Tests

Turbine Shroud/Stators Screening Rig

Testing of ceramic turbine shrouds and stators was performed during this reporting period according to the data in Table 28. There are several noteworthy items that deserve further expansion and explanation:

- In testing on July 11, 1984 a Sintered Alpha Silicon Carbide turbine shroud was successfully screened to a 1400F temperature, which represents a peak stress of 45.7 ksi in the part. On a subsequent run to 1600F, the turbine shroud fractured approximately 80 seconds into the test cycle. At this point in time the calculated stress in the part was 48 ksi, indicating that the part had just barely survived the 1400F cycle. Due to its limitations under thermal stress conditions, SASC is not viewed as a favorable candidate for the current turbine shroud design.

- On August 6, 1984 an RBSN turbine shroud was screened with a Ford integral stator ring (SRBSN). All parts survived an initial 1600F (15-second transition) cycle. During the second cycle to 1800F (15-second transition), the stator ring broke and caused the shroud to fail on shutdown. The stator ring fracture origins were approximately 180 degrees apart; both origins were in the trailing edges where the stator vane meets

Table 28. Turbine Shroud and Stator Screening Tests.

Date	Test Items	Transient Cycle, Flow	Result
7-5-84	Turbine Shroud S/N 544 (RBSN)	15 sec to 1600F, 10 lb/min	OK
7-10-84	Turbine Shroud S/N 547 (RBSN)	15 sec to 1600F, 10 lb/min	OK
7-11-84	Turbine Shroud S/N 101 (SASC)	15 sec to 1400F, 10 lb/min	OK
7-11-84	Turbine Shroud S/N 101 (SASC)	15 sec to 1600F, 10 lb/min	Fracture
7-18-84	Turbine Shroud S/N 548 (RBSN)	15 sec to 2000F, 10 lb/min	OK
8-6-84	Ford Stator No. 5 (RBSN)	15 sec to 1800F, 10 lb/min	Fracture
11-16-84	Stator Set 8 (RBSN)	Normal start per Figure 70	OK
12-7-84	Turbine Shroud 116 (SSN)	Normal start per Figure 70	OK
2-1-85	Turbine Shroud 117 (SSN)	Normal start per Figure 70	OK
2-4-85	Stator Set 5 (SASC)	Normal start per Figure 70	Fracture
3-6-85	Stator Set 9* (RBSN)	Normal start per Figure 70	OK
5-3-85	Turbine Shroud 694 (RBSN)	Normal start per Figure 70	OK
5-3-85	Stator Set 4* (SASC)	Normal start per Figure 70	OK
5-8-85	Turbine Shroud 124 (SSN)	Normal start per Figure 70	OK

*Stators with 0.120 inch radius cutback at trailing edge. Reference Figure 69.

the shroud. Analysis indicated that the failure was due to thermally induced stresses. Contact stress during shutdown between the shroud and the stator ring caused shroud failure. Development efforts since this test have concentrated on the segmented stator concept. On November 16, 1984 a stator thermal screening test was run using the turbine shroud screening rig. The test objective was to thermally shock stator segments (RBSN) to engine normal start conditions (plus 25-percent stress margin), as described by Figure 70. Following the test, no cracks were found in stator trailing edges. On February 4, 1985, a segmented stator set (SASC) was run to a similar cycle as mentioned above. The test was unsuccessful; nearly all of the stator segments were fractured, and two were fully parted down the vane centerline. Fractures were seen to initiate from the stator vane trailing edge area, which is the most highly stressed portion of the part. As a result of this testing it became apparent that survivability of stators is a concern under thermal transient conditions. In order to improve the survivability of stators a design modification was made which incorporates a 0.120-inch radius cutback at the trailing edge. This scallop of the trailing edge represents approximately a 1-percent penalty in performance, but drastically improves the survivability of the stators under thermal transient conditions. This can be seen in subsequent testing, as for example, an RBSN stator set on March 6, 1985 and another SASC stator set on May 3, 1985. The cutback employed is illustrated in Figure 69.

3) The tabular data in Table 28 notes the successful thermal screening of turbine shroud S/N 694 (RBSN) and stator set No. 4 (SASC) on May 3, 1985. Even though the turbine shroud survived the normal start screening cycle, as defined in Figure 70, the shroud did fracture shortly after shutdown following the stator test cycle for the stator set. A review of the transient cycles (Figure 70) shows that the stator screening cycle is to a higher temperature and at a higher airflow than the turbine shroud screening cycle. However, the shorter duration of the stator screening cycle gives a relatively low calculated stress in the turbine shroud. The stators reach their maximum principle stress at approximately 20 seconds into the cycle. At this point in time the turbine shroud is not yet a highly stressed member.

The fracture of turbine shroud S/N 694 during the stator screening cycle, after successfully completing two turbine shroud screening cycles, is not yet fully understood. Fracture occurred 20-seconds after shutdown of the test, when no air or fuel were flowing. Fractography indicates that the fracture was thermally induced with origin at the seal land fillet.

A hypothesis is made that the increased airflow of the stator screening cycle may alter the boundary conditions of the test. Increased turbulence at the stator area and shroud line could alter heat transfer coefficients from those used in the analysis. A test employing an instrumented stator (metal) is planned to verify heat transfer coefficients.

Inner Diffuser Housing and Outer Diffuser Housings Screening Rig

During the report period from July 1984 to June 1985, four sets of inner and outer diffuser subassemblies were successfully screened to normal start conditions plus 25-percent (Figure 70). Table 29 details the test conditions and the hardware that was screened.

Additionally, these tests incorporated a new serialization procedure. All components were laser marked in the area of lowest stress. No failures occurred during this screening.

Transition Duct and Combustor Baffle Screening Rig

During this reporting period, six sets of transition duct and combustor baffle subassemblies were thermally screened as

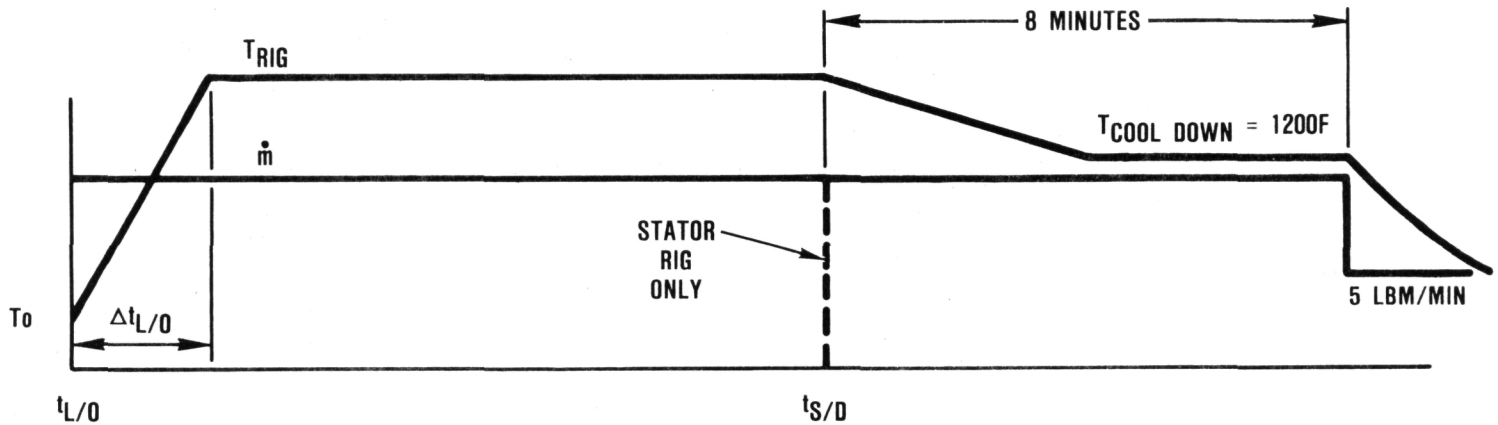

Components(s)	Material	$\dot{m}$, lbm/min	To, F	T_{rig}, F	$\Delta t_{L/O}$, sec	$t_{S/D}$, sec	Number of Cycles
Transition Duct, Baffle	All Materials	22.6	70	1800	10	600	1.5
Inner + Outer Diffusers	RBSN SSN	17.1	70	2000 2000	10	600	1.5
Turbine Shroud	RBSN SSN SASC	10.0	200	1575 1630 1720	15	600	1.5
Stators	All Materials	17.1	70	2225	10	35	1.5

Figure 70. AGT101 Static Components Proof Test Cycles.

Table 29. Inner and Outer Diffuser Housing Screening Results

Airflow	17.1 lb/min
Preheat Temperature	80 - 100F
Max Temperature	2000F
Transient Time to T_{MAX}	10 sec
Time at Temperature	10 min
Downshock Transient	4 min from T_{MAX} to 1200F (T_{min})
Hold Time at T_{MIN}	4 min
Total Cycles each set	2

Test Configuration 1

Component	S/N	Material
Inner Diffuser Housing	110-2	SN-50
Outer Diffuser Housing	109-2	SN-50
Outer Diffuser Housing Spacer	108-6	SN-50
Rockers	116, 117, 118	SN-220M
Eccentrics	134, 135, 136	NC-132
Bolts	034, 035, 036	SN-220M
Upper Contact Washers	135, 136, 137	SN-54
Lower Contact Washers	123, 134, 125	SN-220M
Crowned Washers	130, 131, 132	SN-220M

Test Configuration 2

Component	S/N	Material
Inner Diffuser Housing	111	SN-50
Outer Diffuser Housing	115	SN-50
Outer Diffuser Housing Spacer	108-4	SN-50
Rockers	119, 120, 121	SN-220M
Eccentrics	014, 015, 137	SN-220M
Bolts	038, 039, 040	SN-220M
Upper Contact Washers	138, 139, 140	SN-54
Lower Contact Washers	126, 127, 128	SN-220M
Crowned Washers	133, 134, 135	SN-220M

Table 29. Inner and Outer Diffuser Housing Screening Results (Contd)

Test Configuration 3		
Component	S/N	Material
Inner Diffuser Housing	553	RBSN
Outer Diffuser Housing	590	RBSN
Rockers	122, 123, 124	SN-220M
Eccentrics	120, 121, 122	SN-220M
Bolts	030, 031, 032	SN-220M
Upper Contact Washers	125, 126, 127	SN-220M
Lower Contact Washers	129, 130, 131	SN-220M
Crowned Washers	136, 137, 138	SN-220M
Test Configuration 4		
Component	S/N	Material
Inner Diffuser Housing	588	RBSN
Outer Diffuser Housing	591	RBSN
Rockers	116, 117, 118	SN-220M
Eccentrics	123, 124, 125	SN-220M
Bolts	002, 006, 009	NC132
Lower Contact Washers	132, 133, 1134	SN-220M
Crowned Washers	139, 140, 141	SN-220M

All components were successfully screened through 2 start transients as indicated above.

detailed in Table 30. All test were performed to engine normal start conditions, with 25-percent stress margin, as defined in Figure 70. In one case, however, it was necessary to decrease airflow to 19.7 lb/min and increase the maximum temperature to 2000F to successfully accomplish the screening test. This yields the same stress result as would the cycle defined in Figure 70. Reason for the variation was difficulty in making the liquid fuel burner perform at the required airflows. Since that time, a burner using natural gas has been substituted for the liquid fuel burner, with markedly improved light-off and control characteristics.

This rig uses as a support platform a piece of Lockheed HTP-12 insulation, which is formed to provide both support and a portion of the discharge flow path. As shown in Figure 71, erosion has taken place which may eventually require substitution of the HTP-12 material for a more erosion-resistant insulation. An alternative insulation supplied by Zircar (ZAL-45, 45 lb/ft^3 density) is being investigated.

Table 30. Transition Ducts/Combustor Baffles Screened

(All Screening Tests Run at Normal Start Plus 25 Percent Stress Margin)					
Date	Transition Duct		Baffle		Results
	S/N	Material	S/N	Material	
01/31/85	116	SASL	123	SASC	OK
02/28/85	640	RBSN	120	SASC	OK
03/14/85	115	SASC	108	SASC	OK
03/18/85	114	SASC	109	SASC	OK
06/07/85	131	SSN	371	RBSN	OK
06/11/85	118-4	SASC	108	SASC	OK

Ceramic Static Structures Rig

Build 11

In August 1984 ceramic static structures rig (Figure 72) was built with the components listed in Table 31 and tested to a rig inlet temperature of 1600F at a mass flow rate of 18 and 23 lb/min. A standard 3-inch laboratory combustor and an engine combustor respectively were utilized to achieve these conditions. The test was terminated prior to achieving the desired maximum transient temperature of 1800F due to the occurrence of coupled AE on the turbine shroud and flow separator housing accompanied by a simultaneous drop in rig inlet pressure. Disassembly revealed fracture of the components as noted in Table 31. Fractography results in conjunction with thermal and stress analysis for monitored rig conditions have concluded the cause of failure to have originated from thermally induced stress in the turbine backshroud. The components are believed to have reached fracture stress as a result of a rig burner/control instability at the time of maximum (transient) stress in the above listed components. The shock wave created by the strain release in the backshroud at fracture is believed to have caused the failure in the interfacing components.

The solution to the rig failure is two-fold. First, the turbine backshroud was partially stress-relieved by redesigning, and machining a 3-inch diameter hole through the center of the component. The void area is then filled with Lockheed HTP-12 insulation. The 3-inch diameter hole removes the current peak stress area of the component effectively lowering the maximum principal stress by 88-percent. Secondly, an improved fuel metering system was installed to preclude burner/control instability, thereby minimizing the probability of a rig induced failure. Estimates of ceramic component stresses at the time of fracture are shown below. Assumption for these estimates are as follows:

- All estimates are based on the engine condition analysis with adjustments for the higher mass flow and operating cycle.

C-2

- The assumed heat transfer coefficients have been correlated with test data for the turbine shroud only and in a more limited degree on the outer diffuser housing.

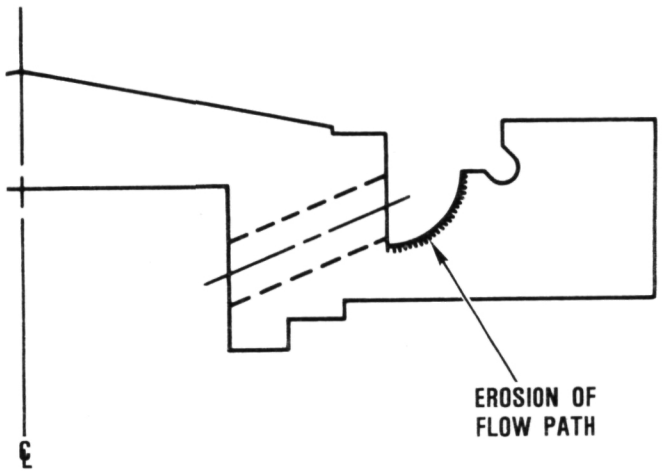

Figure 71. Erosion of Lockheed HTP-12.

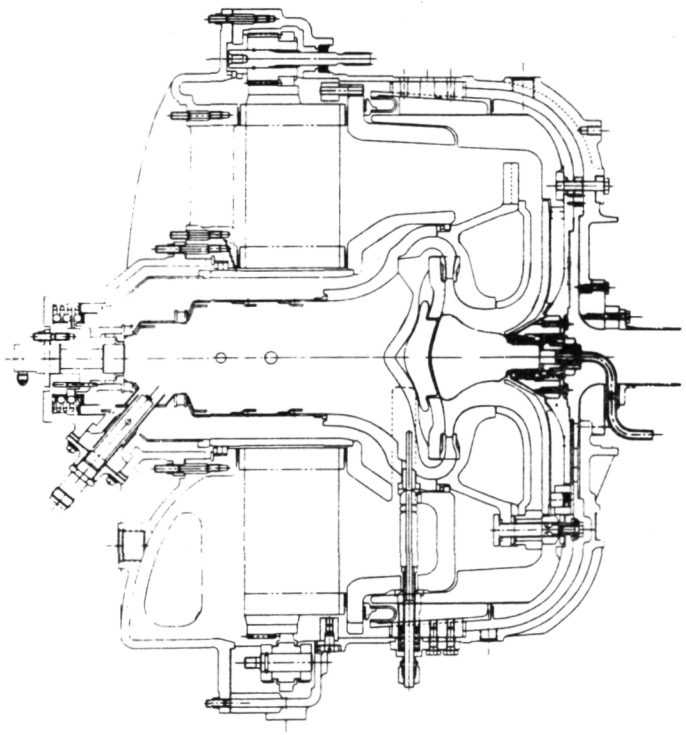

Figure 72. Static Structures Rig.

- The absence of a turbine rotor in the static structures rig should significantly affect the heat transfer coefficients on all three of the below listed components:
  - Turbine Backshroud: 29.4 ksi at 120 seconds after light-off.
  - Turbine Shroud: 21.5 ksi at 140 seconds after light-off.
  - Outer Diffuser: 12.1 ksi at 100 seconds after light-off.

Build 12

In September 1984, the static structures rig was operated to subject a set of ceramic hardware (Table 32) to a stator inlet temperature increase from ambient to 1800F, in 15 seconds. Airflow through the rig was set at 23 lb/min, which corresponds to the transition duct and baffle screening cycle. At the time this test was performed, this thermal transient cycle was intended to duplicate engine development start conditions (plus 25-percent stress margin). Since that time, a similar calculation was performed to simulate engine normal start conditions. The results revealed that stress levels in the ceramic static structures under development start conditions and under normal start conditions show only a very slight difference. Lower temperature but increased airflow for the development start essentially creates the same stresses as the normal start condition. For this test, the desired cycle was attained after first achieving light-offs to lower temperature of 1400F and 1600F. Temperature and flow conditions were maintained for 10 minutes after which flow to the burner was shut off. The regenerator was left turning so that its thermal inertia would allow the rig to slowly cool.

Five cycles to 1800F were accumulated, after which the rig was removed from the test cell and disassembled. All major ceramic components were intact; only a few minor discrepancies were observed. These included chips on two of the three spacers separating the inner and outer diffusers; two very small

Table 31. Fractography Results

Component				Test			Location	Circum* Position	Fracture Stress Plane	Propagation Direction	Mirror Size	Branching	Material Condition	Character-ization
Name	S/N	Configuration	Material	Data	Build	Cycle								
T-Shroud	544	B3E	RBSN	8/24	SR 11	18 lbm/min -1600F + Thermal		4:30 o'clock	Axial/ Circum	Short Circum Then Radial		From Peak Stress Area Below Seal	No Oxidation	Thermal
Back-Shroud	103A	A1	SASC			Spike to 2300F +	Turbine Surface 0.75 inch Off Center	9 o'clock	Radial/ Axial	Radial out-ward		3	No Oxidation	Thermal
T-Duct	110	B2						5:30 o'clock	Radial/ Circum	Radial			No Oxidation	Contact + Thermal Propagation + Contact Secondary
Outer Diffuser	339	A3	RBSN				Axial face, At T-Shroud ODH Contact	Near T-shroud Slots	Radial/ Axial	Radial Inward		Some	No Oxidation	Thermal + Contact & Mechanical
Bolt														
Stators	441 444 454 460 453						Shroud							

*Clockwise as looking through the combustor, TDC = 12 o'clock

Table 32. Ceramic Components Tested in Structures Rig, Build 12, September 12-14, 1984.

Test Date: September 14, 1984

Test Type/Purpose: Proof/Screening Test

Cycle Description: Good; 5 cycles at 1800F and 22.6 lb/min

Rig/Engine/Build: SR 12

Cycles: 5 (Total) Hours: 1.33 (0.83) (Total)

Parts	Part Number	Source	Serial Number	Status
Inner Diffuser	3609638-1	NGK	110-1	OK-2 tiny chips
Outer Diffuser	3609637-1	NGK	109-1	OK
Outer Diffuser Spacer	3609639-1	NGK	108-1	OK
Rocker (3)	3609619-1	GTEC	010, 011, 012	013, 014 chipped
Eccentric (3)	3609658-1	GTEC	013, 014, 015	OK
Bolt (3)	3609622-1	GTEC	016, 019, 021	OK
Contact Washer Upper (3)	3609626-1	GTEC	207, 208, 209	OK
Contact Washer Lower (3)	3609625-1	GREC	207, 208, 209	OK
Crowned Washer	3609621-1	GTEC	207, 208, 209	OK
Transition Duct	3846159-1	CBO	112	OK
Baffle	3609614-1	CBO	124	OK
Stator	3846122-1	ACC	006	OK
Shroud	3609679-1	ACC	547	OK
Backshroud	3846148-1	CBO	106A	OK
Flow Separator Seal Ring	3610206-1	ACC	596	OK - chip on OD
Wave Washer	3609653-1	ACC	268	OK
T Shroud Seal Ring	3609651-1	ACC	361	OK
Flow Separator Housing	3846134-1	Corning	12	OK
Regenerator Shield	3846154-1	CBO	101A	OK
Regenerator Shield Seal Ring	3609650-1	Pure Carbon	103, 104	OK
Insulation	---	B&W	012 SR	OK
Transition Duct Bushing (3)	3609632-1	CBO	211, 212	OK
$T_{4.1}$ TC Inner Seal (Female) (3)	3609631-1	GTEC	207, 208, 209	OK
$T_{4.1}$ TC Inner Seal (Male) (3)	3609630-1	GTEC	207, 208, 209	OK
$T_{4.1}$ TC Inner Seal Spacer (3)	3609633-1	GTEC	207, 208, 209	OK
$T_{4.1}$ TC Inner Load Spacer (3)	3609629-1	GTEC	207, 208, 209	OK
$T_{4.1}$ TC Outer Seal (Female) (3)	3609620-1	GTEC	207, 208, 209	OK
$T_{4.1}$ TC Outer Seal (Male) (3)	3609610-1	GTEC	207, 208, 209	OK

Regenerator Core: MIT 6W

Rotor/: N/A

chips on the inner diffuser, and a small chip due to contact stress on the flow separator housing seal ring.

The backshroud employed in this test had the 3-inch diameter hole at its center, with a piece of Lockheed HTP-12 insulation to fill the resulting void. Successful completion of this test represents the first time that a full set of ceramic static structures was proof-tested to such severe thermal shock conditions.

Build 13

In March 1985 the ceramic static structures rig was built using the ceramic hardware listed in Table 33. In early April 1985 a successful screening test was performed to engine normal start conditions (plus 25-percent), thus qualifying these components for engine use. Thermal transient cycles employed to simulate the engine normal start conditions is given in Figure 70 as the transition duct/baffle screening cycle. Three successful test cycles were run to the required condition. Late in the third cycle, high level AE was noted, indicating a possible fracture of ceramic components. The test was terminated. Subsequent rig disassembly revealed only a chipped stator segment (reusable) and erosion of the high temperature ZAL-45 fiber insulation. The high level AE indications may be contributed to the insulation breaking up, or perhaps to the effect of a too rigidly mounted AE probe sweeping a surface as the rig expands and contracts. The test was considered complete.

Confidence in screening rigs has now reached a point that a check screen of the entire ceramic structural assembly is no longer felt necessary to qualify hardware for engine use. The static structures rig is therefore currently being modified for use as a hot regenerator seal leakage test rig.

2500F Testing

On August 2, 1984 the AGT101 Hot Stator Rig was run for the first time. The original intent for this rig was as a vehicle for performing tests at 2500F of major structural components, including transition duct, baffle, stators, and turbine shroud. The original configuration as given in Figure 73 incorporated a flow separator housing as well. This configuration was used for the first build of the hot stator rig. Note that the flow path of the incoming air to the hot stator rig differs from previous screening rigs in that the incoming air enters via the flow separator housing "smile" prior to combustion in the rig burner. For this initial test a natural gas pre-heater was not used, as originally intended, due to concerns about rig inlet housing integrity when exposed to heated inlet air. This means that incoming air prior to combustion was in the range of 200-250F. The heating effect of the regenerator core was not simulated in this test.

Goals for this initial test were to establish proper rig setup in the test cell, verify rig build procedure and operation, and achieve a 2500F temperature. The components used in Build 1 are listed in Table 34. The intended maximum temperature of 2500F was not achieved because of the fracture of ceramic components (as evidenced by AE signals). The fracture indications came at 10 minutes into the Cycle 3 at a temperature of 1500F, a condition that had already been seen in Cycle 2. The test was halted by manually stopping the air and fuel flows.

Rig disassembly revealed the following ceramic component damage:

- The turbine shroud was fractured with origin at approximately 2 o'clock position as situated in the rig (corresponding to bolt position No. 3). Origin axial location was at a point where the fillet radius of the seal land meets the seal land flat (Figure 74)
- The integral stator fractured in several places with origins in the highly stressed vane trailing edge area
- All seal components were fractured

Table 33. Parts Built Into Static Structures Rig, Build 13

Parts	Source	Material	S/N
Inner Diffuser	NGK	SN-50	110-2
Outer Diffuser	NGK	SN-50	109-2
Outer Diffuser Spacer	NGK	SN-50	108-6
Rocker (3) Eccentric (3) Bolt (3)	Kyocera Norton/GTEC Kyocera	SN-220M NC132 SN-220M	116, 117, 118 134, 135, 136 034, 035, 036
Contact Washer Upper (3)	NGK	SN-54	135, 136, 137
Contact Washer Lower (3)	Kyocera	SN-220M	123, 124, 125
Crowned Washer	Kyocera	SN-220M	130, 131, 132
Transition Duct	CBO	SASC	116
Baffle	CBO	SASC	123
Stator	ACC	RBSN	009
Shroud	NGK	SN-54	117
Backshroud	CBO	SASC	105A
Flow Separator Seal Ring	ACC	RBSN	—
Wave Washer	ACC	RBSN	716
Turbine Shroud Seal Ring	ACC	RBSN	319
Turbine Shroud Spacer Ring	NGK	SN-50	108-3
Flow Separator Housing	Corning	LAS	30
Regenerator Shield	CBO	SASC	104A
Regenerator Shield Seal Ring	Pure Carbon	RSSiC	103, 104
Insulation	Zircar	ZAL-45	Z 451
Transition Duct Bushing (3)	Norton/GTEC	NC-132	—
$T_{4.1}$ TC,* Inner Seal (Female) (3)	Kyocera	SN-220M	207, 208, 209
$T_{4.1}$ TC, Inner Seal (Male) (3)	Kyocera	SN-220M	210, 211, 213
$T_{4.1}$ TC, Inner Seal Spacer (3)	Kyocera	SN-220M	221, 224, 225
$T_{4.1}$ TC, Inner Load Spacer (3)	Kyocera	SN-220M	212, 221, 213
$T_{4.1}$ TC, Outer Seal (Female) (3)	Kyocera	SN-220M	210, 211, 213
$T_{4.1}$ TC, Outer Seal (Male) (3)	Kyocera	SN-220M	210, 211, 213

*TC = Thermocouple

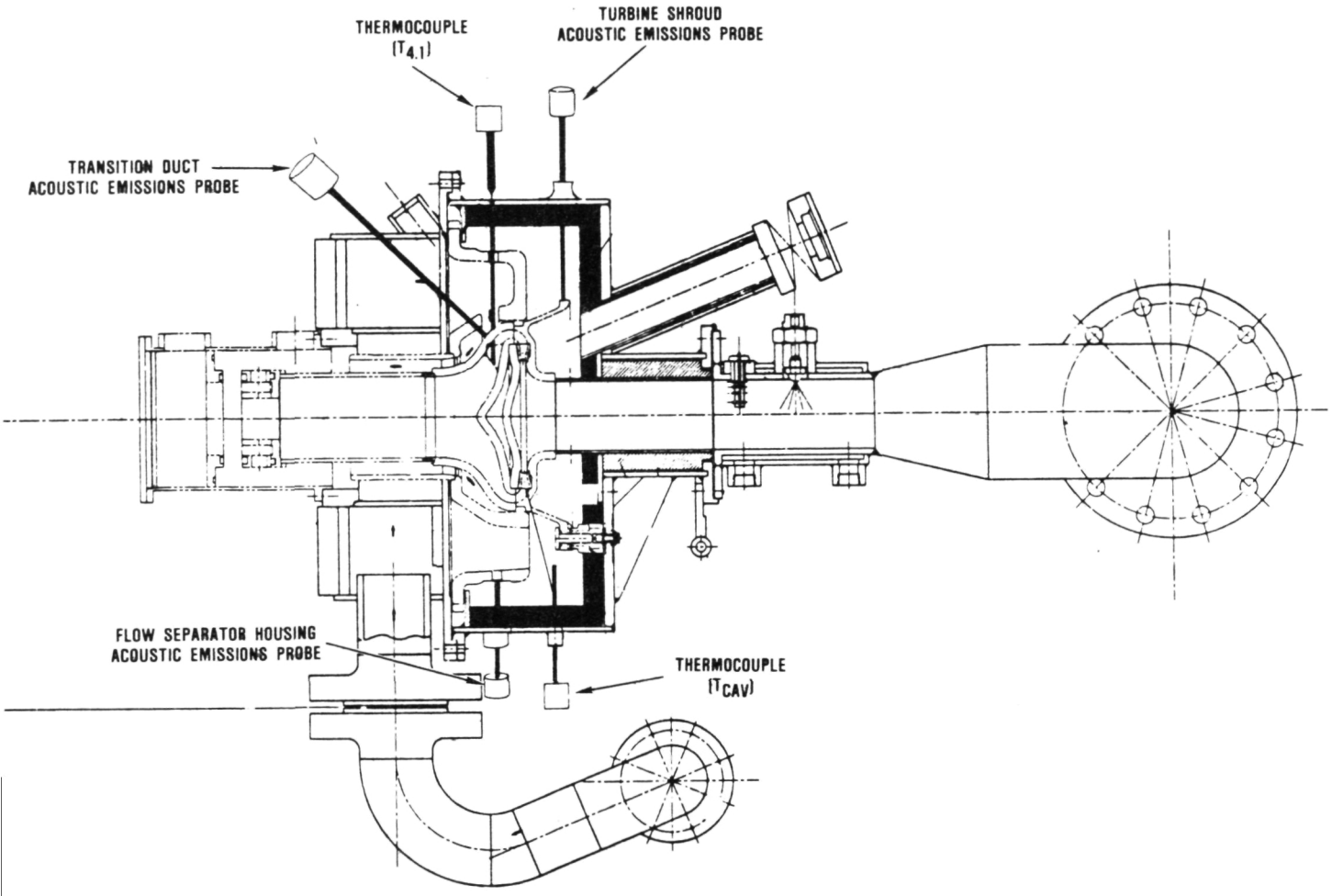

Figure 73. Diagram of Rig With Associated Instrumentation.

- The lower contact washer at shroud location 2 (6 o'clock orientation in the rig) was cracked.

The most likely cause for the fracture is a contact stress near the fillet area of the shroud, where a mismatch of fillet radius (on the shroud) and the mating round (on the flow separator housing seal ring) would have allowed contact loading.

Further testing at 2500F was conducted in October 1984 using the turbine shroud screening rig as a test bed in lieu of the previous hot stator rig. This was done for two reasons: to avoid thermal growth damage to the hot stator rig inlet housing due to different heating rates in different areas, and to avoid risking the flow separator housings, which are not required for the 2500F testing. The ceramic hardware listed in Table 35 was subjected to 30 minutes of operation at 2500F and 10 lb/min airflow. No fractures occurred during the operation. Note that the thermal transients employed were gentle and not intended to impose severe thermal shock to the parts, but rather to determine if interfacial sticking or other problems would be revealed at the 2500F temperature.

Two significant observations were made during rig disassembly. Insulation which supports the turbine shroud and the rest of the ceramic hardware, consisting of a silicon

Table 34. Hot Stator Rig, Build 1

PN	Name	S/N	Supplier	Material	Comments
PA3609679	Turbine Shroud	546	ACC	RBSN	2500F screen OK
PA3609628	Bolt Assembly	013	Norton	HPSN (NC-132)	Shroud hole 2
PA3609628	Bolt Assembly	014	Norton	HPSN (NC-132)	Shroud hole 1
PA3609628	Bolt Assembly	015	Norton	HPSN (NC-132)	Shroud hole 3
PA3609619	Alignment Spacer	004	Norton	HPSN (NC-132)	Shroud hole 2
PA3609619	Alignment Spacer	005	Norton	HPSN (NC-132)	Shroud hole 1
PA3609619	Alignment Spacer	006	Norton	HPSN (NC-132)	Shroud hole 3
3846122	Turbine Stator	205	Ford	RBSN	1-piece stator
PA3609616	Turbine Backshroud	105A	CBO	SASC	2500F screen OK
PA3609615	Combustor Baffle	122	CBO	SASC	2500F screen OK
PA3609649	Transition Duct	112	CBO	SASC	2500F screen OK
PA3609652	Flow Separator Seal Ring	102	ACC	RBSN	Gap at 12:00 o'clock position
PA3609653	Wave Spring	249	ACC	RBSN	
PA3609651	Shroud Seal Ring	321	ACC	RBSN	Gap at 6:00 o'clock position
None	Spacer	None		LAS	To accommodate short T. duct
3846154	Regenerator Shield	101B	CBO	SASC	
PA3609655	Flow Separator	18	Corning	LAS	Crack at 10:00 o'clock
PA3609610	Plug Seal	104, 105, 106	Duramics	Alumina	104 at 10:00 o'clock position 105 at 12:00 o'clock position 106 at 2:00 o'clock position
PA3609620	Mounting Platform	104, 105, 106	Duramics	Alumina	104 at 10:00 o'clock position 105 at 12:00 o'clock position 106 at 2:00 o'clock position
PA3609629	Inner Load Spacer	104, 105, 106	Duramics	Alumina	104 at 10:00 o'clock position 105 at 12:00 o'clock position 106 at 2:00 o'clock position
PA3609630	Male Seal	104, 105, 106	Duramics	Alumina	104 at 10:00 o'clock position 105 at 12:00 o'clock position 106 at 2:00 o'clock position
PA3609633	Thermocouple Spacer	104, 105, 106	Duramics	Alumina	104 at 10:00 o'clock position 105 at 12:00 o'clock position 106 at 2:00 o'clock position
PA3609631	Female Seal	204, 205, 206	Norton	HPSN	204 at 10:00 o'clock position 205 at 12:00 o'clock position 206 at 2:00 o'clock position

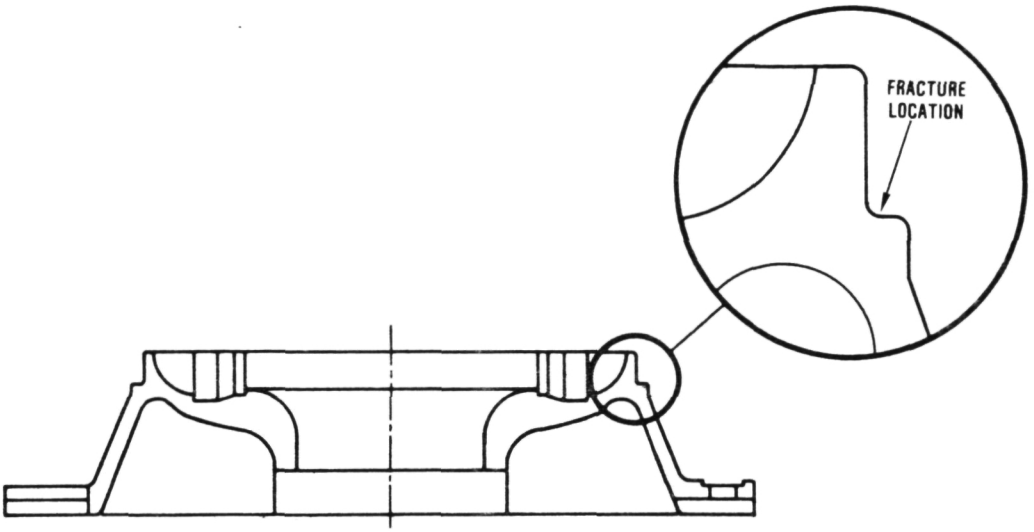

Figure 74. Origin of Turbine Shroud Fracture.

dioxide insulation with an alumina based rigidizer, yielded during the test, allowing the parts to drift axially by approximately 0.050- to 0.100-inch. The insulation also stuck to the turbine shroud when the latter was removed from the rig. Further, examination under magnification on the three struts on the combustor baffle and the mating areas of the transition duct revealed glazing in these areas, although no component sticking (the parts were freely disassembled) was observed. Successful completion of this test represented the first time that these components had been exposed over a long period (30 minutes plus) to 2500F temperatures.

A subsequent attempt to repeat the test, but substituting a turbine shroud of RBSN for the SSN turbine shroud, was aborted approximately 5 minutes after reaching the 2500F temperature. The rig was shut down after a shift in the stack of the ceramic parts was noted. Subsequent disassembly revealed that this was due to relaxation of the insulation, as had previously occurred. Unfortunately, quench water used to cool the discharge ducting backed up into the rig, passed a dam intended to contain it, and as a result the turbine shroud and backshroud both were fractured. The fractures originated in areas where high stress levels normally would not occur. Also, several stators were noted to have stuck to the turbine shroud. This phenomenon was analyzed and it is felt that the sticking is due to metallic deposits emanating from the metal-sheathed thermocouples employed in the rig.

In April 1985, further 2500F testing was conducted, this time employing a new rig design similar in configuration to the turbine shroud screening rig, but oriented in a vertical position. This is done for two reasons: 1) to allow a dead weight to supply the required load to the ceramic stack, and 2) to preclude the possibility that discharge quench water will back up into the rig.

The dead weight employed was made of 300 Series stainless steel, insulated for protection. Unfortunately, it reached a high enough temperature at approximately 25 minutes after achieving the 2500F test temperature that premature shutdown of the rig was thought prudent. The parts employed in this test are listed in Table 36.

Table 35. Components Used in 2500F Turbine Shroud Screening Rig

October 15, 1984 (Completed 30 minutes at 2500F)		
Parts	Source (Material)	S/N
Transition Duct	CBO (SASC)	117
Baffle	CBO (SASC)	122
Stator	ACC (RBSN)	Set 007
Shroud	NGK (SSN)	116
Backshroud	CBD (SASC)	104A
Spacers (2)	ACC (RBSN)	A, B
Wave Washer	ACC (RBSN)	261
T Shroud Seal Ring	ACC (RBSN)	319
October 24, 1984 (Aborted After 5 Minutes at 2500F)		
Parts	Source (Material)	S/N
Transition Duct	CBO (SASC)	117
Baffle	CBO (SASC)	122
Stator	ACC (RBSN)	Set 007
Shroud	NGK (SSN)	551
Backshroud	CBD (SASC)	104A
Seal Spacers	ACC (RBSN)	A, B
Wave Washer	ACC (RBSN)	261
T Shroud Seal Ring	ACC (RBSN)	319

In May 1985, additional testing at 2500F was attempted. To extend the running time at the 2500F temperature, the dead weight system was changed to incorporate ceramics. However, the amount of weight that can be physically installed in the rig envelope was found insufficient. A pressure differential at light-off between the flow path and the cavity surrounding the test pieces caused the transition duct to move upward (axially) and then bounce back down upon the rest of the stack of parts. The parts employed in this test, and the fractures which they suffered, are given in Table 37. Further modifications to the loading system for this rig are anticipated so as to allow extended operation at 2500F test temperature.

Mechanical Screening

During late November 1984, two turbine shrouds (S/N 117, SN-54, NGK and S/N 639,

Table 36. April 18, 1985 Testing at 2500F (Vertically Configured Rig)

Component	P/N	Source	Material	S/N	Condition
Transition Duct	3609649	CBO	SASC	114	OK
Baffle	3609612	ACC	RBSN	592	OK
Insulation	PAP255800	Zircar	ZAL-45	2453	OK
Stator	3846122	ACC	RBSN	Set 7	OK - 4 stuck lightly
Shroud	PAP255853	ACC	RBSN	659	OK - existing cracks in feet
Backshroud	3846148	CBO	SASC	107A	OK
Spacer	---	Corning/ GTEC	LAS	001	Failed - melted
Wave Washer	3609653	ACC	RBSN	717	OK
T Shroud Seal Ring	3609631	ACC	RBSN	323	OK
Flow Separator Housing					
Regenerator Shield					
Regenerator Shield Seal Ring					

RBSN, ACC) were subjected to mechanical proof test. The objective of this test was to subject the shroud to a 4000-lb axial load to simulate the pressure load (plus 25 percent) at maximum power conditions. Figure 75 shows the configuration used. Turbine shroud S/N 117 was successfully loaded to 4000 lbs with no reportable incidents. During the next test, turbine shroud S/N 639 was being loaded from 2500 lbs to 3000 lbs when failure occurred (approximately 2900 lbs). The origin of the fracture was located in the radius of the slot on a foot of the shroud. Figure 76 depicts the failure.

During December 1984, two additional shrouds (S/N 116, SN-54, NGK and S/N 653, RBSN, ACC) were subjected to the mechanical proof test. Once again, the SN-54 (S/N-116) turbine shroud passed the test and the RBSN (S/N-653) failed at approximately 2900 lbs load. The origin of the fracture was located in the same area as the previous failure.

Due to the two failures of slotted RBSN turbine shrouds during mechanical screening, a design modification was implemented to strengthen the area where these failures initiated. This modification resulted in removing the slots on the feet of the shroud as shown in Figure 77.

The first modified RBSN turbine shroud was mechanically screened during April, 1985.

Table 37. May 13, 1985 Testing at 2500F (Vertically Configured Rig)

Part	P/N	Source	Material	S/N	Condition
Transition Duct	3609649	CBO	SASC	114	OK
Baffle	3609612	ACC	RBSN	592	Chipped foot (failed)
Insulation	PAP255800	Zircar	ZAL-45	2453	OK
Stator	3846122/ 3846162	ACC/ CBO	RBSN/ SASC	Set 7	OK - 4 stuck lightly
Shroud	PAP255853	ACC	RBSN	659	Failed
Backshroud	3846148	CBO	SASC	107A	OK
Spacer	3610206	ACC	RBSN	695	OK
Wave Washer	3609653	ACC	RBSN	717	OK
T Shroud Seal Ring	3609631	ACC	RBSN	323	OK
Flow Separator Housing					
Regenerator Shield					
Regenerator Shield Seal Ring					

As shown in Figure 78, the test rig was positioned below a hydraulic press with the load cell centered on a steel ball to assure uniform loading. Four dial indicators were placed in areas of interest (Figure 79) to determine both radial and axial deflections. The load was applied in 500-lb increments up to 3000 lbs and increased by 200-lb increments thereafter. At the 4000-lb level the load was removed and all indicators read to compare to the initial zero reading. Deflection data versus applied load is tabulated in Table 38. The zeros checked very well which adds credence to this deflection data and to the success of this screening test of the RBSN redesigned turbine shroud.

This was the first successful mechanical screening of a RBSN turbine shroud and indicates that eliminating the stress concentration of the slot increased the load carrying capacity up to the required level.

4.5.5 Ceramic Turbine Rotors

AGT ceramic rotors are subjected to a number of inspection steps, tabulated below. These steps are used in determining engine quality rotors. To date, no rotor has been found acceptable for engine testing.

- o Dimensional inspection
- o Density determination

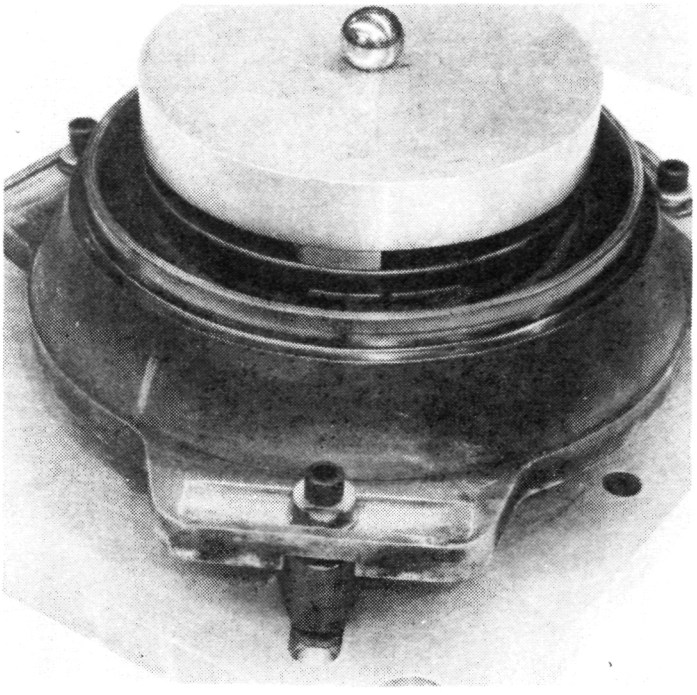

Figure 75. Turbine Shroud Mechanical Screening Test Setup.

- o Visual inspection
- o Ultrasonic inspection
- o Cold spin testing
- o Hot spin testing

Testing has shown a definite correlation between rotor density and burst speed (Figure 80). Rotors with a density of 3.25 g/cm^3 or higher, typically have sufficient strength to pass the cold spin test. Low density rotors are immediately rejected, thus eliminating costly inspection and testing.

Five rotors were cold spin tested during the past year. The test results are summarized in Table 39. Figure 81 shows rotor S/N 344 installed in the spin pit. Due to the unique handling characteristics of ceramics, a new spin arbor was designed to provide a safer method of attaching the rotors to the arbor. The new design is based on the tie bolt arrangement used in the engine. Rotors can be

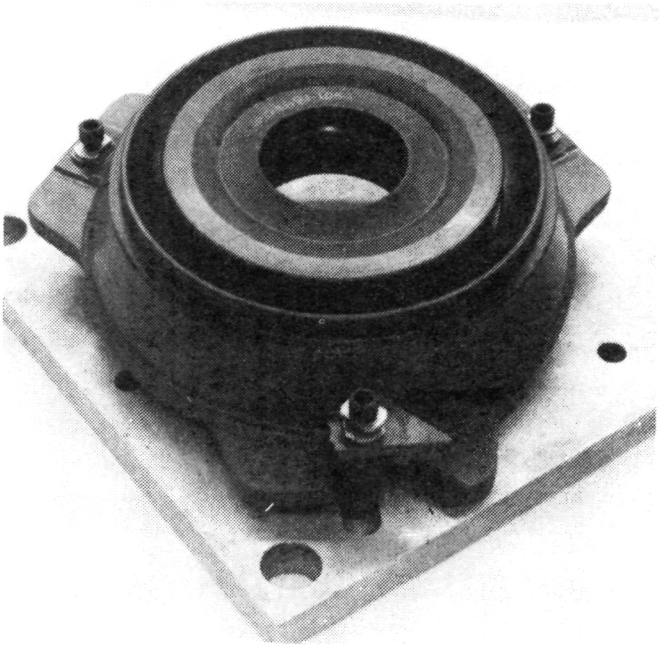

Figure 76. RBSN Turbine Shroud Showing Failure in Mechanical Screening Test.

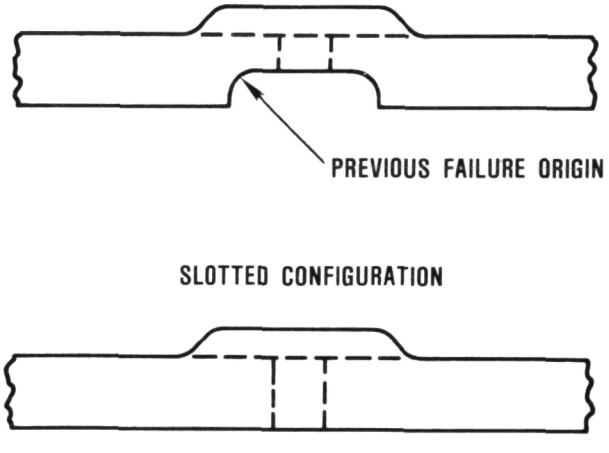

Figure 77. Slotted Versus Slotless Turbine Shroud Configuration.

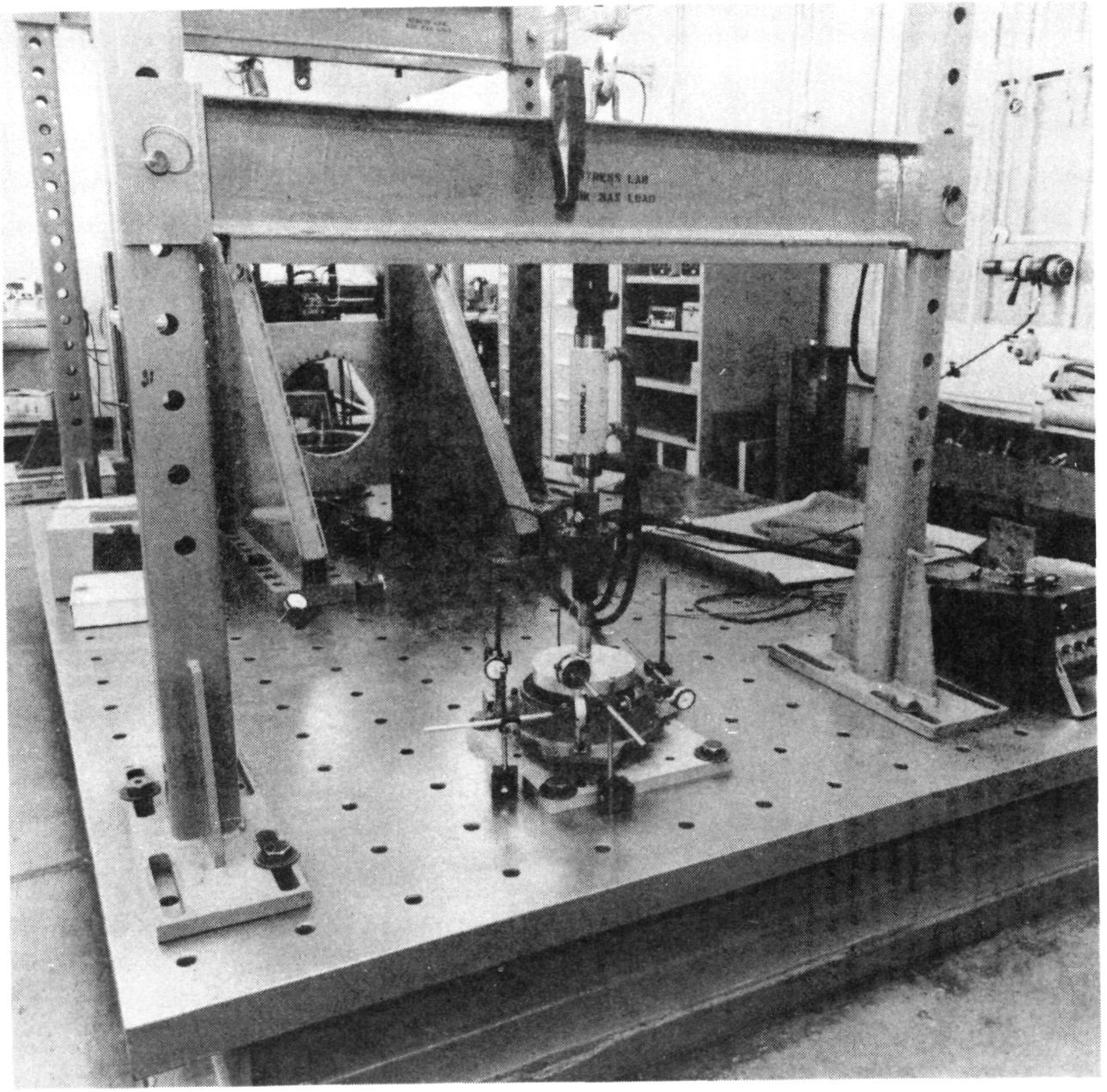

Figure 78. Mechanical Screening Rig Test Setup.

quickly attached to the new arbor with a minimum risk of incurring handling damage. Figures 82 and 83 show the arbor disassembled and installed in the spin pit, respectively.

As part of the computerized tracking system, all AGT101 hardware will be serialized and permanently identified by laser marking. Rotor S/N 552 was selected as the test rotor to ensure the proper location of the laser etched serial number. The rotor was successfully proof tested to 115,000 rpm after being marked on the hub as shown in Figure 84.

Simulated rotor S/N 315 was to be proof tested to 105,000 rpm for use in the rotordynamics test rig. However, at 93,000 rpm the rotor failed. From examination of the direction of crack propagation on a hub piece remaining attached to the arbor, it was determined that the origin of the wheel burst was in the hub. Inspection of the rotor, both visual and ultrasonic, gave no indication of any flaws in this piece. The most likely cause of the burst is a subsurface flaw too small to be detected by ultrasonic inspection.

As part of the continuing materials evaluation, rotors S/N 652 and 688 were selected as spin-to-burst candidates. Rotor S/N 652, due to its high density, was selected to provide an additional data point to correlate burst speed with density. Burst occurred at 121,000 rpm, resulting in a maximum principal stress of

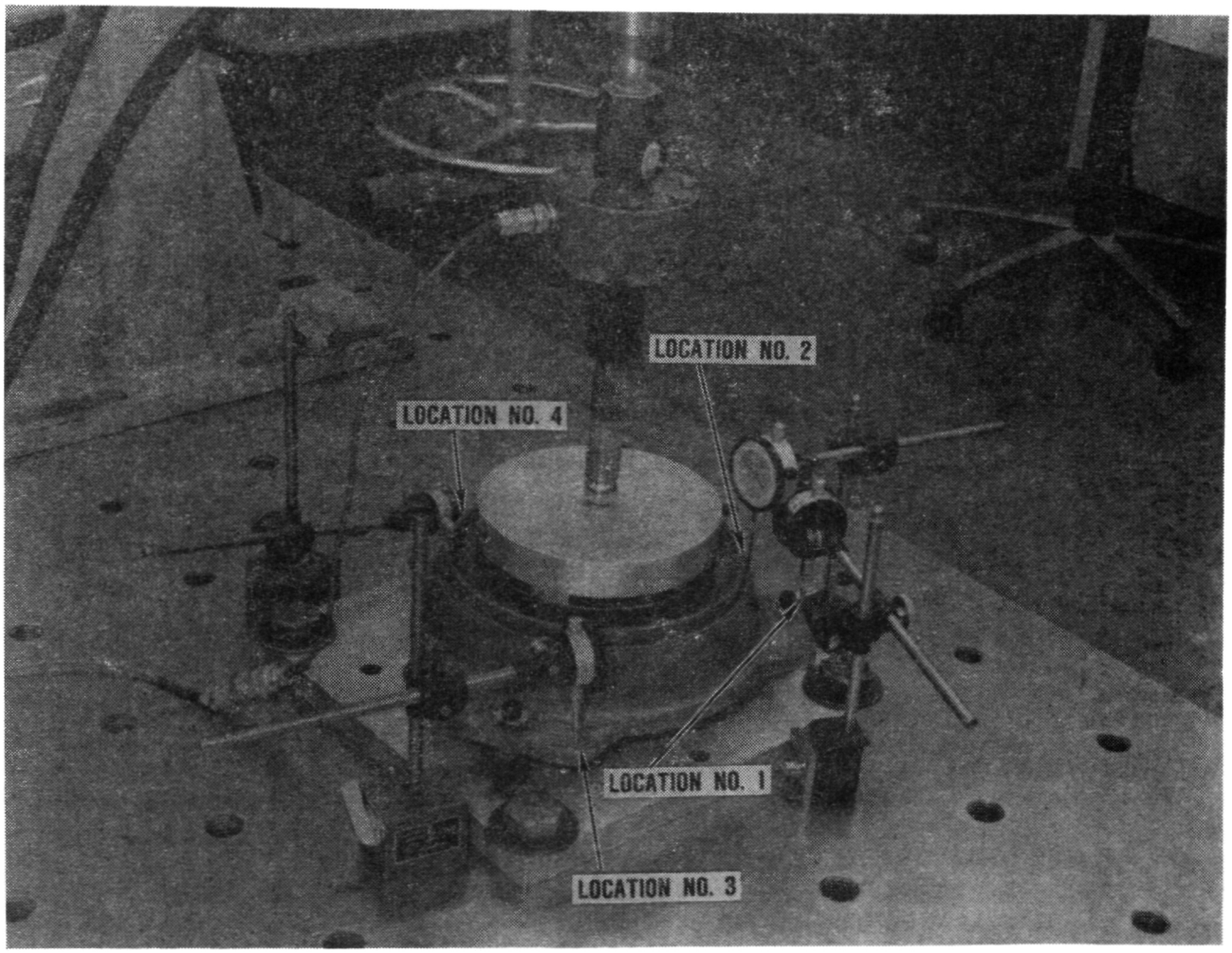

Figure 79. Dial Indicator Locations for Turbine Shroud Load Test.

Table 38. Axial and Radial Deflections of RBSN Turbine Shroud During Mechanical Screen Test.

Load, lbs	Deflection, inches			
	Location 1	Location 2	Location 3	Location 4
500	0.0001	0.0009	0.0006	0.0000
1000	0.0004	0.0015	0.0010	0.0000
1500	0.0008	0.0025	0.0015	0.0000
2000	0.0009	0.0030	0.0017	0.0005
2500	0.0010	0.0036	0.0019	0.0007
3000	0.0011	0.0041	0.0021	0.0010
3200	0.0012	0.0043	0.0022	0.0010
3400	0.0012	0.0045	0.0022	0.0010
3600	0.0012	0.0047	0.0023	0.0012
3800	0.0013	0.0049	0.0024	0.0014
4000	0.0013	0.0051	0.0024	0.0015
0	-0.0002	0.0002	0.0005	0.0001

48.2 ksi. As shown in Figure 80, this correlates favorably with previous high density rotor data. Ultrasonic inspection of rotor S/N 688 revealed a large flaw, approximately one inch from the backface, rendering this rotor unsuitable for engine testing. Due to the size of the flaw, expectations were that the rotor would burst in the 70- to 80,000-rpm range. The actual burst speed was 101,000 rpm, with a maximum principal stress of 34.2 ksi. The failure of rotor S/N 688 reinforces the reliability of ultrasonic inspection in revealing flaws and the need for additional data correlating flaw size with burst speed and density to determine a maximum allowable flaw size.

4.5.6 Ceramic Components Received

The following components were received during this reporting period.

ACC delivered 14 turbine shrouds, 2 truncated turbine shrouds, 1 transition duct, 2 outer diffuser housings, 3 combustor baffles, 3 back shrouds, 10 flow separator housing seals, 8 turbine shroud seal rings, 8 wave washers and 103 stator segments all fabricated from RBSN.

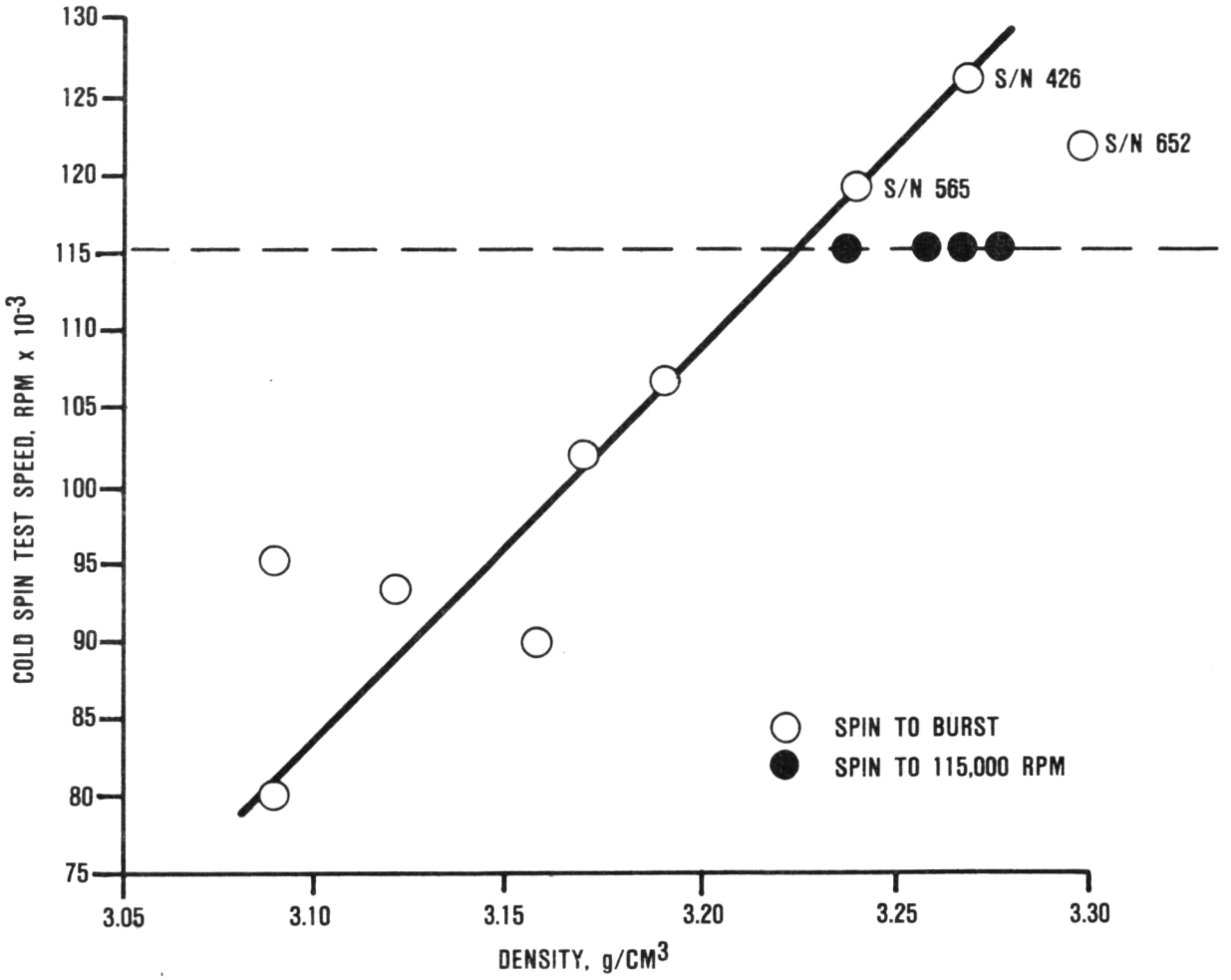

Figure 80. Increasing Consistency Evident in Cold Spin Test.

Table 39. Cold Spin Test Results

S/N	Density, g/cm^3	Speed, rpm	Test Objective
344	3.30	115,000	Proof test rotor after blade turning to eliminate the critical resonance frequency from the operating range.
		115,000	Proof test new spin pit arbor.
552	3.27	115,000	Proof test rotor after laser marking the serial number.
315	3.15	93,000	Proof test simulated rotor to 105,000 rpm.
652	3.30	121,000	Spin to burst to provide data correlating burst speed with density.
688	3.27	101,000	Spin to burst to provide data correlating flaw size with strength.

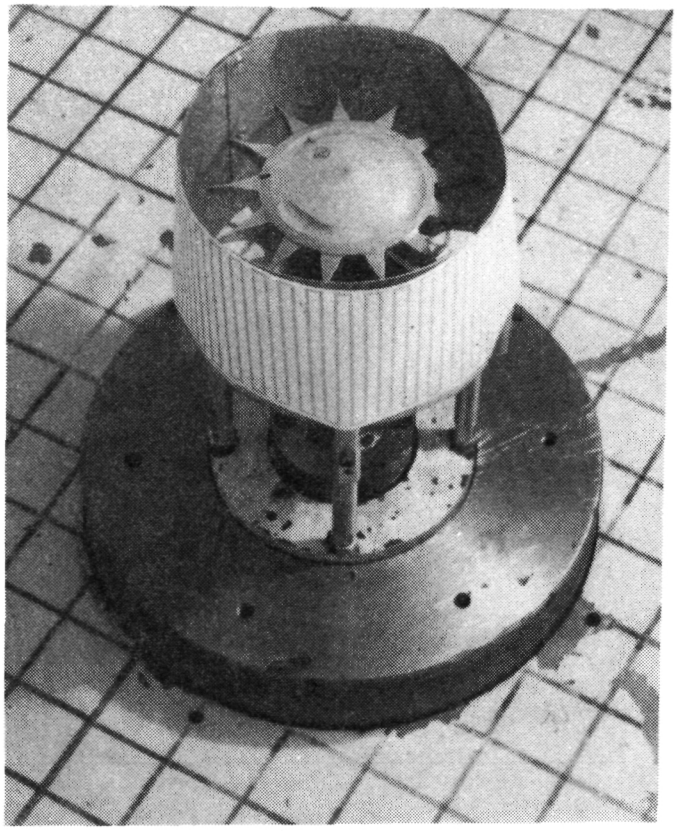

Figure 81. Ceramic Rotor S/N 344 Installed in Cold Spin Pit.

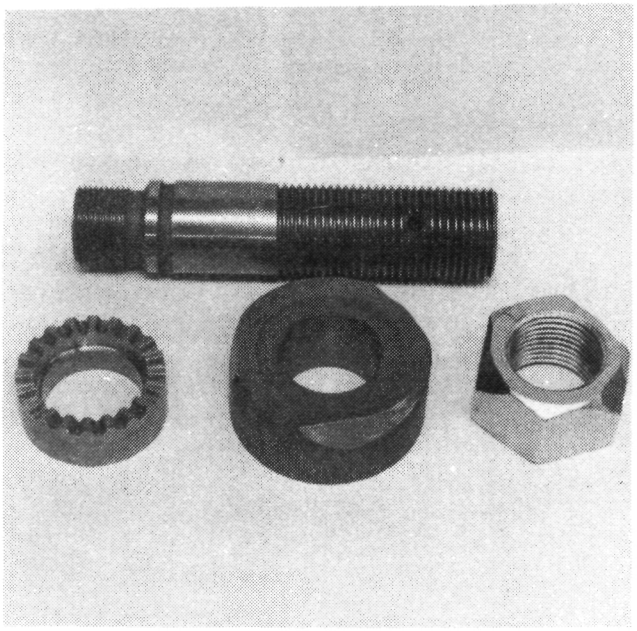

Figure 82. New Design Spin Pit Arbor.

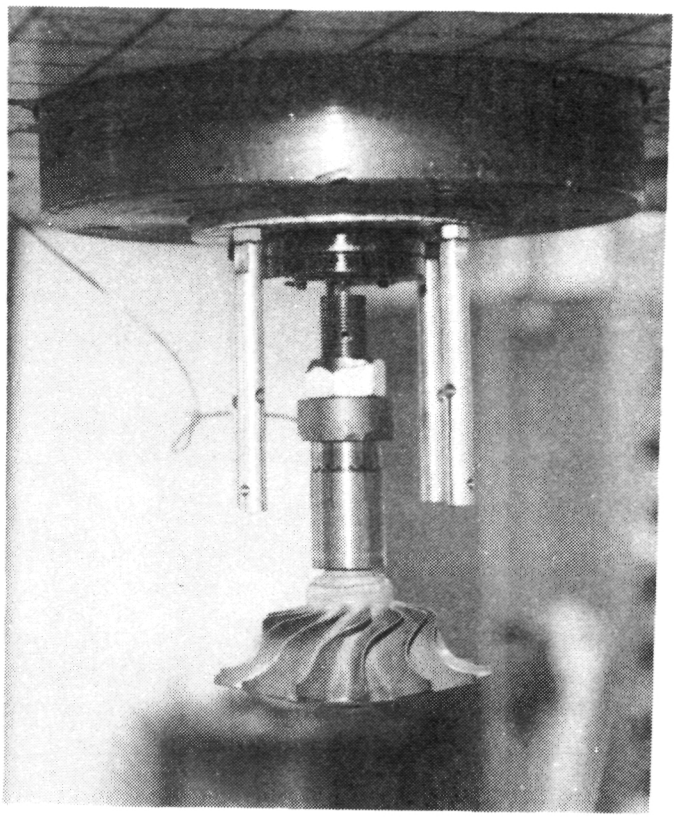

Figure 83. Ceramic Rotor S/N 344 Installed in Spin Pit With New Arbor Arrangement.

Carborundum delivered 8 combustor liners, 4 regenerator shields, 2 transition ducts, 1 combustor baffle and 132 stator segments all fabricated from SASC.

NGK delivered 5 turbine shrouds fabricated from SN-54.

Kyocera delivered 12 sets of rockers, eccentrics, bolts and washers, 6 combustor liner supports, 6 fuel nozzle holders and 6 spacer sleeves all fabricated from SN220M. Six combustor liner supports fabricated from SC201 were also received.

Corning delivered 3 flow separator housings fabricated from LAS.

Duramics delivered 162 pieces of thermocouple hardware fabricated from Al_2O_3.

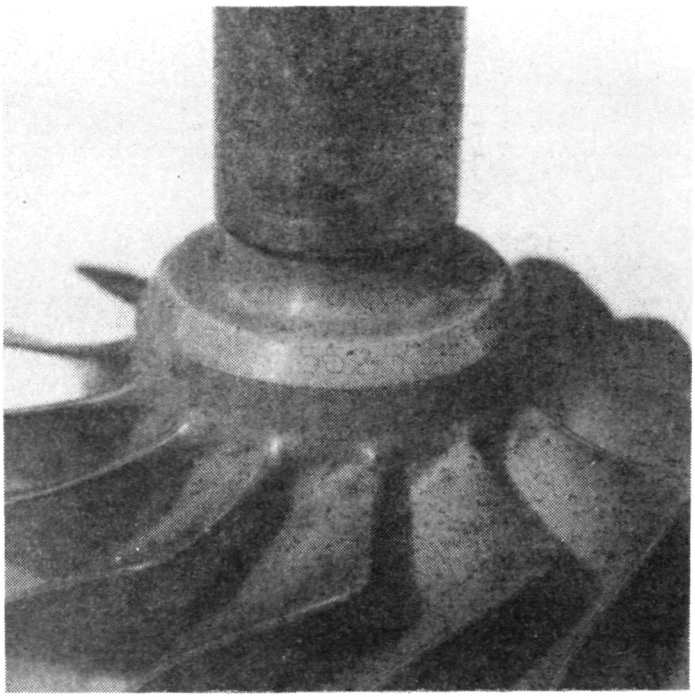

Figure 84. Laser Marking of Ceramic Rotor S/N 552.

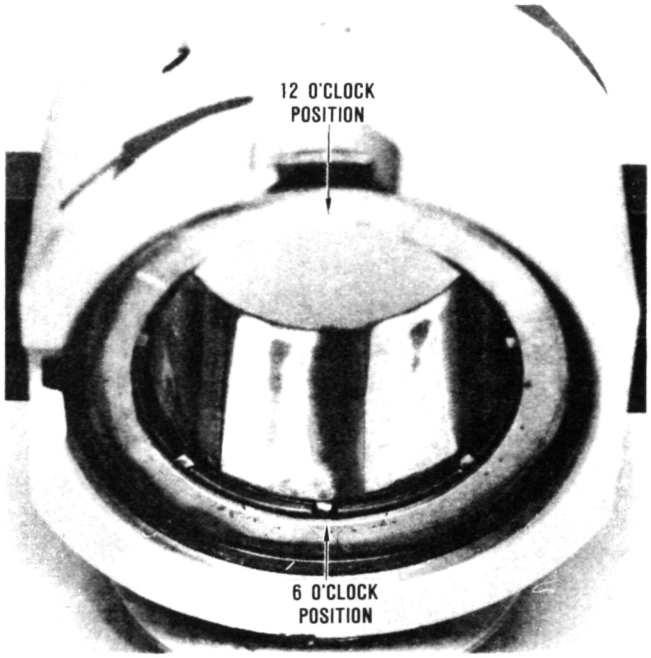

Figure 85. Wear on Foils Supporting The Shaft Loads After 263 Starts.

4.6 High Temperature Foil Bearing Development

Previous high temperature foil bearing programs (Reference 10) resulted in selection of a foil and journal coating combination capable of operation at 1200F. A sputtered TiC foil coating was used with Kaman SCA (Silica-Chromia-Alumina) journal coating. However, when tested in the AGT single bearing rig at a 1-g equivalent load, almost complete foil coating wear-through occurred during 263 starts. Figure 85 shows the bearing wear. Testing was stopped when bearing start torque exceeded test rig starting torque capability.

In addition to a high wear rate, the TiC coated foil bearing did not demonstrate the required load capacity of 6-g for 0.2 sec. The lower load capacity exhibited was determined to be due to the use of an extremely thin (0.0002 inch) hard foil coating. The softer, thicker (0.0008-0.0012 inch) low temperature coatings (Polyimide, Teflon) produced high load capacities because the soft coating loses high spots resulting from foil thickness variations (0.0002-0.0004 inch) allowing the bearing to develop an air film having extremely uniform thickness. Thus, it is necessary to develop an ablative thick film high temperature foil coating that quickly wears in to match journal contour when loaded.

The AGT foil bearing is unique in several areas in comparison to other Garrett developed foil bearings:

- High unit loading at 1-g load - 4.3 psi with ceramic rotor, 5.6 psi with metal rotor whereas previous high-temperature foil bearings were subjected to loads in the 1.1 to 2.1 psi range.
- Rotor excursions can exceed calculated bearing sway space because the bearing is not hydrodynamic when the first critical rotor speed occurs.

- The foil coating must be usable with both a ceramic and a coated metal journal.

Coatings and Materials Evaluation - A test program was initiated to develop suitable bearing coatings for the AGT. Table 40 summarizes the coating combinations and test temperatures. Figure 86 summarizes the methods used in this effort. The rationale of this process was to reduce the initial coating combination matrix to the two or three best suited coating combinations for a 1200F bearing application. Dynamic properties rig testing was used first since previous materials work indicated that if a coating combination gave good results in this rig, the probability of good bearing performance was very high. Test rig features are depicted in Figure 87.

The rotating wear ring, simulating the bearing journal, contacts a thin flat metal sheet simulating the bearing foil. Candidate journal and foil coatings are applied on the contact surfaces. The ring is driven by a variable speed motor, and is capable of axial translation along its axis of rotation. The ring contact surfaces can either be lifted off the foil surface, or held against it with a controlled force, simulating the contact force in an actual bearing. Provisions are incorporated for measuring the torque created by the rotating ring contacting the foil specimen. Friction coefficients then are derived from the torque and load applied to the ring-foil interface. Recent test rig improvements have made static (breakaway) as well as dynamic friction measurements possible.

Table 40. Summary of Foil and Journal Coatings Evaluated.

Journal Coating or Material \ Foil Coatings (IN-X750 Foils)	Au Knoop 200 (Electroplated)	YSZ (Thick Columnar)	IN-X750 (Heat Treated Uncoated)
Silicon Nitride (Hot Pressed or ISO-Pressed	X Amb, 800, 1000, and 1200F	X Amb	0
Tin (PVD)	X Amb, 800, 1000, and 1200F	0	0
Kamatics Karamite (Plasma Spray)	X Amb, 800, 1000, and 1200F	0	0
IOSSO (Proprietary Process)	X Amb, 800, and 1000F	#	0
Boronized IN-718 (Boron Diffusion)	X Amb	X Amb	0
YSZ (EBPVD)	#	0	X Amb

X - Tested, test temperatures noted
\# - Proposed but not tested
0 - No testing considered

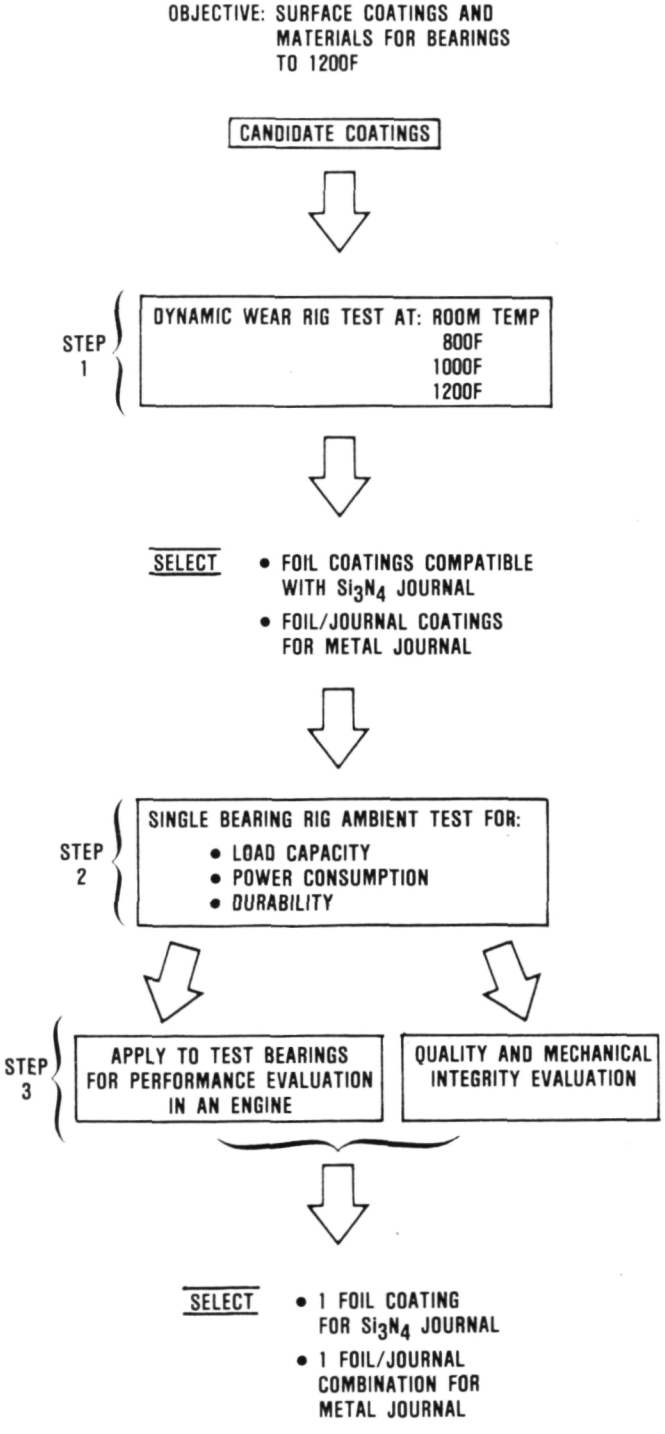

Figure 86. Foil Bearing Surface Coating Development.

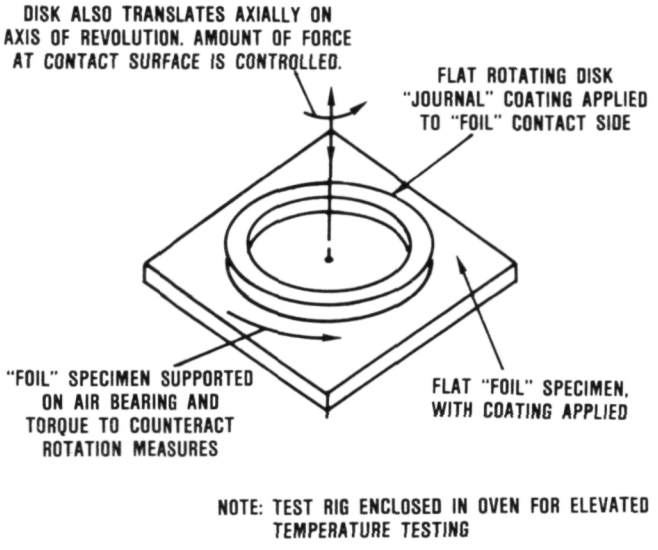

Figure 87. Dynamic Properties Test Rig Schematic.

The dynamic properties rig test procedure used is described in Table 41. This methodology was chosen to replicate bearing starts as closely as possible within the limitations of the test rig. Si_3N_4 versus Au and TiN versus Au were tested to this procedure. Although both TiN and Si_3N_4 have relatively high coefficients of friction at higher temperatures, durability was excellent. Figure 88 is typical of the results obtained during testing. Friction coefficients ranged from those shown in Figure 88 to as much as 0.2 higher for breakaway and dynamic values throughout 800-1200F testing. Ambient friction coefficient values were much lower for both coating combinations ranging from 0.1 to 0.2 at breakaway to 0.1 to 0.15 dynamic.

Single Bearing Rig Testing - To date, Si_3N_4 versus Au has been thoroughly tested in the single bearing rig while evaluation of TiN has not been completed. This test rig is depicted in Figure 89. Test bearing torque is measured via a torque arm and load cell attached to the test bearing housing.

Table 41. Wear Test Sequence.

Step	Condition	Temperature, F	Rig Speed, rpm	Load, psi	Procedure and Time
1	500 Cold Starts	Ambient	0-2000-0	4.3	Accel to 2000 rpm and roll down 2.5 sec, static dwell 15 sec
2	500 Hot Starts	800 1000 1200	0-2000-0	4.3	Accel to 2000 rpm and roll down 2.5 sec, static dwell 15 sec

NOTES:
1. Average wear ring surface speed: 200 rpm = 1.42 ft/sec, 2000 rpm = 14.2 ft/sec
2. 1.96 lb load on load arm = 4.3 psi load on test specimens
3. Large increase in torque requires stopping test, visual examination of test specimen
4. Visual inspection to determine continuation of test at next temperature level

Load is a function of the pressure on the load piston. The test procedures used for bearing testing was as follows:

- Ten no load starts to 50,000 rpm - measure bearing breakaway torque before and after starts
- Ten 1-g load starts to 50,000 rpm - measure bearing breakaway torque before and after starts
- Remove bearing. Visually examine and if no damage is present re-install in rig and measure breakaway torque
- Measure power consumption at loads from 1-g to maximum load sustainable for 2 or more seconds
- Remove bearing and examine
- Replace bearing foils and shaft if necessary. Measure breakaway torque. Run 1000 1-g load starts. Measure breakaway torque, then examine bearing

During the load capacity test a bearing is usually tested to the point at which some foil damage occurs in order to determine ultimate load capacity. Therefore, a new bearing and an undamaged shaft are used for durability testing. Table 42 compares the results obtained for Si_3N_4 versus Au and SCA versus TiC (original AGT high temperature bearing). Figure 90 shows the extent of wear on this bearing. Note the extremely small wear area on the foil; only polishing occurred with no measurable wear. Load capacity also equalled that achieved with the low temperature bearing tested in the single bearing rig.

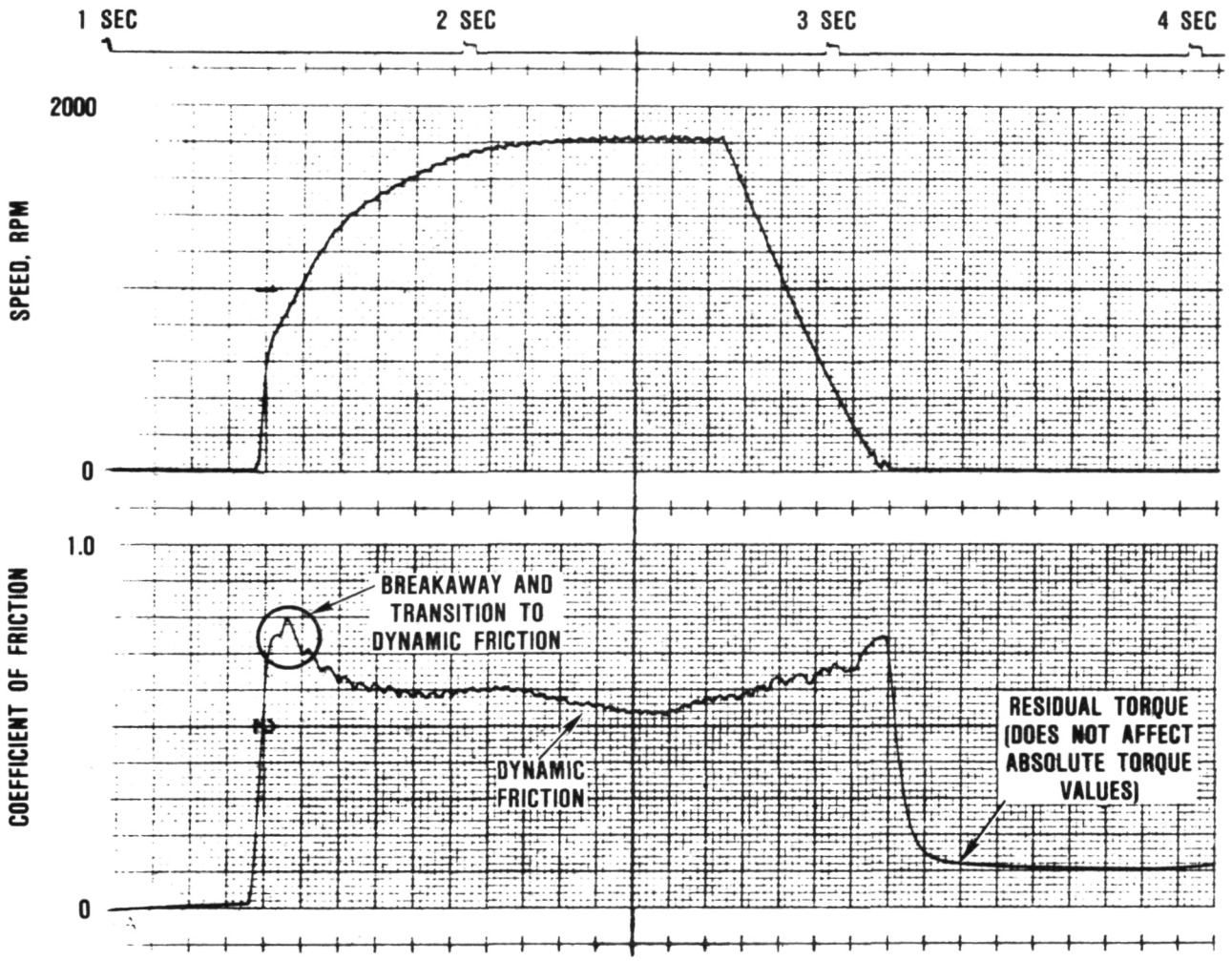

Figure 88. Typical Results of Dynamic Friction Test.

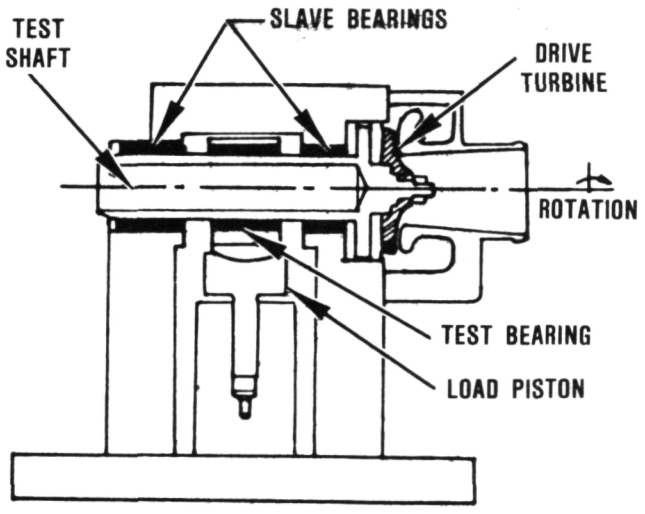

Figure 89. AGT101 Single Bearing Test Rig Schmatic.

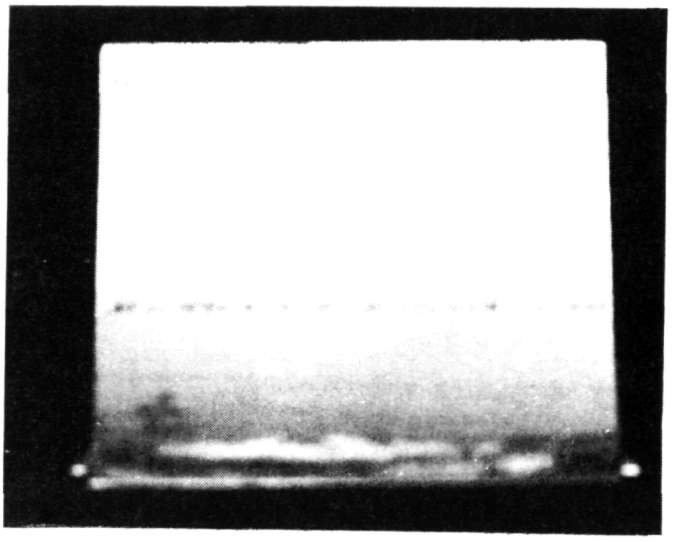

Figure 90. Wear Typical of 1000 Starts at 1-g Load, Aμ Coated Foil Versus Si_3N_4 Journal.

Table 42. Comparison of Test Results For High Temperature Foil and Journal Coatings at Ambient Conditions.

Coating System	Load Capacity and Conditions	Durability
Foils: Tic Shaft: Kaman SCA	19.2 pounds for 2 seconds, 75 krpm	263 starts, 1-g load, complete TiC wear-through
Foils: Au Shaft: HPSN	24.6 pounds for 30 seconds, 75 krpm	1000 starts, 1-g load, no measurable wear
NOTE: All foil dimensions were the same for both of the tabulated tests		

Rig testing has shown Au to be a viable bearing coating for use with a Si_3N_4 journal in the 2500F AGT engine. Proof of this concept will be testing in the engine. Figure 91 shows an integral Si_3N_4 rotor/bearing journal design for accomplishing this goal. TiN is currently considered a viable coating for a metal journal attached to a ceramic rotor when used with Au coated foils. Bearing load capacity also has been maintained in making the transition from low to high temperature foil coatings, a goal not previously accomplished.

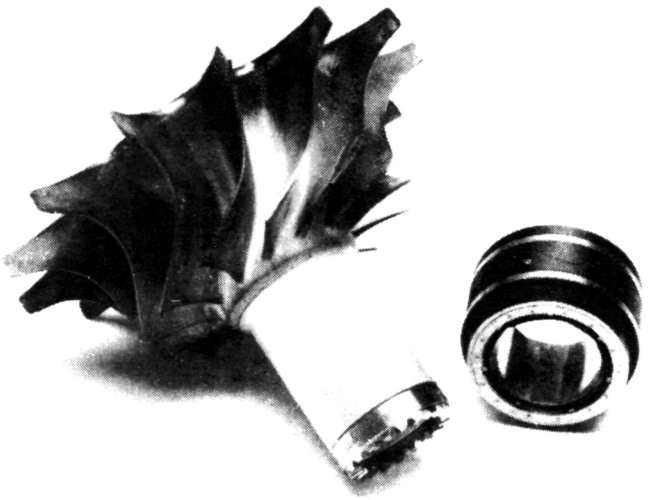

Figure 91. Si_3N_4 Turbine Rotor with Integral Bearing Journal and Aμ Coated Foil Bearing.

APPENDIX A

FORD MOTOR COMPANY
ADVANCED GAS TURBINE (AGT)
TECHNOLOGY DEVELOPMENT PROJECT
1985 ANNUAL
TECHNICAL PROGRESS REPORT

1.0 TASK 2.3 - Ceramic Rotor

1.1 RM-20 Silicon Nitride

RM-20 is a silicon-nitride based material originally developed by Ford for cutting tools and other wear type applications. This material is made by pressureless sintering using silicon nitride chemistries. The process concept involves a form of SRBSN, and the use of yttria as a major sintering aid. Property data and the inherent process flexibility of RM-20 indicates that this material is suitable for slip casting of the AGT rotor.

During this reporting period, attention was focused on a number of process areas relative to the fabrication of rotors using the RM-20 material. These areas were:

- o Primary and secondary reduction of process powders
- o Slip cast development
- o Rotor casting using the fugitive wax process
- o Pre-sintering and sintering of the rotor
- o Heat treatment of RM-20 rotors

Each of these process areas is discussed in the following paragraphs.

1.1.1 RM-20 Powder Reduction

Primary Reduction - The process for manufacturing RM-20 powder consists of dry ball milling selected silicon powders and additives to yield an intimate mix, that are cold pressed under a uniaxial pressure into round plates. Plates are nitrided to yield silicon nitride contents greater than 70-percent concentration by weight and second phase oxynitride crystallites of $Y_{10}Si_6O_{24}N_2$ composition. Thereafter, the plates are broken into coarse particles (14 mesh) suitable for primary reduction by roll crushing.

The nitrided plates have densities in the 1.9 to 2.1 g/cm^3 range and, therefore, the process for reducing the plates by way of primary reduction is difficult and time consuming. Experiments were conducted to determine if lower density (<1.5 g/cm^3) preforms or loose agglomerates could be nitrided to form the desired Si_3N_4 and oxynitride compositions, and as a result become more suitable for reduction into powder. Three component powder blends were nitrided as either loose powders or as briquettes (formed under minimal pressures). The nitrided products were subsequently analyzed by x-ray diffraction, and the formation of the $Y_{10}Si_6O_{24}N_2$ was found to be insufficient to yield a pressureless sinterable powder. Nitrided densities of 1.5 g/cm^3 or greater must be achieved to provide the formation of required powder composition.

Secondary Reduction - Ball milling is used to further reduce the particle size after roll crushing. Dry milling with alumina grinding media will produce powders suitable for the manufacture of slips. By most standards, the resultant powder distribution is relatively coarse for slip casting, but stable slips can be prepared when using deflocculant systems that provide both physical and chemical suspension mechanisms. Two additional secondary milling operations, noted as Secondary Reduction II (SRII) and Secondary Reduction III (SRIII), were instituted to produce finer powders for slip/casting evaluation, (i.e. powder property evaluation).

PRECEDING PAGE BLANK NOT FILMED

SR II utilizes an additional dry milling step and yields a broad particle distribution with no particles larger than 100 mesh. The third reduction technique, SRIII, is wet milling in methanol for 24 hours, which produces a steep distribution curve with all particles less than 325 mesh. Figure 92 reveals the procedure followed in a flow chart of RM-20 powder production. These powders, as shown in the Slip section of this report, are being evaluated for casting suitability.

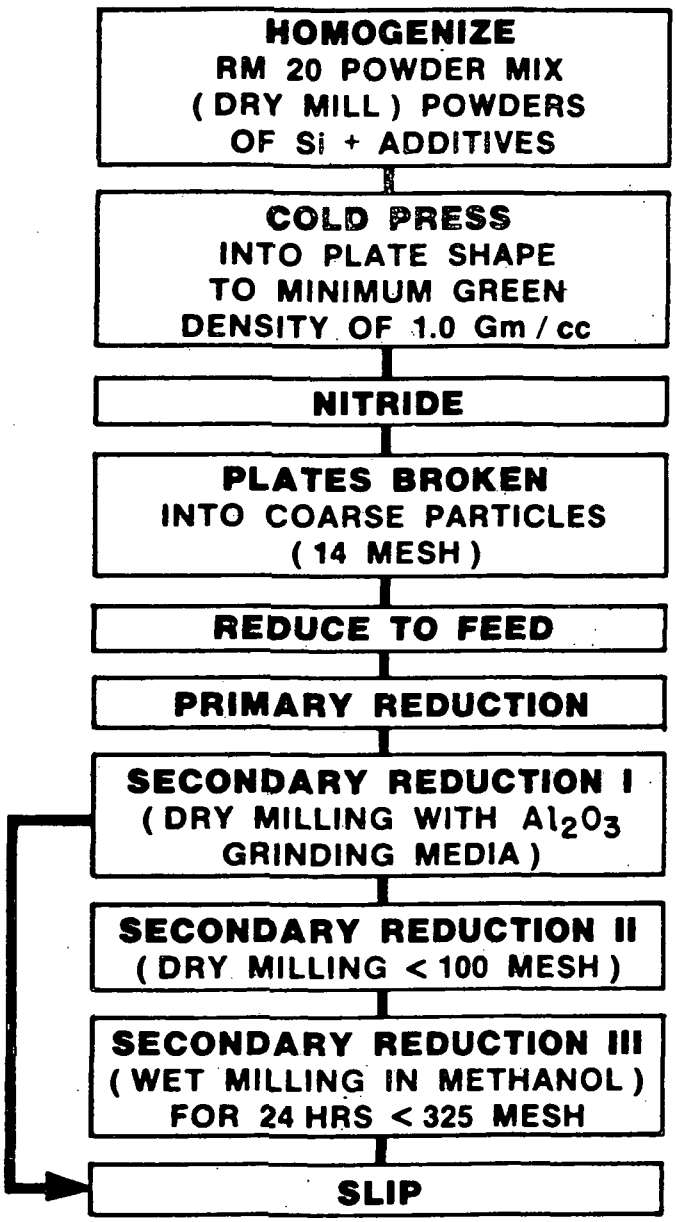

Figure 92. RM 20 Powder Reduction Flow Chart.

1.1.2 RM-20 Slip Formation

Slips were formulated for study using powders representative of SRII and SRIII techniques. Three deflocculants were evaluated: a) Keltex, b) Dispex A-40, and c) Colloids of California 226/35. All deflocculants show chemical and physical suspending mechanisms and are appropriate for the relatively large particle size systems presently used for rotor castings.

The objective of this study is to optimize the slip and casting behaviors for rotors that are cast to net shape on the back face contour (see Casting section for details). The optimum slip must be free of out gassing, show good flow characteristics, show stability within the casting time period, and demonstrate little thixotropic behavior upon casting.

Results thus far show that SRII type powders, reference Figures 93 and 94, show good rheological behavior at low deflocculant concentration levels, whereas the finer SRIII powders reference Figure 95 and 96, produce relatively high viscosity slips with pronounced thixotropy. Dispex A-40, reference Figure 93, at a concentration level of 0.26 percent yielded slips that demonstrated excellent stability and batch to batch reproducibility.

Casting quality to date has been unpredictable. Casting flaws, particularly blade cracking, have been difficult to define as to cause. A study was initiated to assist in determining the cause by evaluating all aspects of the casting process. In general, the casting process can be defined as to technique, hardware and slip. The last item has been optimized and discussed in the previous section; this section will highlight some notable observations and changes that were made as a result of this ongoing analysis.

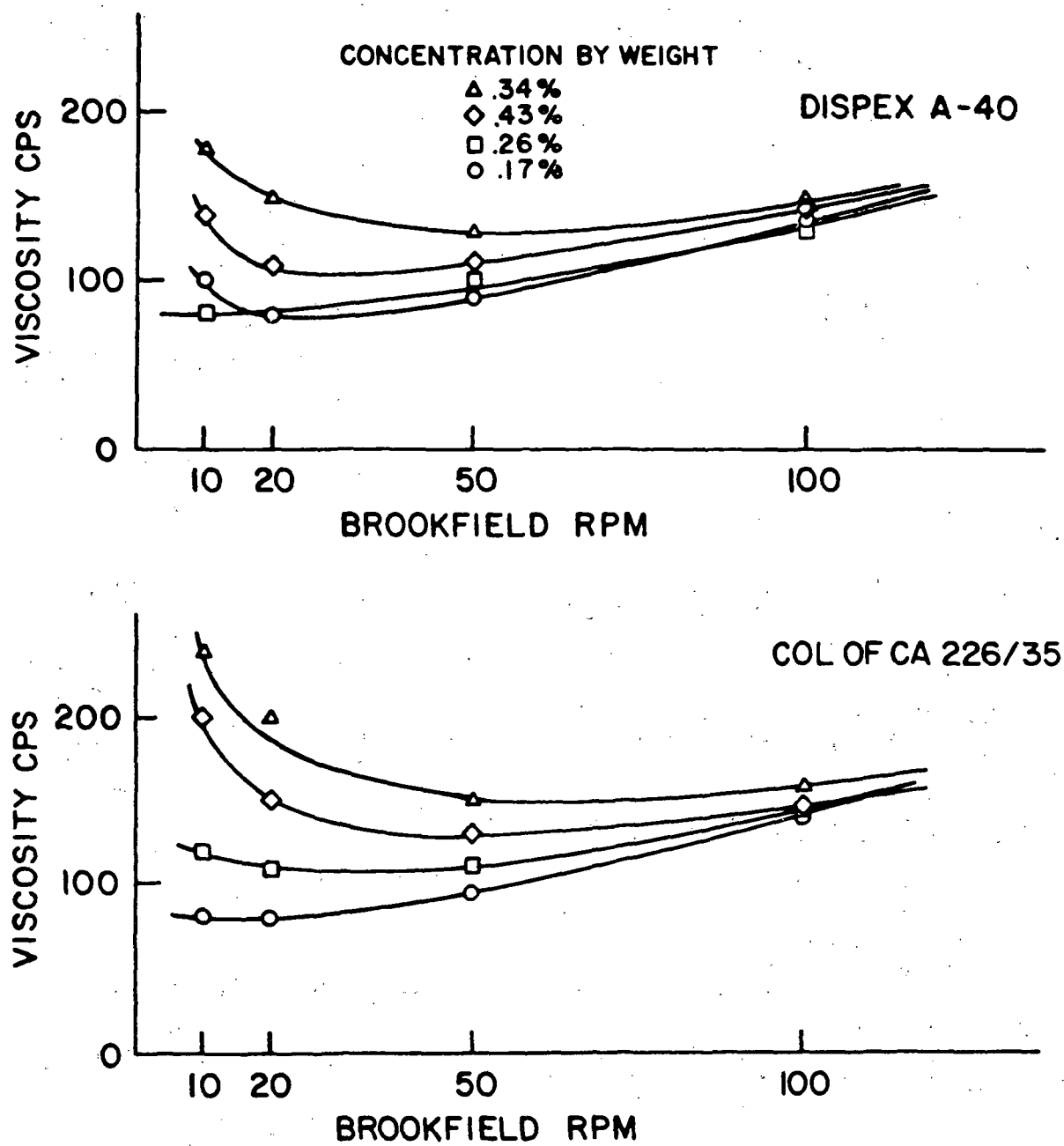

Figure 93. Dispex A-40 and Colloids of California 226/35 SRII Powder.

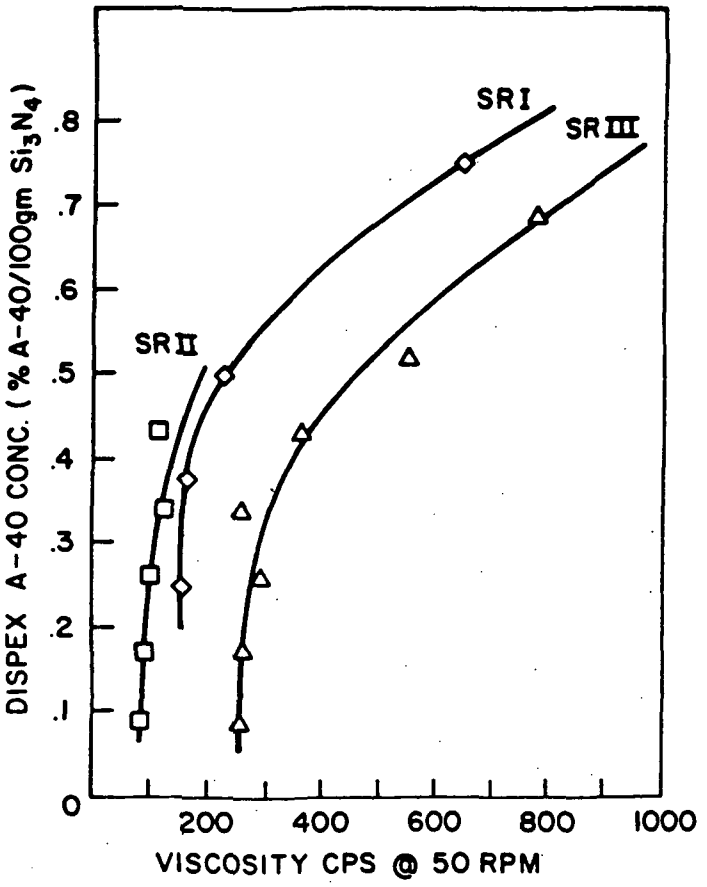

Figure 94. Dispex Concentration Versus Viscosity for 3 Powder Distributions.

1.1.3 Rotor Casting - Fugitive Wax Process

A revised casting procedure for rotors was initiated to reduce the amount of machining of the rotor back face contour to eliminate blade/tip tear during sintering and improve the uniformity of the rotor material. The new procedure enables casting to the specific profile, plus machining stock, by directly piloting the wax mold to an appropriately contoured plastic base.*

*Note: This new procedure has also introduced casting flaws heretofore not present; i.e. the new process is much more sensitive to casting techniques.

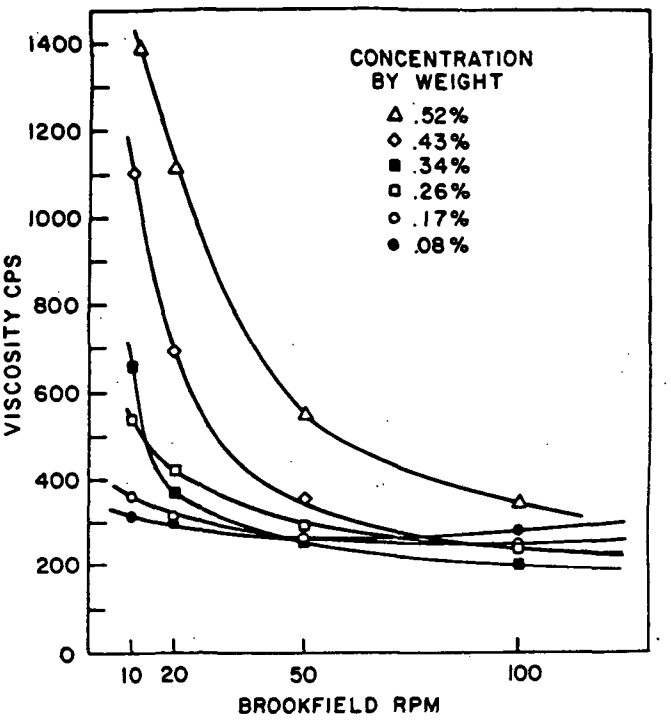

Figure 95. Dispex A-40 SRIII Powder.

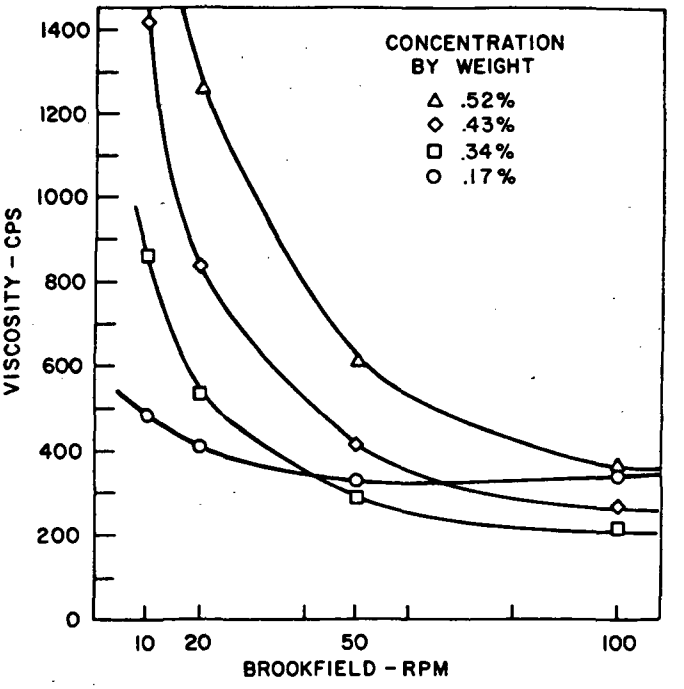

Figure 96. Colloids of California 226/35 SRIII Powder.

The fugitive wax molds are now entirely made with Freeman Manufacturing dip seal wax, which provide more rigidity than the previous wax blends that were formulated for ease of removal in the solvent bath. The original waxes were prone to pseudo-elastic distortion under even slight mechanical loading. The dip seal system is somewhat more stable but also shows the same distortion tendencies. this type of action has resulted in blade cracking in several rotors during the mechanical fixturing of the wax/mold or during removal of same. A new technique was developed to preclude all clamping of the mold to the plaster body. This technique improves rotor quality from the standpoint of blade cracking but makes establishing a uniform seal between the wax and plaster more difficult. This new procedure will be continued; in addition, wax manufacturers are being surveyed to find a more rigid wax to replace the dip seal material.

A Tergitol rinse of the dip seal wax rotor before casting was instituted to provide more efficient wetting of the slip/wax interfaces. This technique has significantly improved casting quality with respect to fill.

Wax molds after casting are being removed by solvents at room temperature. The bath removal process is now completed within 24 hours. Longer soak times were shown to cause slaking of the casting surface.

A one-to-one relationship between positive wax quality and resultant casting quality has been established. Imperfection in the wax (flash, surface irregularities, cracks, etc.) yield gross flaws in the final sintered rotor. These flaws may initially appear after casting, after bisque firing or after sintering. Steps were taken to improve the quality of the wax positives. Ford tooling was reworked for additional wax molding. Assistance was provided to Ford's wax fabricator in developing a wax molding process for manufacturing the positive wax patterns to the quality specification required. This process was successful and waxes of the required quality have been received.

Blade tip casting density uniformity has varied when using primarily a static casting technique. This variation resulted in blade cracking due to differential green shrinkage and/or differential sintering shrinkage. This problem went undetected because this density variation exists below the casting skin. The skin itself appears to be uniform and is only detected when removed via glass beading. Therefore, several casting trials were conducted using centrifugal casting during the latter stages of casting consolidation, particularly during the time increment before blade consolidation occurs. Results show that these variations in density can be reduced using a centrifugal casting technique. This has now been verified on two individual castings.

1.1.4 RM 20 Rotors Pre-Sintering of Rotor

Once dried, the casting becomes extremely fragile and is difficult to handle for inspection and for subsequent sintering. The problem is particularly severe during the placement or "packing" of the rotor in a powder blanket for sintering. Therefore, a pre-sintering or "bisque" firing treatment was developed to partially consolidate the casting and provide the required handling strength.

The bisque firing uses a slow heat-up schedule to 1600C and is held there under N_2 for 4 hours. During this cycle the casting will undergo partial consolidation as indicated by 1/2-percent linear shrinkage, which is sufficient to impart suitable handling strength. An additional advantage of the bisque firing is that the casting can be readily machined using standard high speed steel tools (this ability will reduce diamond grinding of the final component). Results also show that the pre-sintering cycle does not impede the final sintering kinetics. This process is now being used on all castings.

1.1.5 Sintering of Rotor

Cycle - The sintering temperature profile that was initially developed was a single-step densification cycle. Such a cycle was adequate for the densification of the original

platformed rotors but yielded unpredictable blade distortion in the newly designed rotor castings and, in addition, considerable fusing of the packing powder. The packing powder became extremely difficult to remove particularly between the blades. Packing powder compositional changes reduced the observed effects but did not eliminate the problem.

A two-step sintering was therefore developed and optimized to reduce blade distortion and to facilitate the removal of the packing powder. The first sintering step of the dual cycle utilizes a packing powder containing boron nitride and a temperature ramping schedule that has three discrete temperature holds. The cycle is 12 hours in duration with the typical casting undergoing a 8-12 percent sintering shrinkage during this step. Negligible fusion occurs within the packing powder and can easily be removed.

The second step of the sintering cycle utilizes a compositional change in the packing powder and a single temperature hold at 1800C. The compositional change requires the boron nitride content to be decreased to 25-percent of the packing powder mix which effectively increases the Si_3N_4 powder component. This increase provided greater availability of $SiO_{(g)}$ during the sintering cycle, thereby maintaining the required oxynitride composition within the rotor so that full densification can be achieved. Again, after sintering, the packing powder is readily removed.

Upon conclusion of the two-step cycle a nominal 18-percent sintering shrinkage is realized and a final density of 3.24-3.28 g/cm^3 obtained. Observed blade distortion was minimal.

Equipment - The pressureless sintering process utilizes a cold walled vacuum furnace and a refractory metal hot zone. The major drawback of this system is the reactivity of the $SiO_{(g)}$ with the refractory metal hot zone. The hot zone was limited to approximately 15 to 18 cycles before a complete rebuild was required. Significant in-house modifications have increased the furnace life to approximately 25-28 cycles, which is still inadequate (two complete rebuilds were required during this reporting period).

As a consequence, a furnace manufacturer was contracted to redesign the hot zone and other deficient furnace areas to accommodate the sintering environments.

The new design provided for a smaller, more efficient hot zone, faced with tungsten. The new hot zone was constructed, installed, and evaluated with approximately one dozen cycles logged to date. After several cycles, deterioration was noted and rapidly accelerated with subsequent cycles. The furnace manufacturer has analyzed the performance and feels that the 0.005 thickness W was insufficient under the sintering condition. The hot zone has been removed and is being returned to the vendor for corrective action.

1.1.6 Heat Treating of RM-20 Rotor

All pressureless sintered rotors thus far have shown a duplex zoning fracture. The exterior casing is generally dark in color and shows a well crystallized secondary phase. The interior region of the rotor is lighter in color and shows by x-ray diffraction a predominately glassy phase. The densities of both regions appear to be equal. Cold spin testing in a vacuum of rotor SC-8 produced blade separation failures at speeds of 93,586 rpm, 104,849 rpm, and 110, 846 rpm. Fracture origins could not be identified but separation in all blades occurred near the interface of the duplex zones. The zoning interface may be acting as a stress riser and thereby producing premature failures.

An investigation was initiated to develop techniques for crystallization of the interior region of the rotor and for elimination of the duplex interface.

Techniques evaluated were primarily heat treatments that have been successful in producing secondary phase crystallization in hot pressed materials similar in composition to

RM-20. Six different heat treatment experiments were designed and conducted on representative RM-20 specimens. Results show that crystallization could not be achieved using heat treatments appropriate for hot pressed materials. Therefore, a detailed scanning electron microscope (SEM) and micro-probe analysis was conducted to provide additional compositional and material "state" information.

All combinations of nucleation and growth temperatures tested showed second phase crystallization. The resultant second phases were not the oxynitrides as expected by yttrium silicate Y_2SiO_5. This silicate formation (rather than the oxynitride) is due to extensive oxygen pick-up during RM-20 powder preparation - specifically during the primary and scondary reduction steps.

These results indicate that oxygen must be reduced from the powder before sintering to produce the required oxynitride. Experiments are underway to determine if oxygen can be reduced during bisque firing or during the initial stages of sintering.

These results also indicate that the oxygen content in RM-20 materials may be at a sufficient level to preclude the use of packing powders. Seven rotors of the RM-20 composition are currently in the nitriding process.

1.2 RM-2 Rotors

One rotor of the RM-2 composition successfully passed the 115,000 rpm test at room temperature. This rotor, designated V-26, had a sintered density of 3.245 g/cm^3, and has been delivered to Garrett for further testing.

Five RM-2 composition rotors (V-30, 37, 38, 42 and 43) were shipped to ASEA for HIP. Nitrided densities ranged from 2.38 to 2.48 g/cm^3 and after HIP the densities were 3.30 to 3.32 g/cm^3. Four of the rotors were crack free. The fifth had several large cracks on the bottom surface and all rotors had bottom blade tips broken off either during HIPping or handling prior to HIPping.

Microstructural examination revealed some surface interaction between the cladding material and the Si_3N_4. The interior surface was dense and appeared to be flaw free.

Rotor V-43 has been spin tested three times with a loss of blade fragments at 64,500 rpm during the last test.

Rotor V-30, HIPped by ASEA, reached a speed of 106,400 rpm when two blades separated. After rebalancing, a second test ended with complete uniform failure at a speed of 110,400 rpm.

Rotor V-42, which has large cracks, will be sectioned and test bars cut from various locations.

Rotors V-37 and V-38 are being prepared for spin testing.

2.0 Task 2.7 - Stators

2.1 Molding Development

Because of a termination of funding, stator molding development was conducted for only one month during this report period. The tool was reassembled with the additional central electrical heating element. A new batch of molding mix was prepared using a modified procedure in which the silicon powder was blended before mixing the batch.

Initial molding attempts using previously established machine settings and sequencer times proved unsuccessful. Several parametric studies were made resulting in improved as-molded quality. The studies did not include the effects of the new heater because of time constraints.

Parts molded during the parametric studies yielded seven good quality stators for further processing. Three of these have no vane root leading edge cracks and three or less small trailing edge cracks.

2.2 Stator Processing

Stator processing through burn out, nitriding and machining continued throughout the report period:

- o Burn out - 26 stators (4 runs)
- o Nitriding - 11 stators (3 runs)
- o Machining - 6 stators

During the report period twelve stators were delivered to Garrett:

1 - Fully machined and flash oxidized
5 - Fully machined
6 - Nitrided castings

3.0 Task 2.7 - Flow Separator Housing

Six AGT flow separator castings were delivered to Ford for non-destructive evaluation. Of this group, two castings were accepted for machining, and a third casting, S/N 28 was accepted under deviation because of component need. One of the two accepted castings, S/N 30 was machined and delivered directly to Garrett. The second casting, S/N 33, could not be completed because of a machining error at Corning. The casting, S/N 28, was accepted under deviation and was machined and delivered in October 1984.

Overall, the reject-accept ratio of 4:2 was not an improvement over components delivered during earlier reporting periods. On the positive side, the components shipped by Corning during this period had fewer and smaller casting voids. However, new problems were encountered with the last two castings. These problems were cracks in the crossarm - base radius of S/N 34 and insufficient base wall thickness in S/N 37.

In the second quarter of 1985, funding for this activity at Ford was terminated and the NDE technology was transferred from Ford Motor Company to Garrett.

APPENDIX B

AIRESEARCH CASTING COMPANY
ADVANCED GAS TURBINE (AGT)
TECHNOLOGY DEVELOPMENT PROJECT
1985 ANNUAL
TECHNICAL PROGRESS REPORT

1.0 INTRODUCTION

This report, submitted by AiResearch Casting Company (ACC), will cover the efforts of ACC in support of the Garrett/Ford AGT101 program. The ACC effort was conducted as a Garrett subcontractor. This report covers the ACC materials and fabrication development efforts during the period July 1, 1984 through June 30, 1985. These efforts mainly were concerned with the materials development and fabrication of rotors and ceramic structures by slip casting and the fabrication of stator vane assemblies by injection molding.

2.0 SUMMARY

Considerable effort was expended in locating alternate sources for silicon nitride powder. Nine companies, domestic and foreign, have been contacted, most of whom favorably responded. Powder from each of these sources has been obtained and is being evaluated. Several powder samples appear to be satisfactory candidates for slip casting of AGT101 rotors.

Difficulty with the General Telephone and Electronics (GTE) SN-502 baseline Si_3N_4 powder was experienced due to a change in properties of incoming material. This was attributed to a manufacturing process variation which changed the particle shape from whisker to spherical and drastically increased the surface area of the powder.

Seventy rotors were cast during this reporting period using the GTE SN-502 Si_3N_4 powder. The rotors passing inspection after pre-sintering were further densified at Ford, ASEA and ACC by sintering, encapsulation plus HIP and by sinter-HIP. Rotors sinter-HIPped at ACC showed higher flexure strength values. Other rotors cast were SRN-SNN mixtures that were part of an internally funded program. Three rotors were cast using UBE Si_3N_4; three were cast from Starck H-2 powders and five were cast using Denka Si_3N_4 powders, all of which are part of the ongoing program to locate suitable alternate sources of supply for Si_3N_4 material. Nineteen rotors were successfully densified and shipped to Garrett for further evaluation.

During this reporting period, several design changes were made, both on rotor and static structure components. The change from "A" (open blades) to "B" generation (closed blades) rotors drastically increased the time required for complete casting due to the reduction in contact area of slip to plaster. Vacuum-assist casting was initiated which reduced the casting time by as much as 50 percent. The effect of this process is still under study.

During this period, 50 turbine shrouds were cast. Several of these cracked during the early stages of drying, but a change in the drying environment dramatically improved the yield. Fifteen fully processed shrouds and 3 truncated shrouds have been shipped to Garrett. Additional shrouds are in various stages of processing.

3.0 ROTOR MATERIALS AND FABRICATION DEVELOPMENT

3.1 Raw Materials

3.1.1 Availability of Si_3N_4 Powder

Table 43 provides a list of companies, both domestic and foreign, currently producing Si_3N_4 powder. Cost and availability also are indicated. Several sources provide powders having different nomenclatures, which indicate variations in chemistry (purity) particle size distribution (PSD) and surface area. Tables 44 through 54 are typical material properties specified by each manufacturer. Figures 97 and 98 are PSD curves also supplied

Table 43. Silicon Nitride Survey

Country/ Vendor	Commercially Available ?	Price per lb, $ (100 lb Minimum)
United States		
GTE Sylvania	Yes	50.00
Norton	No	---[1]
Elkem	Yes (10/85)[2]	10.00-13.00
Japan		
Asahi Glass	No	---[3]
Denka	Yes	10.00-14.00
Toshiba	Yes	40.00
Toyo Soda	Yes	30.00
UBE	Yes (1/86)[2]	30.00
West Germany		
H.C. Starck	Yes (7/85)[2]	17.50
Sweden		
Kemanord	Yes	22.50

[1]Will supply Si_3N_4 on licensing agreement only

[2]Tentative time when Si_3N_4 will become commercially available

[3]Asahi will use their Si_3N_4 powder only to produce components of their brand

Table 44. GTE Sylvania Si_3N_4 - Manufacturer's Analysis.

SN-502 Alpha Silicon Nitride Powder			
	Typical Range of Purity (% by Weight)	Crystalline Phases	
O_2	0.5-3.0	α Si_3N_4	92-98%
Al	<0.0100	β Si_3N_4	2-8%
Ca	<0.0010	Si_2N_2O	<0.5%
Mg	<0.0020	SiO_2	<0.5%
Total Cations	<0.0500	Si	<0.2%
Chlorine	<0.050		
Fe	<0.005		
Surface Area (m^2/g)			2-5
Color			Tan

by the manufacturer (Denka and Toyo Soda); whereas, Figures 99, 100, and 101 present PSD curves of UBE and Starck powders obtained at ACC as-received and after some milling. All of the powders shown to be available have been obtained and are being evaluated.

3.2 Productivity

Seventy rotors were cast using GTE SN-502 Si_3N_4 powder during this reporting period. Rotors that passed final inspection after presintering were densified at Ford, ASEA and ACC by sintering, encapsulation and HIP, and by sinter-HIP. Densities of Code 1 rotors ranged from 3.25 to 3.30 g/cm^3. Densities of Code 2 rotors ranged from 3.24 to 3.27 g/cm^3.

Four rotors were cast with SRN-SNN mixtures as part of an internally funded program; one was densified at ACC by sinter-HIP to 3.27 g/cm^3, two are in nitriding and one is in the drying stage.

Three rotors were cast using UBE Si_3N_4 (SN-EX, SN-E10, SN-E02 and SN-E05). SN-E02 and SN-E05 have been selected as the most likely candidates for producing rotors and work is progressing on further development of these powders.

Three rotors were cast using Starck H-2 material with sufficiently promising results to warrant further developmental effort.

Table 45. Denka Si_3N_4 Powder - Manufacturer's Analysis.

Representative Examples of Mineral and Chemical Compositions				
Grades		SN-7	SN-9S	SN-9FW
α-Conversion Rate (%)		74.	91.	91.
Chemical Composition (%)	Si	59.4	58.9	59.7
	N	38.2	38.5	38.8
	Fe	0.3	0.2	0.04
	Al	0.2	0.2	0.2
	Ca	0.2	0.2	0.1
	Mg	0.04	0.04	0.005
	C	0.25	0.25	0.25
	O	1.6	2.0	0.9
	Free-Si	0.2	0.2	ND

Other Properties				
Grades	Bulk Density (g/cm^3)	Tap Density (g/cm^3)	Repose Angle (deg)	Specific Surface (m^2/g)
SN-7	0.80	1.20	44	4
SN-9S	0.55	0.88	42	7
SN-9F	0.69	1.14	40	10
SN-9FW	1.05	1.18	32	12

Table 46. ELKEM Si_3N_4 Powder - Manufacturer's Analysis.

Product	Alpha Content (%)	Aluminum (%)	Calcium (%)	Iron (%)	Free Silicon (%)	Carbon (%)
Low-Impurity Grade	>80	<0.2	<0.01	<0.05	<0.5	<1.0
	60 to 80	<0.2	<0.01	<0.05	<0.5	<1.0
Regular Grade	>85	<0.3	<0.05	<0.4	<0.5	<1.0
	60 to 85	<0.3	<0.05	<0.4	<0.5	<1.0

Product	(140 Mesh) 100 Microns	(200 Mesh) <75 Microns	(325 Mesh) <45 Microns	<10Microns
Low-Impurity Grade (>80% α)	$6.75	$8.50	$11.50	$12.00
Low-Impurity Grade (>60 to 80% α)	$4.50	$6.50	$ 8.50	$ 9.50
Regular Grade (>85% α)	$6.25	$8.00	$11.00	$12.50
Regular Grade (>60 to 85% α)	$4.00	$6.00	$ 8.00	$ 9.00

		Price per lb of Alloy
Quantity Extras	2,000 to 29,999 lb	$0.08
	Less than 2,000 lb	$0.16
Packaging Extras	50 lb bags	$0.03
	500 lb drums	$0.055

Table 47. Kemanord Si_3N_4 Powder - Manufacturer's Analysis.

Data Sheet: Siconide™ Grades		
o Purity The following typical analyses are quoted for Standard (S) - and Purified (P) - grades.		
Element	Siconide™ (S)	Siconide™ (P)
	by Weight %	
N	38.2 ±0.1	38.4 ±0.1
O	≤1.5	≤1.5
Si_{elem}	≤1	≤1
Al	0.3	0.1
Ca	≤0.05	0.01
Cr	≤0.005	≤0.005
Cu	≤0.005	≤0.005
Fe	0.2	0.05
K	≤0.005	≤0.005
Li	≤0.002	≤0.002
Mg	0.004	0.004
Mn	0.004	0.004
Na	0.008	0.008
Ti	0.01	0.01
V	≤0.005	≤0.005
W	≤0.01	≤0.01
o Phase Composition Siconide™ 75, 85 and 95 have a nominal alpha-phase content of approximately 75, 85 and 95% respectively.		

Table 47. Kemanord Si_3N_4 Powder - Manufacturer's Analysis (Contd).

Data Sheet: Siconide™ Grades	
o Particle Size/Specific Surface Area	
Siconide™ C is coarsely-ground to 200 US Standard Mesh	
Siconide™ L, M and H micronized powders with low, medium and high specific surface area respectively (range 5-20 m^2/g).	
o Chemical and Physical Data	
Formula	Si_3N_4
Molecular weight	140.28
Silicon (theoretical)	60.06 wt %
Nitrogen (theoretical)	39.94 wt %
Crystallography	
Alpha form	Hexagonal S.G. P31c a_o 7.758 A c_o 5.623 A
Beta form	Hexagonal S.G. $P6_3/m$ a_o 7.603 A c_o 2.909 A
Density	3.185 g/cm^3
Hardness	9 (Moh)
Dissociation temperature (at 1 atm. N_2)	ca. 1900C

Table 48. H.C. Starck H-1 Si_3N_4 Powder - Manufacturer's Analysis.

Powder Characteristics:

o Fine particles below 5 μm # High Alpha Phase ϕ High Purity

o Morphology	Specification
BET Specific Surface Area	7-10 m^2/g
FSSS Particle Size	Maximum 0.8 μm
Apparent Density	0.35-0.55 g/cm^3
Tap Density	0.6-0.8 g/cm^3

Particle shape and size distribution according to scanning electron micrograph

# Crystallographic Phases	Specification
Alpha-Si_3N_4	Minimum 90% by wt
Beta-Si_3N_4	Approximately 4% by wt
Free Si	Maximum 0.1% by wt

ϕ Chemical Composition	Specification
Nonmetallic Constituents	N minimum 38.2% by wt
	O 1.0-1.5% by wt
	C maximum 0.5% by wt
	F approximately 0.08% by wt
Metallic Impurities	Fe maximum 0.05% by wt
	Al maximum 0.15% by wt
	Ca maximum 0.03% by wt
	Na maximum 0.005% by wt

Table 49. H.C. Starck H-2 Si_3N_4 Powder - Manufacturer's Analysis.

Powder Characteristics:

o Coarse Powder # High Alpha Phase ϕ High Purity

o Morphology	Specification
BET Specific Surface Area	2-5 m^2/g
FSSS Particle Size	1.2-2.0 μm
Apparent Density	0.4-0.6 g/cm^3
Tap Density	0.7-0.9 g/cm^3

Particle shape and size distribution according to scanning electron micrograph and figure response on the back

# Crystallographic Phases	Specification
Alpha-Si_3N_4	Minimum 90% by wt
Beta-Si_3N_4	Approximately 4% by wt
Free Si	Maximum 0.1% by wt

ϕ Chemical Composition	Specification
Nonmetallic Constituents	N minimum 38.2% by wt
	O 0.9-1.4% by wt
	C maximum 0.5% by wt
	F approximately 0.05% by wt
Metallic Impurities	Fe maximum 0.05% by wt
	Al maximum 0.15% by wt
	Ca maximum 0.04% by wt
	Na maximum 0.005% by wt

Table 50. Toshiba Si_3N_4 Powder - Manufacturer's Analysis.

Alpha phase, no amorphous phase being included.

(a) Size and shape of particles are extremely uniform with a mean particle size of below 1 μm.

(b) The purity is excellent with total metallic impurities below 0.05%, except aluminum. The aluminum content is approximately 0.2%, and the carbon content is approximately 0.9%.

(c) Excellent sinterability and good sintering performance can be obtained.

Typical Properties

(a)	Phase analysis:	
	Alpha phase	98%
	Beta phase	2%
(b)	Chemical analysis:	
	Si	59.0%
	N	37.5%
	O	2.0%
	C	0.9%
	Fe	0.007%
	Ca	0.01%
	Al	0.2%
	Mg	0.003%
(c)	Mean particle size:	0.9 μm
(d)	Particle size distribution:	
(e)	Tap density	0.6 g/cm^3

Table 51. Toyo Soda Si_3N_4 Powder - Manufacturer's Analysis.

Advantages		
	TS-7	TS-8
Ultra-fine particle size	+	+
High purity	+	+
Low oxygen content	±	+
High α-phase	+	±
Compactabilty	+	±
+ Good		
± Excellent		

Typical Analysis			
		TS-7	TS-8
Metal Impurities	Fe (ppm)*	50	50
	Al (ppm)	maximum 10	maximum 60
	Ca (ppm)	maximum 10	maximum 10
	Na (ppm)	maximum 10	maximum 10
	K (ppm)	maximum 10	maximum 10
Oxygen	(wt %)	1.0	1.5
Chlorine	(wt %)	0.1	0.1
Carbon	(wt %)	0.1	0.1

Physical Properties of Powders		
	TS-7	TS-8
Crystalite size	400	400
FSSS particle size	0.6	0.6
Specific surface area	12	15
α-phase content	86	93
Green density	1.55	1.65
	($1.5T/cm^2$ C.I.P.)	

*ppm = parts per million

Table 52. UBE SN-E02 Si_3N_4 Powder - Manufacturer's Analysis.

CUSTOMER	AiResearch Casting Company		
DATE OF ORDER:	May 23, 1985	ORDER NO.:	414-116785
SHIPPING DATE:	May 24, 1985	QUANTITY:	5 KG
GRADE:	UBE-SN-E02	LOT NO:	B-18

Chemical Analysis:

N	(alkali fusion)	38.9% by wt
O	(inert gas fusion)	0.6% by wt
C	(Hempel method)	0.0% by wt
Cl	(ion electrode)	<100 ppm*
Fe	(atomic absorption)	<100 ppm
Ca	(atomic absorption)	<50 ppm
Al	(atomic absorption)	<50 ppm

Phase Analysis:

Degree of Crystallinity:	~100%
Beta/(Alpha+Beta):	0%

Specific Surface Area: 2 m^2/g

*ppm = parts per million

Table 53. UBE SN-E05 Si_3N_4 Powder - Manufacturer's Analysis.

CUSTOMER:	K.H. Styhr, AiResearch Casting Company
ORDER NO.:	P.O. #815-11216-5
DATE OF ORDER:	February 1985
DATE OF DELIVERY:	Shipping Date: March 9, 1985
QUANTITY:	Net. 10 kg
GRADE:	SN-E-05
LOT NO.:	F-1

Chemical Analysis:

N	(alkali fusion)	38.9% by wt
O	(inert gas fusion)	1.0% by wt
Cl	(ion electrode)	<100 ppm*
Fe	(atomic absorption)	<100 ppm
Ca	(atomic absorption)	<50 ppm
Al	(atomic absorption)	<50 ppm

Phase Analysis:

Degree of Crystallinity:	~100%
Beta/(Alpha+Beta):	1.5%

Specific Surface Area: 5.8 m^2/g

*ppm = parts per million

Table 54. UBE SNE-10 Si_3N_4 Powder - Manufacturer's Analysis.

POWDER SPECIFICATION			
Properties	Powder Grade		
	SN-E-10	SN-E-X	SN-N-X
Morphology	Equiaxed	Equiaxed	Needle-like
Particle Size	0.1~0.3μm	0.3~1.0μm	0.2X(10~20)μm
Specific Surface Area	10~14m^2/g	2~8m^2/g	10m^2/g
Purity	N	>38.0%	
	O	<2.0%	
	C	<0.2%	
	Cl	<100 ppm*	
	Fe	<100 ppm	
	Ca	<50 ppm	
	Al	<50 ppm	
Phase Composition	Degree of Crystallinity	100%	100%
	α Phase	95%	90%
	β Phase	5%	10%

*ppm = parts per million

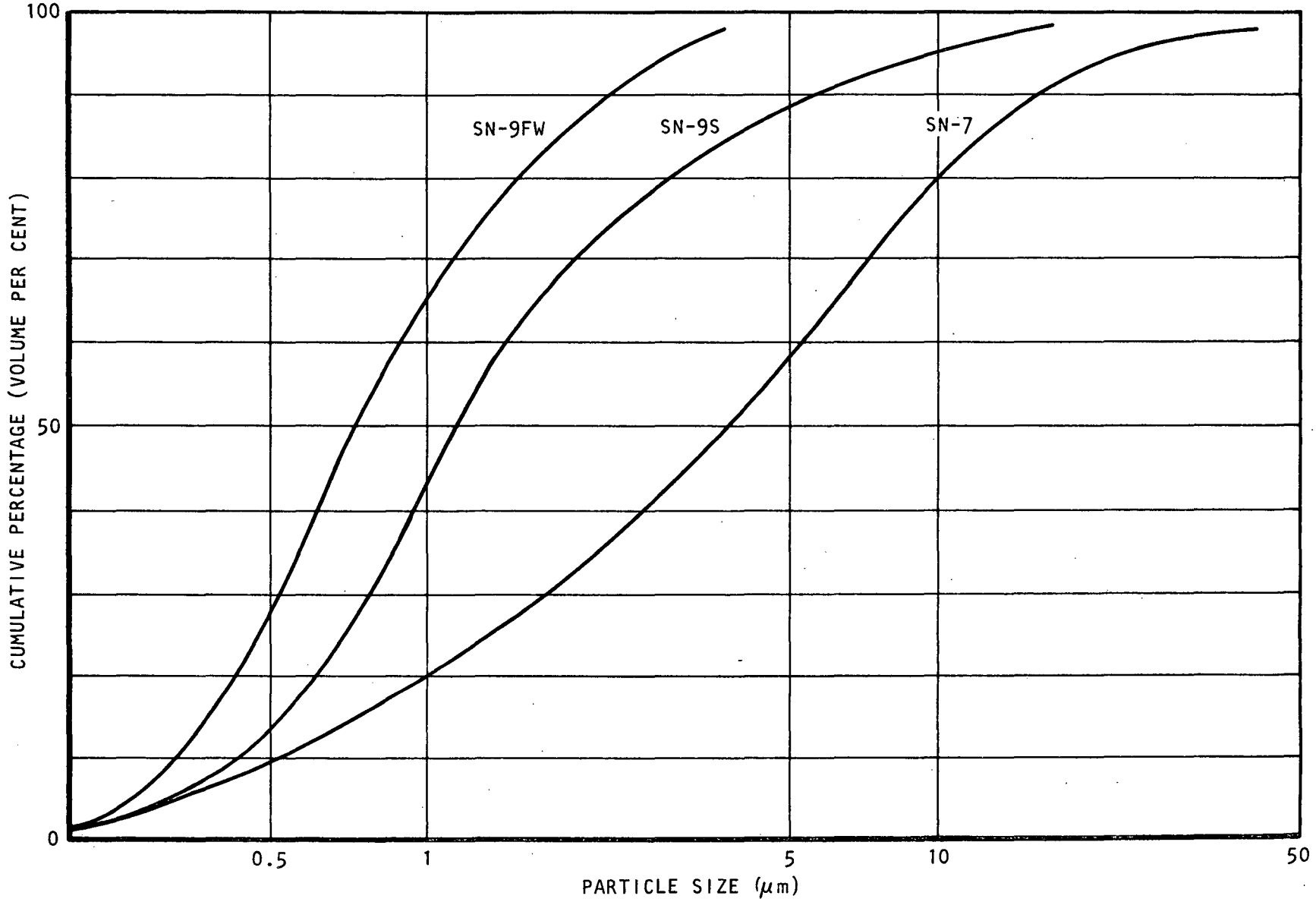

Figure 97. Particle Size Distribution of Several Denka Si_3N_4 Powders - Manufacturer's Data.

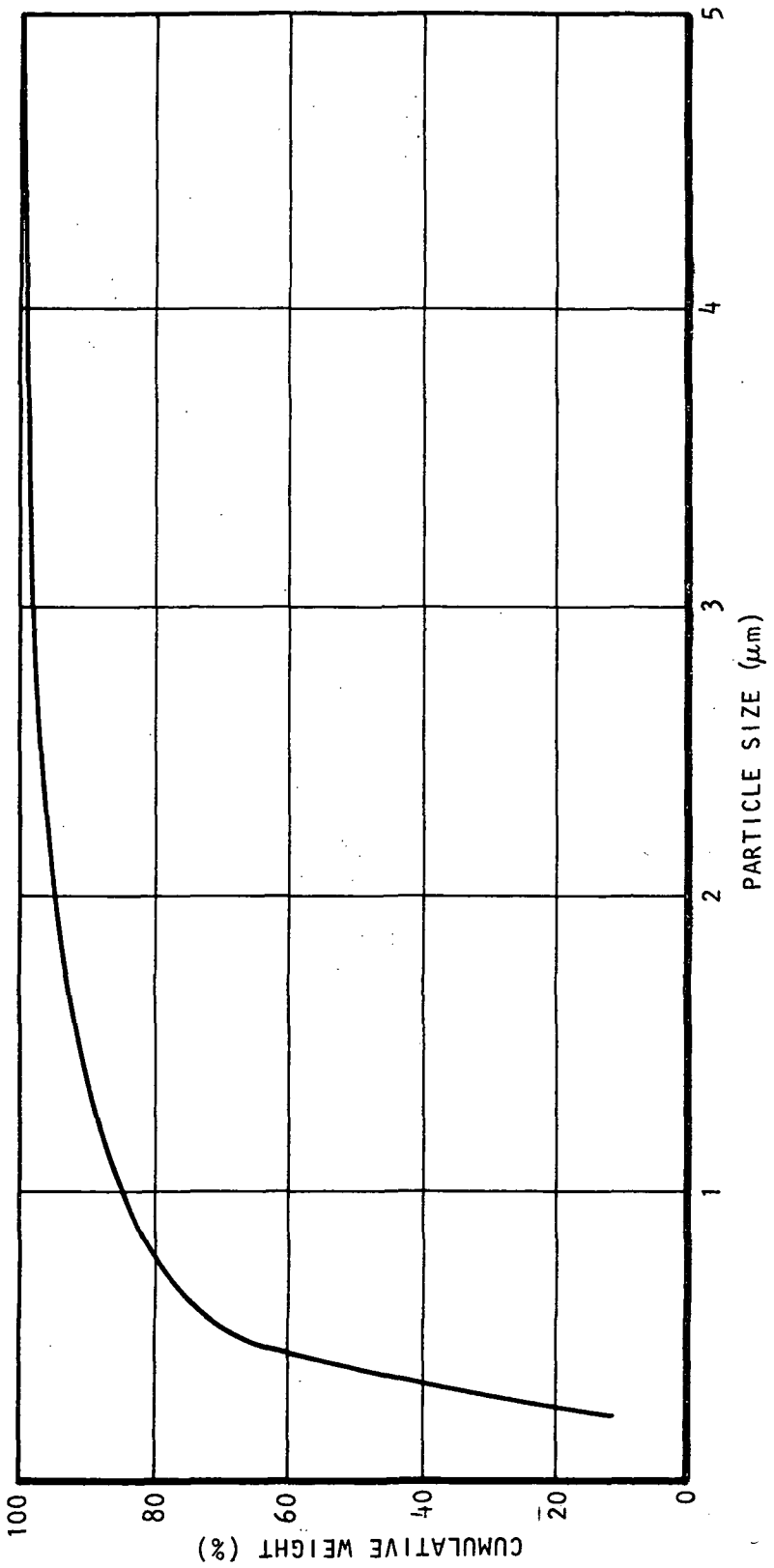

Figure 98. Particle Size Distribution Curve of Toyo Soda Si_3N_4 Powder - Manufacturer's Data.

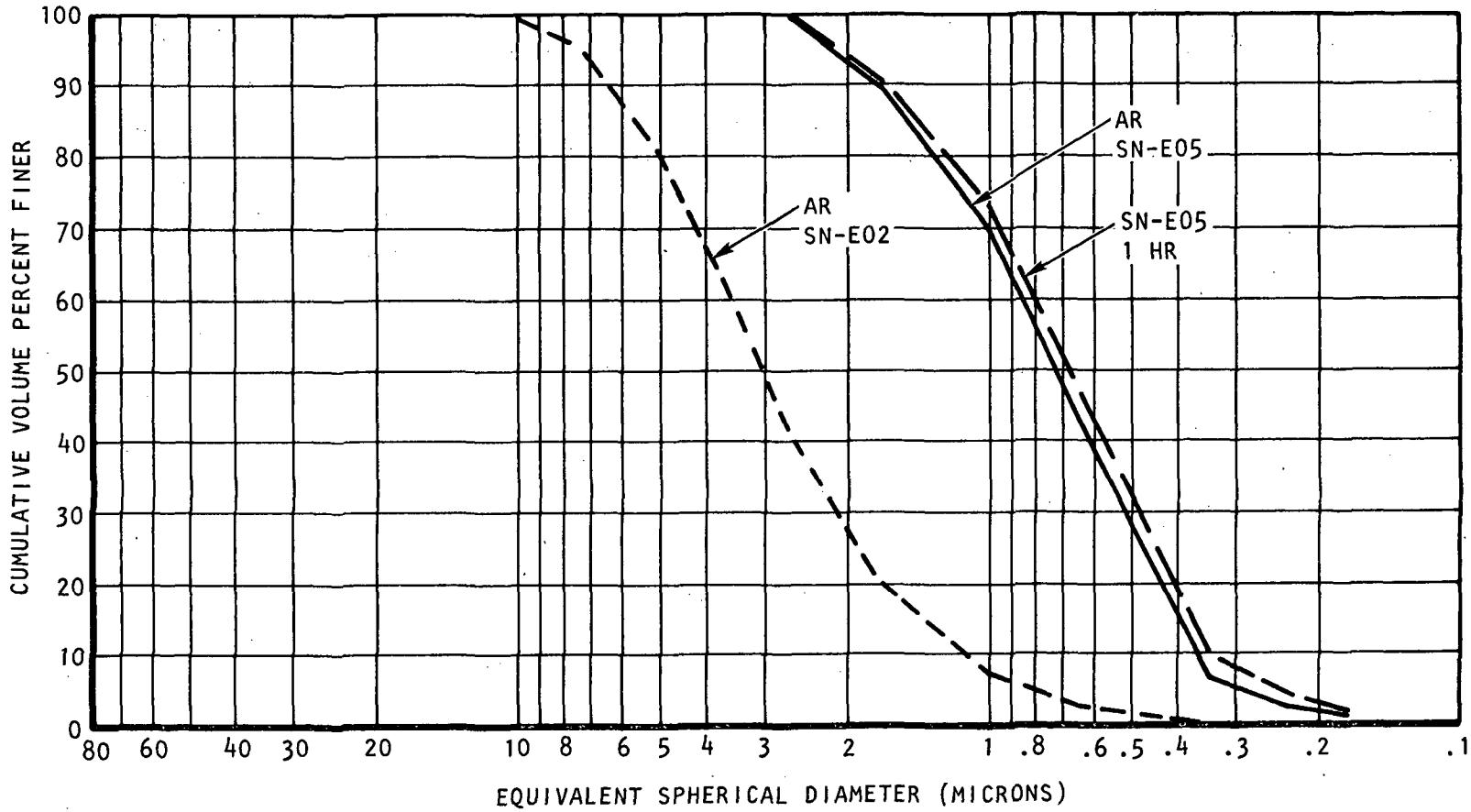

Figure 99. Particle Size Distribution of As-Received UBE Si_3N_4 EO-2 and EO-5 Powders and EO-5 After Milling for 1 Hour.

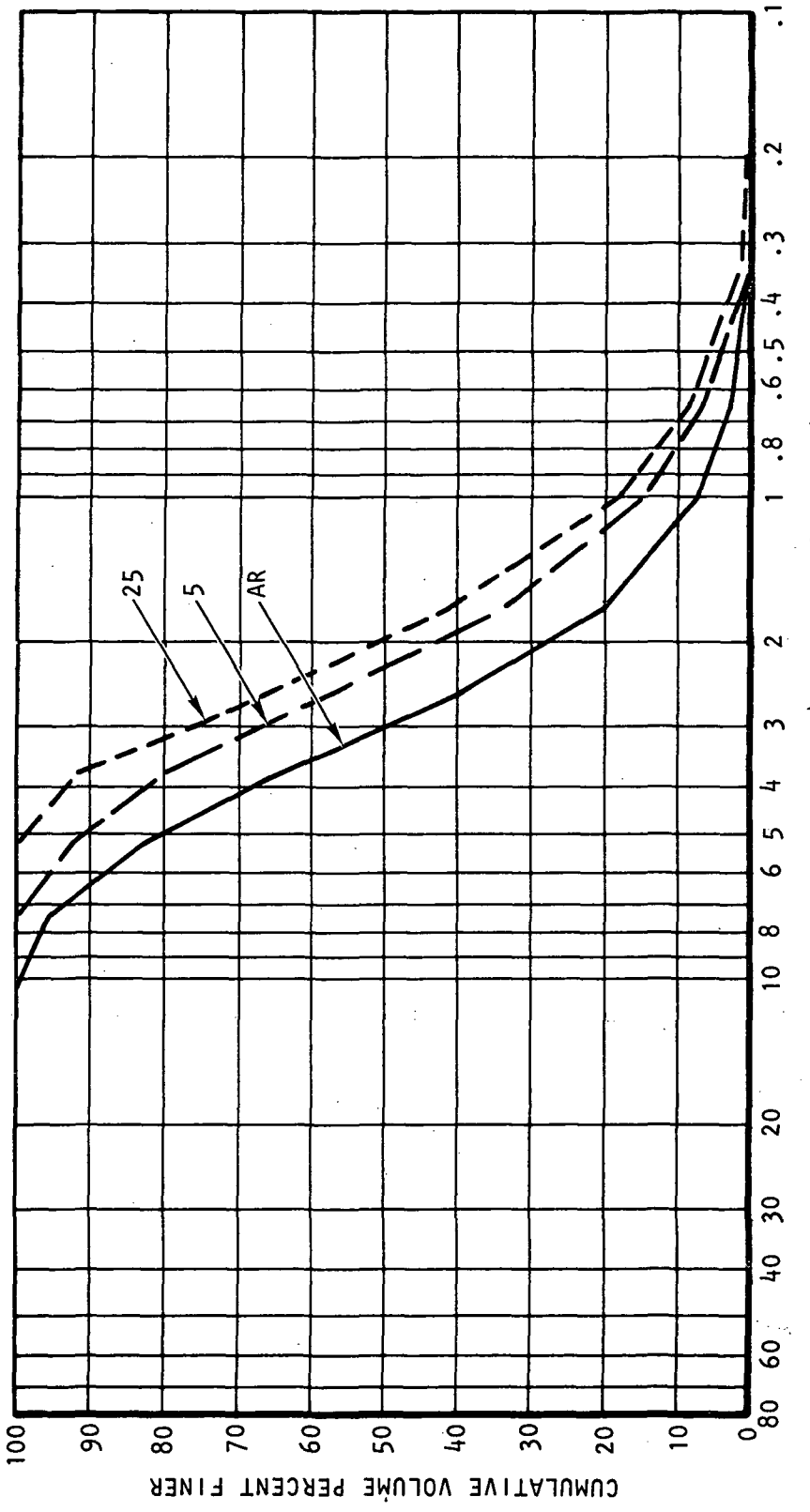

Figure 100. Particle Size Distribution of As-Received UBE EO-2 Si_3N_4 Powder and the Effective Change in Distribution After 5 and 25 Hours Milling.

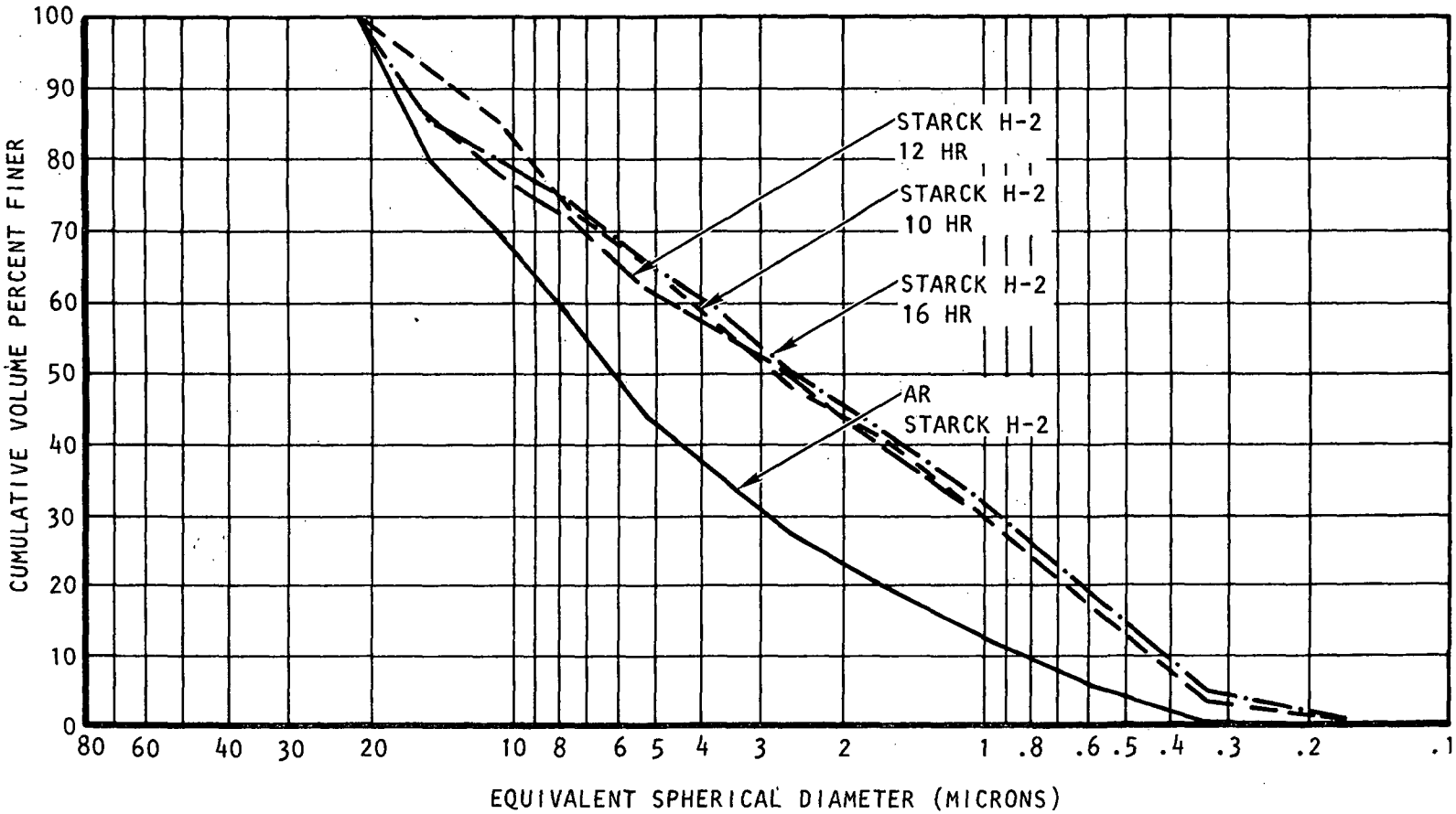

Figure 101. Particle Size Distribution of As-Received Starck H-2 Si_3N_4 Powders and Effects of 10, 12, and 16 Hours Milling Time.

Five rotors were cast with Denka SN-9, SN-95 and SN-7 Si_3N_4 powders. Of these, SN-7 has been selected for further study.

An ACC comparison of the particle size distribution obtained by Microtrack particles analyzer and surface area obtained by BET analysis of as-received Si_3N_4 powders from different suppliers is presented in Table 55.

Table 56 presents a listing of the rotors shipped to Garrett, comparing the treatment and final density of each.

3.3 Technical Progress

3.3.1 Stress Rupture, Room and Elevated Temperature Testing.

Six rotors are currently being evaluated at Garrett for stress rupture and both room and elevated temperature flexure strength. Results are shown in Table 57.

One plate cast with rotor S/N 552 had specimens cut for stress rupture, and room and elevated temperature flexure tests. The results are shown in Figure 102.

Three Code 1 and 3 Code 2 rotors, each achieving final density at Ford, ASEA and ACC, were cut into specimens for room temperature flexure testing. Figure 103 presents the high, low, and median values resulting from the testing of 10 test bars from each casting. Figure 104 is a typical sintered rotor prior to shipping to Garrett for shaft mounting assembly. Figures 105 and 106 show the rotor ready for engine assembly.

3.3.2 Sinter-HIP

One of the most important innovations to date has been the introduction of the sinter-HIP method of densifying ceramics. This technique not only provides better control of operating parameters, but also eliminates the necessity for encapsulation of components while producing higher density parts than can be achieved either by sintering or HIPping alone. The advantages of sinter-HIP as opposed to other densification processes with respect to flexure strength are graphically depicted in Figure 103.

Two sinter-HIP furnaces are presently available for use. One contains a fiber mantel

Table 55. Comparison of PSD and Surface Area of Si_3N_4 From Various Suppliers.

Supplier	Type	Lot No.	Particle Size Distribution, μm percentile			Surface Area, m^2/g
			90%	50%	10%	
GTE	SN-502	SN-160	18.0	7.7	1.30	4.80
UBE	SN-E02	B-16	6.5	3.0	1.20	1.50
UBE	SN-E05	F-1	1.8	0.72	0.37	5.80
Starck	H-2	S-6176B	18.0	6.1	0.82	3.80
Denka	SN-7	7205	18.0	5.1	0.47	4.00

Table 56. Rotors Shipped July 1984 - June 1985.

Serial No.	Code	Casting No.	Densification	Density, g/cm^3
637	1	03154	Sintered at Ford	3.27
638	1	03194-02	Sintered at Ford	3.27
641	1	04254	Sintered at Ford	3.29
642	1	04244-02	Sintered at Ford	3.28
643	1	05014	Sintered at Ford	3.29
648	1	04164-02	Sintered at Ford	3.27
650	2	05144	Sintered at Ford	3.27
651	1	05084-01	Sintered at Ford	3.30
652	1	05084-02	Sintered at Ford	3.29
658	1	05174	Sintered at Ford	3.29
686	1	03194-01	HIPped at ASEA	3.26
687	1	04124	HIPped at ASEA	3.25
688	1	04184	HIPped at ASEA	3.24
689	2	04383	HIPped at ASEA	3.24
690	2	05023-01	HIPped at ASEA	3.24
691	2	05023-02	HIPped at ASEA	3.24
692	2	05093	HIPped at ASEA	3.25
723	1	12184	HIPped at ACC	3.25
724	2	02045	HIPped at ACC	3.24

Table 57. Rotors in Stress Rupture, Room and Elevated Temperature Testing.

Rotor S/N	Material	Densification	Density, g/cm^3
542	Code 1	ACC Sinter HIP	3.26
687	Code 1	ASEA HIP	3.25
634	Code 1	Ford Sintered	3.29
723	Code 2	ACC Sinter HIP	3.25
692	Code 2	ASEA HIP	3.25
650	Code 2	Ford Sintered	3.27

heating element capable of 1400C in vacuum and up to 1950C in 15,000 psi N_2. The other furnace contains a graphite rod and heating element capable of 1500C in vacuum and 2000C in 15,000 psi N_2. One system is also capable of achieving pressures up to 30,000 psi in Argon.

3.4 Problem Areas

3.4.1 Contamination

Discoloration at the blade tips has been evident for some length of time and cracking within or at the interface of the discolored and clearer portions plus blade distortion appears to be coincident.

Earlier work involved flowing air through the slip which created bubbles. Large quantities of black specks could be seen congregating on the bubbled surface. These were submitted for analysis and found to be high in carbon content. Figures 107 and 108 are energy dispersive x-ray (EDX) analyses obtained at two different energy levels which clearly show the extent of carbon contamination. Efforts to resolve what appeared to be obvious organic contamination by evaluation of different deflocculents were pursued by the blade tip discoloration persisted.

Later an actual blade sample was submitted for EDX analysis of both the discolored and clear portions of the blade. Figures 109 and 110 revealed a high yttrium content in the discolored portion which was not evident in the clear part. Repeated washing of the powder prior to slip preparation did not significantly reduce the amount of discoloration. Spin casting apparently causes higher concentration in the smaller area at the tip of the blades. Higher viscosity slip appears to diffuse the discoloration but higher viscosity is not amenable to good castability.

Because of the small particle size and high surface area of the as-received yttria, it was theorized that this component would be highly reactive. To increase the stability of the slip containing yttria it was decided to evaluate the effect of pre-reacting the yttria at 850C in 90 psig N_2. This work is still in progress.

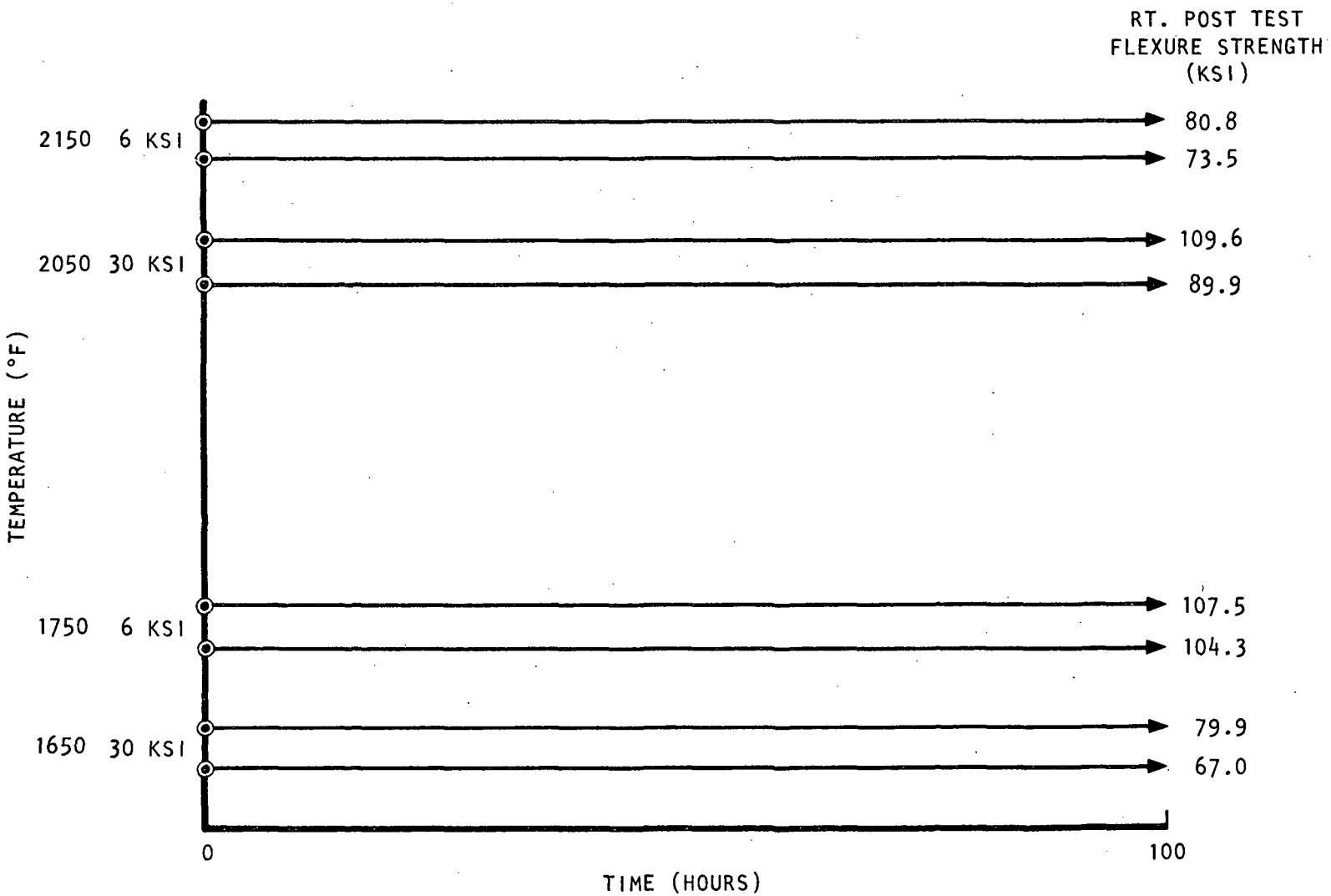

Figure 102. Stress Rupture, Room and Elevated Temperature Flexure Test (Specimens Cut from Plate Cast with Rotor S/N 552).

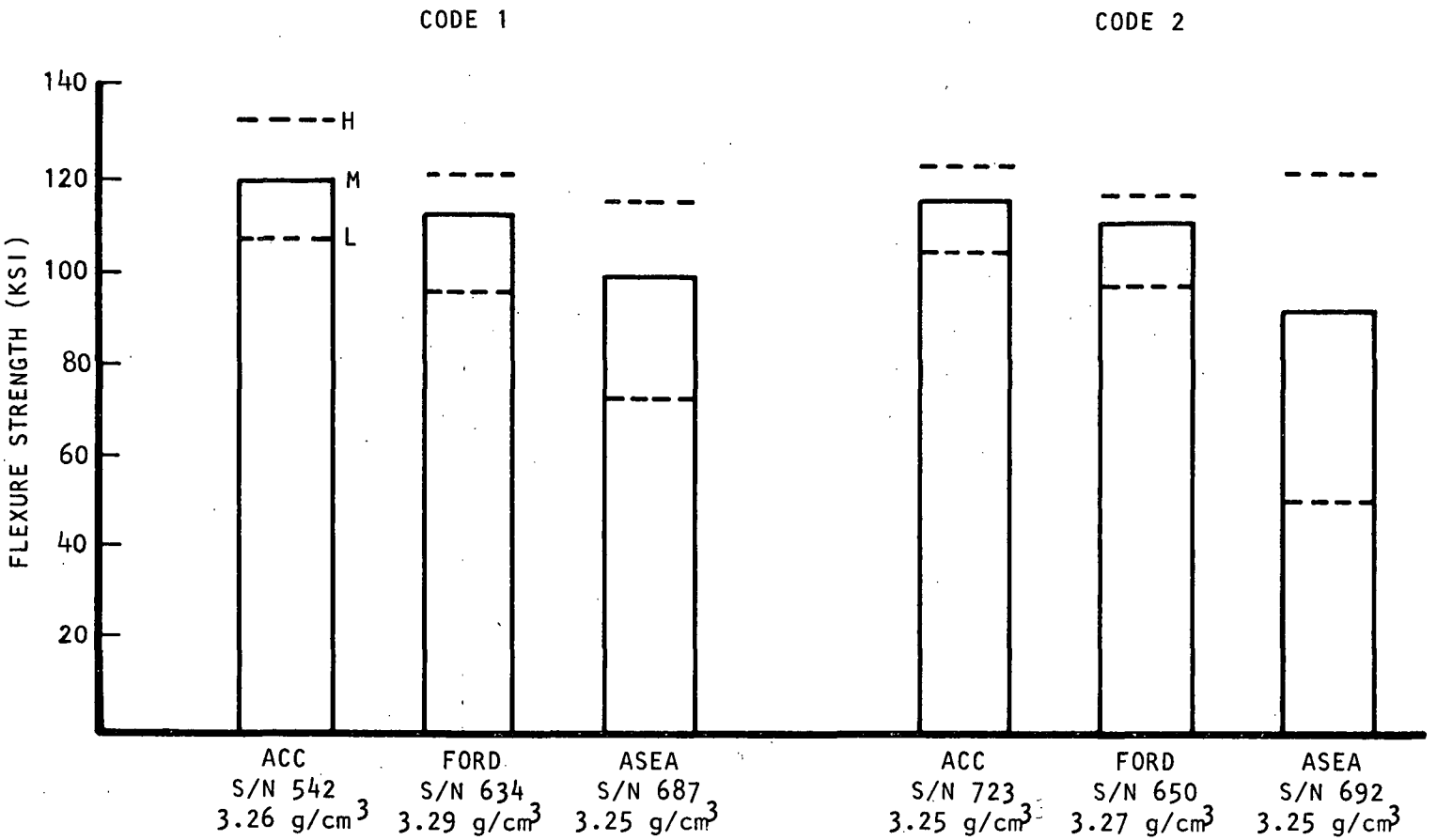

Figure 103. Room Temperature Flexure Testing.

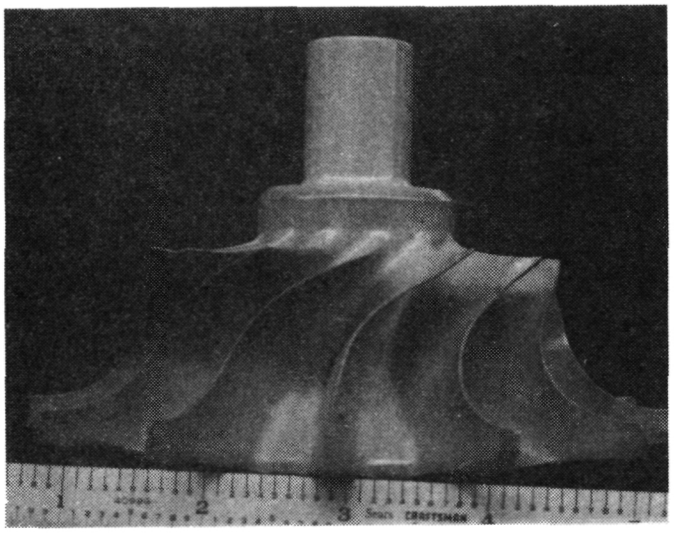

Figure 104. Ceramic Slip Cast AGT101 Turbine Rotor.

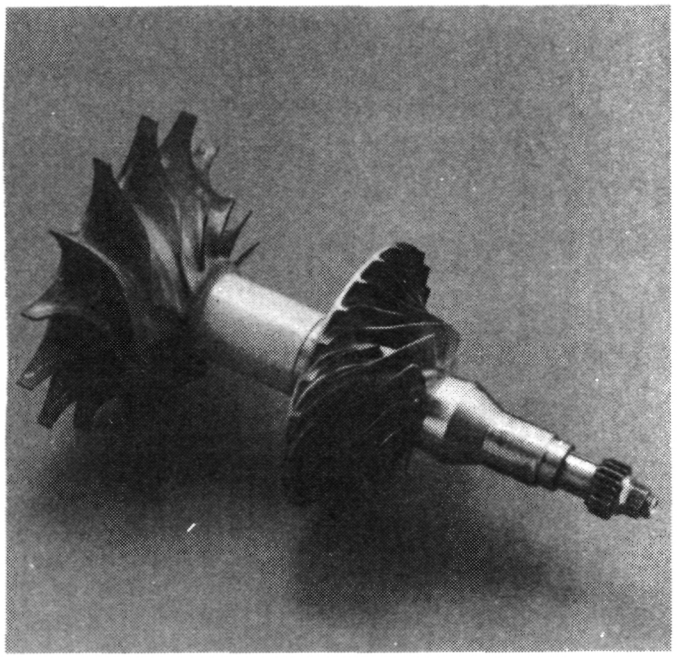

Figure 106. Si_3N_4 Rotor Completely Assembled for Engine Test.

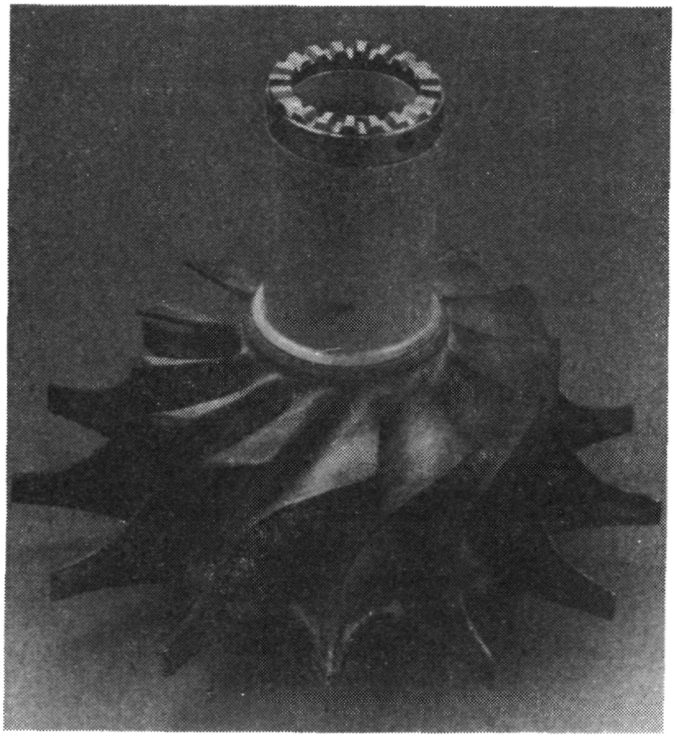

Figure 105. Si_3N_4 Rotor with Shaft Attachment Ready for Spin Testing.

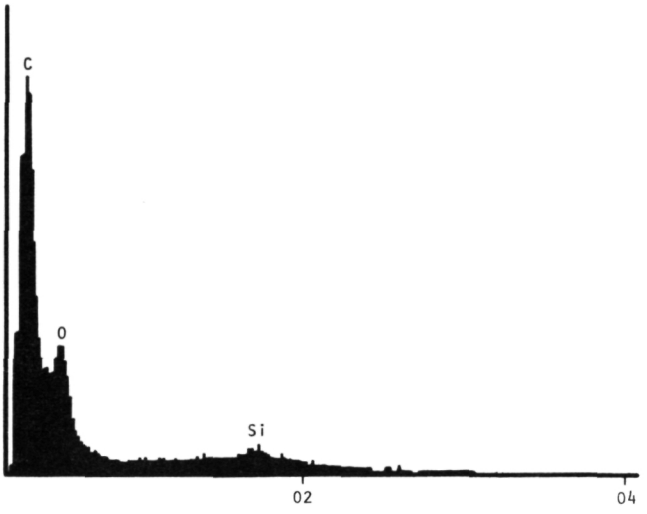

Figure 107. EDX at 2,700 KEV of Powder Samples.

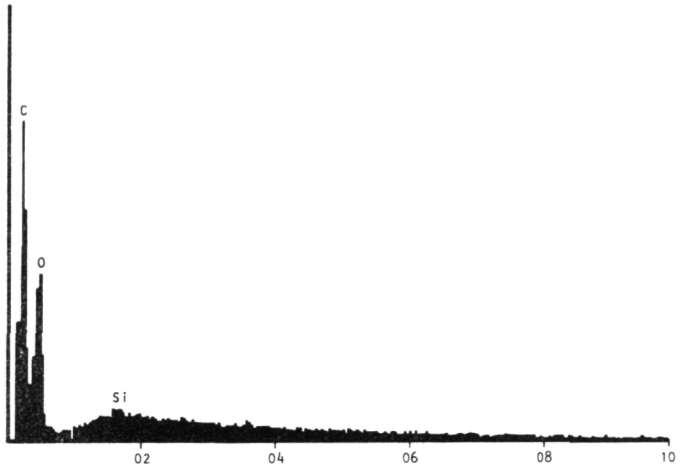

Figure 108. EDX at 5.2 KEV of Powder Samples.

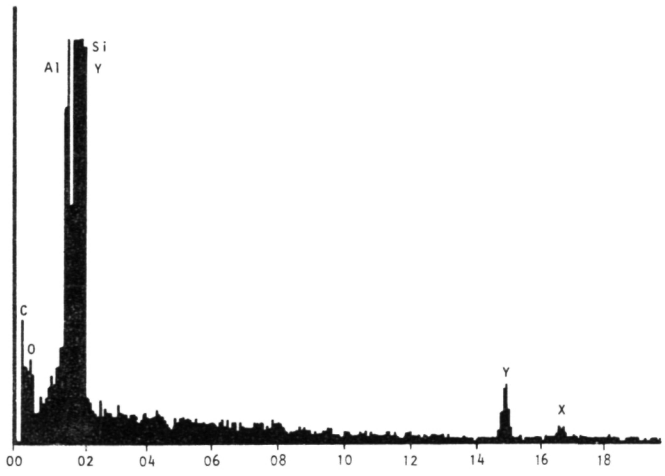

Figure 109. An Expanded EDX Microprobe Spectrum of Blade Sample.

3.4.2 Variations in As-Received Powder

GTE SN-502 Si_3N_4 powder has been the baseline material since the programs inception. However, as-received powders have varied from lot to lot with respect to chemistry, particle size distribution and surface area.

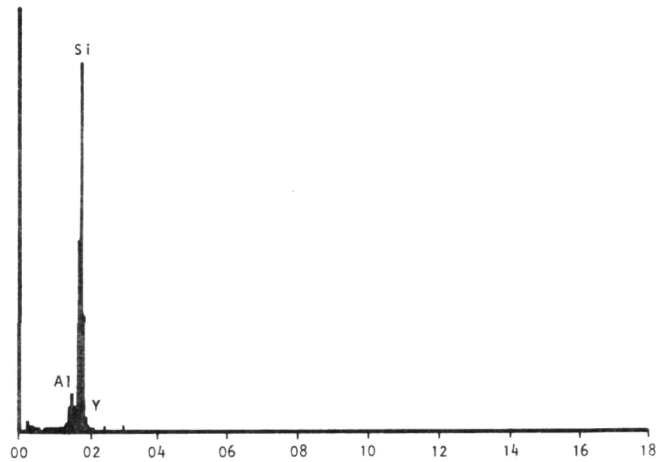

Figure 110. An EDX Microprobe Spectrum Obtained on the Cleaned Area of the Sample Using a 39kV Beam Voltage.

Table 58 shows the changes that have occurred over the past several years. This has led to difficulty in producing a slip with consistent and reproducible properties. Table 59 is an analysis of the range of chemical components of the powder content. Subsequent analyses by ACC confirms the fact that these elements are within the specified amounts. However, the analysis does not show the surface area and pH variations that exist. Material originally received had a needle-like structure, but a change in the manufacturer's process now provides a more spherical shaped particle, which changes the parameters required to produce a good, castable slip.

Several methods to eliminate these problems have been evaluated. These include blending of coarse and fine grain fractions and blending with Si_3N_4 powder supplied by other manufacturers. This work is still in progress.

3.4.3 Design Changes

Design modifications necessary for engine fabrication and performance were made during this period. The changes included a conversion from solid shaft to hollow shaft, as seen in Figure 111, mold design from "A" (open blades)

Table 58. Comparison of GTE Powders Received October 1983 - June 1985.

Date Received	Lot Number	Surface Area m^2/g	Particle Size Distribution, µm Percentile			pH	Bulk Density, g/cm^3
			90%	50%	10%		
Oct. '83	SN-27	4.47	22.0	12.0	2.00	7.87	0.12
Nov. '83	SN-42	3.47	20.0	8.0	2.70		0.25
Feb. '84	SN-33-37	3.33	20.0	8.5	1.70	7.51	0.14
May '84	SN-85	1.35	16.0	5.6	1.20	7.38	--
June '84	SN-92	3.53	17.0	5.7	1.10	--	--
Jan. '85	SN-127	3.34	18.0	6.8	1.40	--	--
Feb. '85	SNE-3R	6.19	18.0	7.6	1.20	--	--
April '85	SN-145 + 27% EV-12-2884	7.20	18.0	7.5	1.30	5.70	0.10 0.04
May '85	SN-160	4.80	18.0	7.7	1.30	5.25	0.14
June '85	SN-165	4.50	17.0	8.0	1.30	--	0.14

Table 59. Chemical Analyses of GTE Powders.

Date Received	Lot Number	Purity, % by Weight, O	C1	Ca	Mg	Mo	Ni	A1	Cr	Fe	Cu
April '85	73% SN-145 + 27% EV-12-2884	1.6 3.8	0.05 0.02	<0.0005 <0.0005	<0.0001 <0.0001	0.0047 0.0173	0.0014 0.0015	0.0303 0.0010	0.0021 0.0017	0.0034 0.0018	<0.0001 <0.0001
May '85	SN-160	3.2	0.04	<0.0005	<0.0001	0.0041	0.0017	0.0139	0.0020	0.0021	<0.0001
June '85	SN-165	2.95	0.03	<0.0005	<0.0001	0.0046	0.0042	0.0040	0.0016	0.0018	<0.0001

*Ledoux Analysis of SN-160	Na	Li	Y	Mo	Ni	A1	Cr	Fe	
	0.001	0.001	0.001	0.003	0.001	0.015	0.001	0.003	

*Spectrographic Analysis

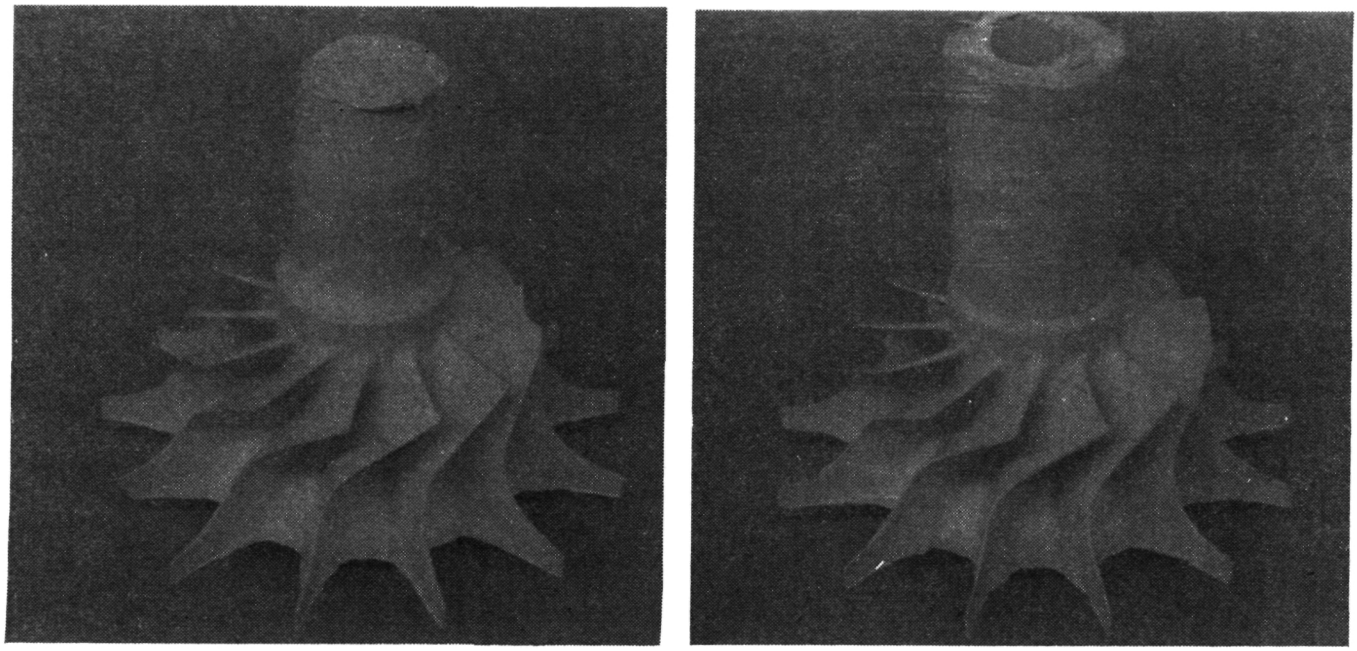

View A. Solid Shaft

View B. Hollow Shaft

Figure 111. Modification of "A" Generation Rotor.

to "B" generation (closed blades) shown in Figure 112 and additional stock added to blades to compensate for shrinkage. These modifications required tooling rework and, in some instances new tooling, which created delays in component delivery.

The conversion from "A" to "B" generation molds drastically increased the length of casting time.

In an effort to reduce the time required for complete casting, vacuum assist was introduced, which reduced the casting time by 50 percent.

3.5 Ongoing Activities

- Continue slip development using Si_3N_4 powder supplied by alternate manufacturers.
- Decrease casting time required for "B" generation molds by further evaluation of vacuum assist and higher porosity plaster molds.
- Continue development and evaluation of SRN-SNN compositions with internal funding.
- Develop methods and/or chemistries to eliminate exducer blade discoloration.

4.0 CERAMIC STRUCTURES

4.1 Turbine Shroud

Fifty turbine shroud castings were prepared during this reporting period. Many of these cracked during the early stages of drying. After a change was made in the drying environment, the yield dramatically improved. Fifteen turbine shrouds and 3 truncated shrouds have been fully processed and shipped to Garrett. Two additional shrouds are presently being nitrided and one has been prenitrided and is being machined. Several modifications to the original shroud design have been made during this period. Highly concentrated stresses were found to occur in the slotted bolt attachment area. The latest design change eliminated the slots as shown in Figure 113, Views A and B. Also, the thick-

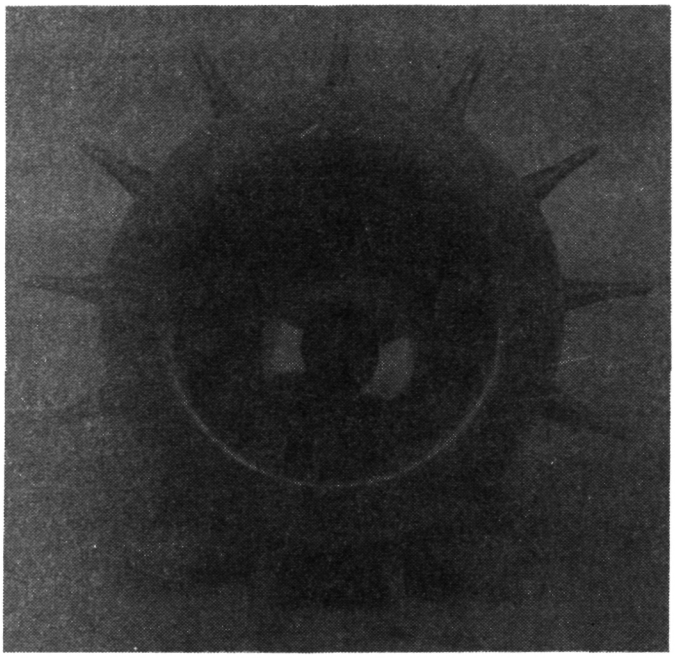

View A. Wax Mold

View B. Wax/Plaster Mold Assembly

Figure 112. Changes in Mold Design.

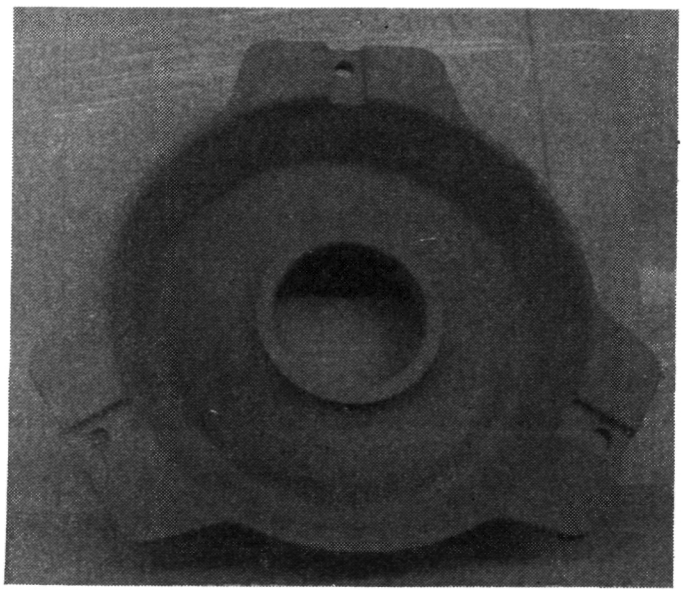

View A. Previous Design

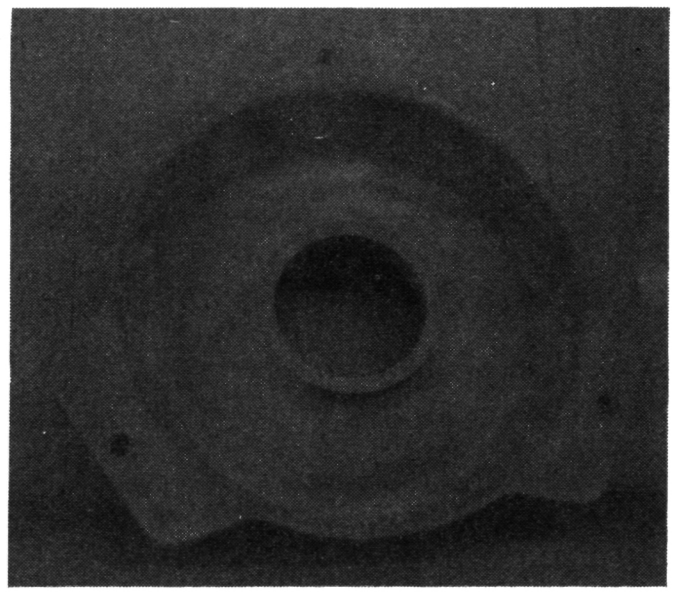

View B. Current Design

Figure 113. AGT101 Turbine Shroud Evolution.

ness of the attachment area was increased to better withstand the high stresses. This modification is considered to be the final design for the turbine shroud and near net-shape tooling is being made. Analyses showed that for the turbine shroud to survive an environment of 2500F, higher component density would be required. A sintered reaction bonded (SRN) shroud was cast and nitrided. This shroud will be cut into three equal sections and each will be sintered in three different sintering furnaces for final density comparisons.

4.2 Turbine Inner Diffuser Housing

One SRN inner diffuser housing was sintered to a 3.18 g/cm^3 density and shipped to Garrett to be cut into test bar specimens. Room temperature flexure strength averaged 85 ksi. At both 2000F and 2200F the average MOR was 55 ksi. ACC was not scheduled to deliver additional inner diffuser housings during this period.

4.3 Turbine Backshroud

Ten turbine backshrouds were cast. Six of these were fully processed and shipped to Garrett. No additional backshrouds were required during this period.

4.4 Combustor Transition Duct

Prior modifications to the combustor transition duct were accomplished by machining the actual cast component. The most recent change required modification to the tooling. View A in Figure 114 shows the configuration of the previous design and View B is the most recent modification.

Difficulty was experienced in casting with the new tool, with cracking occurring during casting, drying, and machining. Rework of the tool was required to eliminate cracking problems. One transition duct has since been fully processed and shipped to Garrett. Four additional components are currently being machined.

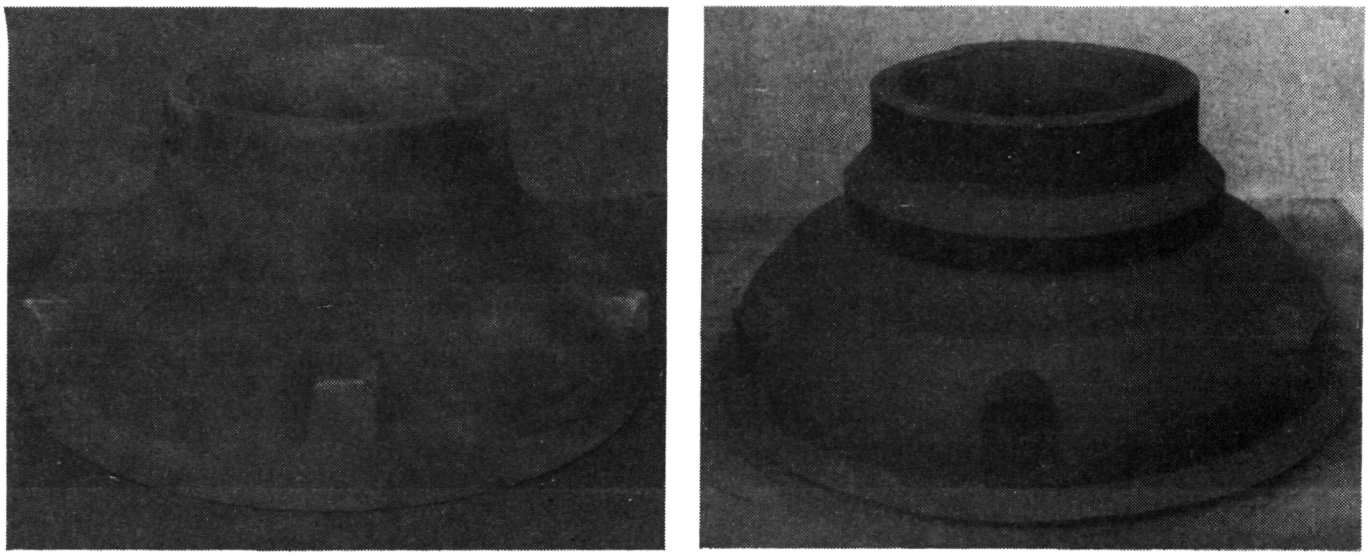

View A. Previous Design **View B. Current Design**

Figure 114. AGT101 Transition Duct Evolution.

4.5 Flow Separator Housing

Several modifications of the original design to produce molds for casting were made. Some were deemed necessary for component engine performance, while others were required in order to produce satisfactory plaster and rubber molds.

Views A, B, and C in Figure 115 respectively show the plaster molds produced from the first three design iterations. The rubber top portion of the complete mold is not shown. The plaster shown in View C is the most recent design and castings will be made during the next report period. Figure 116 shows the trial casting made from the first plaster mold design, which revealed complications that necessitated subsequent tooling design changes.

4.6 Ring Components

Various ring components have been fully processed and delivered to Garrett. These are as follows:

Turbine Shroud Seal Ring	15
Flow Separator Housing Seal Ring	13
Wave Spring	8

Figure 117 shows several of each of the processed ring components. The quantities shown only reflect those components processed to the most recent design iteration.

5.0 INJECTION MOLDED STATOR VANES

During this period, 92 RBN-124 stator vanes were shipped to Garrett for evaluation and engine testing. As an ongoing effort, stators were processed using lower sintering aid compositions (Codes 11, 12, and 13) and are awaiting further processing.

6.0 ANALYTICAL EQUIPMENT

- **PSD Instrumentation** - PSD analyses are obtained with a Leeds and Northrop Microtrack PSD analyzer as shown in Figure 118. PSD measurements in the range of 0.12 to 42.2 μm are made by light scattering techniques.

- **Viscosity Instrumentation** - Figure 118 also shows a Haake rotational viscometer, which is used for characterizing the flow behavior of casting slips. This test apparatus utilizes HP-87 computer enhancement capabilities.

- **Rheology Instrumentation** - The Haake torque rheometer shown in Figure 119, is used to characterize the flow behavior of injection molding feed material in either a small batch mixer or a continuous twin screw extruder.

- **Surface Area Instrumentation** - The Micromeritics Flow Sorb II 2300 shown in Figure 120, is used for measuring the surface area of powder samples. It provides single point, multi-point and total pore volume analytical capabilities.

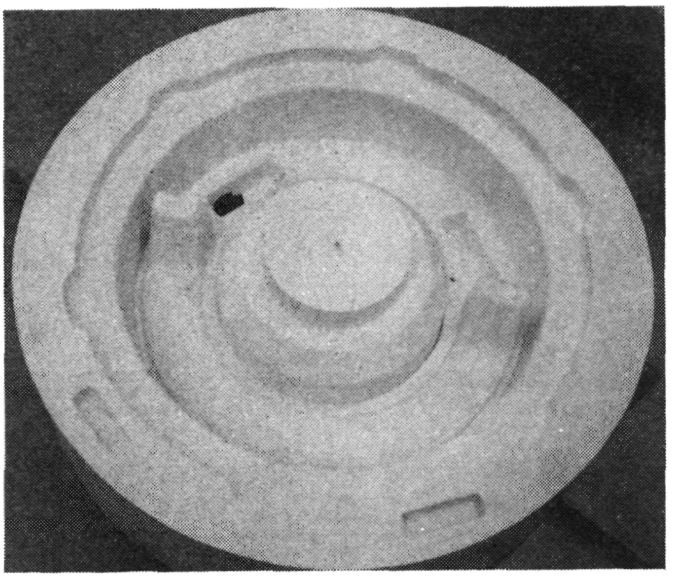

View A

First Iteration Plaster Mold.

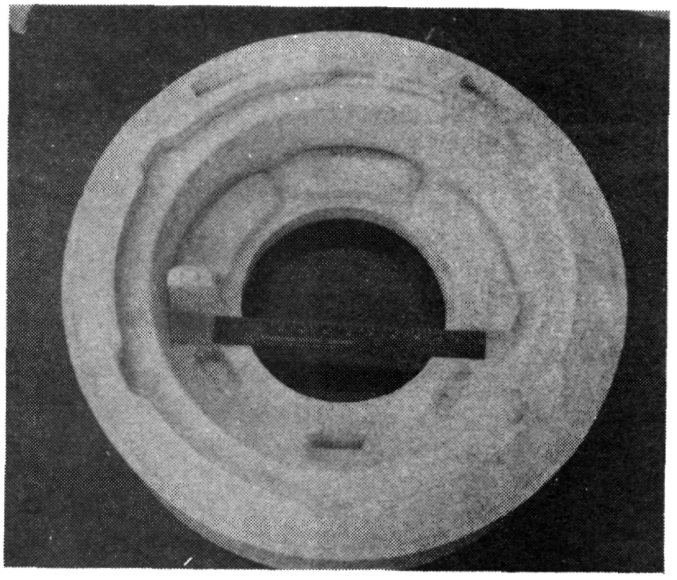

View B

Second Iteration Plaster Mold.

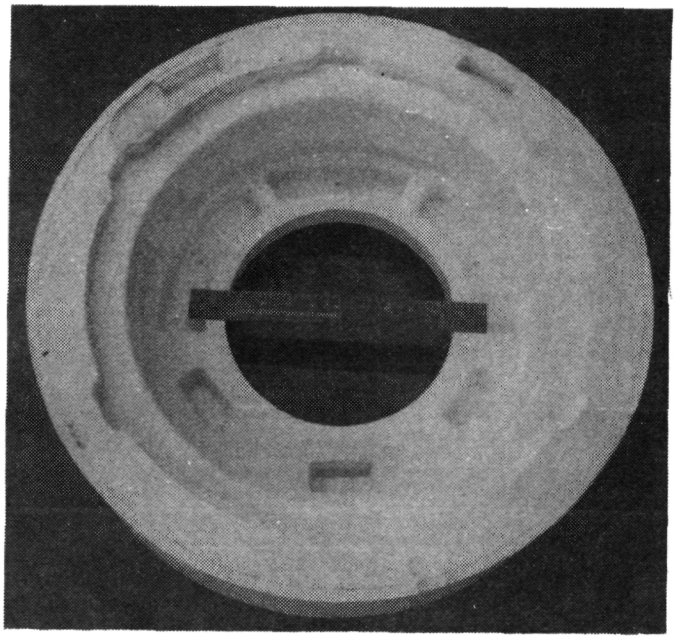

View C

Third Iteration Plaster Mold

Figure 115. Iterations in Plaster Mold - Flow Separator Housing.

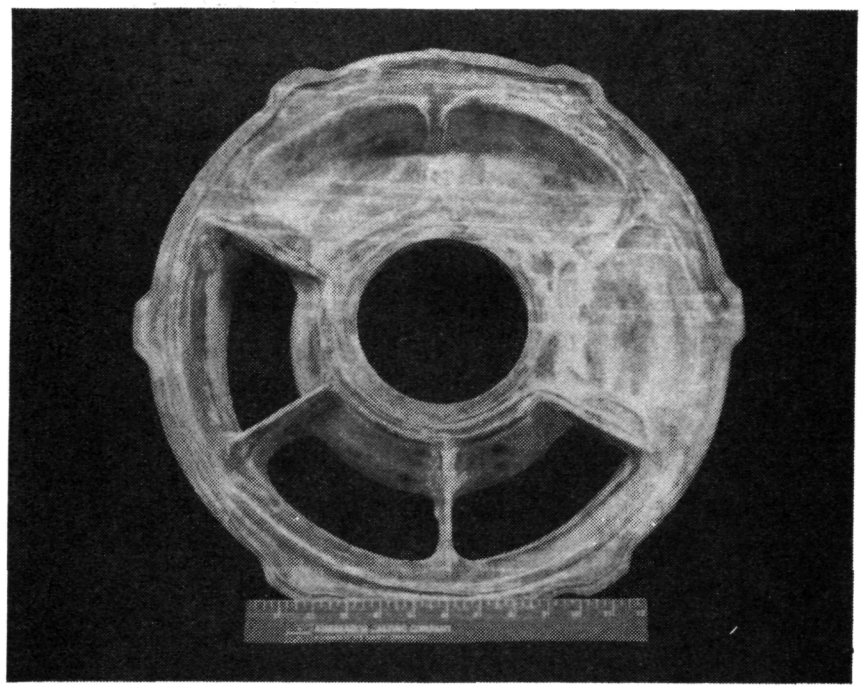

Figure 116. Trial Casting from First Iteration Mold Design - Flow Separator Housing.

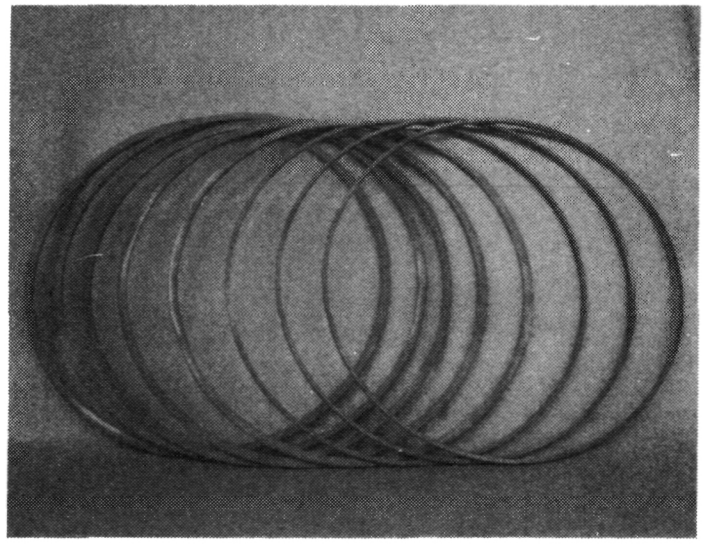

Figure 117. AGT101 Ceramic Ring Components.

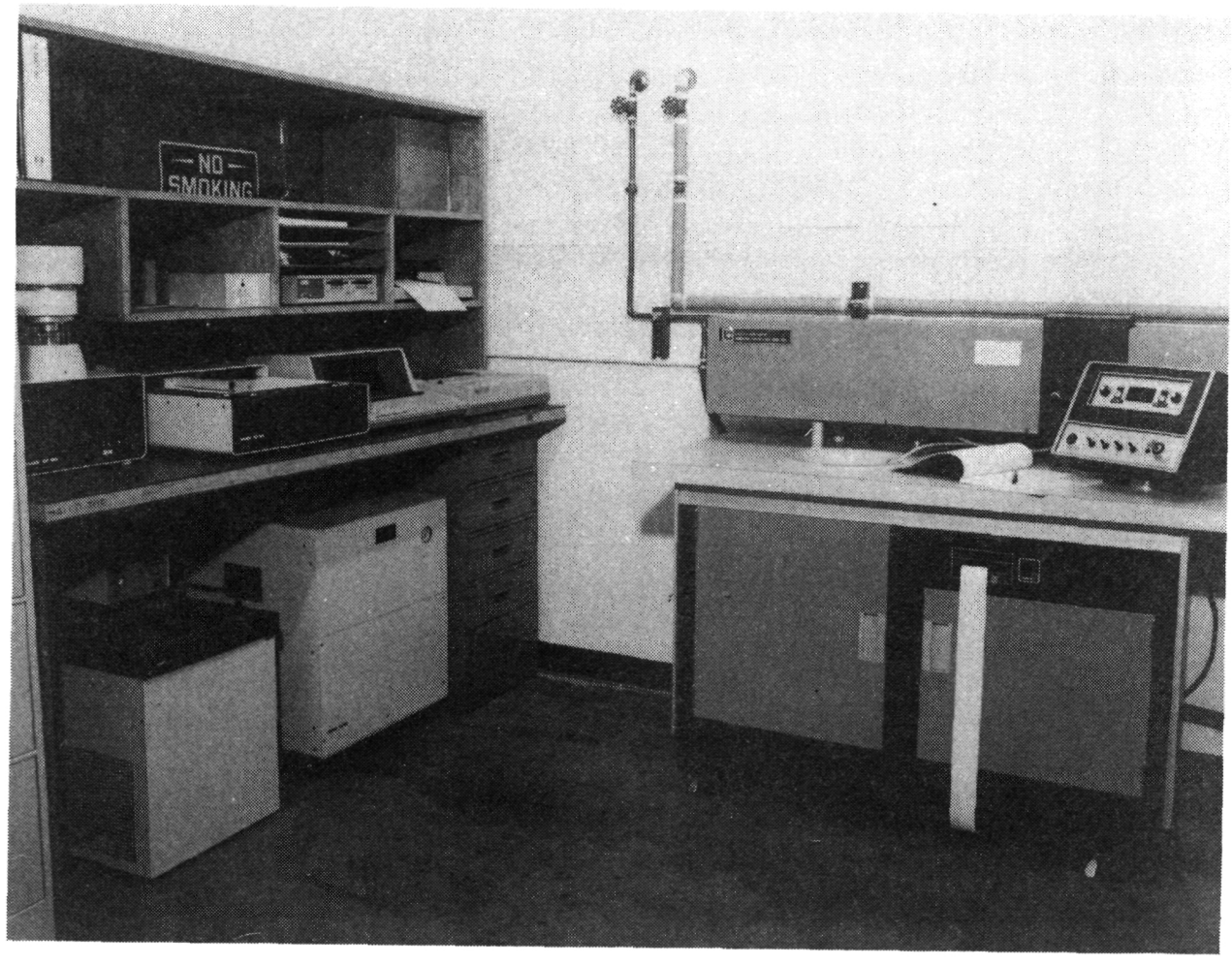

Figure 118. On Right Side of Photograph is a Leeds and Northrup Microtrak Particle Size Distribution Analyzer. On Left is a Haake Rotor Viscometer.

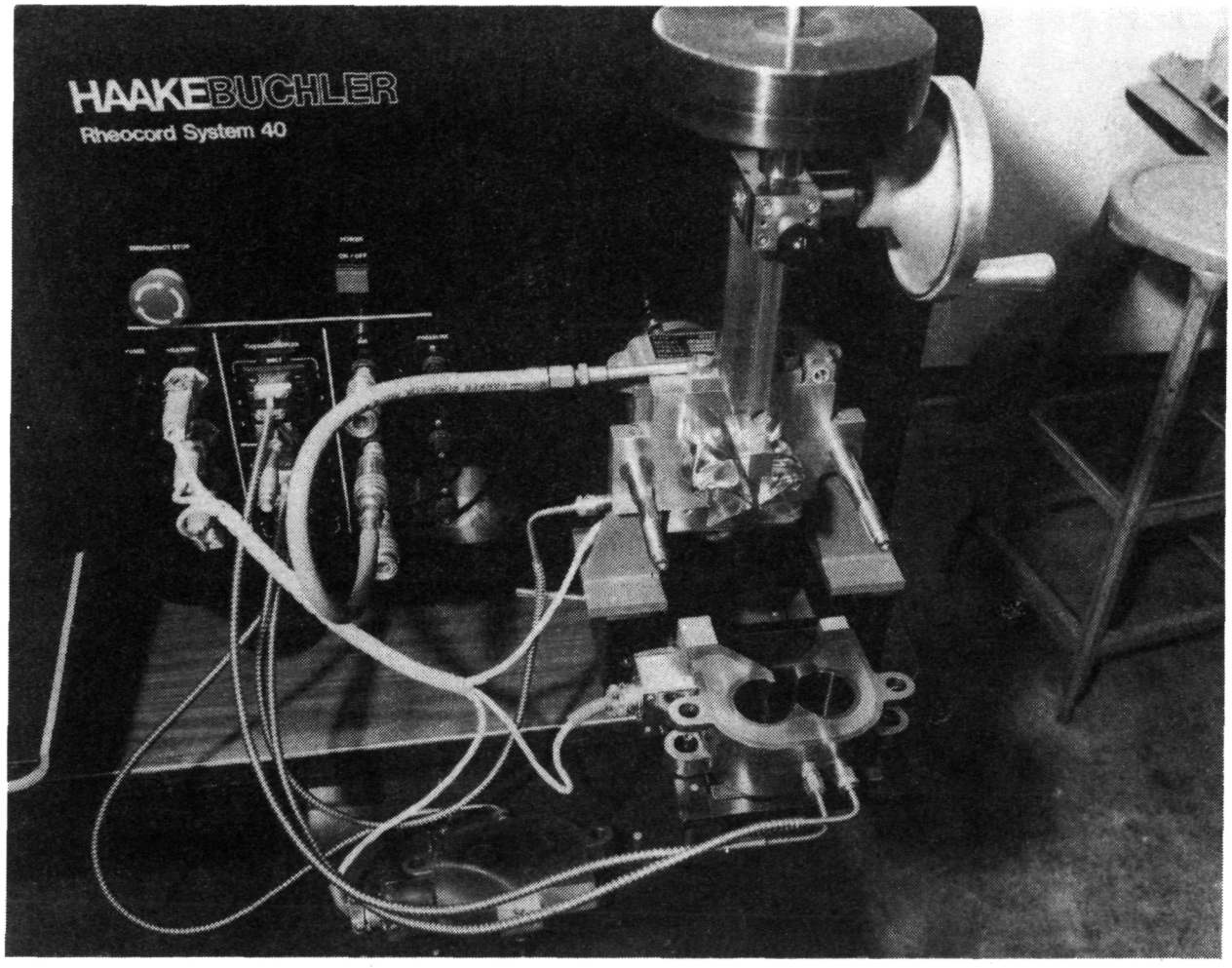

Figure 119. Haake Rheometer for Characterizing Flow Behavior of Injection Molding Mixes.

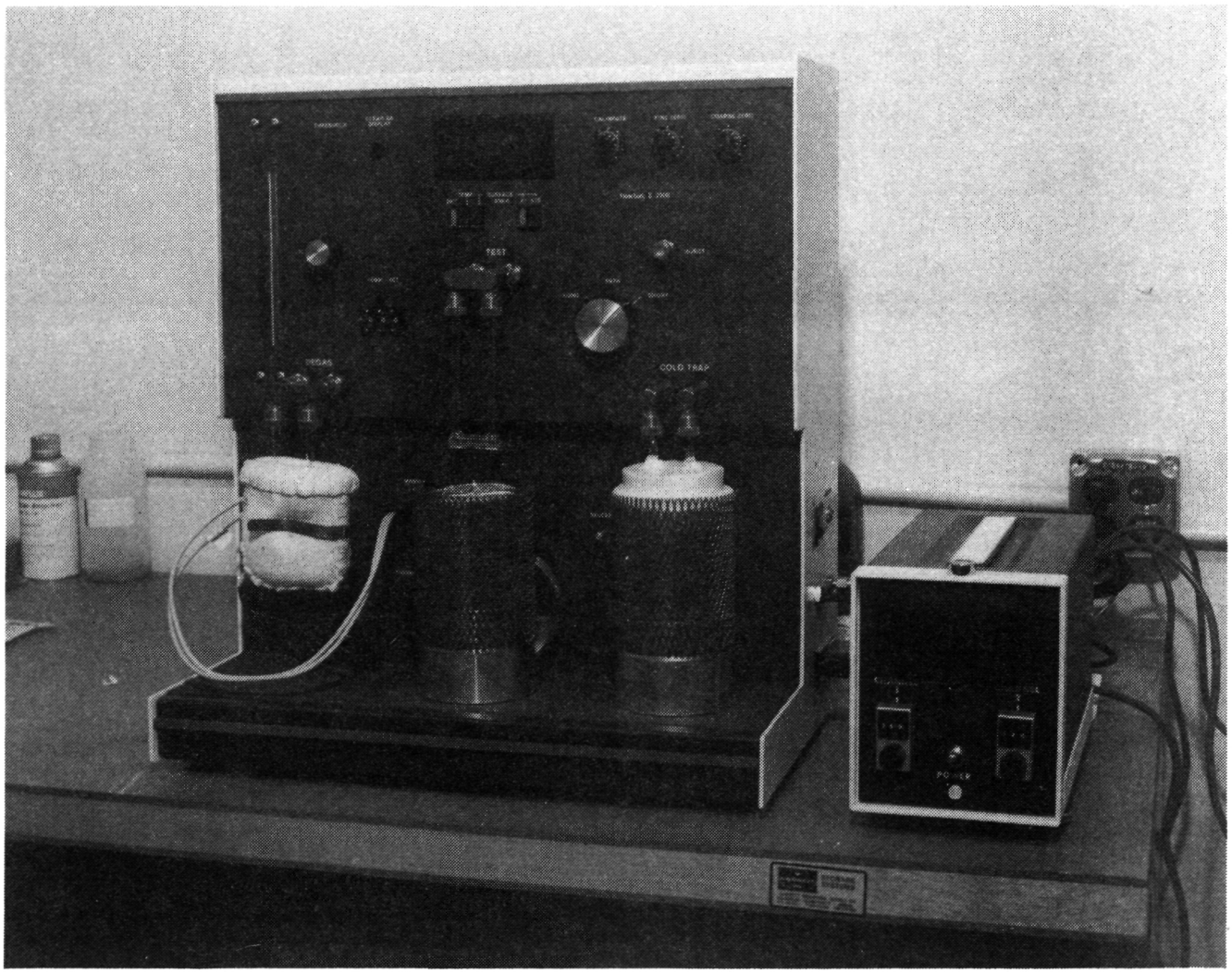

Figure 120. Micromeritics Flow Sorb II - 2300, Surface Area Analytical Equipment.

This Page Intentionally Left Blank

APPENDIX C

CARBORUNDUM UNIQUE WORK ADVANCED GAS TURBINE (AGT) TECHNOLOGY DEVELOPMENT PROJECT 1985 ANNUAL TECHNICAL PROGRESS REPORT

1.0 SUMMARY

This report summarizes the tasks performed by Sohio Engineered Materials Company/Carborundum during the period from July 1, 1984 through June 30, 1985. Work continued on six different sintered alpha silicon carbon (SASC) static structures. During this time period, fabrication activities focussed on injection molding development through optimization of tooling and fixturing to obtain better dimensional control during sintering. Isopressing and green machining continued to be used for select components. A summary of all component deliveries is give in Table 60. Each of these parts was accompanied by 10 ground modulus of rupture (MOR) test bars made from the same powder lot and processed in the same fashion as the respective component.

2.0 TURBINE STATOR

Each stator shipment consisted of 22 individual stator segments that were made by injection molding. The vane profile was closely controlled through sintering fixtures and required no green machining or final finishing. Stock has been added to the outside of the platforms to allow for grinding. Complete fixturing of the platforms to minimize distortion has been attempted and was successful on the trailing edge spacing. Additional work is required to reduce distortion near the leading edge.

Two molding trials were conducted and 7 sets of stator segments (154 individual parts) were sent in the as-fired state as agreed upon in the 1985 work statement. All grinding fixtures were supplied to Garrett for their in-house grinding.

Table 60. Component Delivery.

July 1, 1984 - June 30, 1985		
Component	**Total Parts Shipped**	**S/Ns**
Combustor Liner	8	107 through 116
Regenerator Shield	6	105 through 110
Transition Duct	2	118,119
Combustor Baffle	1	127
Stator Segment Sets (22/set)	7	269 through 422
Turbine Shroud	-	---

Minor mold modifications were necessary between the two molding runs to increase fillet radii between vane and platforms and to eliminate a positive imperfection on the trailing edge. The last three sets of stator segments shipped had these changes incorporated.

Activities on this project were reduced during the second half of this reporting period because of increased priorities on other static components and because sufficient hardware suitable for testing was available at Garrett. New fixturing techniques are currently under investigation to reduce thermal stresses in the stator trailing edge experienced by the SASC components during testing.

3.0 TURBINE SHROUD

Turbine shrouds molded late during the last reporting period were processed through sintering. These shrouds were molded using two different compounds (B, C) which varied in particle size distribution. This molding trial was carried out on a 1000 ton single screw machine at a custom molding house. The mold had been modified to produce a component according to drawing PA3609679. Because of insufficient stock on the tool steel, some green machining in the vane and rotor vicinity was necessary.

Special emphasis was placed on the optimization of the sintering cycle to obtain density without jeopardizing the microstructure through exaggerated grain growth. The balance between these two criteria is harder to control with increased component size and wall thicknesses.

Another critical area successfully addressed was fixturing during sintering. Incorrect fixturing, or no fixtures at all, resulted in shrouds of noticeable triangular shape between the three locating tabs. This problem was eliminated through proper sizing of the ID mandrel and adjustments to other supporting fixtures. In addition, warpage in the horizontal planes and of the tabs was largely reduced through optimized vertical fixtures.

Six turbine shrouds passed all green processing and non-destructive evaluation (NDE) steps and were sintered using fixtures of the latest design iteration. Densities for these components are given in Table 61.

Moldability, densification, and shape control for compound B and C were very similar. As-fired NDE, however, exhibited minor X-ray and fluorescent penetrant inspection (FPI) indications on component P/Ns 24-6 and 24-9. P/N 23-18 showed a crack on one of the tabs. The remaining three shrouds passed FPI and X-ray inspection, with shrouds P/Ns 23-20 and 23-22 being closest to the desired dimensions. Both of these are grinding candidates.

Work was put on hold at the end of the first quarter of this reporting period because of design reevaluations at Garrett with emphasis on lowering maximum stress in SASC components during thermal testing. Further design modifications will likely require a new tool.

Table 61. Turbine Shroud Densities.

P/N	Date Sintered (1984)	Compound	Density (g/cm^3)
24-6	7/18	B	3.10
24-9	7/27	B	3.08
23-17	8/28	C	3.14
23-18	9/7	C	3.07
23-22	9/18	C	3.10
23-20	9/24	C	3.09

4.0 COMBUSTOR BAFFLE

SASC combustor baffles tested at Garrett in rig and engine tests have performed extremely well. All units tested to date have been fabricated from a bimodal composition using the slip casting and green machining approach. Injection molding of a bimodal compound was chosen to obtain a near net shape fabrication process which would yield components with characteristics similar to previously supplied units.

Three different compounds varying only in the fractions of the two basic SiC powders were compounded and molded into MOR bars using a 100-ton machine and components using a 250-ton machine. Different furnacing conditions and fixturing techniques were investigated. The dimensional results and densities showed high variability and most components appeared to be oversize.

An in-depth investigation showed that contaminants in the furnace atmosphere had affected previous firings. Adjustments were made and three sets of MOR bars were processed through sintering, checked for density, ground and submitted for room temperature strength determination and microstructure. Data are expected by August 1985.

The mandrel design used to fixture the component during sintering was found to prohibit the components from reaching the desired shape. Some of the inconsistencies were also attributed to inadequate or uneven packing during the molding process caused by the relative low clamping pressure available on the in-house equipment.

The tool was sent out to be modified to accommodate the backface according to drawing PA3609614 which was obtained during the fourth quarter of this reporting period. The tool was increased on the ID to obtain sufficient grinding stock on the outside flow profile of the baffle. New mandrels are being designed. Arrangements were made to mold at a custom molder using a larger machine.

5.0 TRANSITION DUCT

All transition ducts supplied to GTEC to date were fabricated using isopressed tube stock and green machining to near final shape. This process has produced high quality parts that performed well in various thermal tests, but the process is a highly inefficient fabrication technique. Only about 5 percent of the raw material necessary to form the tube stock is required for the ultimate shape. A manual lathe, CNC lathe and mill are used to obtain the green shape.

Design modifications that Garrett incorporated in the past quarters have complicated the machining because of added features such as 3 thermocouple ports and a 180 degree flow diverter (Drawing PA3610213, Rev A). At the beginning of this fiscal year a dual fabrication approach was chosen. The currently proven technique is being used to supply components which have joined ports and no flow diverter. Injection molding is being developed to incorporate all design features to obtain a near net shape component.

An injection molding tool was designed and received at the end of the third quarter of this reporting period. After initial qualification with plastic components, two lots of transition ducts were molded on a 700-ton machine at an outside vendor. The first lot consisted of 37 ducts which had the ports incorporated without the holes to reduce the probability of flow line related defects. The second lot was made up of 22 transition ducts with port holes. The first of these latter ducts has been processed through sintering and is shown in Figure 121. This transition duct was 97.5 percent dense, showed good integrity and was submitted for in-depth dimensional analysis. Two additional ducts completed binder removal and six are currently in binder removal.

Two isopressed/green machined transition ducts with shrinkfit/brazed thermocouple ports were delivered. The joints were tested up to 5 psi air pressure and no leakage had been observed. Two joining methods have been under investigation. A shrinkfit approach

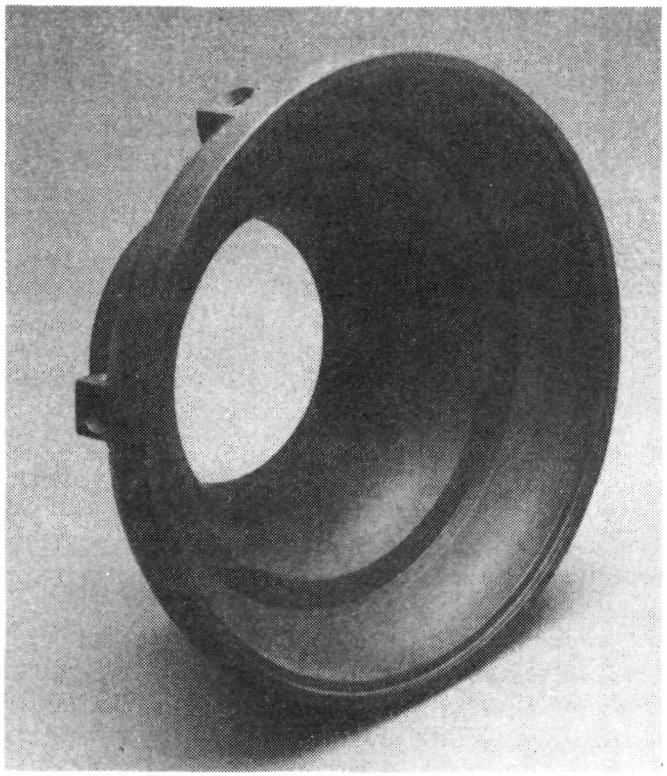

Figure 121. Injection Molded Transition Duct with Port Holes.

was thought to deliver the quickest and best results. However, some misalignment or uneven shrinkage of the inserts, caused insufficient bonding. Subsequent brazing of these joints was moderately successful. The second approach uses a braze and requires grinding on both surfaces to assure a tight fit. This method has been used with good success on other components. Trials with a transition duct are in progress. Fixturing of the ground inserts has to be developed to avoid ID contour grinding after brazing.

In response to Garrett's request for closer control of all dimensional aspects for each component, special emphasis has been placed on the determination of the contour with a contour reader. Holding fixtures were fabricated and base and center lines were established. Generated contours from as-fired components are being used to determine the optimum amount of stock removal from the inside platform (combustor to baffle interface). One trial transition duct and one potential deliverable duct await grinding.

6.0 COMBUSTOR LINER

Isopressing and green machining was chosen as the fabrication method for combustor liners during the past year. This approach represents the least costly method for this shape, volume, and desired delivery schedule. Because of budget constraints and other priorities for fabrication development, the extrusion program was dropped.

Eight liners and their corresponding MOR bars were supplied to Garrett. Billets were isopressed and one of each lot was green machined using calculated shrinkage values. The test pieces were sintered and checked for their dimensions. Adjustments were made when necessary and the remaining billets were machined to these newly specified dimensions. This methodology made it possible to obtain components within the specifications without any final grinding.

7.0 REGENERATOR SHIELD

Regenerator shields requiring close tolerance OD grinding were made from isopressed billets that were then green machined into blanks. These blanks were machined to the final ID with excess stock left on the OD and length.

Each of these premachined tube sections was fired on an individual mandrel and checked for density, dimensions, fluorescent dye penetrant, and microfocus X-ray indications prior to final grinding. Each component was subjected to a final NDE consisting of dimensional and FPI after completion of all grinding steps. Following these routine inspection procedures the units were sterilized and annealed. A total of six machined regenerator shields were shipped, four of these corresponded to Drawing 3846154, the last two were made to Revision A of this drawing.

APPENDIX D

LIST OF SYMBOLS, ABBREVIATIONS, AND ACRONYMS

Acronym	Definition
ACC	AiResearch Casting Company
AE	Acoustic emissions
AGT	Advanced gas turbine
AGT101	AGT model being developed by Garrett/Ford
Al_2O_3	Aluminum oxide
ASEA	ASEA Pressure Systems, Inc., Los Angeles
ATS	Air turbine starter
CBO	Carborundum Company, Niagara Falls, NY
CFDC	Combined Federal Driving Cycle
dB	Decibel
DF	Diffusion flame (relates to combustor/nozzle)
DF-2	Diesel fuel grade 2
DOE	Department of Energy
ECU	Electronic control unit
EPA	Environmental Protection Agency
F	Fahrenheit (degrees of)
FC	Film-cooled (relates to fuel nozzle)
Ford	Ford Motor Company
FPI	Fluorescent-penetrant inspection
FSH	Flow separator housing
Fuller's earth	fine, dust-life material for detecting flow paths
Garrett	Garrett Turbine Engine Company, Division of The Garrett Corporation
GE-Cordierite	Coating material made by General Electric
g	Gravity, 1-g = force equal to one gravity
g/cm^3	Grams per cubic centimeter
HIP	Hot isostatic pressing
HPSN	Hot pressed silicon nitride
HTP	High temperature protection insulation made by Lockheed Corporation
Hz	Hertz, cycles per second
ID	Inner diameter
IGV	Inlet guide vane
inch	U.S. customary linear unit centimeters
in-lb	Inch-pounds (work)
I-85	Copper base coating material (regenerator seals)
I-151	Zinc oxide base coating material (regenerator seals)
JP-4	Kerosene base aviation jet fuel
ksi	One-thousand pounds per square inch
Kyocera	Kyocera International, Inc., Kyoto, Japan
LAS	Lithium alumina silicate ceramic material
LBO	Lean blowout (combustor fuel-air mixture)
lb-in	Pound-inch (torque)
lb/min	Pounds per minute (flow)
LVDT	Linear variable displacement transformer
mil	One-thousandth of one inch

APPENDIX D

LIST OF SYMBOLS, ABBREVIATIONS, AND ACRONYMS

Acronym	Definition
MOR	Modulus of rupture
NASA	National Aeronautics and Space Administration
NDE	Nondestructive evaluation
NGK	NGK - Locke, Inc.
NO_x	Nitric oxides
OD	Outer diameter
pH	Relative acidity to alkalinity balance
psid, ΔP	Differential pressure, pounds per square inch
pound, lb	U.S. customary weight measure 0.373 kilograms
p-p	Peak-to-peak
P_{rig}	Rig pressure psi
PSD	Particle size distribution
RBSN	Reaction cured glass, Lockheed Corp.
Rene 41	High temperature heat resistant superalloy
RM-1	Ford rotor material, first generation
RM-2	Ford rotor material, second generation
RM-3	Ford rotor material, third generation
rpm	revolutions per minute
SASC	Sintered alpha silicon carbide ceramic material
SC201	Silicon carbide ceramic material
SIMCAB	Simplex cone air blast fuel nozzle
Si_3N_4	Silicon nitride
S/N	Serial Number
SNN	Sintered silicon nitride ceramic material
shp	Shaft horsepower
TBC	Thermal barrier coating
TF	Tensile face
Ti	Titanium
TIT	Turbine inlet temperature
T_{max}	Maximum temperature
TSF	Temperature spread factor
$T_{3.5}$	Rating point - combustor inlet temperature
$T_{4.1}$	Rating point - turbine inlet temperature
UCLA	University of California at Los Angeles
VIGV	Variable inlet guide vane
Wayne-Kerr	Rotor dynamic measuring devices
watt	Electrical power - one volt x one ampere
Waspalloy	Heat resistant, high temperature superalloy
Y_2O_3	Yttrium oxide
μ	Micron, one millionth meter
2-D	Two-dimensional
3-D	Three-dimensional

REFERENCES

1) Garrett Turbine Engine Company, "Advanced Gas Turbine (AGT) Powertrain System Development for Automotive Applications," Semiannual Progress Report Number 1 (Octob er 1979 through June 1980), NASA Report CR-165175, November 1980, Contract DEN3-167.

2) Garrett Turbine Engine Company, "Advanced Gas Turbine (AGT) Powertrain System Development for Automotive Applications," Semiannual Progress Report Number 2 (July 1980 through December 1980), NASA Report CR-165329, June 1981, Contract DEN3-167.

3) Garrett Turbine Engine Company, "Advanced Gas Turbine (AGT) Powertrain System Development for Automotive Applications," Semiannual Progress Report Number 3 (January 1981 through June 1981), NASA Report CR-167901, December 1981, Contract DEN3-167.

4) Garrett Turbine Engine Company, "Advanced Gas Turbine (AGT) Powertrain System Development for Automotive Applications," Semiannual Progress Report Number 4 (July 1981 through December 1981), NASA Report CR-167983, June 1982, Contract DEN3-167.

5) Garrett Turbine Engine Company, "Advanced Gas Turbine (AGT) Powertrain System Development for Automotive Applications," Semiannual Progress Report Number 5 (January 1982 through June 1982), NASA Report CR-168104, December 1982, Contract DEN3-167.

6) Garrett Turbine Engine Company, "Advanced Gas Turbine (AGT) Powertrain System Development for Automotive Applications," Semiannual Progress Report Number 6 (July 1982 through December 1982), NASA Report CR-168246, June 1983, Contract DEN3-167.

7) Garrett Turbine Engine Company, "Advanced Gas Turbine (AGT) Powertrain System Development for Automotive Applications," Semiannual Progress Report Number 7 (January 1983 through June 1983), NASA Report CR-174694, December 1983, Contract DEN3-167.

8) Garrett Turbine Engine Company, "Advanced Gas Turbine (AGT) Powertrain System for Automotive Applications," Semiannual Progress Report 8 (July 1983 through december 1983), NASA Report CR-174809, June 1984, Contract DEN3-167.

9) Garrett Turbine Engine Company, "Advanced Gas Turbine (AGT) Powertrain System for Automotive Applications," Semiannual Progress Report 9 (January 1984 through June 1984), NASA Report CR-174886 December 1984, Contract DEN3-167.

10) Contract AFWAL-TR-83-2082, Gas-Lubricated Turbine End Foil Bearing Program

1 Report No	2. Government Accession No.	3. Recipient's Catalog No
CR-179485		

4 Title and Subtitle	5. Report Date
Advanced Gas Turbine (AGT) Technology Development Project 1985 Annual Report (July 1, 1984 - June 30, 1985)	December 1985
	6. Performing Organization Code

7 Author(s)	8. Performing Organization Report No
Engineering Staff of Garrett Turbine Engine Company, A Division of the Garrett Corporation	31-3725(10)
	10. Work Unit No.

9 Performing Organization Name and Address	11. Contract or Grant No
Garrett Turbine Engine Company P.O. Box 5217 Phoenix, Arizona 85010	DEN3-167
	13. Type of Report and Period Covered
12. Sponsoring Agency Name and Address	Interim July 1984 - June 1985
Department of Energy Division of Transportation Energy Conservation, Washington, D.C. 20545	14. Sponsoring Agency Code
	DOE/NASA/0167-10

15. Supplementary Notes
Interim Progress Report under Interagency Agreement
Project Manager T.N. Strom, Propulsion Systems Division, NASA-Lewis Research Center, Cleveland, Ohio 44135

16. Abstract

This report is the tenth in a series of Technical Summary reports for the Advanced Gas Turbine (AGT) Technology Development Project, authorized under NASA Contract DEN3-167, and sponsored by the Department of Energy (DOE). This report was prepared by Garrett Turbine Engine Company, A Division of the Garrett Corporation, and includes information provided by Ford Motor Company, the Carborundum Company, and AiResearch Casting Company. The Project is administered by Mr. Thomas N. Strom, Project Manager, NASA-Lewis Research Center, Cleveland, Ohio. This report covers plans and progress for the period July 1, 1984 through June 30, 1985.

17. Key Words (Suggested by Author(s))	18. Distribution Statement
Advanced Gas Turbine Single Shaft Engine Ceramic Turbine Turbine Transmission	Unclassified - Unlimited Star Category 85 DOE Category UC-96

19 Security Classif (of this report)	20. Security Classif. (of this page)	21. No. of Pages	22 Price*
Unclassified	Unclassified	165	

* For sale by the National Technical Information Service, Springfield Virginia 22161